Characterisation of Sludge Rheology and Sludge Mixing in Gas-mixed Anaerobic Digesters

Wei, P.

Publication date
2021

Document Version
Final published version

Citation (APA)
Wei, P. (2021). *Characterisation of Sludge Rheology and Sludge Mixing in Gas-mixed Anaerobic Digesters*. [Dissertation (TU Delft), Delft University of Technology].

Characterisation of Sludge Rheology and Sludge Mixing in Gas-mixed Anaerobic Digesters

Peng WEI

Characterisation of Sludge Rheology and Sludge Mixing in Gas-mixed Anaerobic Digesters

Dissertation

for the purpose of obtaining the degree of doctor
at Delft University of Technology
by the authority of the Rector Magnificus Prof.dr.ir. T.H.J.J. van der Hagen
chair of the Board for Doctorates
to be defended publicly on

Tuesday 13 July 2021 at 10:00 o'clock

by

Peng WEI
Master of Engineering in Environmental Engineering, Graduate University of Chinese Academy of Sciences, China
born in Jiangxi, China

This dissertation has been approved by the promotors.

Composition of the doctoral committee:

Rector Magnificus	chairman
Prof.dr.ir. J.B. van Lier	Delft University of Technology, promotor
Prof.dr.ir. M.K. de Kreuk	Delft University of Technology, promotor
Prof.dr.ir. W.S.J. Uijttewaal	Delft University of Technology, promotor

Independent members:

Prof.dr.ir. C. Poelma	Delft University of Technology
Prof.dr. Z. Kapelan	Delft University of Technology
Prof.dr. J. Bridgeman	University of Bradford, United Kingdom
Prof.dr. W.-W. Li	University of Science and Technology of China, China
Prof.dr.ir. L.C. Rietveld	Delft University of Technology, reserve member

Cover by: Xiaojie Shao (邵晓捷), and Peng Wei
Printed by: Ipskamp Printing
ISBN: 978-94-6421-407-9

Email: P.Wei@tudelft.nl; pweiemail@163.com

To my family

谨以此书献给我的家人

Abstract

Excess sludge handling is as important as treating the wastewater in determining the operational performance and costs in modern municipal wastewater treatment plants (WWTPs). In practice, excess sludge handling is widely implemented using anaerobic digestion (AD), in which the organic matter inside the sludge is not only stabilised and partly degraded, but also converted to methane gas as alternative fuel. Thus, optimal AD performance aims for maximising both sludge reduction and energy recovery, which is sometimes difficult to achieve in practice. Troubleshooting and optimisation are challenging to implement, due to the limited accessibility of anaerobic digesters and uncertainties of key influencing factors, including mixing behaviour and feed sludge characteristics. This thesis is focused on the possible enhancement of AD performance, by characterising the sludge rheology and evaluating its impact on sludge mixing inside the digesters. A full-scale digester, applying the gas-mixing mode, was selected for detailed investigations.

Rheological properties of waste activated sludge (WAS) and digestate (DGT) from the selected WWTP were characterised, using both rheological measurements and rheological model fitting. DGT showed yield-pseudoplastic behaviour well characterised by the Herschel-Bulkley model. However, WAS demonstrated complex yield-pseudoplastic behaviour, which was better characterised by hybrid model fitting. The rheological instability, characterised by the distinct flow status and transitions, and considerable correlations to solids content, could give more insight in viscoelasticity and thixotropy of concentrated WAS. Moreover, recommendations for developing a proper rheological measurement protocol were also formulated.

The thixotropic behaviour was further explored by involving the rheological impacts of shearing duration and temperature. Under the long-term shearing conditions, the complex thixotropic behaviour was well characterised by two limitation states: Initial and Stable, which showed distinct rheological properties for concentrated WAS, while small rheological difference for DGT. These distinct rheological properties of concentrated WAS were clearly reflected in its pipe flow behaviour, which was well assessed using the computational fluid dynamics (CFD) model with effective rheological data integration. Temperature had a striking impact on the sludge rheology, and strongly correlated with the solids content and degree of sludge stabilisation. The discrepancy in impact between long-term shearing and temperature implied different mechanisms responsible for shifting the equilibrium of hydrodynamic and non-hydrodynamic interactions for sludge structural deformation and recovery.

Moreover, the gas-sludge flow and mixing were characterised in detail, firstly using a refined lab-scale CFD model. Bubble size, phase interaction forces, and liquid rheology significantly impacted predictions of the two-phase flows. A more reliable and complete model validation was obtained by performing a critical comparison. The mixing performance approximated a laminar-flow reactor (LFR) that distinctly deviated from the expected continuously stirred tank reactor (CSTR) design. The results underline the importance of a proper phase-interaction description for reliable flow and mixing characterisation.

The developed model setup was further applied to the full-scale digester. Results revealed considerable dependency of the flow and mixing characterisation, with the rheological input data. The predicted dominant shear rate level was out of the effective shear rate range of the Ostwald model. This finding limited the model application, since the apparent viscosity overestimation at low shear rates led to flow and mixing overestimation. However, the Herschel-Bulkley model better fitted low shear rates, and predicted large gradients of apparent viscosity in the poor flow regime. Distinct flow and mixing compartments were obtained based on the gas-sparging height, including a plug-flow compartment above, and a dead-zone below. Although inducing insufficient mixing, the applied gas-sparging may still be useful to mitigate short-circuiting, accumulative sedimentation and effective volume reduction.

Furthermore, recommendations and guidelines on practical operation and design were proposed. The overall shear rate level in the digester should be increased, which cannot be reached by simply intensifying the gas-sparging rate. Nonetheless, it is recommended to reduce the gas-sparging nozzle height, and/or to enlarge the overall bubble size. Thermophilic operation could also be an alternative, if the improved operational performance compensates the additional energy requirement.

Regarding the full-scale modelling, model reliability or effectiveness should not merely rely on experimental validation. Generally, discrepancies in operations and conditions between design and reality are difficult to be thoroughly identified and foreseen, and thus necessary model simplifications have to be employed. With this aspect, sensitivity analysis and assessment, and tendency predictions are more important than an agreement with experimental data.

Contents

Abstract I
Chapter 1. Introduction and thesis setup 1
1.1 Anaerobic digestion of sewage sludge 1
1.2 Mixing in anaerobic digestion 2
1.2.1 Implementation of mixing in full-scale digesters 2
1.2.2 Incomplete mixing and resulting constraints 3
1.3 Rheological characterisation of sewage sludge 4
1.4 Flow and mixing characterisation 7
1.4.1 Experimental approaches 8
1.4.2 Numerical approaches: computational fluid dynamics (CFD) 9
1.4.3 Numerical characterisation using CFD 11
1.5 Research setup and thesis outline 13
1.5.1 Research objectives and questions 13
1.5.2 Thesis outline 14
1.6 References 16
Chapter 2. Experimental and mathematical characterisation of the concentrated waste activated sludge 23
Abstract 24
2.1 Introduction 25
2.2 Materials and Methods 27
2.2.1 Sample characterisation 27
2.2.2 Rheological measurements 27
2.3 Results and Discussion 28
2.3.1 Varying trends in flow curves 28
2.3.2 Mathematical characterisation on the varying trends 30
2.3.3 Further characterisation of the rheological instability 34
2.3.4 Total solids impact on the rheological instability 40
2.3.5 Special rheological behaviour at low shear rates 42
2.3.6 Suggestions on a proper protocol for rheological measurements 43
2.4 Conclusions 45
2.5 References 45
Chapter 3. Further rheological characterisation and flow assessment of sewage sludge 49
Abstract 50
3.1 Introduction 51
3.2 Materials and Methods 52
3.2.1 Sample characterisation 52
3.2.2 Rheological measurements 52
3.2.3 Hydrodynamics and energy assessment 53
3.3 Results and Discussion 54

3.3.1 Characterisation of time-dependent rheological properties by long-term shearing 54
3.3.2 Temperature impact on rheology: role of solids content 57
3.3.3 Further discussion: implication of dynamic structural change 62
3.3.4 Application of the rheological discrepancy: pipe flow assessment 66
3.4 Conclusions 70
3.5 References 70
Chapter 4. Two-phase flow and mixing in a lab-scale digester: importance for scaled-up applications 73
Abstract 74
4.1 Introduction 75
4.2 Materials and Methods 76
4.2.1 Computational domain and mesh 76
4.2.2 Governing equations and models 77
4.2.3 Boundary conditions 82
4.2.4 Main simulation settings 82
4.3 Results and Discussion 82
4.3.1 Grid independence test 82
4.3.2 Impacts of uncertain parameters on flow field 83
4.3.3 Validation and further prediction 88
4.3.4 Mixing evaluation 95
4.4 Conclusions 98
4.5 References 99
Chapter 5. Gas-mixing in a full-scale anaerobic digester: assessments of rheological data integration, mixing and recommendations for optimisation using computational fluid dynamics 103
Abstract 104
5.1 Introduction 105
5.2 Model setup 106
5.2.1 Geometry, computational domain and mesh 106
5.2.2 Model development 108
5.2.3 Boundary conditions and main simulation settings 110
5.3 Results and Discussion 111
5.3.1 Rheological data integration: the Ostwald model 111
5.3.2 Rheological data integration: the Herschel-Buckley model 118
5.3.3 Role of gas-sparging in mixing: assessment and guidelines for optimisation 123
5.4 Conclusions 130
5.5 References 130
Chapter 6. Summary, further discussion and outlook 135
6.1 Summary 135
6.1.1 Rheological characterisation of sewage sludge 135
6.1.2 Flow behaviour of sewage sludge 136
6.1.3 Mixing performance in digesters 137

6.1.4 Practical aspects: recommendations/guidelines for design and operation 137
6.2. Further discussion and outlook 138
6.2.1 Rheological characterisation: method, data accuracy and mechanism 138
6.2.2 Rheological characterisation: effectiveness to practical applications 140
6.2.3 Limitations in modelling of non-Newtonian flows 141
6.2.4 Mixing in anaerobic digesters 143
6.3 References 144
Nomenclature 147
Supplementary 151
A. Fitting results of more rheological models (Chapter 2) 151
B. Supplementary rheological and pipe-flow data (Chapter 3) 153
C. Grid independence test (Chapter 4) 157
D. Sensitivity study on the effective range of the Ostwald model (Chapter 5) 159
Acknowledgements/致谢 165
List of publications 167
Biography 169

Chapter 1. Introduction and thesis setup

This thesis is focused on the possible enhancement of anaerobic digesters treating excess sewage sludge by characterising the sludge rheology and evaluating its impact on sludge mixing inside the digesters. Since the costs for excess sludge handling determine the operational costs of modern municipal wastewater treatment plants (WWTPs), sludge reduction is a focal point of many researchers. The anaerobic stabilisation of excess sewage sludge, applying the anaerobic digestion (AD) process is widely implemented. During AD, about 50% of the organic matter inside the sludge is degraded and converted to methane gas. The achieved sludge reduction, immediately reduces the sludge handling costs, while the biochemical energy enclosed in the sludge biomass is recovered in the form of methane gas. This recovered methane gas is subsequently used as alternative fuel within the WWTP, leading to substantial reduction in fossil fuel consumption and thus to reduction in greenhouse gas emissions during wastewater treatment. Considering the above, there is a worldwide strong interest to maximise the AD process for both sludge reduction and energy recovery. In the below paragraphs, the role of anaerobic digesters in sludge handling, as well the impact of sludge rheology on digester mixing are further discussed. Finally, an overview of the thesis setup is given.

1.1 Anaerobic digestion of sewage sludge

The costs for excess sludge disposal from municipal WWTPs can be as high as 50% of the total operational costs of these plants. Therefore, as above mentioned, substantial research is focused on reducing the amount of excess sludge leaving the WWTP (e.g. (Appels et al. 2008, Baeyens et al. 1997)). Main research goals focus on reducing the organic fraction of waste activated sludge (WAS), improving its dewaterability and by this, reducing the volume for further processing (Appels et al. 2008). AD is proven to be a cost-effective method, accomplishing both organic matter biodegradation and bioenergy recovery. During AD, WAS is physically decomposed and biochemically converted into biogas and digestate (DGT). The biogas is mainly composed of CH_4 and CO_2 with an average calorific content of 24 MJ/m^3, and thus, is a renewable energy source. In practice, the produced biogas is formed as bubbles, released from the sludge matrix and collected at the top part of the anaerobic digester. The stabilised DGT, which is the final product after degradation of the biodegradable organic fraction of the WAS, is eventually discharged from the digester for dewatering and further treatment, such as incineration, land application, and/or landfill. With some few exceptions,

incineration is the only outlet for WAS processing in The Netherlands. AD processes are usually operated at the mesophilic (30-38°C), or thermophilic (50-57°C) temperature range. Optimal AD performance aims for the highest degree of DGT stabilisation, and therefore, also for maximising the biogas production. However, achieving the optimal performance in practice relies on various factors, in which mixing performance and feed sludge characteristics are found to be important (Terashima et al. 2009).

1.2 Mixing in anaerobic digestion

For the sake of optimal mixing performance, digesters are commonly designed as a continuously stirred tank reactor (CSTR), which is considered a completely mixed reactor with a uniform liquid composition throughout the entire reactor volume (Levenspiel 1999). Key functionalities of mixing can be summarised based on the varies published studies (Karim et al. 2005a, Karim et al. 2005b, Kariyama et al. 2018, Lindmark et al. 2014, Mills 1979, Parkin and Owen 1986, Van Hulle et al. 2014), which includes:

- Enhancement of convection and turbulent diffusion throughout the whole reactor, promoting mass and heat transfer between substrates and microorganisms;
- Avoidance of maldistribution of pH, temperature and redox potential (RP);
- Enhanced dispersion of toxic components and metabolic-end products, and release of produced biogas;
- Reduction in overall sludge particle size, maintaining materials suspended, while preventing sedimentation, foaming and stratification;
- Enhanced shock-resistance capacity under high total solids (TS) feeding conditions.

1.2.1 Implementation of mixing in full-scale digesters

AD essentially is a multiphase flow system, in which the reactor content is mixed by the motion of the produced biogas. However, the degree of mixing caused by biogas bubbles is usually not enough to achieve and maintain an efficient operational performance. Therefore, reactor mixing is commonly enhanced by three auxiliary modes in practice: mechanical stirring, pump recirculation, and/or gas-mixing (Lindmark et al. 2014). In a mechanical stirring mode, sludge is mixed by the rotational motion of impeller(s). In a pump recirculation mode, sludge is suctioned out and recirculated back by a pump system, which is usually combined with a heat exchanger system. In a gas-mixing mode, part of the collected produced

biogas is pressurised and recirculated to the digester by a gas compressor system. The recirculated biogas can be released through diffuser(s) in a confined, or unconfined way. Schematic representation of the three mixing modes is shown in Fig. 1-1.

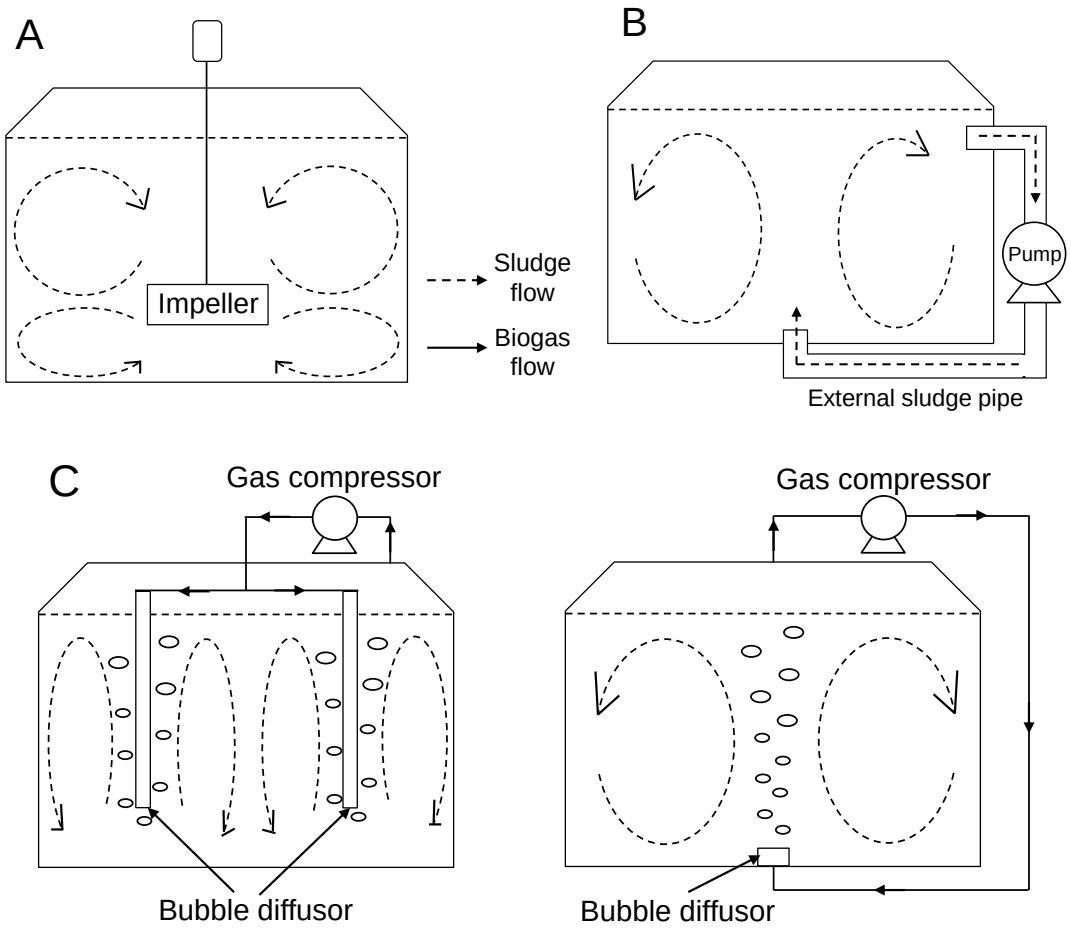

Fig. 1-1 Schematic representation of three auxiliary mixing modes, (A): mechanical stirring, (B): pump recirculation, and (C): gas-mixing, adopted from (Appels et al. 2008).

1.2.2 Incomplete mixing and resulting constraints

Due to a limited dimensional impact, well controlled and maintained mixing is more achievable in lab-scale digesters. However, a dimensional scale-up largely increases the presence of stagnant regions (or dead zone) and short-circuiting, leading to effective volume reduction and deviation of hydraulic retention time (HRT) and/or solids retention time (SRT) between design and reality (Parkin and Owen 1986). Within the context of a CSTR design, it must be realised that HRT and SRT are numerically the same (Hoffmann et al. 2008, Lindmark et al. 2014). The reduced total effective volume because of incomplete mixing can amount up to 75% of the total volume (Monteith and Stephenson 1981), which may coincide

with localised decreased temperature and organic matter removal rate (Parkin and Owen 1986). Hence, good mixing is more difficult to achieve in full-scale installations, and the operational performance can be much lower than the expected CSTR performance, even resulting in malfunctioning or process failure. Besides, resulting accumulative sedimentation of heavy materials like sand and stones, can have an adverse effect on mixing equipment, further weakening the mixing efficiency. Foaming has been found to become another problem under non-mixing (Stroot et al. 2001) and intermittent mixing (Kowalczyk et al. 2013, Stafford 1982) conditions. Persisting scum layer accumulation can further reduce the effective volume and impede the biogas release (Lapp et al. 1975). However, improving the mixing performance cannot be attained by simply enhancing the mixing intensity (power input per unit volume).

Auxiliary mixing requires considerable extra energy for maintaining normal operation (Mills 1979). Energy for mixing can be even over 50% of the total energy consumption in full-scale digesters (Kowalczyk et al. 2013, Rivard et al. 1995). So mixing enhancement needs to be implemented based on an energy valorisation strategy in practice. On the other hand, the effects of intensive mixing on AD performance are still not very clear and contradictory results are found in literature. In some studies, intense continuous mixing only resulted in comparable or even lower biogas production, compared to minimal or intermittent mixing (Hamdi 1991, Karim et al. 2005c, Kim et al. 2002, Stafford 1982, Stroot et al. 2001, Sulaiman et al. 2009, Vavilin and Angelidaki 2005). In addition, some authors reported instable performance under intense mixing conditions, including lower pH, higher RP, and a prolonged start-up period (Hoffmann et al. 2008, Karim et al. 2005b, McMahon et al. 2001, Sulaiman et al. 2009).

Intense mixing may have strong effects on the morphological structure of flocs, such as syntrophic associations of microorganisms. Vigorous shearing has been found to result in flocs disruption (Hoffmann et al. 2008) and less production of extracellular polymeric substances, which facilitates agglomeration and spatial juxta-positioning of the microorganisms (Hoffmann et al. 2008, McMahon et al. 2001, Ong et al. 2002). However, disturbances by intense mixing has not been found to affect long-term and stabilised AD performance in other studies (Hamdi 1991, Hoffmann et al. 2008, Karim et al. 2005a, Karim et al. 2005b).

1.3 Rheological characterisation of sewage sludge

Characterisation and evaluation of mixing in AD rely on accurate knowledge of feed sludge

characteristics. Especially, sludge rheology has been known to be of prime importance to characterise the sludge hydrodynamic behaviour (Slatter 1997), impacting its pumping and mixing processes (Seyssiecq et al. 2003). Assessment of sludge rheology refers to studies on deformation and flow of the sludge under various levels of stress conditions, such as low or high shear. The deformation and flow response can be characterised using a rheogram, which is typically a plot of shear rate versus shear stress.

Generally, rheological properties of a sludge matrix are measured using a rheometer. Two rheometer types are mainly applied for sewage sludge, including capillary and rotational rheometers (Eshtiaghi et al. 2013, Ratkovich et al. 2013). The capillary or tubular rheometers have a simple geometry of a capillary tube. A laminar flow of filled sample is generated by a specified pressure gradient, and the flow rate is used to determine the sample's rheology. The rotational rheometers usually have a concentric cylinder geometry (with single- or double-gap), or a plate and cone geometry. So, shear stress is determined by the imposed torque, and shear rate is determined by rotational velocity. The rotational rheometers have been widely employed in recent years, due to their advantages in measurement compatibility and data collection (Eshtiaghi et al. 2013).

As shown in Fig. 1-2A, different correlations between shear rate and shear stress can be obtained, and thus can be classified into different model fluids. Under an isothermal condition, the correlation of dynamic viscosity μ to shear rate γ and shear stress τ is expressed as

$$\tau = \mu \cdot \gamma \tag{1-1}$$

A Newtonian fluid has a linear correlation between γ and τ, and thus has constant μ. The other curves in Fig. 1-2A represent time-independent non-Newtonian behaviour, and thus μ or named as apparent viscosity, is dependent on γ. Since μ is expressed by a function of γ, Equation 1-1 can be developed as a rheological model to characterise the non-Newtonian behaviour. The Ostwald or power law model is a commonly used rheological model, which is expressed as

$$\tau = K \cdot \gamma^n \tag{1-2}$$

where K denotes the fluid consistency index, and n the flow behaviour index. The n value can determine different types of fluids shown in Fig. 1-2A: (1) Newtonian when $n = 1$; (2) pseudoplastic or shear-thinning when $0 < n < 1$; and (3) dilatant or shear-thickening when $n > 1$. Besides, some materials become a fluid only when the imposed shear stress is over a threshold, which is defined as yield stress. With constant μ over the yield stress, the fluid is Bingham plastic and can be described by the Bingham model:

$$\tau = \tau_0 + \mu_B \cdot \gamma \tag{1-3}$$

where τ_0 denotes the yield stress, and μ_B the constant Bingham viscosity. When μ is shear-dependent, the non-Newtonian behaviour can be described by the Herschel-Bulkley model:

$$\tau = \tau_0 + K \cdot \gamma^n \tag{1-4}$$

When $0 < n < 1$, the Herschel-Bulkley model describes a yield-pseudoplastic fluid shown in Fig. 1-2A.

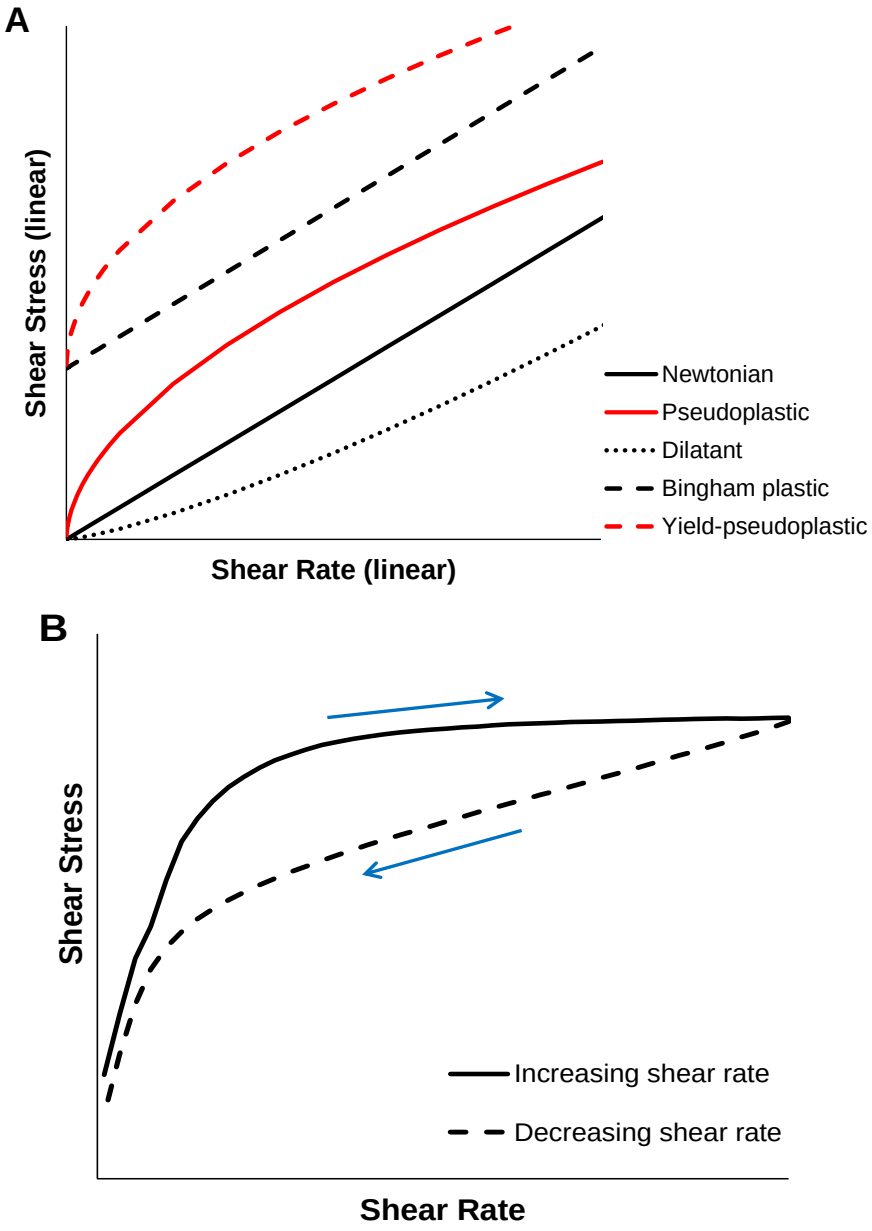

Fig. 1-2 Schematic rheograms of (A): typical model fluids with time-independent rheological behaviour, and (B): thixotropic behaviour.

Nearly Newtonian behaviour has only been found in dilute sewage sludge (Sanin 2002). While characterised by a high solids content, sewage sludge from WWTPs mainly behaves non-Newtonian. However, distinct non-Newtonian behaviour has been reported, including Bingham (Manoliadis and Bishop 1984), pseudoplastic (Bhattacharya 1981, Manoliadis and Bishop 1984) and even dilatant (Bhattacharya 1981). Hence, several rheological models have been widely used, including the Ostwald model, Bingham model and Herschel-Bulkley model (Eshtiaghi et al. 2013, Ratkovich et al. 2013, Seyssiecq et al. 2003). Besides, sludge rheological properties also have been characterised by various models with a higher complexity degree, including the Sisko model (Khalili Garakani et al. 2011, Mori et al. 2006, Pollice et al. 2007, Xia et al. 2009), the Casson model (Khalili Garakani et al. 2011, Pevere et al. 2007), and the Cross model (Eshtiaghi et al. 2012b, Khalili Garakani et al. 2011), which are expressed in Equation 1-5, 1-6, and 1-7, respectively.

$$\tau = \mu_\infty \cdot \gamma + K \cdot \gamma^n \tag{1-5}$$

$$\sqrt{\tau} = \sqrt{\tau_0} + \sqrt{\mu_\infty \gamma} \tag{1-6}$$

$$\frac{\mu - \mu_\infty}{\mu_0 - \mu_\infty} = \frac{1}{1 + \lambda_{Cr} \cdot \gamma^m} \tag{1-7}$$

where μ_∞ denotes the infinite rate apparent viscosity, μ_0 the zero-shear viscosity, λ_{Cr} the time coefficient in the Cross model, and m the rate constant in the Cross model.

All aforementioned rheological models are based on a time-independent assumption, but rheological properties can also be time-dependent. A reversible time-dependent change of apparent viscosity at a constant shear rate or shear stress level is defined as thixotropy. As shown in Fig. 1-2B, thixotropy can be identified when a hysteresis loop is formed in a measurement when combining increasing and decreasing shear rates. Thixotropic behaviour also has been found in sewage sludge, especially with high solids content levels (Battistoni 1997, Eshtiaghi et al. 2013, Seyssiecq et al. 2003), which makes the rheological characterisation more complicated.

1.4 Flow and mixing characterisation

Generally, flow and mixing in digesters are characterised using both experimental and numerical approaches, which are introduced in the following subsections.

1.4.1 Experimental approaches

Application of experimental approaches is a strategy to visualise and quantify flow and mixing in a reactor. However, presence of biogas and stabilised temperature requires a strict air-tight and insulation circumstance for AD in practice. Thus, the commonly used optical techniques, like particle image velocimetry and laser Doppler anemometry, are challenging to implement for straightforward hydrodynamic characterisation. In the last decades, computer automated radioactive particle tracking (CARPT) and computed tomography (CT) have been developed for opaque systems like bubble columns and fluidized beds (Chen et al. 2001, Kemoun et al. 2001, Roy et al. 2001). These advanced non-invasive approaches also have been applied in a lab-scale gas-mixed digester (Karim et al. 2004, Vesvikar and Al-Dahhan 2005). Specific hydrodynamic characteristics were visualised and quantified, including velocity, turbulence of the liquid phase and local gas holdup distribution. Besides, the mixing performance was evaluated by the particle trajectory results. A further application has been carried out to investigate the effects of a specific reactor design on hydrodynamics and mixing in the same system (Varma and Al-Dahhan 2007). CARPT also has been applied in digesters with mechanical stirring to quantify overall shear distribution and local shear levels, and evaluate the influence of the impeller rotational speed (Hoffmann et al. 2008). The aforementioned work has shed light on straightforward hydrodynamic characterisation and mixing in AD. However, the CARPT and CT applications are still limited in lab-scale systems.

Application of a tracer experiment is more feasible to evaluate mixing in large-scale digesters. Generally, a known amount of a chemical (such as LiCl) is used as tracer and injected into the studied digester; and time variation of the tracer concentration is monitored to determine the residence time distribution (RTD) (Levenspiel 1999). The tracer can be injected in a constant flow rate mode, or in a pulse (δ-Dirac) mode. In the constant flow rate mode, tracer concentrations at the endpoint (i.e., the outlet) are monitored until reaching a stabilised level. In the pulse mode, the tracer is injected instantaneously (time scale ~ 0), and the endpoint concentrations are monitored until all the tracer is discharged. Several materials are used as the tracer in AD. Sodium fluoride has been used first, and the results have shown only 50% effective volume in the studied primary digester (Tenney and Budzin 1972). Fluoride tracer also has been used in other primary digesters (Monteith and Stephenson 1981). Large inactive volume (75% of the total volume) and short-circuiting have been found to account for the non-ideal mixing behaviour and shorter HRT. Lithium has been more commonly used as a tracer medium (Anderson et al. 1991, Capela et al. 2009, Olivet et al. 2005, Smith et al. 1993, Terashima et al. 2009), since it is reported to be non-adsorptive and to have no inhibitory

effect on microbial activity (Anderson et al. 1991).

The non-ideal mixing behaviour determined by the tracer experiments usually cannot be well-characterised by ideal models, including CSTR and plug-flow reactor (PFR). Thus more non-ideal models are developed, including the dispersion model, tanks-in-series model and combined models (Levenspiel 1999). These models have been applied to a pilot-scale contact process anaerobic digester, and the results revealed model limitations for an accurate characterisation of the obtained RTD curves (Smith et al. 1993). In addition, a promising computer simulation model has been proposed for the complicated flow pattern in practice. In a study of a gas-lift digester, limitations in the conventional non-ideal models were also reflected by contradictory interpretations on the experimental data (Bello-Mendoza and Sharratt 1999). Authors developed a compartment model for RTD data analysis and for determining correlations between power input and mixing. The model applications have been further extended to a complex industrial-scale digester (Capela et al. 2009). The Gamma distribution model with bypass was found to be the best, and the results determined a good mixing performance with 22% non-effective volume. Besides, some suggestions were addressed to improve the plant-scale operational performance.

1.4.2 Numerical approaches: computational fluid dynamics (CFD)

Since the experimental approaches are still inaccurate to determine the actual flow and mixing performance, also numerical approaches have been developed. Mixing in AD has been numerically characterised since 1970s, and a two-region model has been applied in the early studies (Bello-Mendoza and Sharratt 1998, Keshtkar et al. 2003, Reuss 1991, Sinclair and Brown 1970). However, the two-region model was just simplified without hydrodynamic considerations. Apparently, hydrodynamic modelling is still necessary to give insight into the intrinsic multiphase interactions in AD. Computational fluid dynamics (CFD) is a numerical approach to characterise fluids and flows by means of solving relevant governing equations. Compared to the experimental approaches, CFD modelling is more economical, effective, and applicable to implement for optimisation of operation and design in practice.

In a CFD model based on an isothermal assumption (no heat transfer involved), the governing equations (in a Cartesian coordinate system) for time-dependent single-phase incompressible Newtonian flows include the mass conservation equation (no mass source considered)

$$\frac{\partial v_i}{\partial x_i} = 0 \tag{1-8}$$

and the momentum conservation (or Navier-Stokes) equation

$$\frac{\partial v_i}{\partial t} + v_j \frac{\partial v_i}{\partial x_j} = -\frac{1}{\rho}\frac{\partial p}{\partial x_i} + \frac{\mu}{\rho}\frac{\partial^2 v_i}{\partial {x_j}^2} + \frac{F_i}{\rho} \tag{1-9}$$

where ρ denotes the fluid density, v the fluid velocity, t the time, x the spatial coordinate, p the pressure, μ the dynamic viscosity, and F the external body force. The subscripts i and j refer to the dimensional index. In a 3D scenario, i and j can be 1, 2 and 3. So Equation 1-9 consists of 3 sub-equations; in each sub-equation, i is fixed and j varies from 1 to 3.

When flows are in a turbulence regime, strong nonlinearity leads to challenges in solving the momentum conservation equation. Generally, turbulence modelling is necessary to accomplish closure of the momentum conservation equation, which is widely implemented by Reynolds-averaged Navier–Stokes (RANS) models. The RANS models are based on the ensemble averaging assumption and the Reynolds decomposition concept, and thus, the turbulence-induced unsteady velocity is decomposed into an averaged part ($\overline{v_i}$) and a fluctuating part (v_i')

$$v_i = \overline{v_i} + v_i' \tag{1-10}$$

So the momentum conservation equation is expressed as

$$\frac{\partial \overline{v_i}}{\partial t} + \overline{v_j}\frac{\partial \overline{v_i}}{\partial x_j} = -\frac{1}{\rho}\frac{\partial p}{\partial x_i} + \frac{\mu}{\rho}\frac{\partial^2 \overline{v_i}}{\partial {x_j}^2} - \frac{\partial}{\partial x_j}\left(\overline{v_i' v_j'}\right) + \frac{1}{\rho}F_i \tag{1-11}$$

Generally, the term $\overline{v_i' v_j'}$ accounting for the fluctuating velocity part is defined as the Reynolds stress, and solved by specific models, including k-ε, k-ω, Reynolds stress modelling, etc.

Multiphase flow modelling should be involved to simulate the biogas-sludge flows in AD, in which the sludge is defined as the primary phase and the biogas is the second phase. A two-phase model is generally developed based on an Eulerian-Eulerian method, or an Euler-Lagrange method.

The biogas-sludge flows were mainly simulated using the Eulerian-Eulerian method, in which the second phase is assumed as a continuum, similar to the primary phase. So a volume fraction equation is involved to determine phase fraction in each control cell

$$\begin{cases} V_i = \int_V \alpha_i \, dV \\ \sum_{i=1}^{N} \alpha_i = 1 \end{cases} \tag{1-12}$$

where V denotes the volume, α the volume fraction, N the total number of phases, and the subscript i refers to the phase (primary or second).

The tracer particle motion in the sludge was simulated using the Euler-Lagrange method, in which the second phase is typically assumed as a number of spherical particles. So the second

phase motion is determined by the particle's force balance equation

$$\begin{cases} m_{pt}\frac{\partial \overrightarrow{v_{pt}}}{\partial t} = m_{pt}\frac{\overrightarrow{v_l}-\overrightarrow{v_{pt}}}{\tau_{pt}} + m_{pt}\frac{\vec{g}(\rho_{pt}-\rho_l)}{\rho_{pt}} + \vec{F} \\ \tau_{pt} = \frac{\rho_{pt}d_{pt}^2}{18\mu_l}\frac{24}{C_D Re_{pt}} \\ Re_{pt} = \frac{\rho_l d_{pt}|\overrightarrow{v_{pt}}-\overrightarrow{v_l}|}{\mu_l} \end{cases} \quad (1\text{-}13)$$

where m_{pt} denotes the particle mass, $\bar{F}$ the additional force on the particle, τ_{pt} the particle relaxation time (Gosman and loannides 1983), d_{pt} the particle diameter, C_D the drag coefficient, Re_{pt} the relative Reynolds number (Re), and the subscript *l* and *pt* refer to the primary phase and the particle, respectively.

1.4.3 Numerical characterisation using CFD

In the last few decades, CFD has been reported as a promising tool, applied to various biological processes, including anaerobic water/sludge treatment systems (Wicklein et al. 2016, Wu 2013). Regarding AD systems, many CFD studies have focused on the mechanical stirring mode. The first CFD modelling was incorporated with the CARPT measurements to visualise and quantify the velocity and shear stress in the lab-scale digesters with different stirring speeds (Hoffmann et al. 2008). Results of the followed-up study revealed good model validation and more flow characteristics (Yu et al. 2011). Besides, effects of the impeller design on flow and mixing have been widely investigated (Shen et al. 2013, Wu 2009, 2010a, Wu 2011, 2012a, Yu et al. 2011). Application of a specific impeller type is found to affect axial/radial flow patterns, agitating performance and energy input in the lab-scale digesters (Wu 2012a). Different mechanical stirring design, including impeller location (top-entry or side-entry) and number (single or multiple), was evaluated in a full-scale digester as well, and the optimal mixing design was proposed (Wu 2009, 2010a, Wu 2011). Mixing has been further assessed based on predictions of the velocity gradients induced by the stirring operation, and a correlation to the biogas production performance (Bridgeman 2012, Sindall et al. 2013). However, delicate flow and mixing predictions in the lab-scale models have been found to be limited when involving sludge rheology, and rely on the methods for simulating the rotational motion (Bridgeman 2012, Wu 2012c), and for turbulence modelling (Bridgeman 2012, Wu 2011, 2012c).

Regarding the pump recirculation mode, different sludge recirculation patterns have been characterised using CFD studies. Wu and Chen (2008) developed 3D models for both lab-scale and pilot-scale digesters with a relatively simple pumping set-up from bottom to top.

Authors determined the optimal power input and found that the validated flow field was sensitive to the inlet pipe diameter and the power input. Generally, an additional draft tube system is applied to achieve effective recirculation performance. Different designs of draft tube configurations have been simulated, including draft tube location (externally or internally), and the number of draft tubes constructed (single or multiple). These differences in design have resulted in considerable differences in flow and mixing characteristics in full-scale digesters (Mendoza et al. 2011, Meroney and Colorado 2009, Wu 2009, Wu 2010d). Similar to the mechanical stirring mode, turbulence modelling applying the pump recirculation mode was also evaluated by employing different RANS models (Wu 2010d). Design of the internally located draft tube(s) usually contains an impeller system to enhance flow and mixing. This impeller(s) addition also has been evaluated using numerical models, generally predicting a good mixing performance, e.g. (Meroney and Colorado 2009). Other authors proposed specific impeller characteristics, such as rotational speed and blade tilt angle, for enhancing the flow performance (Manea and Robescu 2012). In addition, various changes in the conventional cylindrical structure of digesters have been considered, including a conical bottom (Wu 2010d, 2012b), and a different egg-shaped structure (Terashima et al. 2009, Wong 2005, Wu 2010c, 2012b). In the egg-shaped CFD models, important influences on flow and mixing were found, resulting from changes in the design of the draft tube mixer and nozzles, specific operational parameters, and sludge rheology (Terashima et al. 2009, Wong 2005, Wu 2010c, 2012b). In addition, the egg-shaped structure is found to achieve more efficient mixing performance than the cylindrical structure (Wu 2010c).

Vesvikar and Al-Dahhan (2005) reported the first CFD model for gas-mixing digesters based on the aforementioned lab-scale setup for the CARPT and CT experiments of Karim et al. (2004). Model validation to the experimental data was done first, and effects of configuration changes on flow and mixing were investigated afterwards (Karim et al. 2007, Vesvikar and Al-Dahhan 2005). Although reported as the earliest CFD modelling work in AD, the gas-mixing mode only has been limitedly addressed, compared to the mechanical stirring and pump recirculation modes. Major constraint is the increased model complexity due to the gas phase consideration. As a result, the simplification of the biogas-sludge flow to a single-phase flow is still applied in several studies (Coughtrie et al. 2013, Karim et al. 2007). Besides, generally, sludge rheology is not properly considered, since it is not part of the different models (Coughtrie et al. 2013, Vesvikar and Al-Dahhan 2005). Moreover, inconsistent rheological impacts on mixing are found, including both negligible (Karim et al. 2007) and considerable (Wu 2010b). In addition, different RANS models also have been applied in turbulence modelling (Coughtrie et al. 2013, Wu 2010b). Moreover, the aforementioned

models are based on lab-scale digesters with confined gas-mixing, which has a considerable discrepancy to unconfined gas-mixing that is commonly applied in full-scale digesters (Wu 2010b). The unconfined gas-mixing has been investigated more recently, but the applied gas-mixing resembles a bubble-column pattern (Dapelo et al. 2015, Dapelo and Bridgeman 2018a, b), and is different to the (semi)gas-lift pattern that is widely pursued in practice. Hence, limited knowledge is available on gas-mixing digesters; the prevailing multiphase flow and resulting mixing performance are still unclear and require further characterisation.

1.5 Research setup and thesis outline

1.5.1 Research objectives and questions

The scope of this thesis is in line with the objectives of the Dutch STOWA project "Community of Practice - Menging slibgisting", that studied the influences of retrofitting sludge digesters on mixing performance and biogas production (STOWA 2021). For the current research, a full-scale anaerobic digester, applying the gas-mixing mode, was selected for detailed investigations. The anaerobic digester is located at WWTP de Groote Lucht (Hoogheemraadschap van Delfland, Vlaardingen, The Netherlands). At the start of the research, the following 5 research objectives were identified:

(1) Characterisation of the complex rheological properties of concentrated sewage sludge, particularly at low shear rates, which correlate to the poor flow or mixing regimes in practice. In-depth attention was paid to the potential rheological instability related to thixotropy;

(2) Characterisation of the flow behaviour related to the complex rheological properties in the (raw) sludge pumping process;

(3) To unveil the phase interactions between injected-biogas and sludge, and to investigate the impacts of sludge rheology and other influencing factors on induced flow and mixing;

(4) Characterisation and assessment of flow and mixing performance by the applied gas-mixing operation in the studied full-scale digester.

(5) To propose recommendations or guidelines for the optimisation of operation and design of anaerobic digesters in practice.

In agreement with the above research objectives, the following 5 research questions were formulated:

(1) How the complex rheological properties of sewage sludge can be better characterised,

and how can these be correlated with the poor flow or mixing performance in practice?

(2) How the determined rheological complexity and instability can be translated to the sludge pipe flow behaviour?

(3) What are the key factors that affect the phase interactions between biogas and sludge, and thus also affect the resulting flow and mixing performance in the studied digesters?

(4) What flow and mixing performance can be predicted, and is it possible to determine whether the applied gas-mixing operation is sufficient to achieve the expected CSTR flow and mixing performance in the full-scale digester?

(5) What recommendations or guidelines can be proposed for the optimisation of operation and design of anaerobic digesters in practice?

1.5.2 Thesis outline

To investigate the aforementioned 5 research objectives and questions, a comprehensive study, including both experimental and numerical work, was implemented and described in the following four chapters (2 to 5). The sludge rheological properties were studied prior to the flow and mixing characterisation. In **Chapter 2**, the potential rheological instability of WAS from the selected WWTP with different TS concentrations is determined. Regarding the complex rheological behaviour, the most suitable characterisation methodology was evaluated, including rheological measurements and rheological model fitting. The prevailing low-shear regime, which correlates to the poor flow/mixing of WAS in anaerobic digesters, was also discussed (for research objective/question 1). The observed thixotropic behaviour, which was considered an important characteristic of the rheological instability and complexity, is further explored in **Chapter 3.** The rheological impacts of shearing duration and temperature were investigated, and the rheological differences between WAS and DGT from the same WWTP were discussed (for research objective/question 1). Thixotropy is of considerable importance for the practical sludge pumping process, which was assessed by integrating the measured rheological data in the CFD model. Particular attention was paid to the potential changes in the pipe flow pattern and pressure drop due to the rheological changes from thixotropy (for research objective/question 2). Multiphase flow and mixing in gas-mixed digesters were characterised in detail and results are presented in **Chapter 4** and **5**. In **Chapter 4**, the biogas-sludge interactions, as the major force that drives sludge motion, are elaborated using a lab-scale CFD model. The model was validated based on referred experimental data, and key influencing factors to determine flow and mixing were evaluated

(for research objective/question 3). The developed model setup was further applied to the full-scale model, and various theoretical mixing models were employed to assess the mixing performance (for research objective/question 3 and 4), which is presented in **Chapter 5**. In the latter chapter, various influencing factors of practical importance were assessed, and recommendations and guidelines on practical operation and design were proposed (for research objective/question 1 and 5). Final conclusions and future perspectives are addressed in **Chapter 6**.

Fig. 1-3 summarizes the framework of all key topics which are discussed in this thesis. The topics are divided into three categories by colour: sludge rheology topics are indicated in red; flow and mixing topics are presented in blue; the topics related to reactor and/or process optimisation are indicated in green. Two types of arrows indicate the perceived relations, connecting the different topics within the same chapter, or between different chapters. A dotted arrow represents an extension or further development in research; a solid arrow represents an impact correlation between the connected topics. More details of these relations are discussed and interpreted in the following chapters.

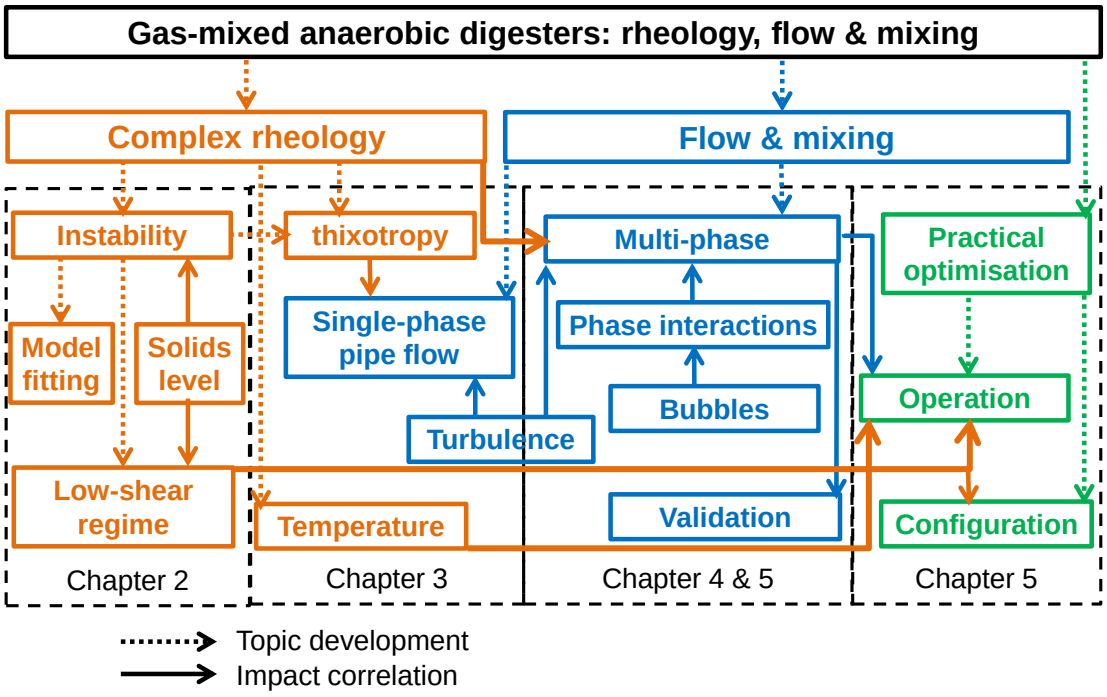

Fig. 1-3 Framework of the thesis. Topics on: sludge rheology are in brown; flow and mixing are in blue; and optimisation are in green.

1.6 References

Anderson, G.K., Campos, C.M.M., Chernicharo, C.A.L. and Smith, L.C. (1991) Evaluation of the inhibitory effects of lithium when used as a tracer for anaerobic digesters. Water Research 25(7), 755-760.

Appels, L., Baeyens, J., Degrève, J. and Dewil, R. (2008) Principles and potential of the anaerobic digestion of waste-activated sludge. Progress in Energy and Combustion Science 34(6), 755-781.

Baeyens, J., Hosten, L. and van Vaerenbergh, E. (1997) Afvalwaterzuivering (Wastewater treatment), Kluwer Academic Publishers, The Netherlands.

Battistoni, P. (1997) Pre-treatment, measurement execution procedure and waste characteristics in the rheology of sewage sludges and the digested organic fraction of municipal solid wastes. Water Science and Technology 36(11), 33-41.

Bello-Mendoza, R. and Sharratt, P.N. (1998) Modelling the effects of imperfect mixing on the performance of anaerobic reactors for sewage sludge treatment. Journal of Chemical Technology and Biotechnology 71(2), 121-130.

Bello-Mendoza, R. and Sharratt, P.N. (1999) Analysis of retention time distribution (RTD) curves in an anaerobic digester with confined-gas mixing using a compartment model. Water Science and Technology 40(8), 49-56.

Bhattacharya, S.N. (1981) Flow characteristics of primary and digested sewage sludge. Rheologica Acta 20(3), 288-298.

Bridgeman, J. (2012) Computational fluid dynamics modelling of sewage sludge mixing in an anaerobic digester. Advances in Engineering Software 44(1), 54-62.

Capela, I., Bilé, M.J., Silva, F., Nadais, H., Prates, A. and Arroja, L. (2009) Hydrodynamic behaviour of a full-scale anaerobic contact reactor using residence time distribution technique. Journal of Chemical Technology & Biotechnology 84(5), 716-724.

Chen, J., Rados, N., Al-Dahhan, M.H., Duduković, M.P., Nguyen, D. and Parimi, K. (2001) Particle motion in packed/ebullated beds by CT and CARPT. Aiche Journal 47(5), 994-1004.

Coughtrie, A.R., Borman, D.J. and Sleigh, P.A. (2013) Effects of turbulence modelling on prediction of flow characteristics in a bench-scale anaerobic gas-lift digester. Bioresource Technology 138, 297-306.

Dapelo, D., Alberini, F. and Bridgeman, J. (2015) Euler-Lagrange CFD modelling of unconfined gas mixing in anaerobic digestion. Water Research 85, 497-511.

Dapelo, D. and Bridgeman, J. (2018a) Assessment of mixing quality in full-scale, biogas-mixed anaerobic digestion using CFD. Bioresource Technology 265, 480-489.

Dapelo, D. and Bridgeman, J. (2018b) Euler-Lagrange Computational Fluid Dynamics simulation of

a full-scale unconfined anaerobic digester for wastewater sludge treatment. Advances in Engineering Software 117, 153-169.

Eshtiaghi, N., Markis, F., Yap, S.D., Baudez, J.-C. and Slatter, P. (2013) Rheological characterisation of municipal sludge: A review. Water Research 47(15), 5493-5510.

Eshtiaghi, N., Yap, S.D., Markis, F., Baudez, J.-C. and Slatter, P. (2012) Clear model fluids to emulate the rheological properties of thickened digested sludge. Water Research 46(9), 3014-3022.

Gosman, A.D. and loannides, E. (1983) Aspects of Computer Simulation of Liquid-Fueled Combustors. Journal of Energy 7(6), 482-490.

Hamdi, M. (1991) Effects of agitation and pretreatment on the batch anaerobic digestion of olive mil. Bioresource Technology 36(2), 173-178.

Hoffmann, R.A., Garcia, M.L., Veskivar, M., Karim, K., Al-Dahhan, M.H. and Angenent, L.T. (2008) Effect of shear on performance and microbial ecology of continuously stirred anaerobic digesters treating animal manure. Biotechnology and Bioengineering 100(1), 38-48.

Karim, K., Hoffmann, R., Klasson, T. and Al-Dahhan, M.H. (2005a) Anaerobic digestion of animal waste: Waste strength versus impact of mixing. Bioresource Technology 96(16), 1771-1781.

Karim, K., Hoffmann, R., Thomas Klasson, K. and Al-Dahhan, M.H. (2005b) Anaerobic digestion of animal waste: Effect of mode of mixing. Water Research 39(15), 3597-3606.

Karim, K., Thoma, G.J. and Al-Dahhan, M.H. (2007) Gas-lift digester configuration effects on mixing effectiveness. Water Research 41(14), 3051-3060.

Karim, K., Thomas Klasson, K., Hoffmann, R., Drescher, S.R., DePaoli, D.W. and Al-Dahhan, M.H. (2005c) Anaerobic digestion of animal waste: Effect of mixing. Bioresource Technology 96(14), 1607-1612.

Karim, K., Varma, R., Vesvikar, M. and Al-Dahhan, M.H. (2004) Flow pattern visualization of a simulated digester. Water Research 38(17), 3659-3670.

Kariyama, I.D., Zhai, X. and Wu, B. (2018) Influence of mixing on anaerobic digestion efficiency in stirred tank digesters: A review. Water Research 143, 503-517.

Kemoun, A., Cheng Ong, B., Gupta, P., Al-Dahhan, M.H. and Dudukovic, M.P. (2001) Gas holdup in bubble columns at elevated pressure via computed tomography. International Journal of Multiphase Flow 27(5), 929-946.

Keshtkar, A., Meyssami, B., Abolhamd, G., Ghaforian, H. and Khalagi Asadi, M. (2003) Mathematical modeling of non-ideal mixing continuous flow reactors for anaerobic digestion of cattle manure. Bioresource Technology 87(1), 113-124.

Khalili Garakani, A.H., Mostoufi, N., Sadeghi, F., Hosseinzadeh, M., Fatourechi, H., Sarrafzadeh, M.H. and Mehrnia, M.R. (2011) Comparison between different models for rheological

characterization of activated sludge. Iranian Journal of Environmental Health Science and Engineering 8(3), 255-264.

Kim, M., Ahn, Y.-H. and Speece, R.E. (2002) Comparative process stability and efficiency of anaerobic digestion; mesophilic vs. thermophilic. Water Research 36(17), 4369-4385.

Kowalczyk, A., Harnisch, E., Schwede, S., Gerber, M. and Span, R. (2013) Different mixing modes for biogas plants using energy crops. Applied Energy 112, 465-472.

Lapp, H., Schulte, D., Sparling, A. and Buchanan, L. (1975) Methane production from animal wastes. 1. Fundamental considerations. Canadian Agricultural Engineering 17(2), 97-102.

Levenspiel, O. (1999) Chemical reaction engineering, 3rd Edition, John Wiley and Sons Inc, New York.

Lindmark, J., Thorin, E., Bel Fdhila, R. and Dahlquist, E. (2014) Effects of mixing on the result of anaerobic digestion: Review. Renewable and Sustainable Energy Reviews 40(0), 1030-1047.

Manea, E. and Robescu, D. (2012) Simulation of mechanical mixing in anaerobic digesters. UPB Scientific Bulletin, Series D: Mechanical Engineering 74(2), 235-242.

Manoliadis, O. and Bishop, P.L. (1984) Temperature effect on rheology of sludges. Journal of Environmental Engineering-Asce 110(1), 286-290.

McMahon, K.D., Stroot, P.G., Mackie, R.I. and Raskin, L. (2001) Anaerobic codigestion of municipal solid waste and biosolids under various mixing conditions—II: microbial population dynamics. Water Research 35(7), 1817-1827.

Mendoza, A.M., Martínez, T.M. and Fajardo, V. (2011) Modeling flow inside an anaerobic digester by CFD techniques. International Journal of Energy and Environment 2(6), 963-974.

Meroney, R.N. and Colorado, P.E. (2009) CFD simulation of mechanical draft tube mixing in anaerobic digester tanks. Water Research 43(4), 1040-1050.

Mills, P.J. (1979) Minimisation of energy input requirements of an anaerobic digester. Agricultural Wastes 1(1), 57-66.

Monteith, H.D. and Stephenson, J.P. (1981) Mixing efficiencies in full-scale anaerobic digesters by tracer methods. Journal Water Pollution Control Federation 53(1), 78-84.

Mori, M., Seyssiecq, I. and Roche, N. (2006) Rheological measurements of sewage sludge for various solids concentrations and geometry. Process Biochemistry 41(7), 1656-1662.

Olivet, D., Valls, J., Gordillo, M.A., Freixo, A. and Sanchez, A. (2005) Application of residence time distribution technique to the study of the hydrodynamic behaviour of a full-scale wastewater treatment plant plug-flow bioreactor. Journal of Chemical Technology and Biotechnology 80(4), 425-432.

Ong, H.K., Greenfield, P.F. and Pullammanappallil, P.C. (2002) Effect of Mixing on Biomethanation

of Cattle-Manure Slurry. Environmental Technology 23(10), 1081-1090.

Parkin, G. and Owen, W. (1986) Fundamentals of anaerobic digestion of wastewater sludges. Journal of Environmental Engineering 112(5), 867-920.

Pevere, A., Guibaud, G., van Hullebusch, E. and Lens, P. (2007) Identification of rheological parameters describing the physico-chemical properties of anaerobic sulphidogenic sludge suspensions. Enzyme and Microbial Technology 40(4), 547-554.

Pollice, A., Giordano, C., Laera, G., Saturno, D. and Mininni, G. (2007) Physical characteristics of the sludge in a complete retention membrane bioreactor. Water Research 41(8), 1832-1840.

Ratkovich, N., Horn, W., Helmus, F.P., Rosenberger, S., Naessens, W., Nopens, I. and Bentzen, T.R. (2013) Activated sludge rheology: A critical review on data collection and modelling. Water Research 47(2), 463-482.

Reuss, M. (1991) Structured modeling of bioreactors. Annals of the New York Academy of Sciences 646(1), 284-299.

Rivard, C.J., Kay, B.D., Kerbaugh, D.H., Nagle, N.J. and Himmel, M.E. (1995) Horsepower requirements for high-solids anaerobic digestion. Applied Biochemistry and Biotechnology 51(1), 155.

Roy, S., Kemoun, A., Al-Dahhan, M. and Dudukovic, M.P. (2001) A method for estimating the solids circulation rate in a closed-loop circulating fluidized bed. Powder Technology 121(2), 213-222.

Sanin, F.D. (2002) Effect of solution physical chemistry on the rheological properties of activated sludge. Water Sa 28(2), 207-211.

Seyssiecq, I., Ferrasse, J.-H. and Roche, N. (2003) State-of-the-art: rheological characterisation of wastewater treatment sludge. Biochemical Engineering Journal 16(1), 41-56.

Shen, F., Tian, L.B., Yuan, H.R., Pang, Y.Z., Chen, S.L., Zou, D.X., Zhu, B.N., Liu, Y.P. and Li, X.J. (2013) Improving the mixing performances of rice straw anaerobic digestion for higher biogas production by Computational Fluid Dynamics (CFD) simulation. Applied Biochemistry and Biotechnology 171(3), 626-642.

Sinclair, C.G. and Brown, D.E. (1970) Effect of incomplete mixing on the analysis of the static behaviour of continuous cultures. Biotechnology and Bioengineering 12(6), 1001-1017.

Sindall, R., Bridgeman, J. and Carliell-Marquet, C. (2013) Velocity gradient as a tool to characterise the link between mixing and biogas production in anaerobic waste digesters. Water Science and Technology 67(12), 2800-2806.

Slatter, P.T. (1997) The rheological characterisation of sludges. Water Science and Technology 36(11), 9-18.

Smith, L.C., Elliot, D.J. and James, A. (1993) Characterisation of mixing patterns in an anaerobic

digester by means of tracer curve analysis. Ecological Modelling 69(3–4), 267-285.

Stafford, D.A. (1982) The effects of mixing and volatile fatty acid concentrations on anaerobic digester performance. Biomass 2(1), 43-55.

STOWA (2021) Optimising excess sewage sludge digestion, community of practice; personal communication.

Stroot, P.G., McMahon, K.D., Mackie, R.I. and Raskin, L. (2001) Anaerobic codigestion of municipal solid waste and biosolids under various mixing conditions—I. digester performance. Water Research 35(7), 1804-1816.

Sulaiman, A., Hassan, M.A., Shirai, Y., Abd-Aziz, S., Tabatabaei, M., Busu, Z. and Yacob, S. (2009) The effect of mixing on methane production in a semi-commercial closed digester tank treating palm oil mill effluent. Australian Journal of Basic and Applied Sciences 3(3), 1577-1583.

Tenney, M.W. and Budzin, G.J. (1972) How good is your mixing. Water & Wastes Engineering 9(5), 57-&.

Terashima, M., Goel, R., Komatsu, K., Yasui, H., Takahashi, H., Li, Y.Y. and Noike, T. (2009) CFD simulation of mixing in anaerobic digesters. Bioresource Technology 100(7), 2228-2233.

Van Hulle, S.W.H., Vesvikar, M., Poutiainen, H. and Nopens, I. (2014) Importance of scale and hydrodynamics for modeling anaerobic digester performance. Chemical Engineering Journal 255(0), 71-77.

Varma, R. and Al-Dahhan, M. (2007) Effect of sparger design on hydrodynamics of a gas recirculation anaerobic bioreactor. Biotechnology and Bioengineering 98(6), 1146-1160.

Vavilin, V.A. and Angelidaki, I. (2005) Anaerobic degradation of solid material: Importance of initiation centers for methanogenesis, mixing intensity, and 2D distributed model. Biotechnology and Bioengineering 89(1), 113-122.

Vesvikar, M.S. and Al-Dahhan, M. (2005) Flow pattern visualization in a mimic anaerobic digester using CFD. Biotechnology and Bioengineering 89(6), 719-732.

Wicklein, E., Batstone, D.J., Ducoste, J., Laurent, J., Griborio, A., Wicks, J., Saunders, S., Samstag, R., Potier, O. and Nopens, I. (2016) Good modelling practice in applying computational fluid dynamics for WWTP modelling. Water Science and Technology 73(5), 969-982.

Wong, T.I. (2005) Numerical flow simulations of an egg-shaped anaerobic sludge digester in wastewater treatment. Thesis (M.Phil.), Hong Kong University of Science and Technology.

Wu, B. (2009) CFD analysis of mechanical mixing in anaerobic digesters. Transactions of the Asabe 52(4), 1371-1382.

Wu, B. (2010a) CFD prediction of mixing time in anaerobic digesters. Transactions of the Asabe 53(2), 553-563.

Wu, B. (2013) Advances in the use of CFD to characterize, design and optimize bioenergy systems. Computers and Electronics in Agriculture 93(0), 195-208.

Wu, B.X. (2010b) CFD simulation of gas and non-Newtonian fluid two-phase flow in anaerobic digesters. Water Research 44(13), 3861-3874.

Wu, B.X. (2010c) CFD simulation of mixing in egg-shaped anaerobic digesters. Water Research 44(5), 1507-1519.

Wu, B.X. (2010d) Computational Fluid Dynamics investigation of turbulence models for non-Newtonian fluid flow in anaerobic digesters. Environmental Science & Technology 44(23), 8989-8995.

Wu, B.X. (2011) CFD investigation of turbulence models for mechanical agitation of non-Newtonian fluids in anaerobic digesters. Water Research 45(5), 2082-2094.

Wu, B.X. (2012a) CFD simulation of mixing for high-solids anaerobic digestion. Biotechnology and Bioengineering 109(8), 2116-2126.

Wu, B.X. (2012b) Integration of mixing, heat transfer, and biochemical reaction kinetics in anaerobic methane fermentation. Biotechnology and Bioengineering 109(11), 2864-2874.

Wu, B.X. (2012c) Large eddy simulation of mechanical mixing in anaerobic digesters. Biotechnology and Bioengineering 109(3), 804-812.

Wu, B.X. and Chen, S.L. (2008) CFD simulation of non-Newtonian fluid flow in anaerobic digesters. Biotechnology and Bioengineering 99(3), 700-711.

Xia, M., Wang, Z., Wu, Z., Wang, X., Zhou, Z. and Lu, J. (2009) Simulation and assessment of sludge concentration and rheology in the process of waste activated sludge treatment. Journal of Environmental Sciences 21(12), 1639-1645.

Yu, L.A., Ma, J.W. and Chen, S.L. (2011) Numerical simulation of mechanical mixing in high solid anaerobic digester. Bioresource Technology 102(2), 1012-1018.

Chapter 2. Experimental and mathematical characterisation of the concentrated waste activated sludge

This chapter is based on

Peng Wei, Qiuman Tan, Wim Uijttewaal, Jules B. van Lier and Merle de Kreuk. Experimental and mathematical characterisation of the rheological instability of concentrated waste activated sludge subject to anaerobic digestion. *Chemical Engineering Journal*. 2018 (349) 318-326. (doi.org/10.1016/j.cej.2018.04.108)

Abstract

For a proper operational performance assessment of excess sewage sludge digesters in practice, a better understanding of waste activated sludge (WAS) rheological behaviour is important, especially regarding the low-shear and poor mixing zones in anaerobic digesters. The potential rheological instability of WAS with different total solids (TS) concentrations was studied in this research. The obtained yield-pseudoplastic behaviour showed varying patterns in a wide shear rate range, of which characterisation depended on hybrid model fitting of defined shear rate segments. Although a new mathematical expression improved the fitting quality, limited applicability of the empiric models reflected the samples' transient rheological behaviour rather than intrinsic properties, challenging the included parameters definition. Characterised by the distinct flow status and transitions, the observed rheological instability gives more insight in viscoelastic and thixotropic effects on sludge flow and mixing behaviour in full-scale WAS treatment systems. Recommendations for developing a rheological measurement protocol were also formulated.

Keywords: waste activated sludge, rheological instability, model fitting, yield-pseudoplastic, thixotropy

2.1 Introduction

Waste activated sludge (WAS) is a complex matrix, diverse and sensitive to origin and condition during transportation, processing and anaerobic digestion (Ratkovich et al. 2013, Seyssiecq et al. 2003). Although crucial for energy input assessments and operational optimisation of mixing in anaerobic digesters at wastewater treatment plants (WWTP), the rheology of thickened WAS is still not fully understood.

Rheological behaviour can differ with the different existing sludge types and can be affected by various factors. Although non-Newtonian behaviour (shear-thinning) was found for activated sludge (AS) in several studies (Lotito et al. 1997, Mori et al. 2006, Seyssiecq et al. 2008), it has also been reported that AS with low total solids (TS) concentrations (<1%) has a relatively constant apparent viscosity with yield stress (Guibaud et al. 2004, Lotito et al. 1997). Sludge with higher TS has generally been found as yield-pseudoplastic (or viscoplastic) (Eshtiaghi et al. 2013); whereas the specific behaviour can be quite different in sludge types (Baroutian et al. 2013, Baudez et al. 2013a, Markis et al. 2014, 2016, Moeller and Torres 1997). So solids content has been found to strongly affect the sludge rheology, including AS (Guibaud et al. 2004, Jin et al. 2003, Lotito et al. 1997, Mikkelsen 2001, Mori et al. 2006, Sanin 2002, Seyssiecq et al. 2008), primary and secondary sludge (Bhattacharya 1981, Lotito et al. 1997, Markis et al. 2014), and the mixture of those two (Baroutian et al. 2013, Bhattacharya 1981, Lotito et al. 1997, Markis et al. 2014, 2016). The interactions of solid particles and the ambient fluid, including hydrodynamic and non-hydrodynamic parameters, were reported to play a major role in the rheological behaviour (Baudez 2008, Baudez and Coussot 2001, Jin et al. 2003). Moreover, the sludge rheology has been found to vary with operational conditions at the WWTP, such as sludge age and/or loading rate (Tixier et al. 2003), flocculation (Chen et al. 2005, Sanin 2002), and aeration gas flow rate (Seyssiecq et al. 2008, Tixier et al. 2003). These operational parameters result in a diversity of sludge types with quite different physicochemical characteristics (Lotito et al. 1997, Moeller and Torres 1997). Conductivity and pH were reported to affect the rheology as well (Sanin 2002). In addition, thixotropy was investigated in some studies, whereas the observed time-dependent rheological behaviour was not further analysed (Baudez and Coussot 2001, Markis et al. 2014).

The rheology of non-Newtonian fluids is usually described by applying mathematical rheological models based on curve-fitting empirical correlation expressions (Chhabra and Richardson 2008). Typical models are shown in Table 2-1, including shear stress models and apparent viscosity models with different degrees of complexity. For sludge matrices, the Bingham model is usually found to fit the rheograms of AS well (Guibaud et al. 2004, Lotito

et al. 1997, Mikkelsen 2001), while the Ostwald (or power-law) model (Baudez et al. 2011, Lotito et al. 1997, Moeller and Torres 1997, Pollice et al. 2007, Seyssiecq et al. 2008) and the Herschel-Bulkley model (Baroutian et al. 2013, Baudez and Coussot 2001, Baudez et al. 2011, Bhattacharya 1981) are found for thickened WAS (>1%) better. There are also a few applications of other models for describing the sludge rheology, such as the Sisko model (Mori et al. 2006) and the Cross model (Eshtiaghi et al. 2012b). Furthermore, mathematical expressions have been developed to further correlate some key influencing factors; exponential (Guibaud et al. 2004, Markis et al. 2014, 2016, Mori et al. 2006), power (Markis et al. 2014) and linear (Baroutian et al. 2013, Markis et al. 2014) relations have been reported to correlate the rheological properties towards the solids content.

Table 2-1 Commonly used rheological models.

Model	Expression		Description
Bingham	$\tau = \tau_0 + \mu\dot{\gamma}$	(2-1)	Constant viscosity with yield stress τ_0
Ostwald (de Waele)	$\tau = K\dot{\gamma}^n$	(2-2)	Power law
Herschel-Bulkley	$\tau = \tau_0 + K\dot{\gamma}^n$	(2-3)	Power law with τ_0
Casson	$\sqrt{\tau} = \sqrt{\tau_0} + \sqrt{\mu_\infty\dot{\gamma}}$	(2-4)	With τ_0 and limiting apparent viscosity μ_∞
Sisko	$\mu = \mu_\infty + K\dot{\gamma}^{n-1}$	(2-5)	Power law coupled with μ_∞
Cross	$\frac{\mu-\mu_\infty}{\mu_0-\mu_\infty} = \frac{1}{1+\lambda_{Cr}\dot{\gamma}^m}$	(2-6)	Four parameters including limiting apparent viscosities of μ_0 and μ_∞
Carreau	$\frac{\mu-\mu_\infty}{\mu_0-\mu_\infty} = (1 + (\lambda_{Ca}\dot{\gamma})^2)^{\frac{n-1}{2}}$	(2-7)	Four parameters including μ_0 and μ_∞
Ellis	$\mu = \frac{\mu_0}{1+(\tau/\tau_{1/2})^{\alpha-1}}$	(2-8)	Function of shear stress, with a critical shear stress $\tau_{1/2}$

In spite of the wide use, applicability of the models in Table 2-1 is specific to one sludge type or measuring condition, while usually the steady flow status at relatively high shear rates (> 10 s^{-1}) is used. The diverse and even contradictory results published, suggest that rheological characteristics of sludge might be too complicated to be described by a single rheological model containing empiric parameters. Moreover, there is a risk to apply one mathematical relation at different shear rates, since varying rheological behaviour has been reported at different shear rates (Baudez and Coussot 2001, Markis et al. 2014, Tabuteau et al. 2006). In full scale sludge treatment installations, the WAS faces changing shear rates throughout the process: from high-shear-level pumping systems to low-shear-level anaerobic digesters, especially in the poor-mixed or dead zones where shear rates can go down towards 0 s^{-1}.

Regarding considerable viscoelasticity observed in the untreated concentrated WAS (Farno et al. 2016), when the sludge with viscoelasticity and maybe thixotropy experiences medium and low shear rates, a good understanding of the potential instable and transitional rheological behaviour becomes important to assess sludge flow and mixing in full scale digesters. Nevertheless, this rheological instability has hardly been reported in literature.

In this study, the rheology of thickened WAS with different TS concentrations was measured and assessed in a wide shear rate range; particular attention was given to the low-shear regime in practice to investigate any rheological instability related to viscoelasticity and/or thixotropy.

2.2 Materials and Methods

2.2.1 Sample characterisation

Excess secondary sewage sludge, sampled after gravitational thickening before feeding into an anaerobic digester at WWTP De Groote Lucht (Vlaardingen, The Netherlands), was used for this study. Considering the solids content impact, the sampled gravitational thickened (GT) sludge (of 1-2% TS) was concentrated by vacuum filtration to different TS concentrations up to 7%. In agreement with literature, the vacuum filtration was used in order to minimise any changes in the physical sludge structure (Markis et al. 2014). All the GT and vacuum-filtration-concentrated (VFC) samples were stored at 4°C and were tested within four days. The solids content was determined by standard gravimetric analysis, TS and volatile solids (VS) analysis following the standard methods (APHA 2012).

2.2.2 Rheological measurements

The rheology was measured using an Anton Paar MCR 302 Rheometer (Anton Paar GmbH, Austria), which has two concentric cylinders (measuring bob and cup) as a rotational Couette geometry. A CC27 measuring system was applied so the radii of the measuring bob and cup are 13.332 mm and 14.466 mm, respectively.

2.2.2.1 Flow curve

The flow curve measurement started with a pre-shear step of 90 s at a constant shear rate (generally 1000 min^{-1}), to minimise concentration gradients and to reach a homogeneous sample distribution. After a pause of 60 s, a flow measurement step in ramp mode was

followed: the applied shear rate was increased from 0.01 s^{-1} to 1000 s^{-1}, with a decreasing corresponding time interval, both of which varied logarithmically.

2.2.2.2 Yield stress

Two methods were applied for yield stress measurements. In method 1, the pre-shear and subsequent steps were similar to 2.2.1. The measuring step was in a torque ramp mode, and the torque imposed on the sample increased gradually from a value below the yielding process, of which the critical moment was determined by monitoring the responsive deflection angle. The second method was in a dynamic oscillation mode by using a PP50 plate system. The sample was in oscillation with a fixed frequency of 1 Hz and varying strains from 0.01 to 200%, and storage modulus and loss modulus were measured to determine yield stress.

2.2.2.3 Creep test

In order to further investigate rheological instability and thixotropy, a creep mode measurement was performed. In each sample test, constant shear stress in series with a duration of 106 s was applied. A shear stress range was set based on relevant flow curve results. Hence, the applied stress started below the yield stress and was successively increased up to the maximum shear rate (e.g. 1000 s^{-1}).

Triplicate measurements were typically performed for each sample. A constant temperature at 20°C was controlled for all experiments, with a tolerance of ± 0.05°C. No apparent stratification was observed when samples were kept static in containers for at least 3 h. Therefore, the influence of sludge settling during the duration of the experiments (maximum 20 minutes) was considered negligible.

2.3 Results and Discussion

2.3.1 Varying trends in flow curves

Rheograms of the GT and the VFC sludge with TS concentrations of 1.2%, 3.6% and 6.0%, are shown in Fig. 2-1. All samples were found to show yielding and shear-thinning (or yield-pseudoplastic) behaviour, and returned flow curves with varying trends. For the GT sludge (TS 1.2%), the shear stress generally increased with the shear rate slightly at low shear rates, while had a faster increase above 12 s^{-1} (Fig. 2-1A). For the VFC sludge (Fig. 2-1B and 2-1C), the rheogram showed two different segments of increasing shear stress (shear stress 2

and shear stress 3 in the graph), with a transition when the shear rate was around 10 s^{-1}. The VFC sludge also showed a decreasing shear stress part with the increasing shear rate at very low shear rates (usually <0.3 s^{-1}), which has not been reported before for secondary sewage sludge (Baroutian et al. 2013, Markis et al. 2014, 2016, Moeller and Torres 1997).

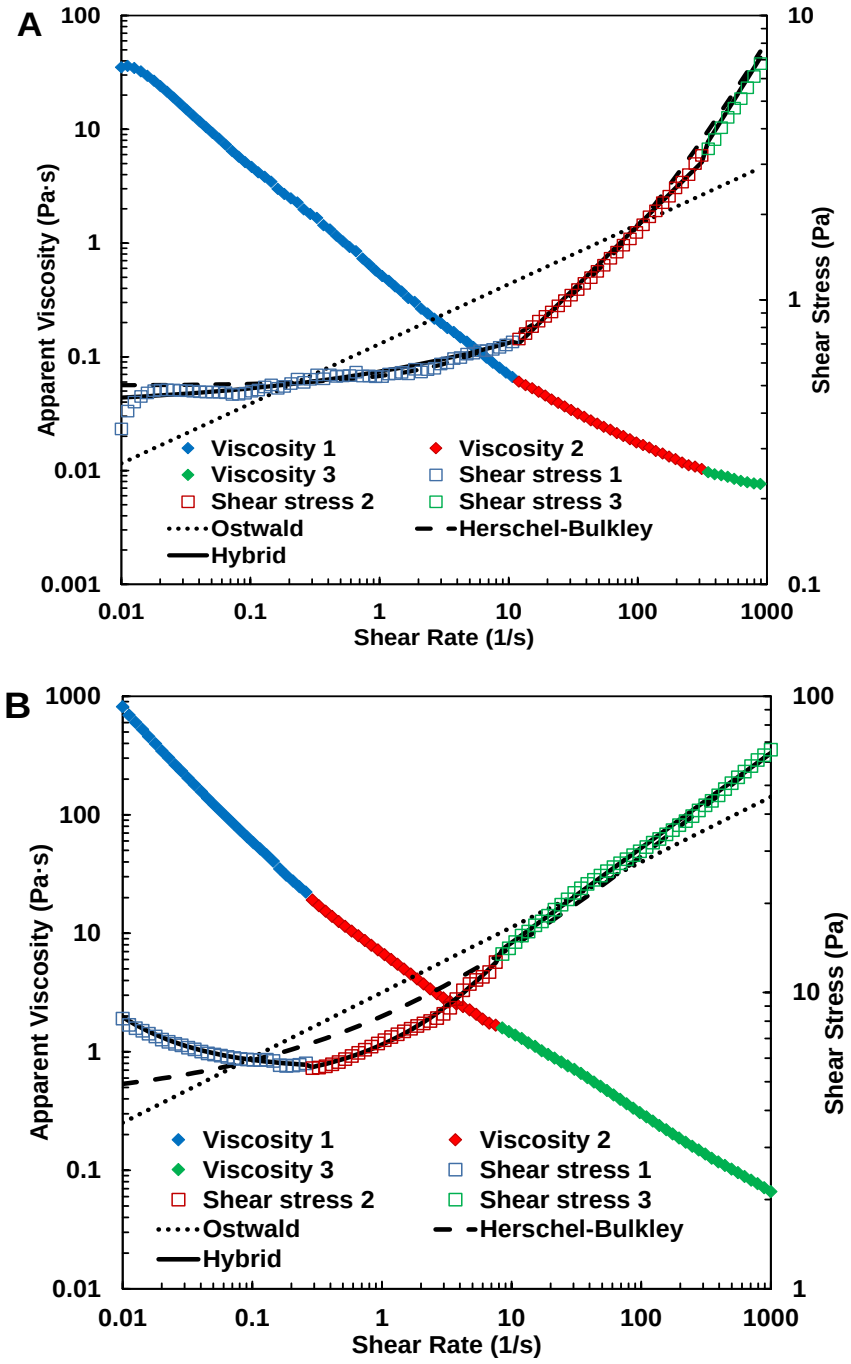

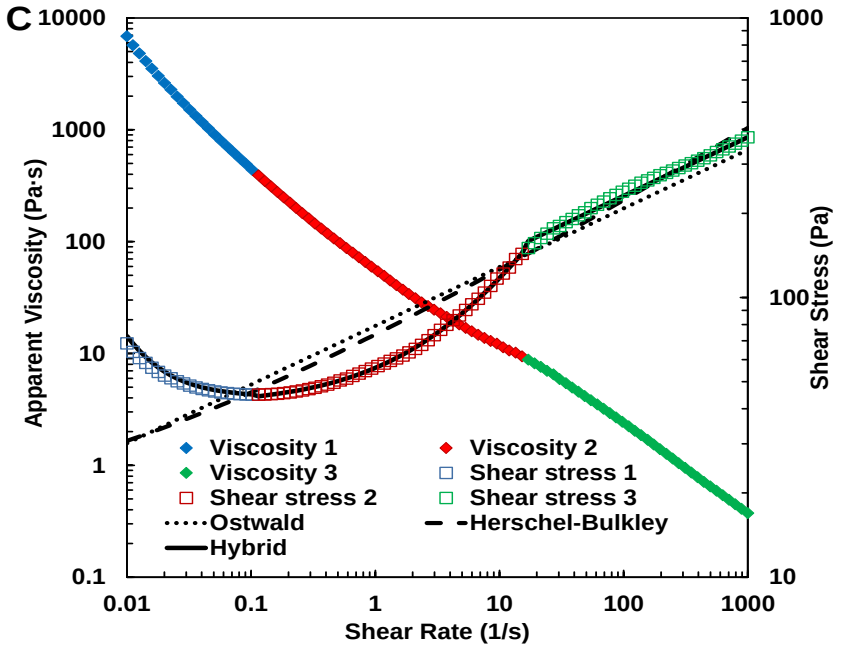

Fig. 2-1 Three distinct segments in the rheograms of A: TS 1.2%, B: TS 3.6% and C: TS 6.0%, and the fitting results of shear stress data.

All apparent viscosity and shear stress curves could be divided into three segments of similar behaviour, to better describe the varying trends in the wide shear rate range. For the GT sludge (Fig. 2-1A), the three segments were identified at shear rates 0.01-12, 12-350 and 350-1000 s^{-1}, respectively. For the VFC sludge (Fig. 2-1B and 2-1C), the first segment was the initial decreasing part of the shear stress curve, and the other two got distinct increasing trends.

2.3.2 Mathematical characterisation on the varying trends

2.3.2.1 The Ostwald model and the Herschel-Bulkley model

Mathematical characterisation on applicability of the segmentation for the varying trends in the rheograms was carried out using various rheological models. The most widely used models, the Ostwald model (Equation 2-2) and the Herschel-Bulkley model (Equation 2-3) were considered for both the whole curve and the defined segments, while the fitting quality was assessed by the sum of squared errors (SSE) and the root mean squared error (RMSE).

Results are presented in Fig. 2-1 and Table 2-2. Fitting of the full curves by both models gave unacceptable deviations (large SSE and RMSE values), but fitting each segment separately returned better results. Although similar performances of the two models were obtained in

some segments, the Herschel-Bulkley model was usually found to better describe the low shear rates (such as segment 1 of all, and segment 2 of the VFC sludge). On the other hand, the Ostwald model fit the data better at high shear rates (segment 3). The good performance of single model fitting in a specific shear rate range agreed with some previous results, but these studies also showed limitation of single model fitting, when applied in a wider shear rate range (Baudez and Coussot 2001, Baudez et al. 2011).

Table 2-2 Fitting results of the sludge with three TS concentrations, using the Ostwald model and the Herschel-Bulkley model.

TS (%)	Model		K	n	τ_0	SSE	RMSE
1.2	Ostwald	Whole	0.70	0.20		$8.8\cdot10^{2}$	$2.9\cdot10^{0}$
		Segment 1	0.57	0.06		$8.2\cdot10^{1}$	$1.2\cdot10^{0}$
		Segment 2	0.23	0.45		$2.8\cdot10^{-5}$	$9.8\cdot10^{-4}$
		Segment 3	0.05	0.73		$8.8\cdot10^{-8}$	$9.9\cdot10^{-5}$
	Herschel-Bulkley	Whole	0.04	0.74	0.49	$2.4\cdot10^{-1}$	$4.5\cdot10^{-2}$
		Segment 1	0.14	0.31	0.42	$2.4\cdot10^{-2}$	$2.0\cdot10^{-2}$
		Segment 2	0.08	0.63	0.39	$7.4\cdot10^{-3}$	$1.7\cdot10^{-2}$
		Segment 3	0.01	0.99	1.22	$1.2\cdot10^{-2}$	$4.4\cdot10^{-2}$
3.6	Ostwald	Whole	10.01	0.22		$5.9\cdot10^{5}$	$7.7\cdot10^{1}$
		Segment 1	4.73	-0.10		$5.3\cdot10^{3}$	$1.4\cdot10^{1}$
		Segment 2	6.95	0.25		$3.6\cdot10^{0}$	$3.5\cdot10^{-1}$
		Segment 3	7.10	0.32		$4.9\cdot10^{-3}$	$1.1\cdot10^{-2}$
	Herschel-Bulkley	Whole	4.08	0.39	4.24	$1.6\cdot10^{2}$	$1.3\cdot10^{0}$
		Segment 1	0.06	-0.83	5.52	$6.5\cdot10^{-2}$	$5.0\cdot10^{-2}$
		Segment 2	1.72	0.74	4.94	$8.1\cdot10^{-1}$	$1.7\cdot10^{-1}$
		Segment 3	3.91	0.39	5.83	$1.7\cdot10^{1}$	$6.6\cdot10^{-1}$
6.0	Ostwald	Whole	79.21	0.21		$3.6\cdot10^{7}$	$6.0\cdot10^{2}$
		Segment 1	28.87	-0.16		$6.9\cdot10^{5}$	$1.8\cdot10^{2}$
		Segment 2	61.86	0.23		$1.1\cdot10^{4}$	$1.6\cdot10^{1}$
		Segment 3	87.81	0.21		$6.0\cdot10^{-1}$	$1.3\cdot10^{-1}$
	Herschel-Bulkley	Whole	60.56	0.27	13.24	$2.4\cdot10^{4}$	$1.6\cdot10^{1}$
		Segment 1	0.03	-1.49	44.14	$6.7\cdot10^{-1}$	$1.9\cdot10^{-1}$
		Segment 2	14.87	0.71	41.16	$1.0\cdot10^{1}$	$5.1\cdot10^{-1}$
		Segment 3	90.80	0.21	~0	$7.9\cdot10^{2}$	$4.9\cdot10^{0}$

Hence, as shown in Fig. 2-1, to better characterise the varying rheological behaviour, hybrid model fitting was needed; the Herschel-Bulkley model at low shear rates and the Ostwald model at high shear rates were combined to describe the entire curve. It indicated that the role of yield stress reflected by the term (τ_0) in the Herschel-Bulkley model was important at low shear rates, however, became less important and even negligible once reaching a high shear rate.

Moreover, two discrepancies in the regressed parameters should be noted in Table 2-2. Firstly, when the GT sludge (TS 1.2%) was fitted by the same model (Ostwald), segment 2 and 3 gave distinct K (0.23 and 0.05) and n (0.45 and 0.73) values, which seemed to express behaviour of two different types of sludge, rather than a transition. Secondly, when the same segment was fitted with Ostwald and Herschel-Bulkley, both models achieved an acceptable regression (segment 2 and 3, TS 1.2%). However, the predicted *K* and *n* values were different, even though having the same definition. Therefore, the discrepancies may highlight the empirical nature of both models, implying a transient rheological status rather than fixed physical properties.

2.3.2.2 Models with higher complexity

In addition to the existing models, more complex models (from Equation 2-4 to 2-8) were used in order to identify if the rheological data could be more accurately predicted. The more complex models included more limiting parameters, such as zero-shear apparent viscosity (μ_0) and infinite rate apparent viscosity (μ_∞). Fitting results applying these models are shown in Fig. 2-2 and Table S-1. It was found that, even with some modifications, the increased complexity did not return satisfactory fitting quality, especially for the flow curves of the VFC sludge.

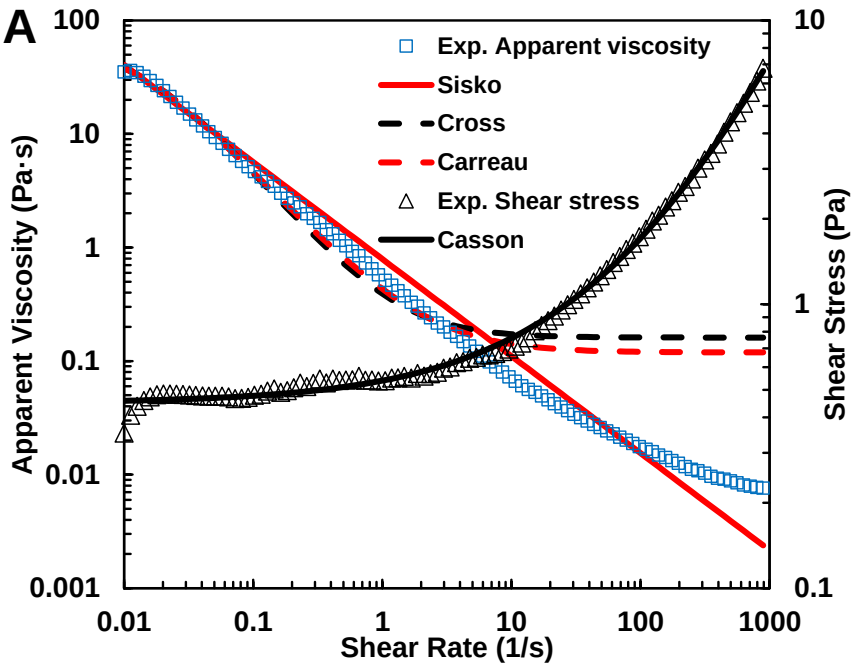

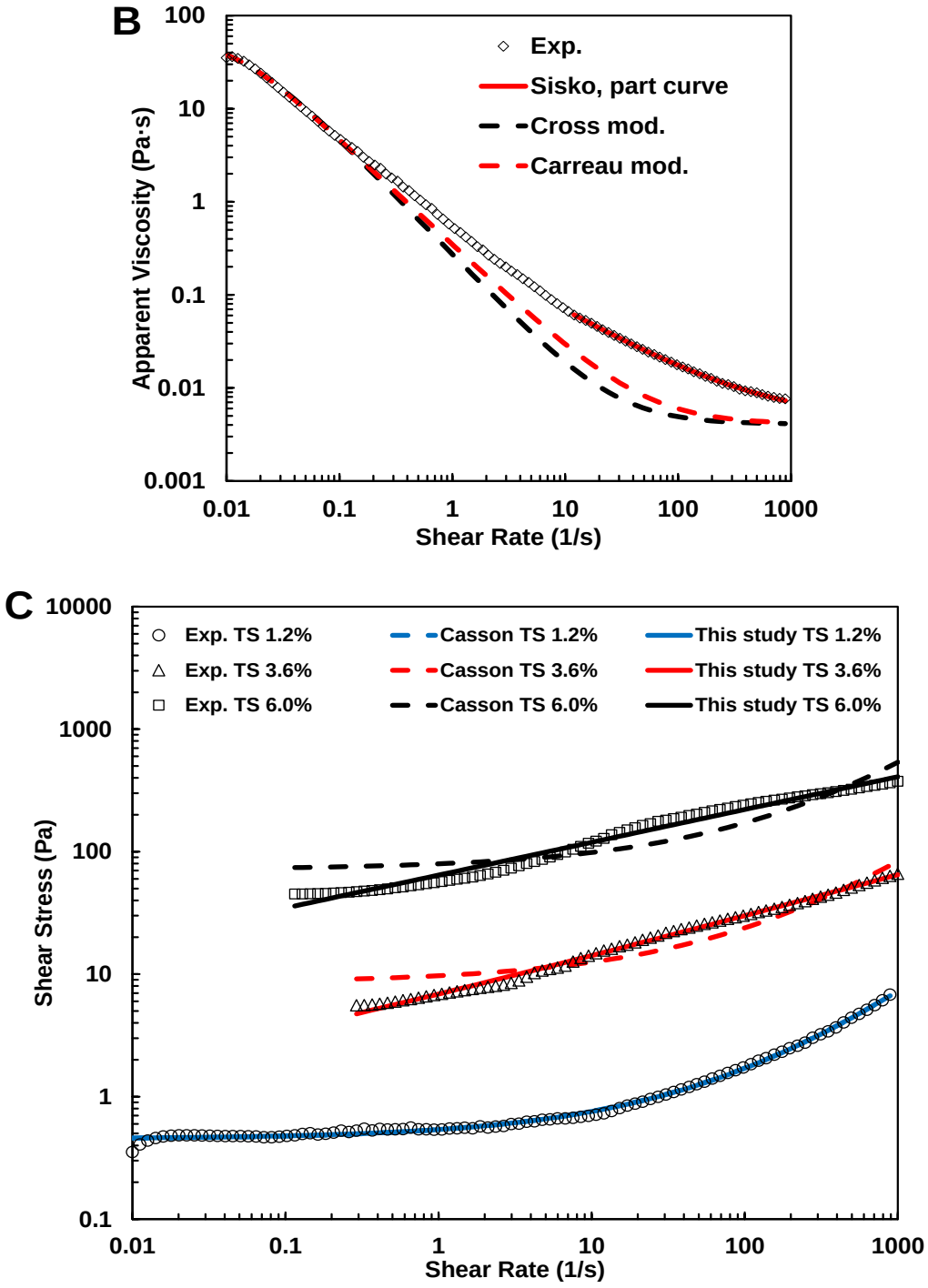

Fig. 2-2 Fitting by the models with limiting parameters, A: original and B: modified models for the GT sludge; and C: Casson and the expression in this study for the VFC sludge.

In order to improve the fitting performance, a new expression was developed that includes critical shear stress (τ_C) and the coefficients n and K_n:

$$\sqrt{\tau} = \sqrt{\tau_C} + K_n \sqrt{\dot{\gamma}}^n \tag{2-9}$$

The fitting results of this expression in Table S-1 and Fig. 2-2C demonstrate an improved fitting quality with much lower SSE and RMSE values than other models used. It seemed that the returned K_n and n were parameters similar to the K and n in Ostwald and Herschel-Bulkley, since consistent varying tendencies were obtained as TS increased. However, although close to yield stress (τ_0) for the GT sludge, the critical shear stress (τ_C) returned decreasing values at increasing TS, so this parameter seemed not only to be related to yield stress but also to TS. The proposed expression was applied to fit rheological data of other WAS, including thermophilic and mesophilic anaerobically digested sludge from WWTP Echten (The Netherlands, data not shown in this paper), showing improved fitting results as well. Therefore, considering the improvements of fitting quality, this empirically developed expression could be recommended to characterise the rheological behaviour of concentrated WAS in a wide shear rate range.

Moreover, it should be noted that verifying the theoretical μ_∞ by rheological measurements was very challenging in this study. For the GT sludge, the asymptote could not be extended further but showed an unreliable transition to shear-thickening (over 890 s^{-1}), which is further interpreted in Section 3.6. For the VFC sludge, a tendency to μ_∞ could not be found even at the upper shear stress limit of the applied rheometer (about 3800 s^{-1}). Hence, understanding the practical meaning of μ_∞ for concentrated sludge is unclear. It is also crucial for the applicability of the relevant rheological models, because an inaccurate prediction of μ_∞ could lead to assessment deviation of the minimum apparent viscosity in the strongest shear regions, e.g. when sludge is pumped or mixed in full-scale reactors.

The three TS concentrations investigated and described above were representative for all measured samples that are not shown here. Essentially, the employed segmentation was a method to improve the poor performance of characterising the total curves in a wide range of shear rates. The number of segments that needed to be applied for a decent description of the measurements was not universal and depended per sample, as can be seen from the different segments found with the GT and VFC sludge (Section 3.4). The inconsistency reflected in the model fitting indicated instable behaviour and changes of the sludge rheology at the specific applied shear rates.

2.3.3 Further characterisation of the rheological instability

In order to further confirm and characterise the instable rheological behaviour, more experimental approaches were applied for the varying trends and relevant transition parts in the flow curves, involved in both yielding and flowing status.

2.3.3.1 Yielding process

Since the strict theoretical concept of yield stress is not yet clear (Chhabra and Richardson 2008) and debate still exists on the correct methodology (Eshtiaghi et al. 2013, Hannote et al. 1991), various methods were used to determine the sludge yield stress experimentally (Baudez et al. 2013a, Mori et al. 2006, Spinosa and Lotito 2003) or by applying different models (Baudez and Coussot 2001, Guibaud et al. 2004, Moeller and Torres 1997, Slatter 1997). In this study, different methods were assessed, determining τ_0 by: (1) the initial point in a flow curve; (2) best model fitting (Herschel-Bulkley); (3) the linear range in a complex modulus curve from the dynamic oscillation measurement; and (4) the abrupt point in a deflection angle curve.

The data in Table 2-3 showed considerable discrepancies between the four methods, especially for the VFC sludge. With TS concentration over 3%, method 2 returned the lowest yield stress values, whereas method 4 showed the highest. The yield stress range determined by method 3 was close to method 1 for the VFC sludge (Table 2-3).

Table 2-3 Results of the yield stress (Pa) determined by four methods.

TS (%)	1 Initial point of flow curve	2 Model fitting (Herschel-Bulkley)	3 Dynamic oscillation measurement	4 Deflection angle measurement
1.2	0.4	0.4	-	0.4
1.5	0.5	0.6	-	0.5
1.6	0.2	-	12.0-15.6	-
2.5	3.5	4.2	-	2.9
3.6	7.8	5.5	-	8.2
4.2	17.8	10.5	-	19.7
4.5	22.6	14.4	-	24.4
4.6	41.3	-	43.0-50.1	-
6.0±0.2*	68.6	44.1	-	77.3
6.3	82.8	-	86.5-100.6	-
7.0	94.9	64.9	-	126.0

*the standard deviation of the other TS data was below 0.06%.

Method 1 could be used when the initial shear rate (0.01 s^{-1}) approximated the yielding process. However, the decreasing shear stress trend indicated the possibility of underestimating the yield stress. Similar deviation was found in method 2, although it has been widely applied in previous research (Baudez and Coussot 2001, Guibaud et al. 2004, Moeller and Torres 1997, Slatter 1997). As indirect approaches, the estimated τ_0 by methods 1 and 2 relies on the trend of the measured curve, similar to the limitation reported in literature (Hannote et al. 1991). Method 3 is a more direct approach by determining the critical shift of the sludge from "solid-like" to "liquid-like" at a certain oscillation frequency. However, as shown in Fig. 2-3A, the shift is smooth in each curve. Although not sharp enough, the

obtained stress range was acceptable for the VFC sludge, which was also similar to literature values with comparable TS concentrations (Baudez et al. 2013a, Farno et al. 2016, Mori et al. 2006). But method 3 was not suitable for the GT sludge, since an unacceptable high value was obtained. When assessing the rheological characteristics of the GT sludge, separation of flocs and supernatant was observed. Hence, instead of the original matrix, the more condensed sludge layer that was formed on the measuring plate may have accounted for the measured curve, which very likely led to a large overestimation of the yielding point.

Since the deflection angle represents the degree of sample deformation, method 4 is straightforward as well. Compared to method 3, the measured deflection angle had a precipitous increase to reflect the yielding process (Fig. 2-3B), with no risk of separation. The obtained τ_0 is as expected and in line with the other methods. Therefore, method 4 is the best recommended approach to determine the yield stress for WAS. However, the discrepancies in the different methods also implied that the yielding was not a stable process and sensitive to shearing conditions.

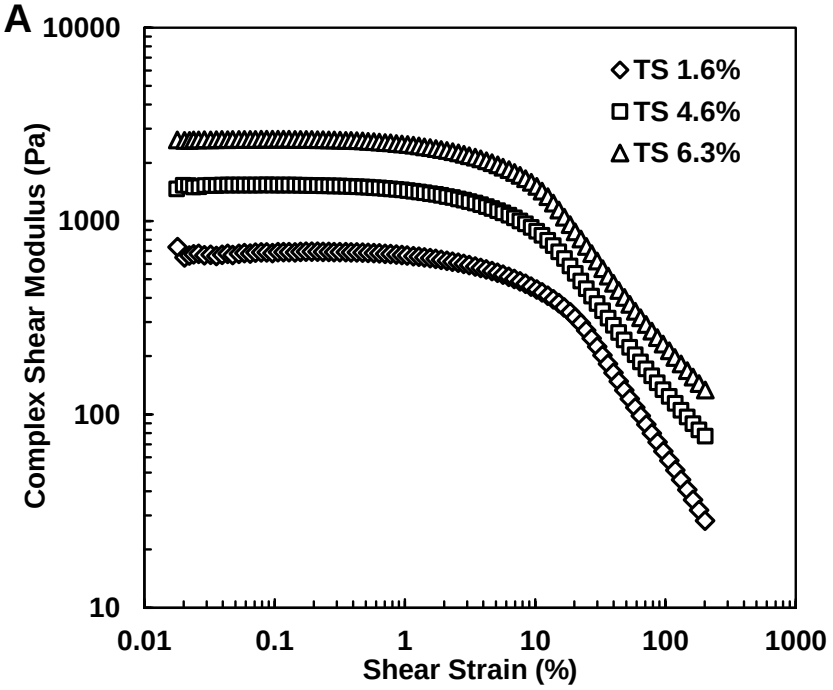

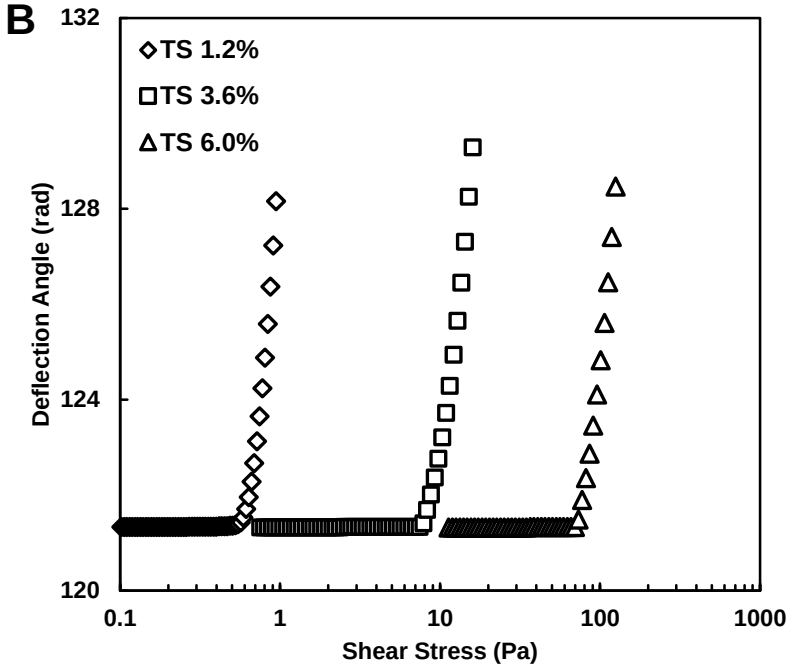

Fig. 2-3 Experimental results for determining the yield stress, A: the dynamic oscillation measurement, B: the deflection angle measurement.

2.3.3.2 Distinct flow status

More rheological instability after yielding was revealed using a creep test. As shown in Fig. 2-4A, the responsive shear rate of the medium VFC sludge (TS 3.6%) decreased in time below the yielding point (≤ 8.0 Pa). However, when the applied shear stress was over the yield stress, an instable flow status was obtained, showing fluctuations and a slightly decreasing averaged shear rate in time. A stable flow with a smooth plateau was achieved above 16 Pa, and thixotropic behaviour was found, since the shear rate kept increasing with time. Results of the corresponding shear strain shown in Fig. 2-4B were different with other studies (Baudez and Coussot 2001, Markis et al. 2014). The different critical stress found in this study could not be distinguished by the concave shape change of the curves of the sludge without thixotropy (Baudez and Coussot 2001), or the asymptotic tendency formed in the sludge with comparable TS levels but much less viscoelasticity (Markis et al. 2014). In addition, compared to the previous results (Farno et al. 2016), the larger magnitude of modulus also indicated stronger viscoelasticity in the studied WAS, resulting in more rheological transitions. The range of the critical transition to flow stability (14-16 Pa) covered the transition between segment 2 and 3 (14.1 Pa in Fig. 2-1B). The same comparison of the critical stress in different TS concentrations is shown in Table 2-4, indicating a good similarity between the results obtained from these methods. Therefore, the rheological

instability was found not occasional or random, but can be revealed by using different methods, including experiments and model fitting.

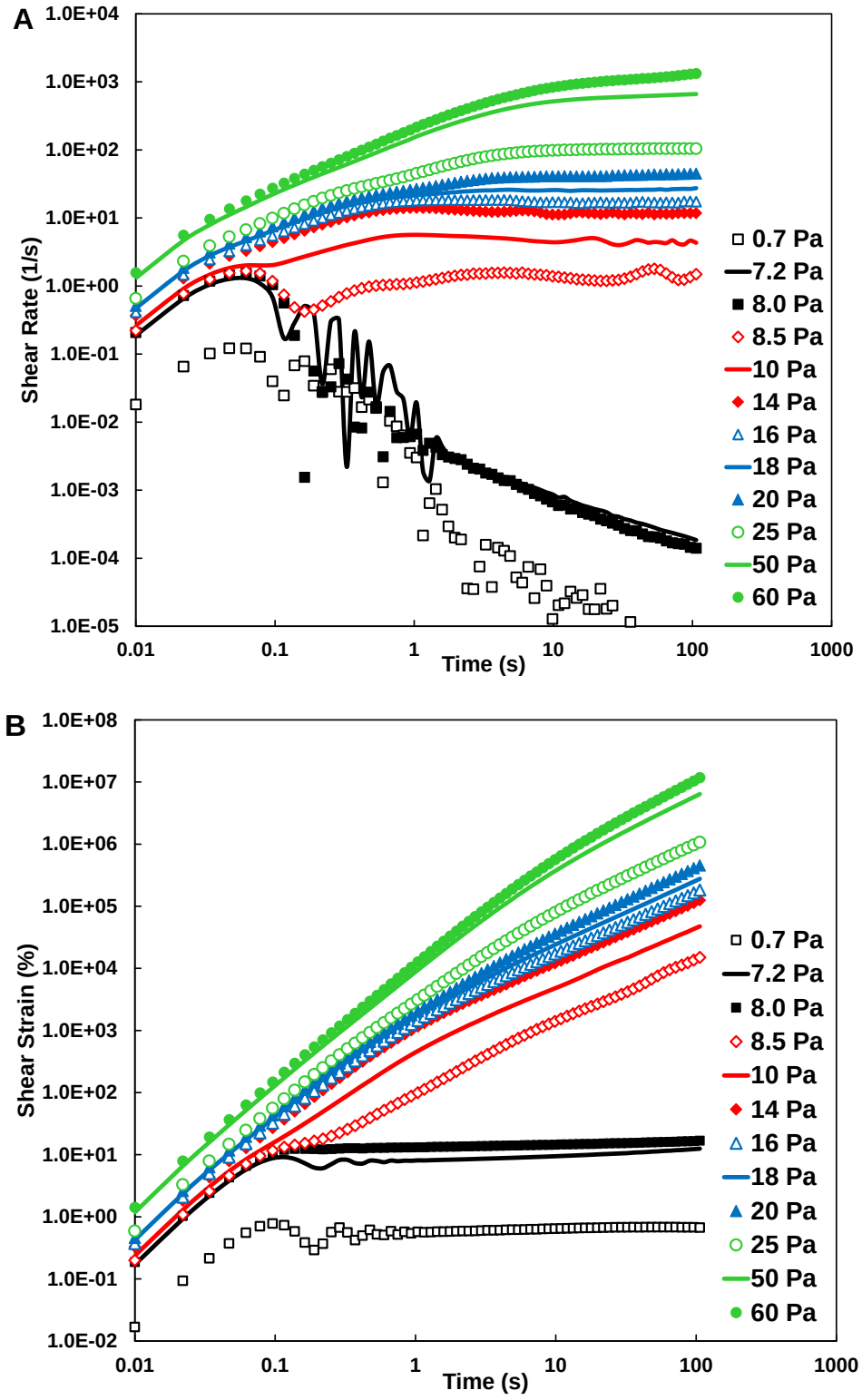

Fig. 2-4 Variation of A: responsive shear rate and B: shear strain in the creep tests (TS 3.6%).

Table 2-4 Critical points of shear stress determined by different experimental methods.

TS (%)	Yield stress (Pa)		Shear stress of transition 2 (Pa)	
	Method 4	Creep test	Flow curve	Creep test
1.2	0.22	0.20-0.25	0.51	0.5-0.6
3.6	8.2	8.0-8.5	14.1	14-16
7.0	95	92-108	286	250-270

2.3.3.3 Thixotropic behaviour

The thixotropic behaviour was further characterised by measuring in an increase-decrease shear mode (from 0 to 100 s^{-1} and back to 0 again). The results shown in Fig. 2-5A demonstrated a larger hysteresis loop at higher TS concentrations, indicating a stronger influence on the rheology by shear time or shear history. Similar results were obtained when measuring sludge rheology in a membrane bioreactor, indicating that thixotropy was more apparent as the biomass concentration increased due to growth (up to 2%) (Pollice et al. 2007). Competition between solids interactions and viscous forces was reported to be responsible for thixotropy (Baudez 2008). Moreover, flocs have been reported to have a re-flocculate ability; due to the physicochemical interactions between separated fragments, fractured flocs can reversibly form and even develop in larger sizes in stagnancy, leading to settling (Jin et al. 2003). Hence, the dynamic floc structure in WAS could lead to these differences in the hysteresis loop. In the shear-increase step, large flocs would undergo breakage and deformation, which could not totally recover in time under durable shearing. Thus in the shear-decrease step, the overall bonding effect on the internal structure of the sludge will be weakened, leading to the hysteresis shown in Fig. 2-5A. Although nearly no hysteresis formed, thixotropy was still present in the GT sludge (TS 1.5%). As shown in Fig. 2-5B, once yielding was overcome, the flow status could be maintained by a shear stress (0.4 Pa) lower than the yield stress (> 0.5 Pa initially).

Therefore, subjecting WAS with considerable rheological instability to anaerobic digestion, requires insight in the conditional changes in practice. Especially in a system with high shear-rate gradients, applying a flow or mixing beyond yielding may not be enough, since an instable flow status may still exist below a critical shear rate level.

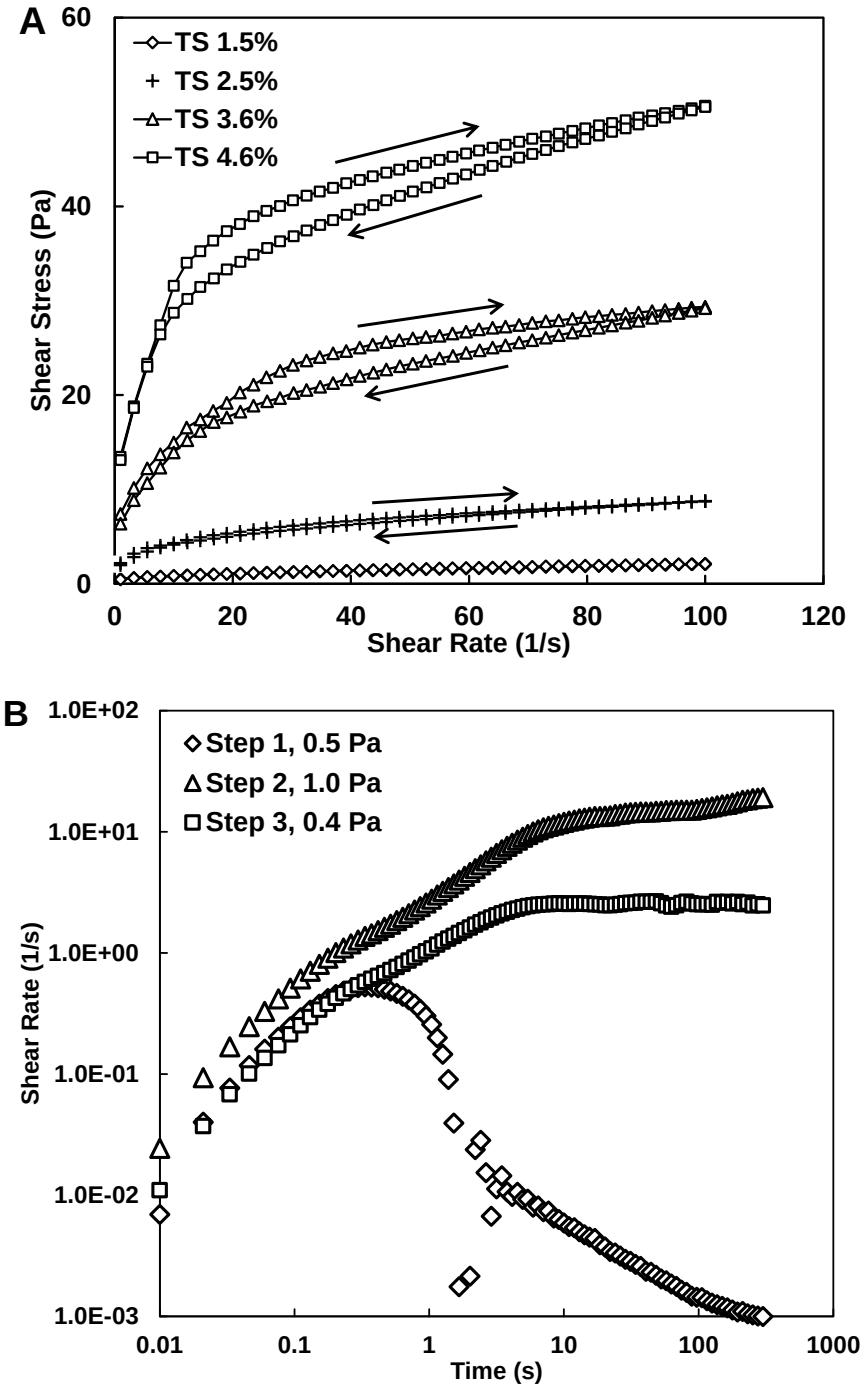

Fig. 2-5 Thixotropic behaviour of the WAS, A: hysteresis in sludge with different TS concentrations; B: time-dependent yielding of the GT sludge.

2.3.4 Total solids impact on the rheological instability

As a key influencing factor on the rheological instability, the impact of the solids content was further investigated. As shown in Fig. 2-6, the correlation between yield stress and TS is better described as exponential in a TS range of 1-5%, which agrees with the previous studies

(Guibaud et al. 2004, Markis et al. 2014, 2016, Mori et al. 2006). However, when the TS range was extended to 7%, the yield stress would be overestimated by the exponential relation at the low TS part, whereas the power law relation described better. Hence, a proper correlation relied on the specific TS range taken into consideration. In addition, the increased normal stress from the sludge on the measuring bob also indicated a stronger force perpendicular to the shear stress as TS increased. Hence, the highly nonlinear increase in stress levels over 3% TS implied that the components in the sludge seem to build a 3D steric network for cohesion that becomes more strengthened at high TS concentrations.

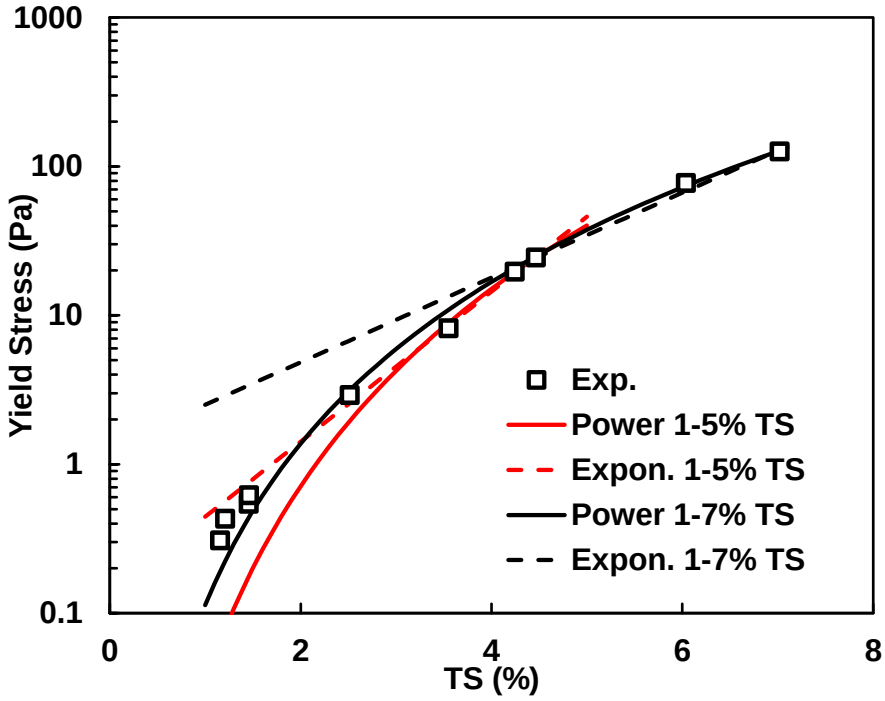

Fig. 2-6 Correlation between the measured yield stress and TS concentrations.

More parameters for the rheological instability correlated to TS are shown in Table 2-5. For the VFC sludge, the critical shear rate for a stable flow (transition 2) increased more linearly to TS (R^2 0.96); but decreased towards a constant level (0.13 s^{-1}) for an instable flow (transition 1), indicating an enlarging instable flow range as TS increased.

For the GT sludge, the thixotropy was not strong enough to clearly show transition 1. However, the increasing *n* in the different indicated segments suggested more 'Newtonian' behaviour as the shear rate increased. The increasing *K* and decreasing *n* obtained in the stable flow status (Segment B) agreed with expected behaviour: increased pseudoplastic at increased TS. However, in the instable flow status (Segment A), the *n* got an abnormal value (>1) and stayed almost constant (0.7) at TS above 3%, indicating an almost TS-independent

level of the flow behaviour index in the low shear rates. Hence, more challenge was confronted to characterise the instable rheological status by the commonly used model fitting, since inconsistent and contradictory results were obtained. The weakened impact from TS on the rheological behaviour at low shear rates, also implied its dependency on the applied shear rate. Moreover, it could be perceived that for non-Newtonian WAS in a digester, the mixing performance difference resulting from the relevant shear rate difference, might be further enlarged by the TS difference on the long term.

Table 2-5 Rheological instability of the sludge with various TS concentrations, characterised by three critical transitions and hybrid model fitting results.

TS (%)	Transition 1 (shear rate, 1/s)	Segment A (instable flow status)		Transition 2 (shear rate, 1/s)	Segment B (stable flow status)		Transition 3 (shear rate, 1/s)	Segment C (stable flow status)	
		K	***n***		***K***	***n***		***K***	***n***
1.2	-	0.13	0.31	12.0	0.23	0.45	351	0.05	0.73
2.5	0.33	0.28	1.15	5.3	2.24	0.36	-	-	-
3.6	0.29	1.72	0.74	9.6	7.10	0.32	-	-	-
4.2	0.13	4.87	0.67	13.5	18.60	0.29	-	-	-
6.0	0.12	14.87	0.71	17.1	87.81	0.21	-	-	-
7.0	0.13	25.55	0.72	19.2	159.14	0.19	-	-	-

2.3.5 Special rheological behaviour at low shear rates

The decreasing shear stress part between the yielding point and transition 1, indicated strong instability caused by viscoelasticity and thixotropy, thus brought more uncertainty to be clearly determined. As discussed in Section 3.3.3, a flow status could be maintained by smaller shear stress after yielding, so it was possible to obtain the decreasing shear stress curve. A similar phenomenon was reported in the study of Pignon et al. (1996), in which the flow pattern was visualised using a transparent colloidal suspension. Localised shear or stick slip was observed in the regime of decreasing shear stress: only part of the sample was activated as a shear layer when imposing quite low shear rates (even to 10^{-4} s^{-1}). So, the sheared layer thickness d_{eff} could be used to roughly calculate the effective shear rate using:

$$\dot{\gamma}_{eff} = \dot{\gamma} d / d_{eff} \tag{2-10}$$

where $\dot{\gamma}$ denotes the measured shear rate and d the whole gap width. Based on this equation, the effective shear rate will be larger than the measured one if d_{eff} is smaller than d. When calculating apparent viscosity,

$$\mu = \tau / \dot{\gamma} \tag{2-11}$$

this could result in an overestimation of the apparent viscosity and thus to abnormal regressed n values (in Table 2-2). So, the expected asymptote to theoretical μ_0 at the very low shear rates might also be covered. An abrupt transition from flow towards stagnation was reported when measuring pasty sludge at high TS concentrations, also indicating that the effective shear was just covering a part of the whole gap (Baudez 2008). Besides, the localised shear could be described in a non-monotonic pattern by a sandwich-like structure model, in which more specific parameters and expressions were used to determine the decreasing part (Coussot et al. 1993). Moreover, the region containing the minimum shear stress after yielding showed an increasing thickness of the sheared layer. This behaviour was proposed as another critical shear condition (transition point 1 in Table 5) (Coussot et al. 1993), below which the flow was extremely instable (Coussot et al. 2002).

Although it seemed not feasible to visualise flow regions in the samples, potential localised shear or sandwich-like structures might account for the special behaviour. Furthermore, as discussed in Section 3.3.3, different to the colloidal suspension, the floc formation in WAS may also be an influencing factor. When overcome yielding, rupture of the dynamic floc structure may further loosen the connection between particles, which reduces the resistance to flow. In addition, the decreasing shear stress part was hardly observed in the measurement of digested sludge with similar TS concentrations (data not shown in this paper) compared to the fresh WAS, indicating that the related physicochemical interactions for the reversible floc formation might become weaker during the sludge aging process.

However, describing the decreasing part is more challenging than the other parts in the rheograms. Regarding the returned abnormal results (n<0), an improved model with time-dependent functioning for thixotropy seems necessary. Moreover, due to thixotropy, the yielding underlying a simple value was dynamic and complicated in the studied WAS samples. Regarding design and operation in practice, the difficulty in estimating apparent viscosity at low shear rates, can bring more challenges for assessing and optimising the energy requirement when continuously pumping WAS, or for assessing the mixing performance in considerable low-shear regions distributed in digesters.

2.3.6 Suggestions on a proper protocol for rheological measurements

Although no standardised laboratory protocol has been established for sludge yet (Eshtiaghi et al. 2013), it is necessary to develop a proper methodology for sludge with diverse behaviour. Hence, several recommendations can be given to improve the rheological

measurements in a concentric rotational rheometer, especially for viscoplastic and thixotropic matrices.

2.3.6.1 Determining the yield stress

The yield stress measurement should be straightforward, and carefully focused on the deformation of the sample whenever thixotropic behaviour is observed. In the present research, determining the abrupt changing point in a measured deflection angle curve was recognized as an effective method.

2.3.6.2 Pre-shear step

Besides a homogeneous distribution of the sample, the rotational speed of pre-shear should not be too intense to further deform the sample structure, especially for thixotropic samples, since it could lead to an underestimation of the shear stress (Fig. 2-5). In literature, the opposite is advised as well (Baudez et al. 2013a, Baudez et al. 2011, Baudez et al. 2013b, Farno et al. 2014, 2015), to apply high pre-shear rates to erase the material memory (or shear history) of the sludge. However, if the rest time is not long enough, this could lead to disruption of the sludge flocs and would therefore give a wrong impression of behaviour of sludge during low mixing conditions, e.g. flowing out of a sludge thickener, being pumped from a sludge buffer, or mixing in large scale digesters in the more stagnant or low mixing zones.

2.3.6.3 Shear rate range in measurement

For concentric rotational rheometers, no distinct indication could be identified when the flow turns from laminar to turbulent (Seyssiecq et al. 2003). However, when flow is not laminar, secondary flows (or Taylor-Couette instability) will be generated and lead to an incorrect shear-thickening result (Ratkovich et al. 2013). In order to avoid this transition, the *Re* or the Taylor number (*Ta*) needs to be estimated for each measurement. In Taylor-Couette flow, *Re*, critical *Re* to turbulent, and *Ta* can be calculated by using Equations 2-12, 2-13 and 2-14 (White 2011), respectively. The critical *Re* and *Ta* for Taylor vortex generation is usually around 145 and 1708, respectively (Drazin and Reid 2004).

$$Re = \omega R_i d/\upsilon \tag{2-12}$$

$$Re_{transition} = 41.3\sqrt{(R_i + R_o)/2d} \tag{2-13}$$

$$Ta = \omega^2 R_i d^3/\upsilon^2 \tag{2-14}$$

where ω denotes the angular velocity, R_i the bob radius, d the gap width and υ the kinematic viscosity of fluid. The *Re* (167.9) and *Ta* (2168) of the maximum shear rate point (1000 s^{-1})

in the GT sludge were found to be above the critical values, and the corresponding apparent viscosity was larger than the result at 890 s^{-1}. The point influenced by Taylor vortex generation could therefore be eliminated. Moreover, the maximum *Re* and *Ta* sharply decreased (41 and 144, respectively, TS 2.5%) into the laminar range as TS increased. Hence, *Re* or *Ta* should always be estimated to control the setting of shear rate range in laminar flow.

2.4 Conclusions

For the yield-pseudoplastic behaviour of the studied WAS, clear rheological characterisation depended on hybrid model fitting of defined shear rate segments. Although a new mathematical expression improved fitting quality, limited applicability of the empiric models reflected the samples' transient rheological behaviour rather than intrinsic properties, challenging the included parameters definition. Characterised by the distinct flow status and transitions, the rheological instability could give more insight in viscoelasticity and thixotropy, which impact sludge flow and mixing in full-scale WAS treatment systems. The observed rheological instability is more pronounced at increased TS concentrations, which are commonly found in WAS digesters.

2.5 References

APHA (2012) Standard Methods for the Examination of Water and Wastewater, 22nd Edition, American Public Health Association, American Water Works Association, Water Environment Federation, Washington.

Baroutian, S., Eshtiaghi, N. and Gapes, D.J. (2013) Rheology of a primary and secondary sewage sludge mixture: Dependency on temperature and solid concentration. Bioresource Technology 140, 227-233.

Baudez, J.-C., Gupta, R.K., Eshtiaghi, N. and Slatter, P. (2013a) The viscoelastic behaviour of raw and anaerobic digested sludge: Strong similarities with soft-glassy materials. Water Research 47(1), 173-180.

Baudez, J.C. (2008) Physical aging and thixotropy in sludge rheology. Applied Rheology 18(1), 8.

Baudez, J.C. and Coussot, P. (2001) Rheology of aging, concentrated, polymeric suspensions: Application to pasty sewage sludges. Journal of Rheology 45(5), 1123-1139.

Baudez, J.C., Markis, F., Eshtiaghi, N. and Slatter, P. (2011) The rheological behaviour of anaerobic digested sludge. Water Research 45(17), 5675-5680.

Baudez, J.C., Slatter, P. and Eshtiaghi, N. (2013b) The impact of temperature on the rheological behaviour of anaerobic digested sludge. Chemical Engineering Journal 215-216, 182-187.

Bhattacharya, S.N. (1981) Flow characteristics of primary and digested sewage sludge. Rheologica Acta 20(3), 288-298.

Chen, B.-H., Lee, S.-J. and Lee, D.J. (2005) Rheological characteristics of the cationic polyelectrolyte flocculated wastewater sludge. Water Research 39(18), 4429-4435.

Chhabra, R.P. and Richardson, J.F. (2008) Non-Newtonian flow and applied rheology: engineering applications, Butterworth-Heinemann, Oxford.

Coussot, P., Leonov, A.I. and Piau, J.M. (1993) Rheology of concentrated dispersed systems in a low molecular weight matrix. Journal of Non-Newtonian Fluid Mechanics 46(2), 179-217.

Coussot, P., Nguyen, Q.D., Huynh, H.T. and Bonn, D. (2002) Viscosity bifurcation in thixotropic, yielding fluids. Journal of Rheology 46(3), 573-589.

Drazin, P.G. and Reid, W.H. (2004) Hydrodynamic stability, Cambridge University Press, Cambridge.

Eshtiaghi, N., Markis, F., Yap, S.D., Baudez, J.-C. and Slatter, P. (2013) Rheological characterisation of municipal sludge: A review. Water Research 47(15), 5493-5510.

Eshtiaghi, N., Yap, S.D., Markis, F., Baudez, J.-C. and Slatter, P. (2012) Clear model fluids to emulate the rheological properties of thickened digested sludge. Water Research 46(9), 3014-3022.

Farno, E., Baudez, J.C., Parthasarathy, R. and Eshtiaghi, N. (2014) Rheological characterisation of thermally-treated anaerobic digested sludge: Impact of temperature and thermal history. Water Research 56, 156-161.

Farno, E., Baudez, J.C., Parthasarathy, R. and Eshtiaghi, N. (2015) Impact of temperature and duration of thermal treatment on different concentrations of anaerobic digested sludge: Kinetic similarity of organic matter solubilisation and sludge rheology. Chemical Engineering Journal 273, 534-542.

Farno, E., Baudez, J.C., Parthasarathy, R. and Eshtiaghi, N. (2016) The viscoelastic characterisation of thermally-treated waste activated sludge. Chemical Engineering Journal 304, 362-368.

Guibaud, G., Dollet, P., Tixier, N., Dagot, C. and Baudu, M. (2004) Characterisation of the evolution of activated sludges using rheological measurements. Process Biochemistry 39(11), 1803-1810.

Hannote, M., Flores, F., Torres, L. and Galindo, E. (1991) Apparent yield stress estimation in xanthan gum solutions and fermentation broths using a low-cost viscometer. Chemical Engineering Journal and the Biochemical Engineering Journal 45(3), B49-B56.

Jin, B., Wilen, B.M. and Lant, P. (2003) A comprehensive insight into floc characteristics and their impact on compressibility and settleability of activated sludge. Chemical Engineering Journal 95(1-3), 221-234.

Lotito, V., Spinosa, L., Mininni, G. and Antonacci, R. (1997) The rheology of sewage sludge at different steps of treatment. Water Science and Technology 36(11), 79-85.

Markis, F., Baudez, J.-C., Parthasarathy, R., Slatter, P. and Eshtiaghi, N. (2014) Rheological characterisation of primary and secondary sludge: Impact of solids concentration. Chemical Engineering Journal 253, 526-537.

Markis, F., Baudez, J.-C., Parthasarathy, R., Slatter, P. and Eshtiaghi, N. (2016) The apparent viscosity and yield stress of mixtures of primary and secondary sludge: Impact of volume fraction of secondary sludge and total solids concentration. Chemical Engineering Journal 288, 577-587.

Mikkelsen, L.H. (2001) The shear sensitivity of activated sludge: Relations to filterability, rheology and surface chemistry. Colloids and Surfaces A: Physicochemical and Engineering Aspects 182(1–3), 1-14.

Moeller, G. and Torres, L.G. (1997) Rheological characterization of primary and secondary sludges treated by both aerobic and anaerobic digestion. Bioresource Technology 61(3), 207-211.

Mori, M., Seyssiecq, I. and Roche, N. (2006) Rheological measurements of sewage sludge for various solids concentrations and geometry. Process Biochemistry 41(7), 1656-1662.

Pignon, F., Magnin, A. and Piau, J.M. (1996) Thixotropic colloidal suspensions and flow curves with minimum: Identification of flow regimes and rheometric consequences. Journal of Rheology 40(4), 573-587.

Pollice, A., Giordano, C., Laera, G., Saturno, D. and Mininni, G. (2007) Physical characteristics of the sludge in a complete retention membrane bioreactor. Water Research 41(8), 1832-1840.

Ratkovich, N., Horn, W., Helmus, F.P., Rosenberger, S., Naessens, W., Nopens, I. and Bentzen, T.R. (2013) Activated sludge rheology: A critical review on data collection and modelling. Water Research 47(2), 463-482.

Sanin, F.D. (2002) Effect of solution physical chemistry on the rheological properties of activated sludge. Water Sa 28(2), 207-211.

Seyssiecq, I., Ferrasse, J.-H. and Roche, N. (2003) State-of-the-art: rheological characterisation of wastewater treatment sludge. Biochemical Engineering Journal 16(1), 41-56.

Seyssiecq, I., Marrot, B., Djerroud, D. and Roche, N. (2008) In situ triphasic rheological characterisation of activated sludge, in an aerated bioreactor. Chemical Engineering Journal 142(1), 40-47.

Slatter, P.T. (1997) The rheological characterisation of sludges. Water Science and Technology 36(11), 9-18.

Spinosa, L. and Lotito, V. (2003) A simple method for evaluating sludge yield stress. Advances in Environmental Research 7(3), 655-659.

Tabuteau, H., Coussot, P. and Baudez, J. (2006) A new approach to the thixotropic behaviour of sewage sludge. Journal of Residuals Science and Technology 3(4), 233-240.

Tixier, N., Guibaud, G. and Baudu, M. (2003) Determination of some rheological parameters for the characterization of activated sludge. Bioresource Technology 90(2), 215-220.

White, F.M. (2011) Fluid mechanics, McGraw-Hill, New York.

Chapter 3. Further rheological characterisation and flow assessment of sewage sludge

This chapter is based on

Peng Wei, Wim Uijttewaal, Jules B. van Lier, Merle de Kreuk. Impacts of shearing and temperature on sewage sludge: rheological characterisation and integration to flow assessment. *Science of the Total Environment*. 2021 (774C). (doi.org/10.1016/j.scitotenv.2021.145005)

Abstract

Accurate rheological characterisation of sewage waste activated sludge (WAS) is of high importance for downstream processing related to optimised sludge pumping and mixing, assessment of energy demands and overall process design. However, to elaborate rheological behaviour is often challenging under dynamic operational conditions in practice. In this study, two practical influencing factors were investigated: long-term shearing and temperature. Compared to anaerobic digestate (DGT), concentrated WAS had more complex and stronger thixotropic behaviour. Under the long-term shearing conditions, the sludge thixotropic behaviour was well characterised by two quantified limitation states. Temperature had a striking impact on the rheological properties, which was strongly correlated to solids content and digestion process. The impact discrepancy between the long-term shearing and temperature, implied different mechanisms to shift the equilibrium of hydrodynamic and non-hydrodynamic interactions for structure deformation and recovery. The distinct rheological properties between the two determined states were clearly reflected in pipe flow behaviour, revealing a concrete link between lab-measured sludge rheology and its practical flow performance. The pipe flows were well assessed using the developed Computational Fluid Dynamics model with effective rheological data integration, which is promising for practical design and optimisation of sewage sludge systems.

Keywords: sewage sludge, rheology, thixotropy, temperature, computational fluid dynamics (CFD), pipe flow

3.1 Introduction

Anaerobic digestion of municipal waste activated sludge (WAS), has been widely applied in wastewater treatment plants (WWTP). Sludge digestion targets both sludge mass reduction and the recovery of biochemical energy in the form of biogas. To enhance operational performance, compact installations for treating highly concentrated sludge matrices are promising and have been in focus (Jiang et al. 2014). Regarding total energy consumption, sludge pumping and mixing can use over 50% of the total energy demand in a WWTP (Kariyama et al. 2018, Kowalczyk et al. 2013). Cost-effective sludge pumping and mixing are hampered by the dynamic and highly viscous rheological behaviour of the WAS (Baudez et al. 2011, Jiang et al. 2014). Hence, to optimise process design and efficiency, proper assessment of the energy consumption for sludge pumping and mixing is of high importance (Eshtiaghi et al. 2012a, Slatter 2001), and relies on accurate sludge rheological characterisation.

Thus far, most researchers focused on describing the complex non-Newtonian behaviour in concentrated WAS with high total solids (TS) levels. Rheological properties of WAS have been found to have nonlinear relations to TS and temperature (Baudez 2006, Baudez et al. 2011, Eshtiaghi et al. 2013, Markis et al. 2016, Ségalen et al. 2015a, Ségalen et al. 2015b, Seyssiecq et al. 2003). Additional rheological complexity results from thixotropic behaviour (Baudez and Coussot 2001, Markis et al. 2016), which is defined as a reversible and time-dependent rheological change to specific shearing conditions imposed on a fluid (Seyssiecq et al. 2003). Moreover, some researchers focused on the application of rheological properties in sludge pumping systems and relevant pipe flows (Eshtiaghi et al. 2012a, Proff and Lohmann 1997, Slatter 1997, Slatter 2001), including pressure drop estimation (Farno et al. 2018, Proff and Lohmann 1997). Although one study linking the sludge thixotropy to pumping energy estimation was published recently (Farno et al. 2020), quantitative correlations between flow behaviour and energy consumption are still limited. The aforementioned thixotropic behaviour (Baudez and Coussot 2001, Markis et al. 2016) complicates the rheological characterisation using a single rheological model (Wei et al. 2018). In practice, this rheological variability or instability could be easily triggered by dynamic operational conditions, such as non-stabilised pumping processes, intermittent feeding/mixing modes and temperature fluctuations. Hence, clear characterisation of the complex and source-dependent rheology is still challenging. Consequently, the rheological-dependent correlations to flow and mixing behaviour has not been well developed, leading to limited application to process optimisation (i.e. energy consumption) in practice.

In this study, the complex rheological behaviour, especially thixotropy of WAS and anaerobic digestate (DGT) from the same WWTP, was investigated based on a long-term shearing condition. Variability to temperature was also combined to the complex rheological characterisation, with a view to potential changes of force interactions and equilibrium in the sludge matrix. Moreover, Computational Fluid Dynamics (CFD) simulations were performed to integrate the rheological properties into prediction and assessment of pipe flow and pressure drop.

3.2 Materials and Methods

3.2.1 Sample characterisation

Sludge samples were taken from WWTP De Groote Lucht (Vlaardingen, The Netherlands), including WAS after gravitational thickening and DGT from the anaerobic digesters. So the samples could be representative to the sewage sludge in both transportation and digestion processes in the studied WWTP. WAS samples with higher TS concentrations were obtained using vacuum filtration to minimise changes in physical sludge structure. All the samples were stored at 4°C and tested within four days. The solids content was measured using the standard methods (APHA 2012).

3.2.2 Rheological measurements

Rheological properties were measured using an Anton Paar MCR 302 Rheometer (Anton Paar GmbH, Austria) equipped with a CC27 coaxial cylinder system (radius of the two concentric cylinders: 13.332 mm and 14.466 mm, respectively). Measurements, including flow curve and yield stress, were carried out based on the proposed methods from our previous work (Wei et al. 2018).

Flow curve. (1) After reaching a stabilised set temperature (tolerance ± 0.05°C), the sample was pre-sheared (16.7 s^{-1}) for 90 s, to minimise concentration gradients achieving a homogeneous distribution; (2) followed by a rest of 60 s; (3) a flow measurement in a logarithmical ramp mode, with an applied shear rate range of 0.01 ~ 1000 s^{-1}. For studying the long-term shearing impact, step (3) was successively repeated in six rounds at 20°C to the same sample. For studying the temperature impact, five temperatures were applied that cover a wide range of operational conditions (transport, heat exchange, digestion), including 10, 20, 35, 45 and 55°C.

Yield stress. The same procedure was used as with (1) and (2); (3) a measurement in a torque ramp mode, starting from a low torque level with a gradual increase to capture the yielding process with a critical change of the monitored deflection angle.

Except the long-term shearing scenario (one-time measurement), triplicate measurements were normally implemented, and good data consistency with small overall standard deviation (≤4%) was obtained. So rheological data of the long-term shearing could be representative to the WAS with the given TS concentration.

3.2.3 Hydrodynamics and energy assessment

A CFD model for flows in a circular pipe was developed based on the sludge pipeline system operated in the aforementioned WWTP, of which the diameter is 20 cm. The preliminary 3D results showed axisymmetric velocity profiles so finally a 2D axisymmetric assumption was applied. A length/diameter (L/D) ratio of 40 was set to ensure generation of fully-developed flows. Physical properties of fluid were specified using the measured data of WAS and DGT. Pressure-driven flows, assuming a fixed pressure gradient along the horizontal pipe, were simulated in both laminar and turbulent cases. The Re-Normalisation Group (RNG) k-ε model was used for turbulence, which supports the simulation of turbulent flows with relatively low *Re* values. Model reliability was first determined by a grid independency study, and a domain with optimal mesh dimensions (characteristic resolution 0.004 m) was selected for the following simulations. In each case, a converged fully-developed flow was determined not only by low residuals ($<10^{-5}$), but also by a force balance (imbalanced force ratio<5%) between wall shear stress and pressure-driven force. Simulations were carried out using the commercial package ANSYS-Fluent 17.1 on a Dell Optiplex 7010 computer, with Intel Core i5-3740 and 8 GB RAM.

A non-Newtonian pipe flow can be characterised using a generalised *Re* (Metzner and Reed 1955)

$$Re_{MR} = \frac{\rho V_p D}{\mu_{eff\_MR}} \tag{3-1}$$

where ρ is fluid density; V_p is mean pipe flow velocity; D is pipe diameter; and μ_{eff_MR} is effective dynamic viscosity depending on applied rheological models. For Ostwald (or power-law) model, the apparent viscosity μ and the Re_{MR} in laminar flow regime (Metzner and Reed 1955) are expressed as

$$\mu = K\gamma^{n-1} \tag{3-2}$$

$$Re_{MR} = \frac{\rho V_p D}{K\left(\frac{8V_p}{D}\right)^{n-1}\left(\frac{3n+1}{4n}\right)^n} \tag{3-3}$$

where γ is shear rate; and K and n are the fluid consistency coefficient and the flow behaviour index, respectively. For Herschel-Bulkley model, the μ and Re_{MR} (Chilton and Stainsby 1998) are expressed as

$$\mu = \frac{\tau_0}{\gamma} + K\gamma^{n-1} \tag{3-4}$$

$$\begin{cases} Re_{MR} = \dfrac{\rho V_p D}{K\left(\frac{8V_p}{D}\right)^{n-1}\left(\frac{3n+1}{4n}\right)^n\left(\frac{1}{1-X}\right)\left(\frac{1}{1-aX-bX^2-cX^3}\right)^n} \\ X = \dfrac{\tau_0}{\tau_W} = \dfrac{4L\tau_0}{D\Delta P}, a = \dfrac{1}{2n+1}, b = \dfrac{2n}{(n+1)(2n+1)}, c = \dfrac{2n^2}{(n+1)(2n+1)} \end{cases} \tag{3-5}$$

where τ_0 is yield stress; L is pipe length; ΔP is pressure difference; and τ_W is wall shear stress. Pressure drop in pipe flows can be estimated as:

$$\frac{\Delta P}{L} = \frac{4f}{D} \cdot \frac{\rho {V_p}^2}{2} \tag{3-6}$$

where f is the Fanning friction factor. For laminar flows f is expressed as

$$f = \frac{16}{Re_{MR}} \tag{3-7}$$

For turbulent flows, f is modified as (Dodge and Metzner 1959):

$$\frac{1}{\sqrt{f}} = \frac{4}{{n'}^{0.75}} \log\left(Re_{MR} f^{\frac{2-n'}{2}}\right) - \frac{0.4}{{n'}^{1.2}} \tag{3-8}$$

where n' is another flow behaviour index and usually has the same value as n. It should be noted that regarding laminar pipe flows of a non-Newtonian fluid characterised by Ostwald model, Equation 3-3 is used to calculate the pressure drop (Metzner and Reed 1955):

$$\frac{\Delta P}{L} = \frac{4}{D} K \left(\frac{3n+1}{4n}\right)^n \left(\frac{8V_p}{D}\right)^n \tag{3-9}$$

3.3 Results and Discussion

3.3.1 Characterisation of time-dependent rheological properties by long-term shearing

Rheological impact of long-term shearing was characterised by the six rounds of flow curve measurements, for both DGT and WAS samples. As shown in Fig. 3-1A, for the DGT sample with a TS concentration of 2.6% (further referred to DGT 2.6%), similar flow curves were obtained for each round. On the contrary, Fig. 3-1B showed a considerable decrease in shear

stress over the shear rate range of the WAS sample with a TS concentration of 6.7% (further referred to WAS 6.7%). The change in shear stress decreased as the rounds were repeated, and almost superposed flow curves were obtained after Round 4. Similarities were also found in the yield stress measurements. As depicted in Fig. 3-1C, yield stress data of all the samples shows an asymptotic tendency, indicating that stabilised rheological properties were achieved under the long-term shearing condition. Hence, besides the initial state in Round 1, another rheological state in Round 6 was determined. From here on, these states are referred to as 'Initial' and 'Stable' state, respectively. This means that at a specific shear rate, the maximum and minimum apparent viscosity of a sample was determined by the Initial and Stable state, respectively. Thus, any time-dependent variation in apparent viscosity would range in this determined range, regardless shearing duration.

Several models were applied to characterise the Initial and Stable flow curves, including Ostwald, Herschel-Bulkley, a modified model developed by Baudez et al. (2011), and the hybrid model proposed in our previous study (Wei et al. 2018). For the WAS curves, Ostwald and Herschel-Bulkley failed to obtain a good fitting. The modified model performance was not satisfactory, despite prior successful reports in a wide range of shear rates (Baudez et al. 2011, Baudez et al. 2013b, Ségalen et al. 2015b). Similar to our previous study (Wei et al. 2018), the hybrid model fitting was the best, in which Herschel-Bulkley fitted the low and medium shear rates, and Ostwald fitted the high shear rates (detailed fitted shear rates are shown in Table S-2). For the DGT samples, Herschel-Bulkley achieved good fitting performance for the whole curves. As shown in Table S-2, large differences were found for WAS: all shear stress values were reduced by about 50% from Initial to Stable. In combination with the considerable changes of K and n, Initial and Stable states demonstrated distinct rheological behaviour. For DGT, the differences in the rheological parameters between Initial and Stable were much lower than for WAS sludge.

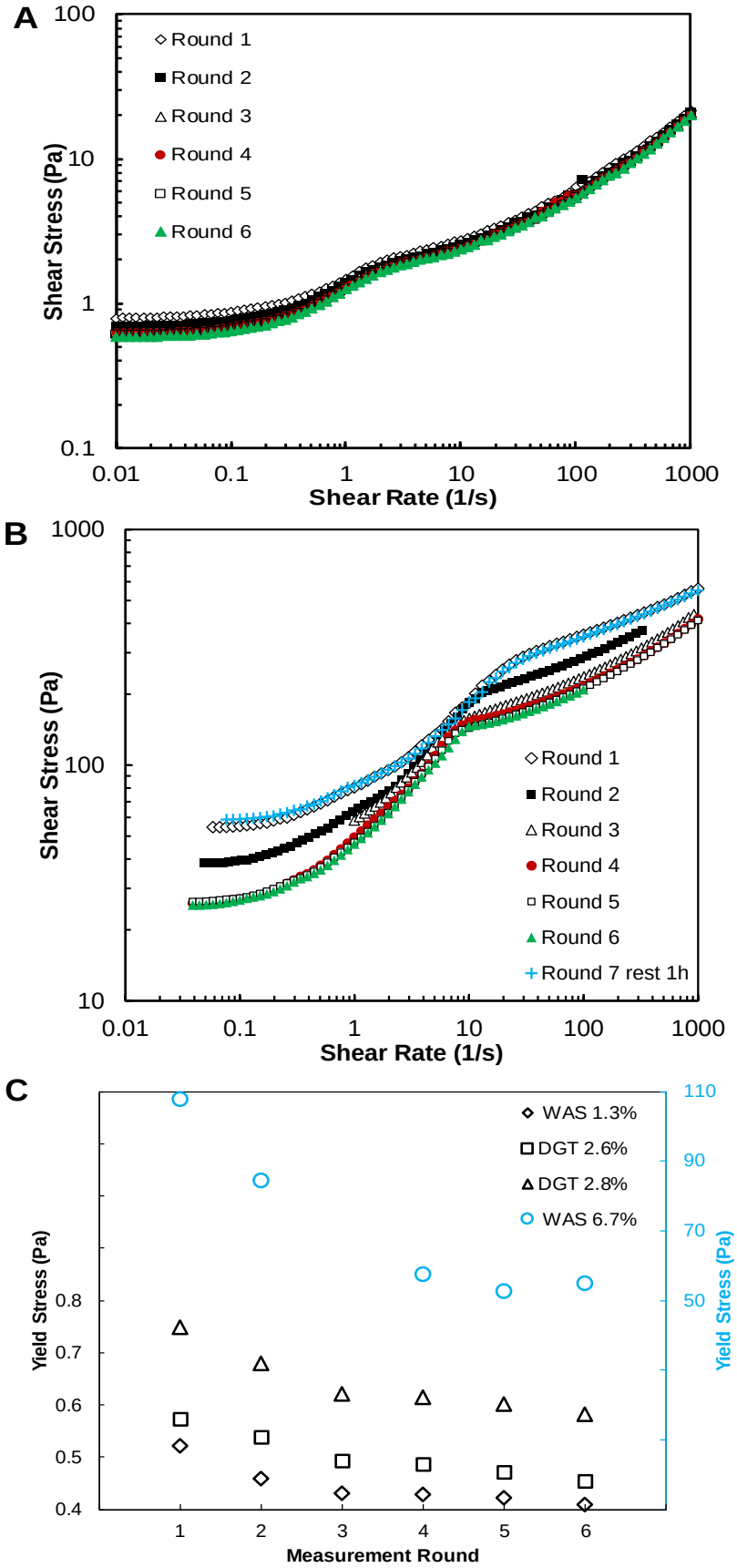

Fig. 3-1 Rheological data measured in 6 rounds, flow curves of A: DGT, TS 2.6%; B: WAS, TS 6.7%; and C: variation of yield stress.

The reduced yield stress and *K* values implied unsteady restructuring of the sludge, in which the viscoelasticity, accounting for both viscous and elastic behaviour, became weakened under the long-term shearing condition. This structural change could eventually lead to a shift of equilibrium between the particles' colloidal forces (non-hydrodynamic) and hydrodynamic forces (Baudez 2008), which was reflected by reaching another stabilised rheological state after the long-term shearing. The structural/rheological evolution, that was characterised by two critical transitions (Table S-2), has similarities to previous reported studies (Baudez 2008, Baudez et al. 2011), but reveals a different pattern. The Stable curve differed completely from the Initial curve, however, rheology changed back to nearly its Initial state after a resting period of about 1 h, indicating reversible structural deformation. In summary, shearing history had a strong and reversible impact on WAS, while the impact on DGT sludge was small. Considering that both WAS and DGT originated from the same WWTP, the obtained results also indicated that the thixotropic behaviour of the sludge was distinctly weakened during the digestion process.

3.3.2 Temperature impact on rheology: role of solids content

Since the studied temperature change was modest and all measurements were done in a relatively short time (~20 min), occurrence of any thermal-treatment/aging process of the samples was negligible. Hence, relevant changes of sludge composition and solubilisation reported in some studies (Farno et al. 2015) were not considered or discussed in this study. Fig. 3-2A and 3-2B show the Initial (Round 1) flow curves of DGT 3.1% and WAS 7.0% at five temperatures, and Table S-3 shows the regressed rheological parameters of WAS 7.0%. In both cases, shear stress decreased as temperature increased, while curve profiles were similar in the whole shear rate range. However, yield stress data show different trends between the two sludge types (Fig. 3-2C): WAS has a monotonic decrease, while DGT has a plateau region. An almost constant yield stress was obtained from 30°C to 45°C, bridging the two decrease regions of 10°C ~ 20°C, and 45°C ~ 55°C. This similarity was also observed in the almost overlapped flow curves of 35°C and 45°C (Fig. 3-2A), and it agrees with a previously reported study of digested sludge, in which a considerable decrease in yield stress was only observed at temperatures over 40°C (Baudez et al. 2013b). These results indicate an insensitive impact on yield stress when the temperature varied within the range of commonly applied mesophilic digestion temperatures, i.e. 35 ± 5°C, at which the anaerobic digester was operated at full scale. WAS rheology revealed a higher sensitivity towards temperature changes, since the yield stress value started to plunge over 20°C.

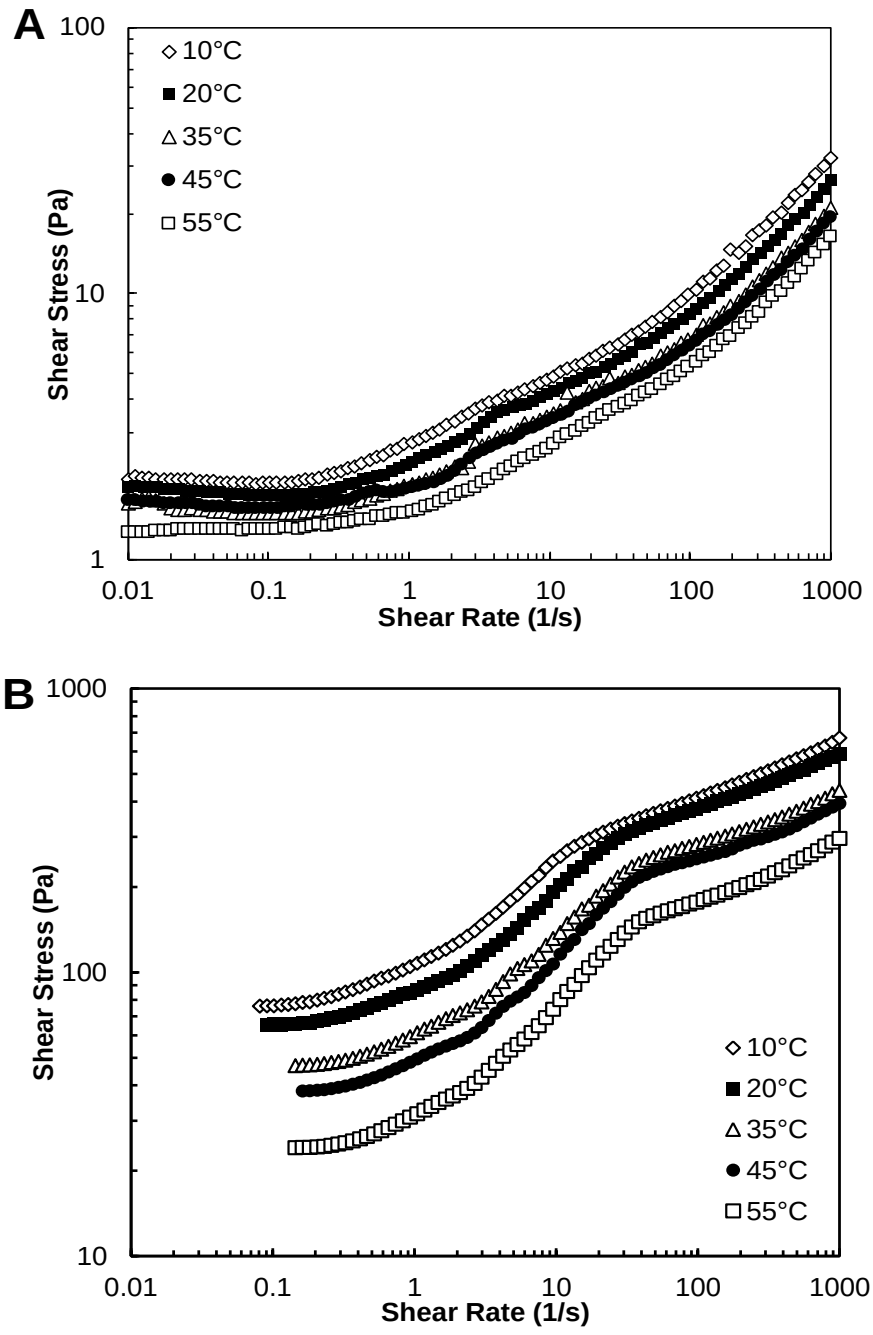
A
100
10
1
Shear Stress (Pa)
10°C
20°C
35°C
45°C
55°C
0.01
0.1
1
10
100
1000
Shear Rate (1/s)
B
1000
100
10
Shear Stress (Pa)
10°C
20°C
35°C
45°C
55°C
0.01
0.1
1
10
100
1000
Shear Rate (1/s)

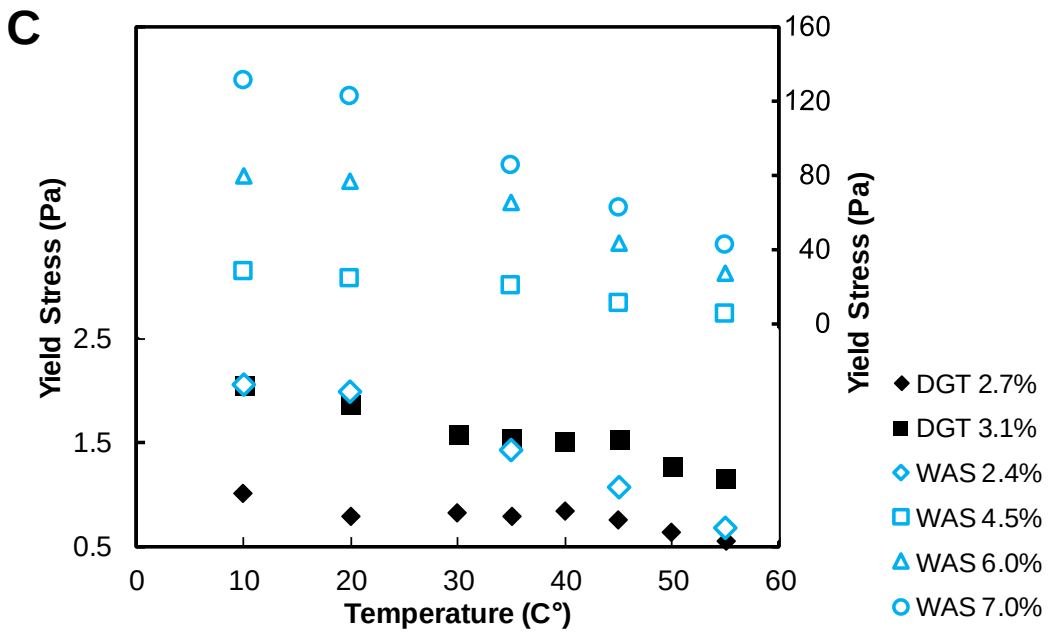

Fig. 3-2 Rheological data at different temperatures, flow curves of A: DGT 3.1%; B: WAS 7.0%; and C: yield stress of DGT and WAS.

Several models have been reported to have a good correlation between temperature and rheological properties, including an exponential relation (Manoliadis and Bishop 1984), the Arrhenius model (Baroutian et al. 2013), and the Vogel-Tammann-Fulcher (VTF) model (Baudez et al. 2013a, Dieudé-Fauvel et al. 2009, Ségalen et al. 2015b). The VTF model is expressed as,

$$\varphi = A \cdot \exp\left(\frac{E_a}{R} \cdot \frac{1}{T - T_0}\right) \tag{3-10}$$

where A is a model coefficient, E_a is activation energy, R is the gas constant, and T_0 is a critical temperature for vitreous, or glassy transition.

The VTF model has been successfully applied for the non-hydrodynamic dominant regime of sludge with a medium TS level (<5%) (Baudez et al. 2013a, Baudez et al. 2013b) and pasty sludge with a high TS level (>10%) (Dieudé-Fauvel et al. 2009, Ségalen et al. 2015b). In this study, it was also found to have the best fit of all WAS yield stress (τ_0) data. However, different temperature correlations were found with other model parameters. For WAS 4.5% (Fig. 3-3A), similar to τ_0, *K2* and τ_1 decreased following the VTF model; whereas the *K1* decreasing trend was best fit by the exponential relation. As temperature increased, *n1* increased while *n2* had no considerable change. Similarities were obtained in the other concentrated WAS with TS concentrations > 2.5%, which are not shown here. The obtained results implied shear rate dependency on the aforementioned structural deformation and the

changes of force interactions in WAS. At low and medium shear rates (segment 1), a good Arrhenius correlation was obtained between *K1* and the water dynamic viscosity (Fig. 3-3B). The increased *n1* indicates a lower degree of shear-thinning, a higher degree of fluidity, and also a higher degree of electrical conductivity status (Ségalen et al. 2015b). Hence, changes in the hydrodynamic interactions affected by temperature were apparently more reflected at low shear rates. At high shear rates, the VTF model better fitted *K2*, which reflected the impact of sludge solids content, and thus implied a more dominant influence of the non-hydrodynamic interactions. However, the negligible *n2* change indicated the shear-thinning degree was almost independent on temperature at high shear rates, which agrees with reported results (Baroutian et al. 2013, Manoliadis and Bishop 1984).

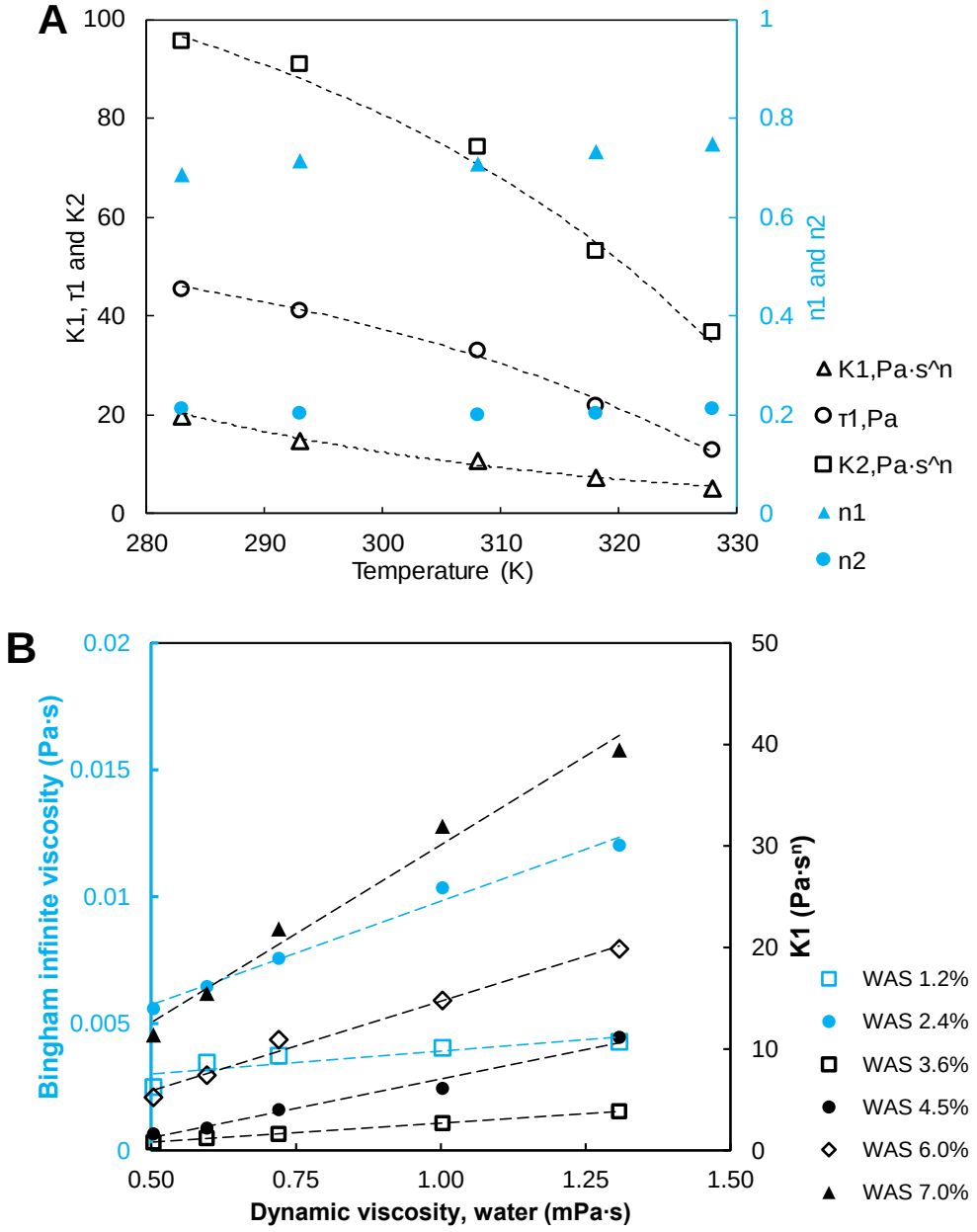

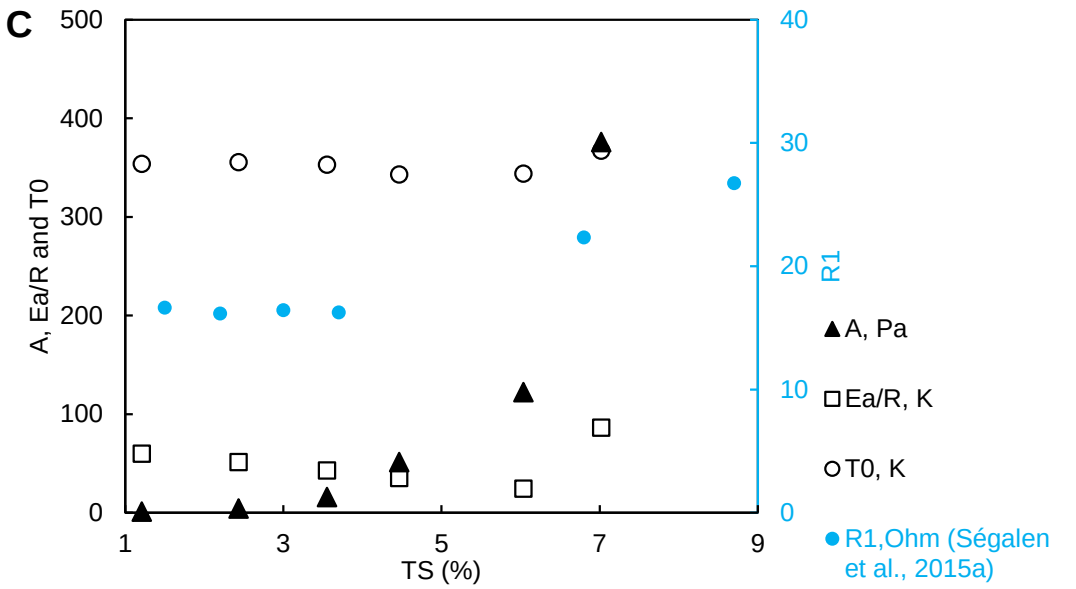

Fig. 3-3 Model correlation results. A: To temperature, WAS 4.5%; B: to water dynamic viscosity, all WAS samples; and C: the VTF model parameters for τ_0 to TS concentration, compared to experimental data (Ségalen et al., 2015a).

The rheological impact of temperature was also strongly correlated to the solids content level. Unlike the fitting results for the more concentrated WAS, both Herschel-Bulkley and the modified model (Baudez et al. 2011) had acceptable fitting performance at TS < 2.5%. For the model derived yield stress, a good correlation with the VTF model was obtained. As shown in Fig. 3-3B (the blue data), the Bingham infinite viscosity α_0 has a good linear relation with the water dynamic viscosity, indicating a good Arrhenius correlation and considerable hydrodynamic interactions over the entire shear rate range. Apparently, these results agree quite well with the previous studies (Baudez et al. 2013b, Dieudé-Fauvel et al. 2009, Ségalen et al. 2015b). However, good temperature correlations to K and n were difficult to achieve with any of the aforementioned models. The VTF model performance was found to be more correlated to the TS level. Comparable values of the regressed E_a and T_0 (in Equation 3-10) in τ_0, $K2$ and τ_1 correlations were only found in a TS range between 2.5% and 6%. However, a large deviation was found between E_a and T_0 when TS < 2.5% and TS > 6%. As reported by Dieude-Fauvel et al. (2009), it indicates similar patterns of involved molecular movements and particle interactions, mainly occurring in a specific TS range.

Fig. 3-3C shows the fitting results of the VTF model for τ_0 at different TS concentrations. All of the three parameters, especially E_a and A (related to activation intensity), have a distinct increase at TS > 6%. It has been reported that the rheological properties also correlate well

to sludge electrical properties (Dieudé-Fauvel et al. 2009, Ségalen et al. 2015a, Ségalen et al. 2015b), which can be characterised by same activation energy (E_a) results between apparent viscosity and electrical resistivity (Dieudé-Fauvel et al. 2009). In their developed equivalent circuit model, an electrical resistance *R1* was defined to represent the interactions and network of solid compounds (the non-hydrodynamic discussed in our study) (Ségalen et al. 2015a, Ségalen et al. 2015b), which was also shown in Fig. 3-3C. The *R1* variation, a slight initial decrease and a critical increase in the range between 3.7% and 6.8% TS (Ségalen et al. 2015a), has a similar trend to our results. Hence, increasing solids content over a threshold may lead to a critical change or evolution of the non-hydrodynamic interaction intensity, illustrated by the considerable rheological changes in Fig. 3-3C.

Moreover, the interactive impacts between temperature and solids content on sludge rheology may change through aging processes. After long-term mesophilic digestion, solids content of DGT can be stabilised (almost constant TS and VS concentrations), which is characterised by similar non-hydrodynamic interactions over a wider temperature range of 30~40°C. This may clarify the aforementioned insensitivity of DGT yield stress change to temperature (Fig. 3-2C).

3.3.3 Further discussion: implication of dynamic structural change

Similarity of rheological behaviour under different conditions can be determined by dimensionless master curves (Baudez and Coussot 2001, Baudez et al. 2011, Coussot 1995). As mentioned before, the DGT flow curves showed a good fit over the whole shear rate range, justifying the use of the following equation (Baudez et al. 2011)

$$\begin{cases} \mathrm{T}_M = 1 + \beta \cdot {\Gamma_A}^n + \Gamma_A \\ \mathrm{T}_M = \frac{\tau}{\tau_0}, \Gamma_A = \frac{\alpha_0}{\tau_0} \cdot \dot{\gamma}, \beta_{mc} = \frac{K}{\tau_0} \cdot \left(\frac{\tau_0}{\alpha_0}\right)^n \end{cases} \quad (3\text{-}11)$$

where α_0 is the Bingham infinite apparent viscosity (Pa·s). For WAS curves, since the modified model (Baudez et al. 2011) was no longer appropriate, another equation with a reference viscosity (Baudez and Coussot 2001, Coussot 1995) was used

$$\begin{cases} \mathrm{T}_M = 1 + \lambda \cdot {\Gamma_B}^n \\ \mathrm{T}_M = \frac{\tau}{\tau_0}, \Gamma_B = \frac{\mu_T}{\tau_0} \cdot \dot{\gamma}, \lambda = \frac{K}{\tau_0} \cdot \left(\frac{\tau_0}{\mu_T}\right)^n \end{cases} \quad (3\text{-}12)$$

where μ_T is the reference viscosity of the interstitial fluid (water). It was found that the curve trend was independent on μ_T. For the sake of simplicity, the μ_T value was set to 1 at 20°C, and varied accordingly with the change in water dynamic viscosity at other temperatures.

As shown in Fig. 3-4A, all DGT curves were very close to form one master curve. In line with the previous results (Baudez et al. 2011, Ségalen et al. 2015b), it implied similar hydrodynamic and non-hydrodynamic interactions in DGT within the studied temperature and TS ranges. The aforementioned weak thixotropic behaviour was only reflected by the small deviation between the Initial and Stable curves when $\Gamma > 2$. However, for WAS, distinct curves were obtained between 10°C and 55°C, with a marked change at around $\Gamma = 0.2$. Unlike the DGT results, the WAS Initial and Stable curves started to separate when $\Gamma > 0.1$, and the difference kept increasing when $\Gamma > 1$. Moreover, separated curves of 10°C and 55°C were also observed in the other concentrated WAS (TS > 2.5%). Hence, a single master curve was only formed in DGT and WAS with low TS concentrations (< 2.5%), but not for the other concentrated WAS, which was, to the authors' knowledge, never reported in previous research.

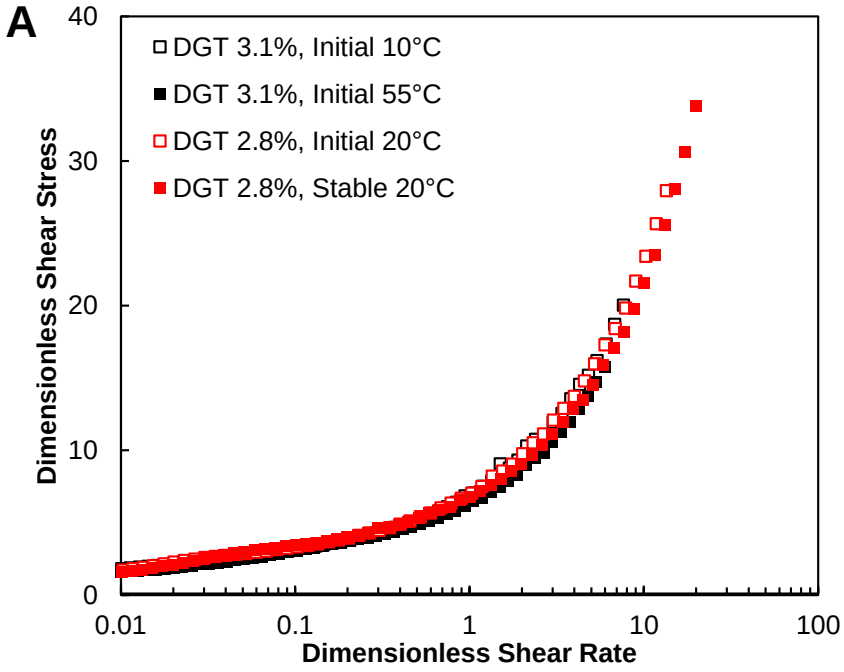

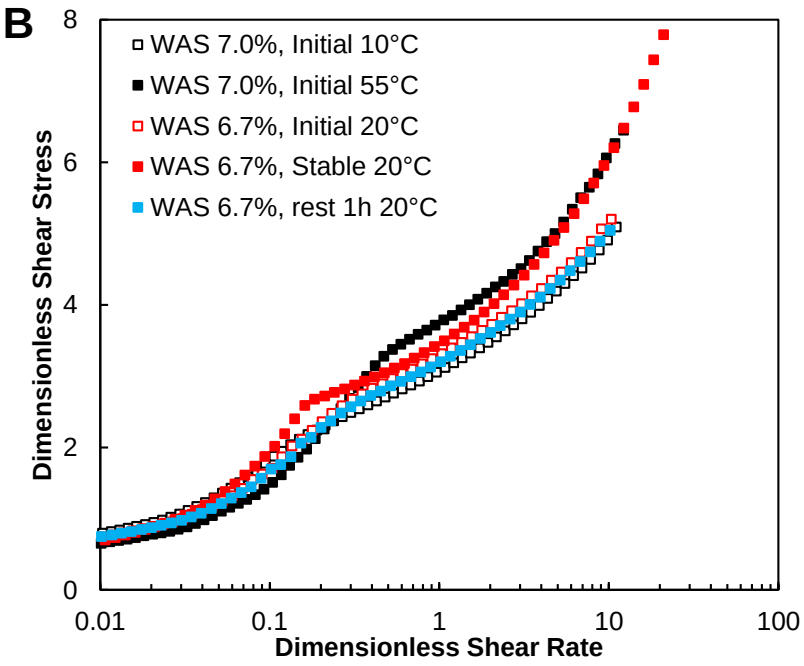

Fig. 3-4 Dimensionless flow curves of A: DGT samples, and B: WAS samples.

However, larger scaled shear stress (T_M) values in Initial 55°C and Stable 20°C curves could be noticed. These indicated a higher viscous or less flowable degree, which was unexpected and is seemingly contradictory to the original data shown in Fig. 3-1 and Fig. 3-2. In Equation 3-12, T_M also represents the relative shear stress to the referred τ_0. When comparing the Initial 10°C and 55°C curves, the trend illustrated variations in the relative shear stress from low to high shear rates, which might be related to dynamic behaviour of the force interactions in WAS. As discussed in Section 3.2, the hydrodynamic interactions could be considerable at low shear rates, similarly to DGT, the two curves were close to each other. As reported in our previous study (Wei et al. 2018), localised shear (Baudez et al. 2011) could occur, as demonstrated by the part of the curve where shear stress was lower than τ_0. As temperature increased, localised shear could be mitigated, which means that WAS became more flowable, leading to lower T_M at 55°C than at 10°C. However, as shear rate increased, collision and interaction probability of the particles increased, and more energy was dissipated for particle dispersion (Coussot 1995, Tsutsumi and Yoshida 1987). Therefore, in Section 3.2 the non-hydrodynamic interactions could become more important at high shear rates. Due to the changes of the hydrodynamic and non-hydrodynamic interactions, the relevant force equilibrium to maintain sludge rheological behaviour would be dynamic and shifting. As shown in Fig. 3-5, the mean shear stress reduction in the flow curves is systematically lower than yield stress reduction. It indicated that, after yielding, the generated destruction degree

of sludge structure was not constant, but became less and towards a more structural reconstruction state at higher temperatures and higher shear rates, resulting in higher T_M values at 55°C than at 10°C. Similarities were also found between Initial 20°C and Stable 20°C: yield stress was reduced by 51.0% while the mean shear stress was reduced by only 33.1±7.7%.

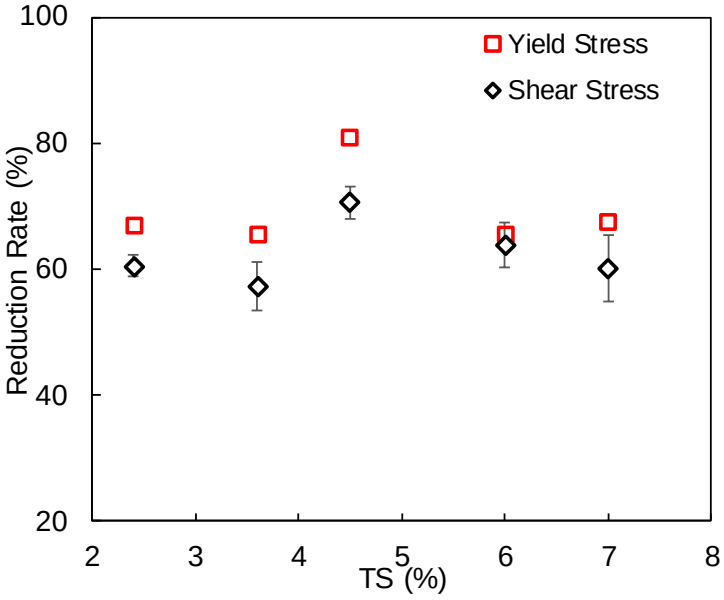

Fig. 3-5 Mean reduction rates (between 10°C and 55°C) of yield stress and shear stress in flow curves (> 5 s^{-1}) at different TS concentrations of WAS.

Moreover, trend differences in the curves between temperature increase (Initial 10°C and 55°C) and shearing time change (Initial and Stable 20°C) also implied different mechanisms of shifting the force equilibrium. The Initial 10°C and 55°C curves in Fig. 3-4B are almost parallel after the cross point at Γ = 0.2. The parallel trend implied that the equilibrium shift and the destruction degree change due to temperature were independent of the shear rate, consistent with the results of decreasing *K2* and constant *n2* shown in Section 3.2. Hence, temperature apparently mainly affected the intensity of the overall hydrodynamic and non-hydrodynamic interactions, but not the pattern and related structure of flocs and agglomerated particles. However, no parallel trend could be observed in Initial and Stable 20°C curves. Since the hydrodynamic interactions were consistent at the same temperature, the long-term shearing effect on the equilibrium shift appears to be related to the non-hydrodynamic interactions. On one hand, the decrease in transition shear rate (Table S-2) indicated less and less localised shear, implying that long-term shearing led to much weaker attractive forces between the flocs and agglomerated particles, and a higher destruction degree. On the other

hand, the consequent characteristic size reduction was accompanied by an increased number of these solids content. This caused the collision and interactive probability to increase along with the shear rate, leading to a T_M trend no longer parallel to that for Initial (Fig. 3-4B). Hence, the long-term shearing apparently affected both the intensity and pattern of the non-hydrodynamic interactions, and eventually resulted in reaching another force equilibrium determined as Stable in this study. The microscopic force and structural changes between Initial and Stable states could be macroscopically demonstrated by the considerable changes of rheological parameters, including *K*, *n* and T_M. In addition, these changes seem reversible since the curve fell back to Initial after a long-time rest.

Hence, essentially this T_M deviation had no contradiction to the original data and referred studies. It supported the theoretical interpretation in literature (Baudez et al. 2011, Coussot 1995, Tsutsumi and Yoshida 1987) and implied different mechanisms of shifting the force equilibrium between the long-term shearing and temperature impacts.

3.3.4 Application of the rheological discrepancy: pipe flow assessment

For both WAS and DGT, flow behaviour of Initial and Stable states was investigated using CFD models. Model validity was first determined using reference data, including Newtonian (water, 20°C) and non-Newtonian (Pinho and Whitelaw 1990) pipe flows. As shown in Fig. S-1, a good agreement was achieved between the referred data and simulation results. However, unlike Newtonian, the non-Newtonian velocity profiles showed a higher rheological dependency.

As shown in Fig. S-2 and Table S-4, the aforementioned rheological discrepancy between Initial and Stable was clearly demonstrated in the hydrodynamic data, especially for WAS. In addition, the difference between Initial and Stable increases as the pressure gradient (Pa/m) decreases. Therefore, it implies a considerable change of flow behaviour when the sludge, especially the WAS, frequently changes between Initial and Stable states under a specific pumping or mixing condition.

Although an optimal rheological characterisation was achieved, the hybrid model did not lead to a satisfactory energy assessment of the WAS pipe flows. In Re_{MR} calculation, the involved sub-models: Herschel-Bulkley and Ostwald with distinct K and n values, could not be well integrated and had to be applied individually. As shown in Table 3-1, different Re_{MR} values were obtained between the sub-models, indicating that both governed shear rate segments played an important role in the flow characteristics. In order to improve flow characterisation, an ‘effective’ Ostwald model was applied, and the parameters K_{eff} and n_{eff} were not

determined by the experimental data fitting but by regression of Equation 3-9 (Metzner and Reed 1955). As expected, it could predict more reasonable Re_{MR} with moderate values (Table 3-1) compared to the two sub-models. The effective model was further validated using the Moody diagram. As shown in Fig. 3-6, the WAS data have a good correlation to the Hagen-Poiseuille line, representing the theoretical relation between the Fanning friction factor and *Re* in the laminar regime (typically *Re* < 2100). A good correlation was also obtained for the DGT data in both the laminar regime and the turbulent regime determined by a modified expression (Equation 3-8, (Dodge and Metzner 1959)).

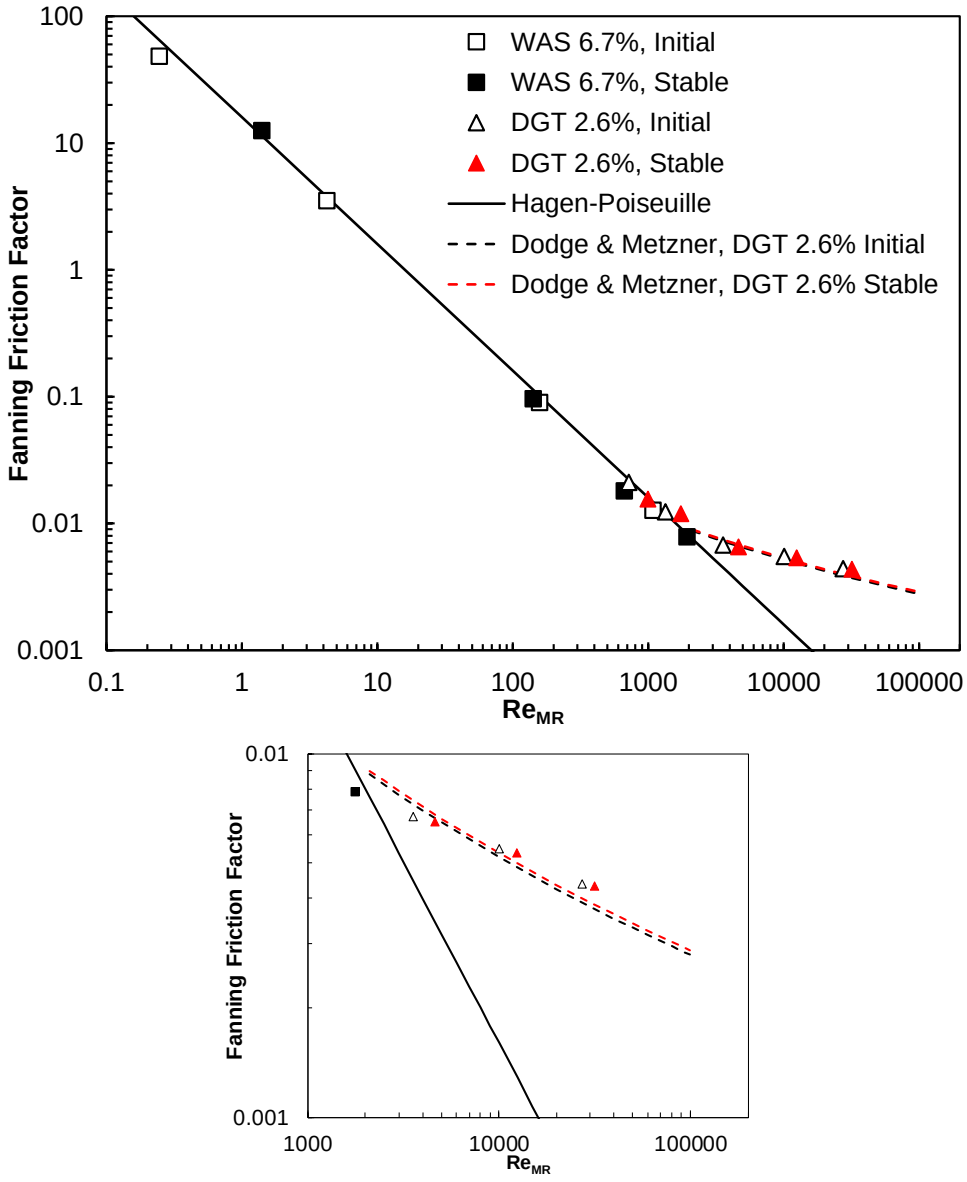

Fig. 3-6 Moody diagram of Initial and Stable of WAS (the 'effective' Ostwald model) and DGT.

Table 3-1 Re_{MR} of WAS and DGT predicted by different models.

	WAS 6.7%				DGT 2.6%	
	Effective *dP/L* (Pa/m)	Re_{MR}, **Hybrid Herschel-Bulkley**	Re_{MR}, **Hybrid Ostwald**	Re_{MR}, **'Effective' Ostwald**	**Effective *dP/L* (Pa/m)**	Re_{MR}, **Herschel-Bulkley**
Initial	2496	0.3	0.2	0.2	67	719
	4955	4.5	3.9	4.2	84	1344
	8392	89.6	175	157	134	3567
	11130	434.5	1346	1085	240	1.0E+4
					466	2.7E+4
					1135	9.8E+4
Stable	2492	1.3	1.0	1.4	60	996
	4596	46	167	142	88	1745
	5430	148	912	666	130	4636
	8349	341	2945	1934	242	1.2E+4
					470	3.2E+4
					1125	1.1E+5

Fig. 3-7 shows pressure drop variations in the studied flow rate range, based on a developed correlation from a more practical aspect (Metzner and Reed 1955)

$$\frac{\Delta P}{L} = 32K\frac{8^{n'-1}}{D^{3n'+1}}\left(\frac{3n+1}{4n}\right)^{n}\left(\frac{4Q}{\pi}\right)^{n'} \tag{3-13}$$

where Q is flow rate. Limitation of the single sub-model use was also illustrated in the correlation performance (Fig. 3-7A): hybrid Herschel-Bulkley was only valid at very low flow rates before getting large deviations; hybrid Ostwald had a considerable underestimation at high flow rates. However, the 'effective' Ostwald model got good correlations for both Initial and Stable states. It again emphasised the importance of determining K_{eff} and n_{eff}; and the considerable pressure drop reduction (> 33%) from Initial to Stable. Correlating to the rheological changes between Initial and Stable, some quantitative solutions were proposed to assess general time-dependent laminar pipe-flow behaviour of the WAS. A range of pressure drop could be determined based on Initial and Stable state, expressed as

$$\frac{\Delta P}{L} = \begin{cases} 1838\cdot\frac{1.54^{0.32}}{D^{1.95}\cdot 8^{0.68}}\cdot\left(\frac{4Q}{\pi}\right)^{0.32}, & min\ \ (by\ \ Stable) \\ 3501\cdot\frac{1.66^{0.28}}{D^{1.83}\cdot 8^{0.72}}\cdot\left(\frac{4Q}{\pi}\right)^{0.28}, & max\ \ (by\ \ Initial) \end{cases} \tag{3-14}$$

Thus, at a specific flow rate, the corresponding pressure drop is expected to vary within the determined range. This is especially useful for achieving an optimised operation for sludge pumping, i.e. in sludge systems with a high and low temperature thermal-hydrolysis process (THP) as pre-treatment. In these systems, the transport of highly concentrated sludge

mixtures and the batch-wise feeding of certain THP configurations leads to high pumping energy consumption, non-optimised heat transfer and even clogging. Switching off or even reducing pumping/mixing power for some time should therefore be considered due to the reversible thixotropic behaviour. After a rest period, the dynamic force equilibrium would shift and reconstruction to Initial could occur, increasing the stagnant and poor flow regions. The installed pump/mixer capacity should be designed to handle the Initial rheology, in order to trigger the sludge motion again.

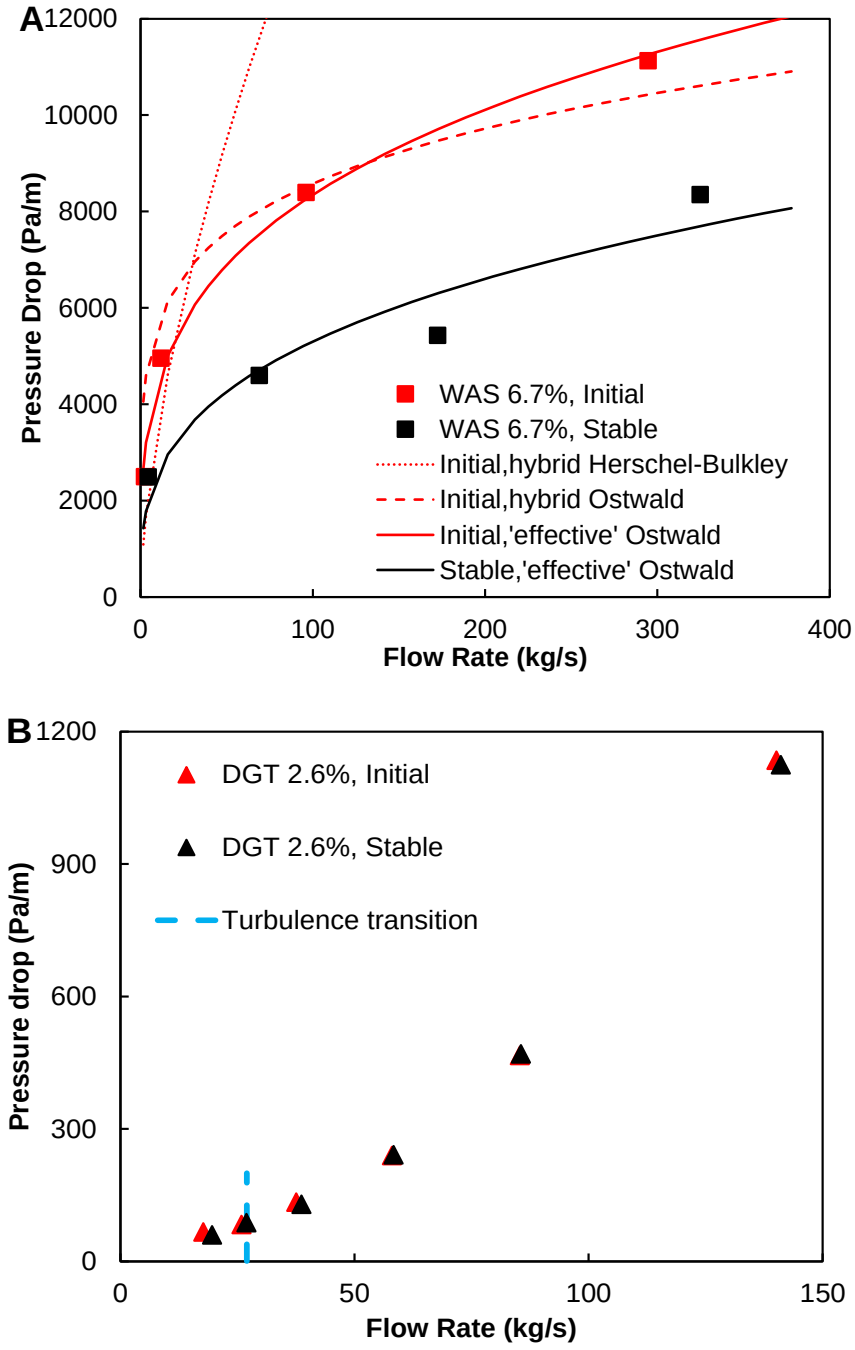

Fig. 3-7 Correlations of the pressure drop to the flow rates, A: WAS, and B: DGT.

Furthermore, it should be noticed that K_{eff} and n_{eff} were mainly developed to characterise flow behaviour under specific flow conditions, i.e., a flow rate/pressure gradient range, which is more related to practical applications such as pump design. For thixotropic materials, it is not easy to determine K_{eff} and n_{eff}, because they are not explicitly derived from the rheogram, which may require systematic experiments or simulations. More attention is also required to the last WAS group and the second DGT group (Fig. 3-7B), since the Re_{MR} values were close to the aforementioned critical value (2100) for turbulence transition. If the imposed pressure gradient increased further, turbulence may occur, which will lead to a considerable increase in pressure drop and thereby might complicate practical operations. Hence, the integration of experimental and CFD approaches developed in this study sheds light on a better solution to the aforementioned issues in practice.

3.4 Conclusions

- The complex thixotropic behaviour of the studied sewage sludge was well characterised by the two quantified limitation states: Initial and Stable.
- Impact discrepancy between the long-term shearing and temperature, implied different mechanisms to shift the equilibrium of hydrodynamic and non-hydrodynamic interactions for structure deformation and recovery.
- The distinct rheological properties between Initial and Stable were clearly reflected in pipe flow behaviour, revealing a concrete link between lab-measured sludge rheology and its practical flow performance.
- The pipe flows with complex rheological properties were well assessed using the developed CFD model with effective rheological data integration, which is promising for practical design and optimisation of sewage sludge systems.

3.5 References

APHA (2012) Standard Methods for the Examination of Water and Wastewater, 22nd Edition, American Public Health Association, American Water Works Association, Water Environment Federation, Washington.

Baroutian, S., Eshtiaghi, N. and Gapes, D.J. (2013) Rheology of a primary and secondary sewage sludge mixture: Dependency on temperature and solid concentration. Bioresource Technology 140, 227-233.

Baudez, J.-C. (2006) About peak and loop in sludge rheograms. Journal of Environmental Management 78(3), 232-239.

Baudez, J.-C., Gupta, R.K., Eshtiaghi, N. and Slatter, P. (2013a) The viscoelastic behaviour of raw and anaerobic digested sludge: Strong similarities with soft-glassy materials. Water Research 47(1), 173-180.

Baudez, J.C. (2008) Physical aging and thixotropy in sludge rheology. Applied Rheology 18(1), 8.

Baudez, J.C. and Coussot, P. (2001) Rheology of aging, concentrated, polymeric suspensions: Application to pasty sewage sludges. Journal of Rheology 45(5), 1123-1139.

Baudez, J.C., Markis, F., Eshtiaghi, N. and Slatter, P. (2011) The rheological behaviour of anaerobic digested sludge. Water Research 45(17), 5675-5680.

Baudez, J.C., Slatter, P. and Eshtiaghi, N. (2013b) The impact of temperature on the rheological behaviour of anaerobic digested sludge. Chemical Engineering Journal 215-216, 182-187.

Chilton, R.A. and Stainsby, R. (1998) Pressure Loss Equations for Laminar and Turbulent Non-Newtonian Pipe Flow. Journal of Hydraulic Engineering 124(5), 522-529.

Coussot, P. (1995) Structural Similarity and Transition from Newtonian to Non-Newtonian Behavior for Clay-Water Suspensions. Physical Review Letters 74(20), 3971-3974.

Dieudé-Fauvel, E., Van Damme, H. and Baudez, J.C. (2009) Improving rheological sludge characterization with electrical measurements. Chemical Engineering Research and Design 87(7), 982-986.

Dodge, D.W. and Metzner, A.B. (1959) Turbulent flow of non-newtonian systems. Aiche Journal 5(2), 189-204.

Eshtiaghi, N., Markis, F. and Slatter, P. (2012) The laminar/turbulent transition in a sludge pipeline. Water Science and Technology 65(4), 697-702.

Eshtiaghi, N., Markis, F., Yap, S.D., Baudez, J.-C. and Slatter, P. (2013) Rheological characterisation of municipal sludge: A review. Water Research 47(15), 5493-5510.

Farno, E., Baudez, J.C., Parthasarathy, R. and Eshtiaghi, N. (2015) Impact of temperature and duration of thermal treatment on different concentrations of anaerobic digested sludge: Kinetic similarity of organic matter solubilisation and sludge rheology. Chemical Engineering Journal 273, 534-542.

Farno, E., Coventry, K., Slatter, P. and Eshtiaghi, N. (2018) Role of regression analysis and variation of rheological data in calculation of pressure drop for sludge pipelines. Water Research 137, 1-8.

Farno, E., Lester, D.R. and Eshtiaghi, N. (2020) Constitutive modelling and pipeline flow of thixotropic viscoplastic wastewater sludge. Water Research 184, 116126.

Jiang, J., Wu, J., Poncin, S. and Li, H.Z. (2014) Rheological characteristics of highly concentrated anaerobic digested sludge. Biochemical Engineering Journal 86, 57-61.

Kariyama, I.D., Zhai, X. and Wu, B. (2018) Influence of mixing on anaerobic digestion efficiency in stirred tank digesters: A review. Water Research 143, 503-517.

Kowalczyk, A., Harnisch, E., Schwede, S., Gerber, M. and Span, R. (2013) Different mixing modes for biogas plants using energy crops. Applied Energy 112, 465-472.

Manoliadis, O. and Bishop, P.L. (1984) Temperature effect on rheology of sludges. Journal of Environmental Engineering-Asce 110(1), 286-290.

Markis, F., Baudez, J.-C., Parthasarathy, R., Slatter, P. and Eshtiaghi, N. (2016) The apparent viscosity and yield stress of mixtures of primary and secondary sludge: Impact of volume fraction of secondary sludge and total solids concentration. Chemical Engineering Journal 288, 577-587.

Metzner, A.B. and Reed, J.C. (1955) Flow of non-newtonian fluids—correlation of the laminar, transition, and turbulent-flow regions. Aiche Journal 1(4), 434-440.

Pinho, F.T. and Whitelaw, J.H. (1990) Flow of non-newtonian fluids in a pipe. Journal of Non-Newtonian Fluid Mechanics 34(2), 129-144.

Proff, E.A. and Lohmann, J.H. (1997) Calculation of pressure drop in the tube flow of sewage sludges with the aid of flow curves. Water Science and Technology 36(11), 27-32.

Ségalen, C., Dieudé-Fauvel, E. and Baudez, J.C. (2015a) Electrical and rheological properties of sewage sludge – Impact of the solid content. Water Research 82, 25-36.

Ségalen, C., Dieudé-Fauvel, E., Clément, J. and Baudez, J.C. (2015b) Relationship between electrical and rheological properties of sewage sludge – Impact of temperature. Water Research 73, 1-8.

Seyssiecq, I., Ferrasse, J.-H. and Roche, N. (2003) State-of-the-art: rheological characterisation of wastewater treatment sludge. Biochemical Engineering Journal 16(1), 41-56.

Slatter, P.T. (1997) The rheological characterisation of sludges. Water Science and Technology 36(11), 9-18.

Slatter, P.T. (2001) Sludge pipeline design. Water Science and Technology 44(10), 115-120.

Tsutsumi, A. and Yoshida, K. (1987) Effect of temperature on rheological properties of suspensions. Journal of Non-Newtonian Fluid Mechanics 26(2), 175-183.

Wei, P., Tan, Q., Uijttewaal, W., van Lier, J.B. and de Kreuk, M. (2018) Experimental and mathematical characterisation of the rheological instability of concentrated waste activated sludge subject to anaerobic digestion. Chemical Engineering Journal 349, 318-326.

Chapter 4. Two-phase flow and mixing in a lab-scale digester: importance for scaled-up applications

This chapter is based on

Peng Wei, Robert F. Mudde, Wim Uijttewaal, Henri Spanjers, Jules B. van Lier and Merle de Kreuk. Characterising the two-phase flow and mixing performance in a gas-mixed anaerobic digester: importance for scaled-up applications. *Water Research*. 2019, 149: 86-97. (doi.org/10.1016/j.watres.2018.10.077)

Abstract

This study aimed to characterise the gas-liquid flow and mixing behaviour in a gas-mixed anaerobic digester by improving phase interaction modelling using Computational Fluid Dynamics (CFD). A 2D axisymmetric model validated with experimental data was set up using an Eulerian-Eulerian method. Uncertainty factors, including bubble size, phase interaction forces and liquid rheology were found to significantly influence the flow field. A more reliable and complete validation was obtained by critical comparison and assessment of the referred experimental data, compared to the models reported in other studies. Additionally, justifiable corrections and predictions in detail were obtained. Mixing was evaluated by trajectory tracking of a large number of particles based on an Euler-Lagrange method. The mixing performance approximated to a laminar-flow reactor (LFR) that distinctly deviated from expected continuous stirred tank reactor (CSTR) design, indicating limited enhancement from the applied gas-sparging strategy in the studied digester. The study shows the importance of a proper phase-interaction description for a reliable hydrodynamic characterisation and mixing evaluation in gas-mixed digesters. Validations, bend to experimental data without a critical assessment, may lead to an inaccurate model for further scaled-up applications.

Keywords: anaerobic digestion, CFD, two-phase flow, hydrodynamics, mixing

4.1 Introduction

Stabilisation of biomass and its biochemical conversion into energy-rich biogas are commonly performed in anaerobic digesters, in which good mass transfer and heat transfer rely on a proper mixing. In digesters designed as a continuous stirred tank reactor (CSTR), mixing is commonly achieved by biogas recirculation (Lindmark et al. 2014). However, the mixing is often insufficient in full-scale gas-mixed digesters, due to unaccounted scale-up effects (Bello-Mendoza and Sharratt 1998, Capela et al. 2009, Terashima et al. 2009). Prevailing short-circuiting or dead zones in practice result in treatment performances below the theoretical potential (Capela et al. 2009, Samstag et al. 2016). In order to optimize mixing, the flow behaviour and mixing performance should be well characterised, and the actual contribution to mixing from the biogas recirculation should be evaluated. Any additional mixing brought forward by the produced biogas resulting from sludge digestion is not taken into account in the design process and the exact impact of evolving biogas has not yet been evaluated.

For research purposes it is very challenging to obtain a clear insight of the mixing behaviour in an opaque and gas tight system when using only experimental approaches. A general mixing pattern can be determined using tracer tests (Capela et al. 2009, Smith et al. 1993, Terashima et al. 2009), but local flow fields responsible for any poor mixing cannot be determined from the results of tracer residence time distribution (RTD). Advanced non-invasive techniques, such as computer automated radioactive particle tracking (CARPT) and computed tomography (CT) can provide detailed information of flow fields (Karim et al. 2004, Varma and Al-Dahhan 2007), but are yet not applicable to full scale facilities.

Computational Fluid Dynamics (CFD) has often been recognised as a promising approach to characterise and optimise hydrodynamics in biological processes (Wicklein et al. 2016, Wu 2013). However, only few studies have focused on gas-mixed anaerobic digesters (Coughtrie et al. 2013, Dapelo et al. 2015, Dapelo and Bridgeman 2018a, Karim et al. 2007, Vesvikar and Al-Dahhan 2005, Wu 2010b). Vesvikar and Al-Dahhan (2005) developed a 3D model to simulate a digester based on a lab-scale experimental study (Karim et al. 2004). A good qualitative agreement to the experimental data was reported, and specific configurational factors were investigated for reducing the poorly-mixed space. Simulations with more configurational modification were carried out using the finite element method (Karim et al. 2007). In addition, some numerical influencing factors on hydrodynamics were considered, including Reynolds-Averaged-Navier-Stokes (RANS) models for turbulence (Coughtrie et al. 2013, Wu 2010b), and single/multiphase approaches for gas-liquid flow (Coughtrie et al. 2013, Dapelo et al. 2015, Dapelo and Bridgeman 2018a).

In the gas-mixed digesters, sludge flow and mixing are mainly driven by energy from the gas-sparging. Therefore, a proper characterisation of the phase interaction between gas and liquid (sludge) is crucial. However, in the aforementioned studies, the two-phase flow modelling was still limited with considerable simplifications and uncertainties. Some studies eliminated the two-phase interaction region and essentially simulated a single-phase flow (Coughtrie et al. 2013, Karim et al. 2007). Although sludge rheology has been recognised as important for design and operation of sludge treatment processes (Eshtiaghi et al. 2013), no rheological measurements of the used sludge were reported (Karim et al. 2007). Hence, different types of liquids were used, including Newtonian (Coughtrie et al. 2013, Vesvikar and Al-Dahhan 2005) and non-Newtonian fluids (Karim et al. 2007, Wu 2010b), to validate the same experimental data (Karim et al. 2004). Despite the different used rheology, similar good agreements were reported. Moreover, the model validations were incomplete involving only a part of the experimental results, thus not convincing enough. Although a more detailed model validation was done by Dapelo et al. (2015), the studied reactor was essentially a bubble column with a bottom-mounted nozzle (Dapelo et al. 2015, Dapelo and Bridgeman 2018a), different from the full scale digesters with vertical-hanging gas lances.

Therefore, the aforementioned description of the two-phase flow and limited model validation, should be improved. This study aimed at developing a reliable CFD model in a scaled-down digester, in order to further guide process assessment and optimisation in scaled-up systems. The focus was on modelling the gas-sludge interaction process, and detailed model validation and mixing evaluations were carried out.

4.2 Materials and Methods

4.2.1 Computational domain and mesh

A computational domain was created based on the gas-lift digester studied by Karim et al. (2004), which was a 7.2 L cylindrical tank concentrically mounted with a gas injection pipe (0.5 cm inner diameter) and a draft tube (4.4 cm inner diameter) (Karim et al. 2004). More detailed information is given in Fig. 4-1A. Considering the geometry and layout, a 2D axisymmetric domain was developed. As shown in Fig. 4-1B, a central axis is used, a free surface for the liquid phase is defined at the top, and the other boundaries are constructed according to the original design.

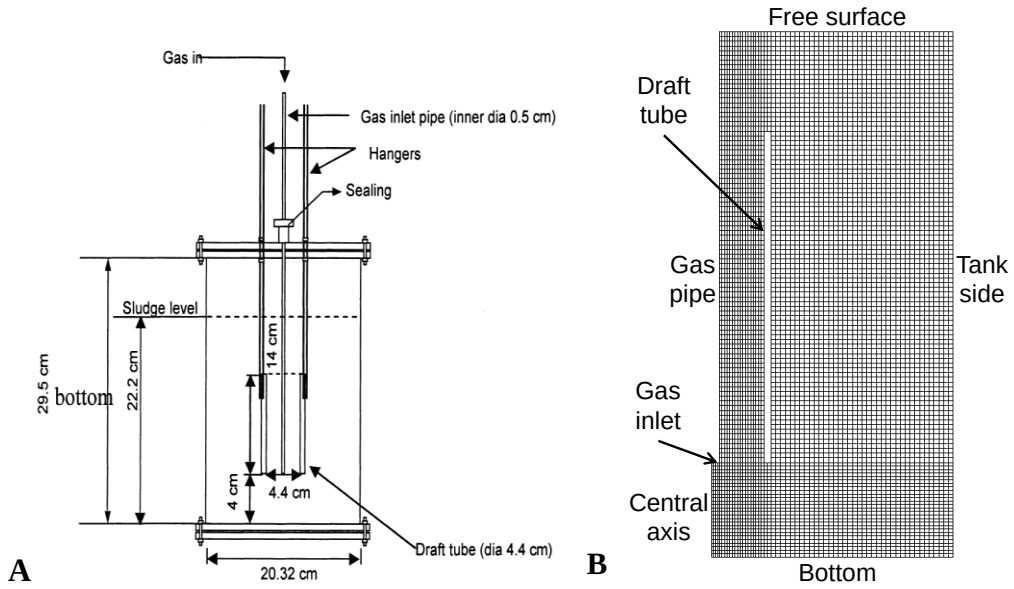

Fig. 4-1 (A) Digester geometry (Karim et al. 2004), and (B) the computational domain with boundaries and typical mesh in this study.

Structured grids were used for meshing, and finer grids were applied within the sensitive regions of phase interaction around the gas pipe and the draft tube (Fig. 4-1B). To check grid independency, 5 characteristic grid sizes (A through E) from coarse to fine were created, which are shown in Table 4-1.

Table 4-1 Mesh setting by 5 characteristic grid sizes.

Mesh	**A**	**B**	**C**	**D**	**E**
Characteristic size (mm)	3.3	1.8	1.1	0.8	0.5
Number of grid cells	2.0×10^3	6.7×10^3	1.9×10^4	3.5×10^4	7.6×10^4

4.2.2 Governing equations and models

Considering the focus on bubbly flow and not on single bubble motion, an Eulerian-Eulerian model was utilised, in which the gas phase is treated as a continuum, similar to the liquid phase. For the sake of simplicity, solid particle motion, interfacial mass transfer and heat transfer were neglected, and a single bubble diameter set for the gas phase. Transient simulations were implemented. Hence, the governing equations given below were solved for each phase.

Volume fraction equation

The volume of each phase in a control cell is determined as

$$V_i = \int_V \alpha_i \, dV \tag{4-1}$$

$$\sum_{i=1}^{N} \alpha_i = 1 \tag{4-2}$$

where V denotes the volume, α the volume fraction, N the total number of phases, and subscript i refers to the phase (liquid or gas).

Mass conservation equation

$$\frac{\partial}{\partial t}(\alpha_i \rho_i) + \nabla \cdot (\alpha_i \rho_i \overrightarrow{v_i}) = 0 \tag{4-3}$$

where ρ denotes the density, and $\vec{v}$ denotes the velocity.

Momentum conservation equation

$$\frac{\partial}{\partial t}(\alpha_i \rho_i \overrightarrow{v_i}) + \nabla \cdot (\alpha_i \rho_i \overrightarrow{v_i} \ \overrightarrow{v_i}) = -\alpha_i \nabla p + \nabla \cdot \alpha_i \boldsymbol{\tau}_i + \alpha_i \rho_i \vec{g} + \vec{F}_{PI,i} \tag{4-4}$$

$$\vec{F}_{PI,i} = \vec{F}_{D,i} + \vec{F}_{L,i} + \vec{F}_{T,i} \tag{4-5}$$

where p denotes the pressure, $\boldsymbol{\tau}$ the stress-strain tensor, and $\vec{g}$ the gravitational acceleration. $\vec{F}_{PI}$ denotes the phase interaction forces between the gas and the liquid per unit volume, in which drag force $\vec{F}_D$, lift force $\vec{F}_L$ and turbulent dispersion force $\vec{F}_T$ are taken into account. Specific models were applied to close these phase interaction forces.

Models for phase interaction forces

1) Drag force

The drag force is represented by solving the interphase momentum exchange term from the gas phase g to the liquid phase l, as expressed in Equation 4-6.

$$\vec{F}_{D,l} = \frac{\rho_g f_D}{6 t_g} d_g A_{in} \left(\overrightarrow{v_g} - \overrightarrow{v_l}\right) \tag{4-6}$$

where t_g denotes the particulate relaxation time, d_g the diameter of the secondary (gas) phase, μ_l the dynamic viscosity of the primary (liquid) phase, and A_{in} the interfacial area per unit mixture volume.

$$t_g = \frac{\rho_g {d_g}^2}{18 \mu_l}; \quad A_{in} = \frac{6 \alpha_g (1 - \alpha_g)}{d_g} \tag{4-7}$$

The drag function f_D is solved by the Schiller and Naumann Model (Naumann and Schiller 1935).

$$f_D = \frac{C_D Re_g}{24} \tag{4-8}$$

where Re_g denotes the relative Reynolds number (Equation 4-9), and C_D the drag coefficient (Equation 4-10).

$$Re_g = \frac{\rho_l |\overrightarrow{v_g} - \overrightarrow{v_l}| d_g}{\mu_l} \tag{4-9}$$

$$C_D = \begin{cases} \frac{24}{Re_g}\left(1 + 0.15 {Re_g}^{0.687}\right) & Re_g \leq 1000 \\ 0.44 & Re_g > 1000 \end{cases} \tag{4-10}$$

2) Lift force

The lift force stems from velocity gradients of the primary phase, and is expressed as

$$\vec{F}_{L,l} = -C_L \rho_l \alpha_g \left(\overrightarrow{v_l} - \overrightarrow{v_g}\right) \times \left(\nabla \times \overrightarrow{v_l}\right) \tag{4-11}$$

where C_L denotes the lift coefficient and is defined by the Legendre-Magnaudet model (Legendre and Magnaudet 1998).

$$C_L = \sqrt{{C_{L,lowRe}}^2 + {C_{L,highRe}}^2} \tag{4-12}$$

where $C_{L,\,lowRe}$, $C_{L,\,highRe}$ and Sr denotes the parameters in the model:

$$\begin{cases} C_{L,lowRe} = \frac{6}{\pi^2} \frac{2.55}{\left(Re_g Sr\right)^{0.5}\left(1 + 0.2\frac{Re_g}{Sr}\right)^{1.5}} \\ C_{L,lowRe} = \frac{1 + 16 {Re_g}^{-1}}{2\left(1 + 29 {Re_g}^{-1}\right)} \end{cases} ; \quad Sr = \frac{Re_\omega}{Re_g}; \quad 0.1 < Re_g < 500 \tag{4-13}$$

and Re_ω the vorticity Reynolds number:

$$Re_\omega = \frac{\rho_l |\nabla \times \overrightarrow{v_l}| {d_g}^2}{\mu_l} \tag{4-14}$$

3) Turbulent dispersion force

The turbulent dispersion force is related to the effect of interphase turbulent momentum transfer, solved using the Lopez de Bertodana Model (de Bertodano 1991).

$$\vec{F}_{T,l} = -\vec{F}_{T,g} = C_T \rho_l k_l \nabla \alpha_g \tag{4-15}$$

where C_T denotes a constant (generally set to 1), and k_l the turbulent kinetic energy of the liquid phase, which is calculated by solving the k-ε model.

Turbulence closure

Regarding the reported considerable turbulent kinetic energy (Karim et al. 2004), turbulence needed to be modelled. In this process, turbulence originates from the large velocity differences induced by gas-sparging, which is strongly correlated to bubbly regions. Moreover, modified RANS models have been found to be appropriate for a low-*Re* non-

Newtonian flow (Wu 2010d). Considering the localised bubbly and turbulent distribution, the RNG k-ε Mixture Turbulence model was applied, which is more suitable to (nearly) stratified and low-*Re* multiphase flows (Orszag et al. 1993).

$$\frac{\partial}{\partial t}(\rho_m k) + \nabla \cdot (\rho_m \overrightarrow{v_m}\ k) = \nabla \cdot \left(\alpha_k \mu_{eff} \nabla k\right) + G_{k,m} - \rho_m \varepsilon \tag{4-16}$$

$$\frac{\partial}{\partial t}(\rho_m \varepsilon) + \nabla \cdot (\rho_m \overrightarrow{v_m}\ \varepsilon) = \nabla \cdot \left(\alpha_\varepsilon \mu_{eff} \nabla \varepsilon\right) + C_{1\varepsilon} \frac{\varepsilon}{k} G_{k,m} - \rho_m C_{2\varepsilon}{}^* \frac{\varepsilon^2}{k} \tag{4-17}$$

where α_k and α_ε are the inverse effective Prandtl numbers for *k* and *ε*, respectively ($\alpha_k=\alpha_\varepsilon$ ≈1.393 for high *Re*). In this model, mixture (denoted by m) properties of both phases are involved and are computed from Equation 4-18.

$$\begin{cases} \rho_m = \sum_{i=1}^{n} \alpha_i \rho_i \\ \mu_m = \sum_{i=1}^{n} \alpha_i \mu_i \\ \overrightarrow{v_m} = \frac{\sum_{i=1}^{n} \alpha_i \rho_i \overrightarrow{v_i}}{\rho_m} \\ G_{k,m} = \mu_{t,m}(\nabla \overrightarrow{v_m} + \nabla(\overrightarrow{v_m})^T) : \nabla \overrightarrow{v_m} \end{cases} \tag{4-18}$$

where $G_{k,m}$ denotes the production of *k*. The Differential Viscosity Model was applied to better solve low-*Re* flows, so the effective viscosity μ_{eff} is computed from a differential equation, in which parameters $\hat{\mu}$ and C_v are involved:

$$d\left(\frac{\rho_m{}^2 k}{\sqrt{\varepsilon \mu_m}}\right) = 1.72 \frac{\hat{\mu}}{\sqrt{\hat{\mu}^3 - 1 + C_v}} d\hat{\mu};\ \ \hat{\mu} = \frac{\mu_{eff}}{\mu_m};\ \ C_v \approx 100 \tag{4-19}$$

The parameter $C_{2\varepsilon}{}^*$ is calculated by Equation 4-20.

$$C_{2\varepsilon}{}^* = C_{2\varepsilon} + \frac{C_\mu \eta^3 (1 - \eta/\eta_0)}{1 + \beta \eta^3};\ \ \eta = S\frac{k}{\varepsilon};\ \ S = \sqrt{2 S_{ij} S_{ij}};\ \ S_{ij} = \frac{1}{2}\left(\frac{\partial u_j}{\partial x_i} + \frac{\partial u_i}{\partial x_j}\right) \tag{4-20}$$

The other constants are shown below:

$$C_{1\varepsilon} = 1.42;\ \ C_{2\varepsilon} = 1.68;\ \ C_\mu = 0.0845;\ \ \eta_0 = 4.38;\ \ \beta = 0.012$$

Due to the finer grids, the first grid layer attaching wall boundaries could be in the viscous sub-layer of turbulence (Y^+<5). Hence, an Enhanced Wall Function was applied to correctly calculate the near-wall region flow field covering both linear and logarithmic patterns.

Phases

The detailed phase physical properties are shown in Table 4-2. For the primary phase, different fluids were used, including Newtonian (water) and non-Newtonian (sludge 1 and 2) that were described by the power law.

$$\mu = K\dot{\gamma}^{n-1} \tag{4-21}$$

where *K* denotes the flow consistency index, $\dot{\gamma}$ the shear rate, and *n* the flow behaviour

(power-law) index. Sludge 1 data were from literature (Achkari-Begdouri and Goodrich 1992). Sludge 2 was the waste activated sludge sampled from Wastewater Treatment Plant De Groote Lucht (The Netherlands); the rheology was measured according to our previous work (Wei et al. 2018), and total solids (TS) were measured according to standard methods (APHA 2012). The secondary phase was set as spherical air bubbles, with a diameter in the range of 1-10 mm.

Table 4-2 Physical properties of the applied phases.

Phase		Density (kg/m^3)	Rheology			Total Solids (%)	Diameter (mm)
			K ($Pa \cdot s^n$)	n	μ (Pa·s)		
	Water	998	-	1	0.001	0	-
Liquid	Sludge 1	1001	0.192	0.56	0.010-0.030	5.4	-
	Sludge 2	1002	18.5	0.30	0.11-2.84	4.9	-
Gas	Air	1.225	-	-	1.79×10^{-5}	-	1-10

Euler-Lagrange method

An Euler-Lagrange method was applied to track particle trajectories and evaluate the mixing. Spherical particles with the same settings to the experiment (Karim et al. 2004) were used in a one-way coupling simulation. The turbulence dispersion (by Discrete Random Walk model), virtual mass and pressure gradient effects on particles were considered. Thus the particle motion is solved by:

$$\frac{\partial \overrightarrow{v_{pt}}}{\partial t} = \frac{\overrightarrow{v_l} - \overrightarrow{v_{pt}}}{\tau_{pt}} + \overrightarrow{F_{VM}} + \overrightarrow{F_{PG}} + \overrightarrow{F_{SL}};\ \ v_l = \overline{v_l} + \zeta\sqrt{\frac{2k}{3}};\ \ \tau_{pt} = \frac{\rho_{pt} d_{pt}^2}{18\mu_l}\frac{24}{C_d Re_{pt}} \tag{4-22}$$

where the subscript *pt* denotes the particles, $\overline{v_l}$ the mean velocity, ζ a normally distributed random number, and τ_{pt} the particle relaxation time. The virtual mass force (F_{VM}), pressure gradient force (F_{PG}) and Saffman lift force (F_{SL}) in unit volume are solved by:

$$\begin{cases} \overrightarrow{F_{VM}} = C_{VM}\frac{\rho_l}{\rho_{pt}}\left(\overrightarrow{v_{pt}}\cdot\nabla\overrightarrow{v_l} - \frac{d\overrightarrow{v_{pt}}}{dt}\right) \\ \overrightarrow{F_{PG}} = \frac{\rho_l}{\rho_{pt}}\overrightarrow{v_{pt}}\cdot\nabla\overrightarrow{v_l} \\ \overrightarrow{F_{SL}} = 81.2\rho_l {d_{pt}}^2(\dot{\gamma}\nu_l)^{0.5}\left(\overrightarrow{v_l} - \overrightarrow{v_{pt}}\right) \end{cases} \tag{4-23}$$

where C_{VM} is the virtual mass coefficient (= 0.5), and ν_l the liquid kinematic viscosity. A larger number of particles (9063) were released and tracked at different gas flow rates.

4.2.3 Boundary conditions

Involved boundary conditions included axisymmetric centreline, velocity inlet, degassing top and wall. The axisymmetric centreline was set for creating a 3D axisymmetric circumstance. The velocity inlet was for gas injection. The degassing top was for discharging the gas phase while retaining the liquid phase. The wall condition including no-slip for liquid and free-slip for gas was set at the other boundaries.

4.2.4 Main simulation settings

In the transient simulations, time step setting obeyed the Courant-Friedrichs-Lewy (CFL) condition and the first order implicit scheme was used. The Phase Coupled Semi-implicit method for pressure linked equations (SIMPLE) scheme was utilised for pressure-velocity coupling. High order schemes including second order Upwind, Quadratic interpolation for convective kinetics (QUICK) (Leonard and Mokhtari 1990) and Monotonic upstream-centered scheme for conservation laws (MUSCL) (van Leer 1979) were set for improving simulation accuracy. Regarding the relatively complicated process modelled and performance achieved, the simulations were done in a stringent way with satisfactory convergence: 1) a desired criterion of 1×10^{-5} was used for residuals of most parameters, while a more reasonable order of 10^{-4} was used for the continuity and gas velocity residuals; because residual values of the aforementioned parameters were difficult to reach 1×10^{-5}, even using a quite small time step of 1×10^{-6} s (1×10^{-4} s already fits the CFL condition). 2) the gas mass flow rate and liquid flux were also monitored and achieved satisfactory balance (imbalance < 5%). The simulations were implemented using the commercial package ANSYS-Fluent 16.2 mainly on a Dell Optiplex 7010 computer, with Intel Core i5-3740 and 8 GB RAM. When running two parallel processors, the computational time ranged between 1 and 10 days.

4.3 Results and Discussion

4.3.1 Grid independence test

A grid independence test was performed first, using the Grid Convergence Index (GCI) method (Celik et al. 2008, Roache 1994). The axial velocities at heights of 11.25 cm and 18.25 cm were used for the assessment. Mesh D and E were found to have quite similar profiles and values of the velocity; and the GCI results (GCI_{CD}: 3.3±3.5%, GCI_{DE}: 0.7±1.1%)

were in an asymptotic range close to 1 (1.02±0.02), indicating that the grid independence was achieved. Considering smaller number of grid cells and less computational consumption, Mesh D was selected as optimal for the following simulations. The detailed results and interpretation can be found in the Supplementary Material (Fig. S-3 and Table S-5).

4.3.2 Impacts of uncertain parameters on flow field

4.3.2.1 Bubble size

As mentioned in the Introduction, several uncertainties needed to be investigated. Although no experimental data are available to support, proper identification of a characteristic bubble size is important in the model calculations. To achieve a clear estimation, only the drag force was applied for phase interaction, and two distinct fluids water (Newtonian) and sludge 1 (non-Newtonian (Achkari-Begdouri and Goodrich 1992)) were used.

According to the references (Lehr et al. 2002, Polli et al. 2002, Schäfer et al. 2002, Vesvikar and Al-Dahhan 2005, Wu 2010b), bubbles with diameters ranging from 1 mm to 10 mm can be expected. Fig. 4-2 shows the liquid axial velocity profiles at 1/2 depth, zooming in inside the draft tube. Although the peak became smaller, similar velocity profiles of the water were obtained as the bubble size increased, especially larger than 3 mm (Fig. 4-2A). However, different profiles were obtained in sludge 1. As the bubble size increased, a more substantial decrease was found in the peak value, and the peak position also moved further from the centreline (Fig. 4-2B). Similar tendencies were found at the other heights in both fluids (data not shown).

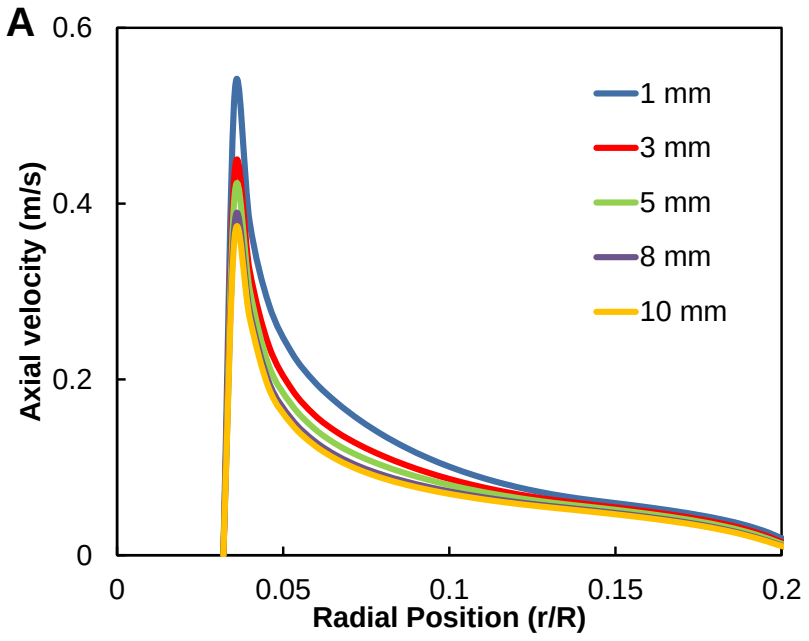

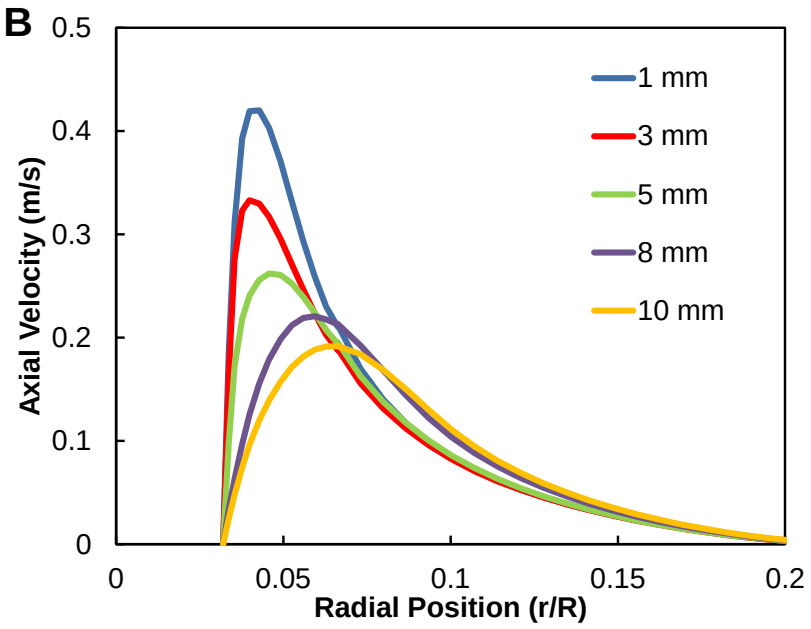

Fig. 4-2 Liquid axial velocity profiles of different bubble sizes inside the draft tube in (A) water and (B) sludge 1 at 11.25 cm height; gas flow rate 28.32 L/h.

The velocity independency on the bubbles over 3 mm agreed with a previous study using water as well (Vesvikar and Al-Dahhan 2005), in which the corresponding bubble size was 2 mm, and 10 mm was set in their simulations. However, the velocity was quite sensitive to the bubble size in sludge 1. Hence, the bubble size setting (1 mm) in the study of Wu (2010) (Wu 2010b) using the same sludge data needs to be evaluated; in experimental measurements, the characteristic bubble sizes in free air-water bubbly flow were reported from 1-5 mm (Lehr et al. 2002, Polli et al. 2002, Schäfer et al. 2002). Moreover, the bubble size was found to increase with the liquid apparent viscosity (Schäfer et al. 2002). Therefore, the bubble size settings in previously reported simulations were not suitable: 10 mm (Vesvikar and Al-Dahhan 2005) seemed too big for water and 1 mm (Wu 2010b) too small for sludge. Considering the typical bubble sizes in reality and the apparent viscosity influence, 5 mm was set in the following simulations.

4.3.2.2 Phase interaction forces

Presence of the pipe and the draft tube in the studied digester created more changes in the local liquid velocity than that in conventional bubble columns; as mentioned in Section 2.2, the bubbly process induces high velocity differences and fluctuations. Hence, several potential influences related to velocity gradient and turbulence need to be considered. Compared to the previous studies (Coughtrie et al. 2013, Vesvikar and Al-Dahhan 2005, Wu

2010b), more phase interaction forces, including lift force and turbulent dispersion force, were involved in this study.

As shown in Fig. 4-3A and B, with the addition of the lift force and/or the turbulent dispersion force, both water and sludge 1 get a lower but wider velocity peak inside the draft tube and a stronger flow outside, even though the liquid phase got low *Re* (10^2). The discrepancy was also reflected in gas phase distribution results, in which the gas phase was distributed over a much larger domain when applying all the forces (Fig. 4-3C). Hence, the results indicated important roles for the two forces, leading to broaden the distribution of the gas phase and the liquid flow.

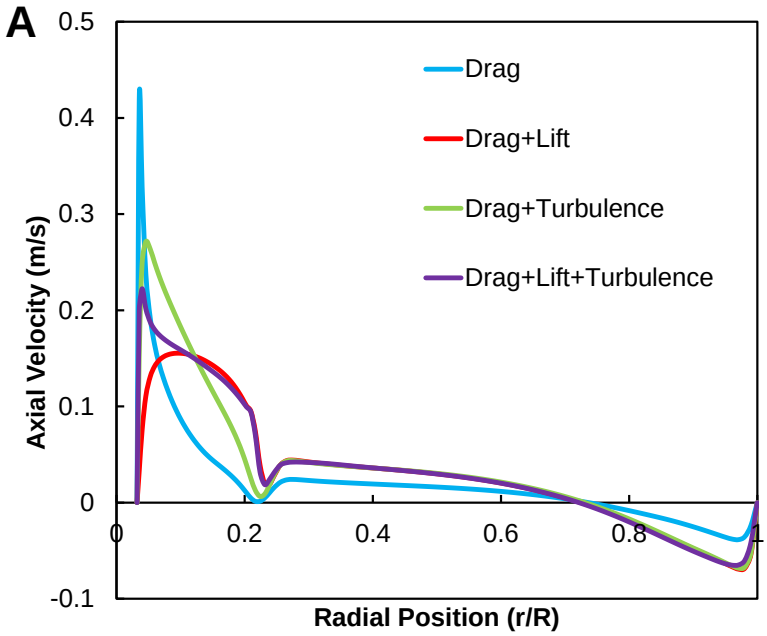

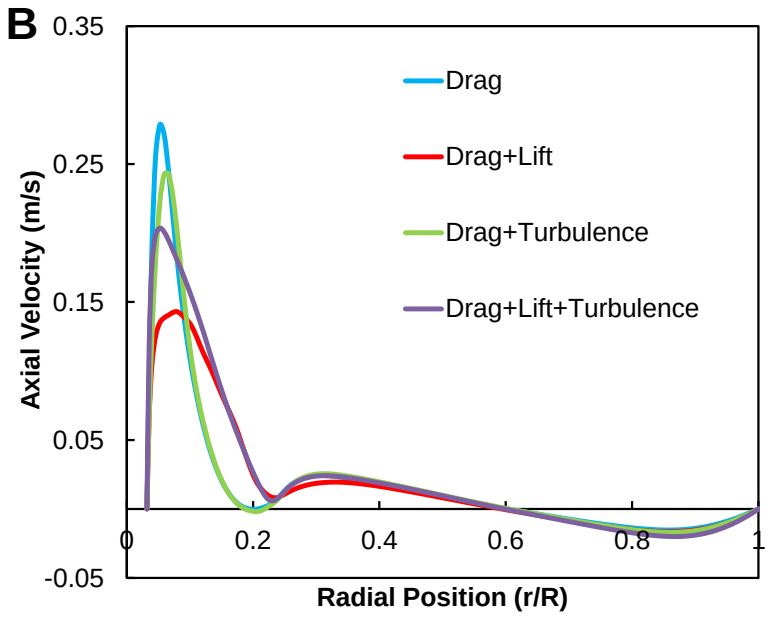

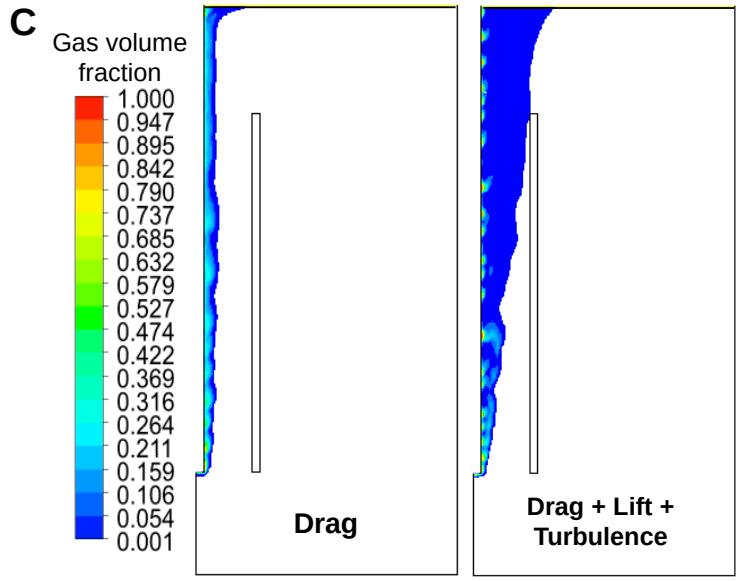

Fig. 4-3 Results of applying different phase interaction forces: axial velocity profiles of (A) water and (B) sludge 1 at 18.25 cm height, and (C) gas phase distribution in sludge 1; gas flow rate 28.32 L/h.

Unlike buoyancy and the drag force causing vertical rising, the lift force accounted for horizontal bubble motion. As shown in Fig. 4-3, the sharp velocity gradient in the near-pipe region ($r/R<0.05$) can result in a considerable bubble dispersion and turbulence, which further induces more liquid flows. However, the more viscous sludge 1 weakened this effect, leading to a smaller velocity change than that of the water. Furthermore, a similar tendency was found by applying larger bubbles and only the drag force in sludge 1 (Fig. 4-2B), which might result from the shear-rate-dependent rheological behaviour. Hence, for a non-Newtonian fluid, the high velocity differences not only induced more phase interaction forces, but also led to localised differences in the apparent viscosity, making the two-phase flow more complicated.

4.3.2.3 Liquid apparent viscosity

Sludge 2 measured in this study was also used to investigate the impact of apparent viscosity. Regarding the reported 4.5% (Karim et al. 2004), sludge 1 and 2 had comparable TS concentrations, but distinct rheological behaviour, due to the sludge origin (Table 4-2).

As shown in Fig. 4-4, the predicted velocity is quite different: sludge 1 shows a more constrained flow than the water, demonstrated by a narrowed velocity profile inside the draft tube, and a smaller vortex outside with a separation point (the liquid velocity is zero and changes direction) closer to the centreline. Moreover, an extremely constrained flow was

found for the much more viscous sludge 2 without the induced vortex or flow. The flow field change also indicated a trend to a highly concentrated and unrealistic gas phase distribution, implying the limitation of the Eulerian-Eulerian method for extremely viscous fluids.

These results were different from previously reported results, in which it was described that a rheological change did not affect mixing behaviour significantly (Karim et al. 2007). It should be noted that in the latter study two fluids were applied that had comparable apparent viscosities (pseudoplastic: 2-9 mPa·s and dilatant: 8-32 mPa·s ($\dot{\gamma}$ range 1-1000 s^{-1})). This is not large enough to cover the rheological differences found in practice. As illustrated in our study, a change in sludge rheology could lead to a quite different flow pattern under the same gas-sparging conditions. It can be concluded that accurate characterisations of sludge rheology are crucial for proper flow prediction and mixing evaluation.

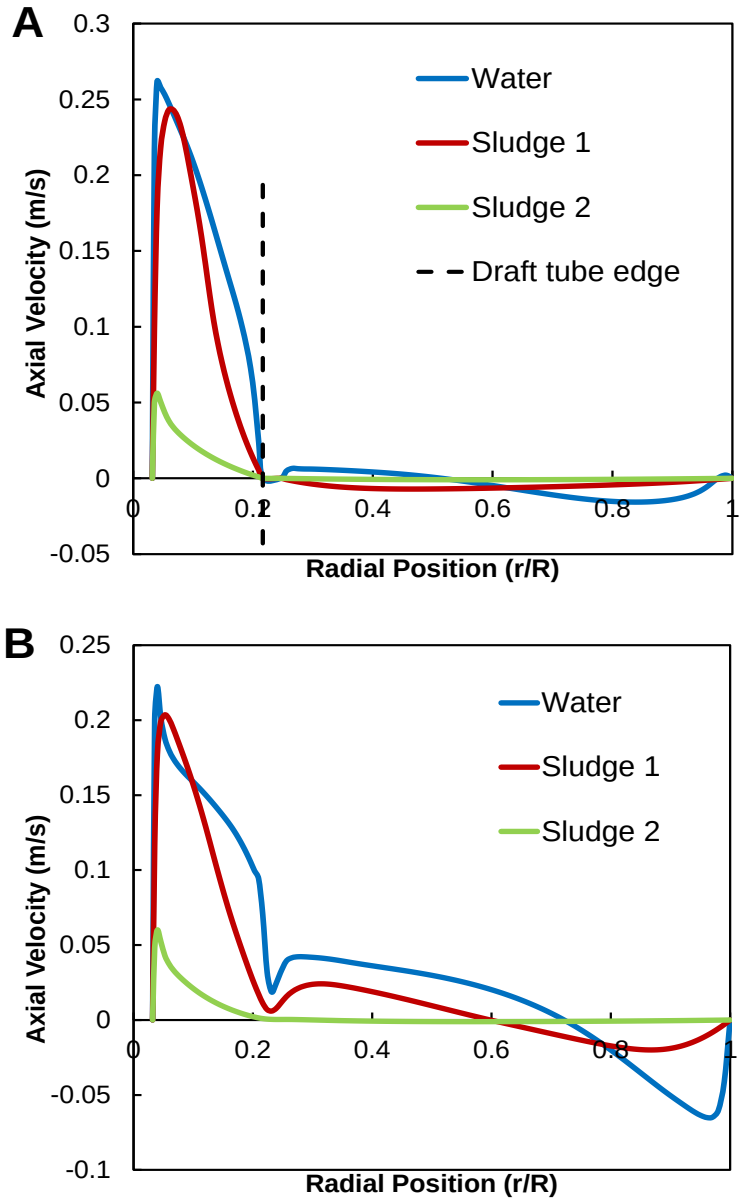

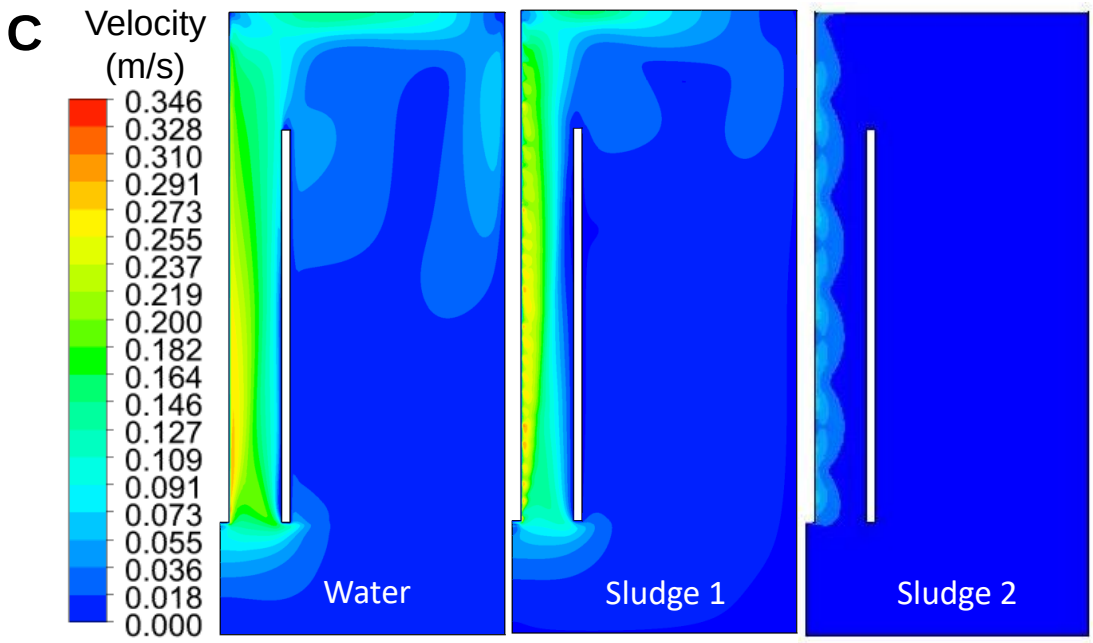

Fig. 4-4 Velocity of water, sludge 1 and sludge 2, profiles at heights of (A) 11.25 cm, (B) 18.25 cm, and (C) contours in the whole domain; gas flow rate 28.32 L/h.

4.3.3 Validation and further prediction

Considering the aforementioned incomplete validation in the previous research (Coughtrie et al. 2013, Karim et al. 2007, Vesvikar and Al-Dahhan 2005, Wu 2010b), and the sensitive impacts on the flow field found in Section 3.2, the validation of the proposed model was improved.

4.3.3.1 Velocity field

Compared to the experimental velocity field in the whole domain (Karim et al. 2004), general flow patterns were in agreement, including the vortex, the major recirculation loop, and the strong/weak flow locations. However, consistent with Section 3.2, discrepancies were considerable between the water and sludge 1. Highly similar to the previous study using water as well (Vesvikar and Al-Dahhan 2005), as shown in Fig. 4-5, the water has a big vortex covering over one half of the whole depth, and the vortex centre is at 17.5 cm height, lower than the top of the draft tube. However, the measured vortex was smaller, covering one third of the whole depth and having a higher centre (19.25 cm height). Hence, this considerable overestimation of the flow cannot be used to conclude a good agreement as reported (Vesvikar and Al-Dahhan 2005). Although predicting a slightly constrained flow field with a smaller vortex closer to the centreline, sludge 1 showed a better approximation. It indicated

that the unreported apparent viscosity of the experimental sludge might have been between that of the water and sludge 1, even better resembling sludge 1.

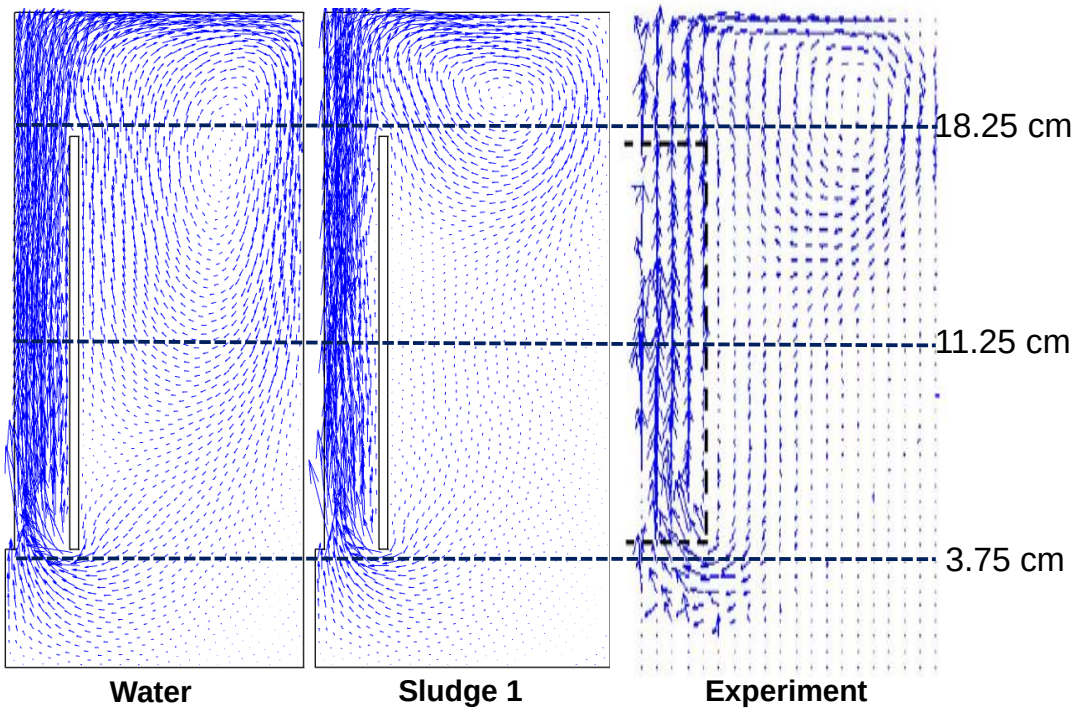

Fig. 4-5 Simulated and experimental (Karim et al. 2004) velocity fileds in the digester, gas flow rate 84.96 L/h.

The axial velocity profiles of sludge 1 at three heights labelled in Fig. 4-5 are shown in Fig. 4-6. Considering the uncertain settings discussed above, the overall agreement was satisfactory. For all gas flow rates, the velocity outside the draft tube (r/R>0.22) only showed small differences with the almost fixed separation point (0.64) that was smaller than the measured 0.71 (Karim et al. 2004). It confirmed the slightly constrained flow mentioned above, and also indicated the difficulty to further enhance this part of the flow under the given gas-sparging conditions. However, more discrepancies were found inside the draft tube, which are further discussed in Section 3.3.3.

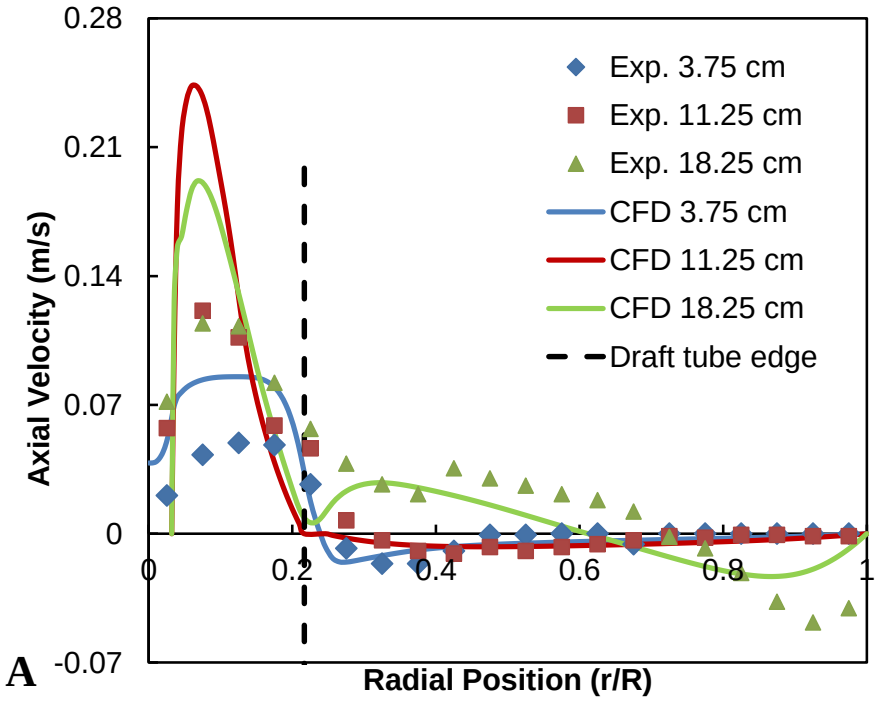
0.28
0.21
0.14
0.07
0
-0.07
Axial Velocity (m/s)
0
0.2
0.4
0.6
0.8
1
Radial Position (r/R)
Exp. 3.75 cm
Exp. 11.25 cm
Exp. 18.25 cm
CFD 3.75 cm
CFD 11.25 cm
CFD 18.25 cm
Draft tube edge
A

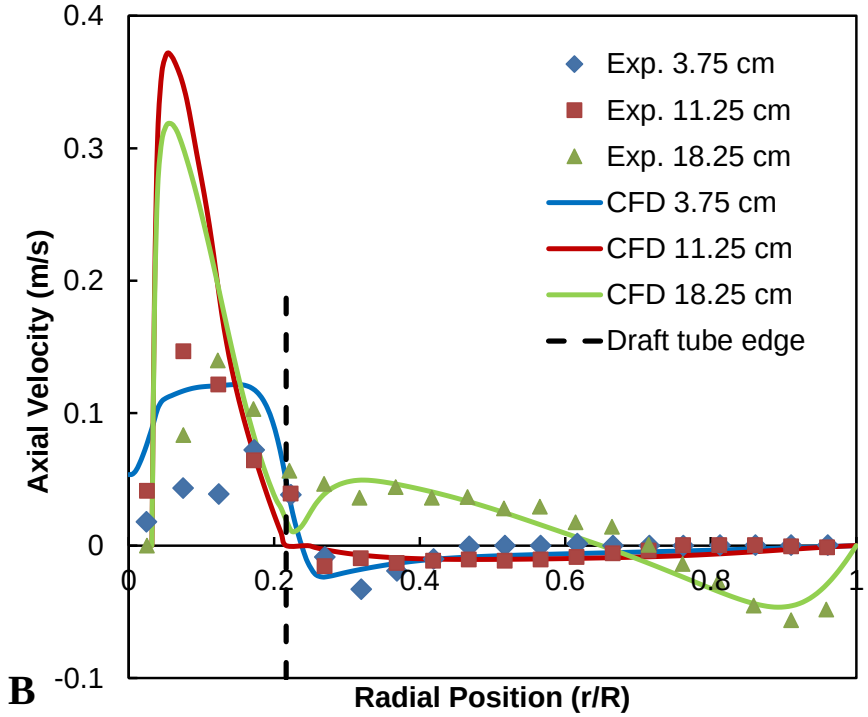
0.4
0.3
0.2
0.1
0
-0.1
Axial Velocity (m/s)
0
0.2
0.4
0.6
0.8
1
Radial Position (r/R)
Exp. 3.75 cm
Exp. 11.25 cm
Exp. 18.25 cm
CFD 3.75 cm
CFD 11.25 cm
CFD 18.25 cm
Draft tube edge
B

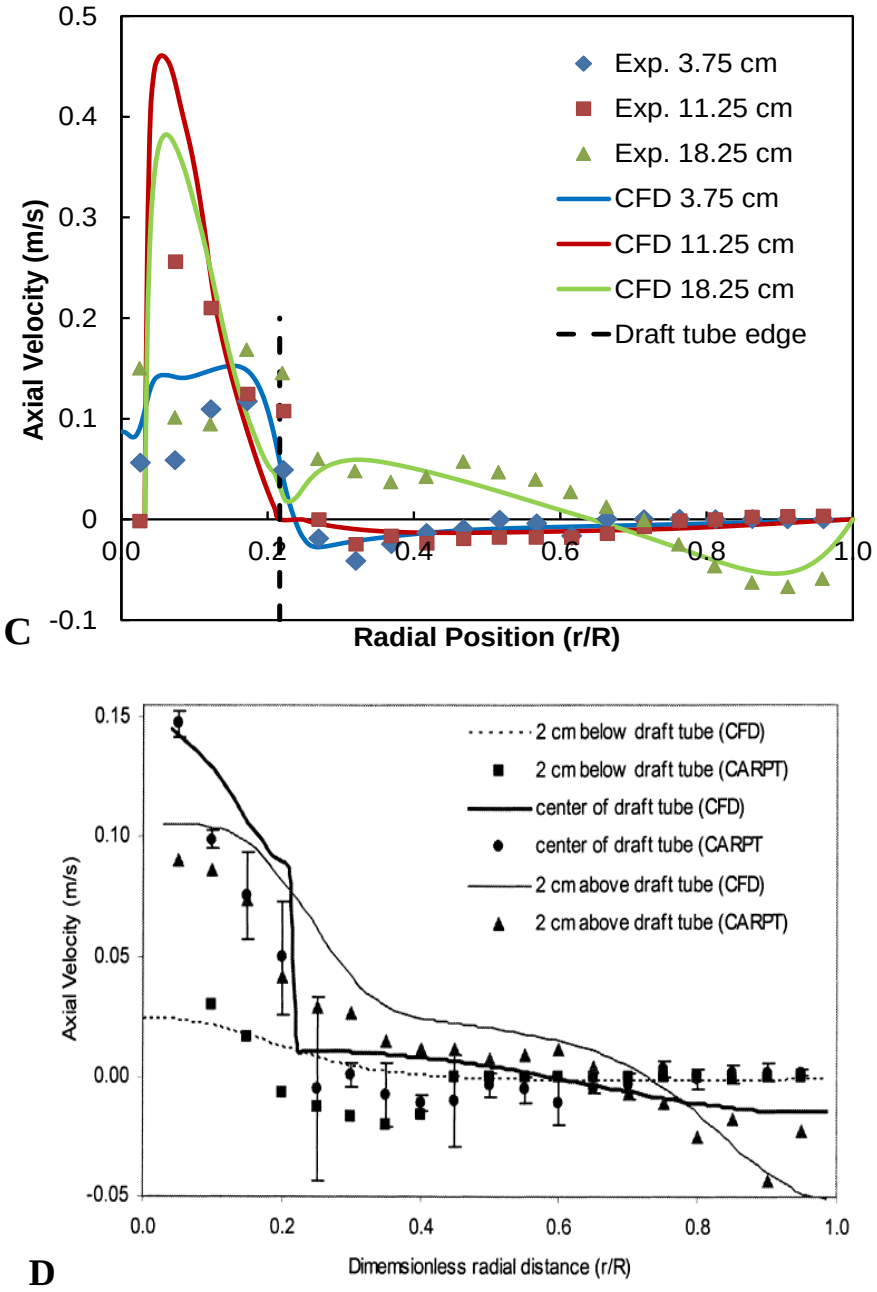

Fig. 4-6 Axial velocity profiles of sludge 1 and measurements (Karim et al. 2004) at 3 heights, gas flow rates of (A) 28.32 L/h, (B) 56.64 L/h, and (C) 84.96 L/h, and (D) the results of Vesvikar and Al-Dahhan (2005).

4.3.3.2 Gas phase distribution

Besides velocity field, gas holdup is another important indicator that has not been validated before. Most bubbles were observed to rise inside the draft tube and were mainly confined in the 1.8 mm radius central region (Karim et al. 2004), while almost no gas was detected

outside the draft tube (Karim et al. 2007). As shown in Fig. 4-7A, the gas phase plume, containing a cluster with high volume fractions (>0.2), is consistent with the descriptions above, and with other observations about separated rising bubbles without coalescence (Dapelo et al. 2015, Vesvikar and Al-Dahhan 2005). In Fig. 4-7B, the predicted maximum gas volume fraction of 0.53 at 20 cm height is comparable to the experimental value of 0.48 (Karim et al. 2004), which is much better than the value (<0.02) reported previously (Vesvikar and Al-Dahhan 2005).

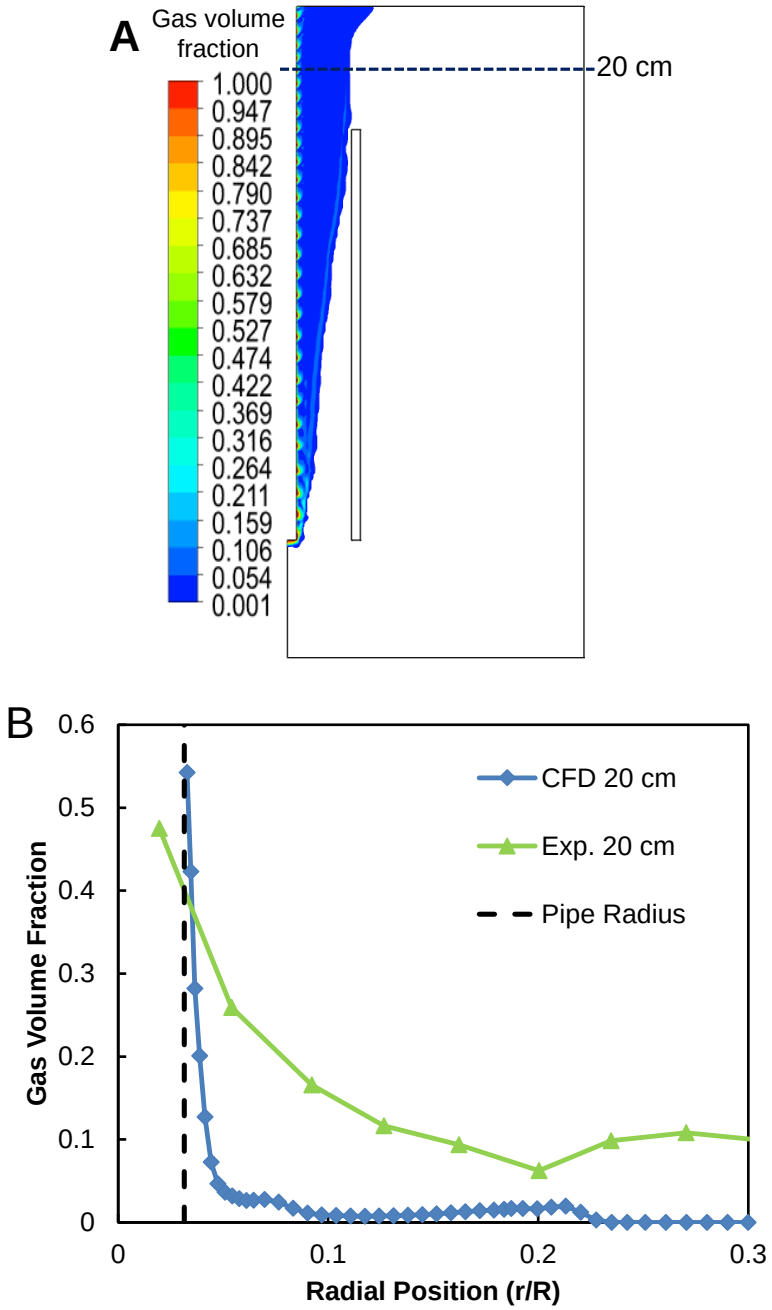

Fig. 4-7 (A) Predicted gas phase distribution in the whole domain, and (B) at 20 cm height combined with experimental data (Karim et al. 2004); gas flow rate 28.32 L/h.

Although a similar tendency with a small gas volume peak was predicted just above the draft tube (r/R = 0.21), the simulation demonstrated a more confined and highly underestimated gas distribution in the other parts of the reactor. To assess this large deviation, the experimental data accuracy had to be evaluated. The measured peak (at 1.8 mm) was positioned inside the pipe (radius 3.2 mm, the dash line in Fig. 4-7B), which seems incorrect. Additionally, a considerable portion of the gas holdup outside the draft tube was reported to result from data discontinuity (Karim et al. 2004). Hence, the deviation could have also originated from inaccurate data collection.

A conserved gas flux calculation (gas flux per cell = gas volume fraction × gas velocity) was performed for the simulation data, but couldn't be done for the experimental results due to lack of reported gas velocity data. The aforementioned rare bubble occurrence outside the draft tube correlated to a quite small effective gas velocity in the studied period, leading to a negligible effective contribution to the total gas flux. Hence, the dominant part of this balanced gas flux was still from the central region where most bubbles occurred and where the predicted and experimental data were close to each other. Additionally, the realistic random motion of a single bubble is essentially difficult to be represented by the applied Eulerian-Eulerian method with a RANS model, also resulting in the constrained gas phase distribution. Therefore, the large deviation in Fig. 4-7B did not mean a failure of the simulation; contrarily, the simulation results of the conserved gas phase had a peak in the key region and a bubbly pattern comparable to the experimental data, still indicating a good agreement.

4.3.3.3 Critical validation and further prediction of the flow field

Considering that the sludge used in the experiment was expected to be a little less viscous than sludge 1, the velocity deviation inside the draft tube requires some further discussion.

To assess data reliability, the flux balance of the liquid axial velocity was evaluated. As shown in Table 4-3, the simulation results were excellent with a mean imbalanced flux of 0.83 ± 0.75%; but the experimental data showed a large value of 11.3 ± 9.4%. The only measured dataset (in Fig. 4-7B) even got higher imbalanced flux values (in parentheses in Table 4-3), also implying that the measured gas holdup may not be accurate enough. In addition, the velocity data were not consistent in different studies, although from the same measurements (Karim et al. 2004, Vesvikar and Al-Dahhan 2005). As shown in Fig. 4-6, the experimental velocity profiles in D showed more discrepancies with A-C, having peaks closer to the centreline and a different profile above the draft tube. Moreover, Fig. 4-6A, B and C show considerable velocity values at the position of the draft tube at 11.25 cm height,

which does not obey the theoretical zero-velocity assumption on the no-slip walls. The large standard deviation bars of the velocity at the same height in Fig. 4-6D demonstrated strong fluctuations. Therefore, the accuracy and consistency of the experimental velocity data were not good enough, which was affected by the strong flow fluctuation and limited resolution inside the draft tube (only 4 data points).

Table 4-3 Imbalanced flux (%) of the axial velocity at the three heights, results in parentheses were based on the measured gas holdup data (Karim et al. 2004).

Gas flow rate (L/h)	Reference direction	3.75 cm		11.25 cm		18.25 cm	
		Exp.	CFD	Exp.	CFD	Exp.	CFD
28.32	upward	8.63	0.19	23.99	0.48	7.01	0.39
	downward	9.45	0.19	31.56	0.48	7.54	0.39
56.64	upward	21.94	0.21	4.36	1.43	5.60	0.96
	downward	28.10	0.21	4.18	1.41	5.30	0.97
84.96	upward	2.16	0.26	16.96	2.59	3.30(10.07)	1.00
	downward	2.22	0.26	20.42	2.52	3.19(9.14)	1.02

Unlike the previous research (Vesvikar and Al-Dahhan 2005, Wu 2010b), the validation in this study was not assessed only by the degree of overlap to the experimental data. Even achieving a high agreement, the obtained model may not be optimised if having no well-balanced mass/flux and some uncertain parameter settings. Hence, adjusting the model to obtain a perfect fit to the experimental data could be risky for any further application of the developed model, which must be carried out with care. The aforementioned deviation may also be related to the nature of the Eulerian-Eulerian method for the model. In the bubble-driven process, the bubbles-concentrated region, represented by a high gas volume fraction, can have a strong buoyancy effect. The generated large velocity difference across the gas-liquid interface can then induce strong shear and fluctuation of the liquid velocity. Hence, the positions of the high gas phase fraction (α_G), the high liquid velocity (v_L), and the strong momentum transfer ($F_{PI,L}$) are correlated. On one hand, measurements with 4 points may be too limited to characterise the quite localised and unstable bubble-induced flow inside the draft tube. On the other hand, the assumption of a fluid instead of separate bubbles for the gas phase, makes the Eulerian-Eulerian with RANS model not specific enough to simulate a bubble-induced non-Newtonian flow. However, the improved two-phase simulation presented in this study not only achieved good agreement with the experimental data, but also made reasonable corrections and further predictions of the hydrodynamics in detail.

Hence, the elaborated scaled-down model could be considered for further scale-up applications.

4.3.4 Mixing evaluation

Fig. 4-8A shows the typical particle trajectories in the simulation, and various paths are obtained in the particles labelled by different colours. Most formed big loops back into the draft tube, which agreed with the experimental data (Karim et al. 2004) shown in Fig. 4-8C. As shown in Fig. 4-8B, the typical instantaneous particle distribution is not homogeneous, but confined to form specific major paths. Some regions, including the big vortex, bottom and corner of the digester, showed almost no particles travelling. Mixing performance and RTD were mainly evaluated using particle recirculation time, defined as the time for a particle to return at the released position. Totally 9063 particles were tracked while applying three gas flow rates, and normalised particle number and time (θ) were applied, which referred to the total particle number and theoretical mean recirculation time, respectively. The ideal models of CSTR, plug-flow reactors (PFR) and laminar-flow reactors (LFR) were also used for evaluation.

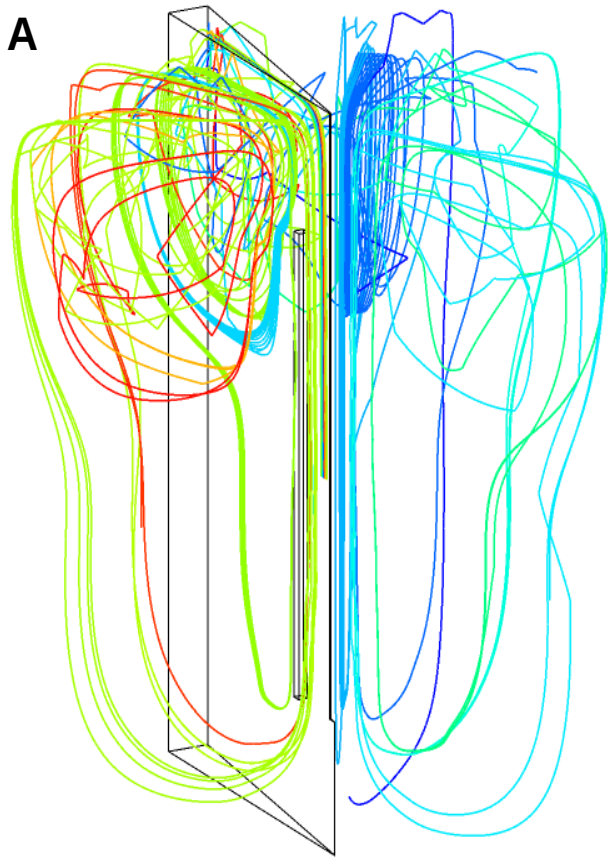

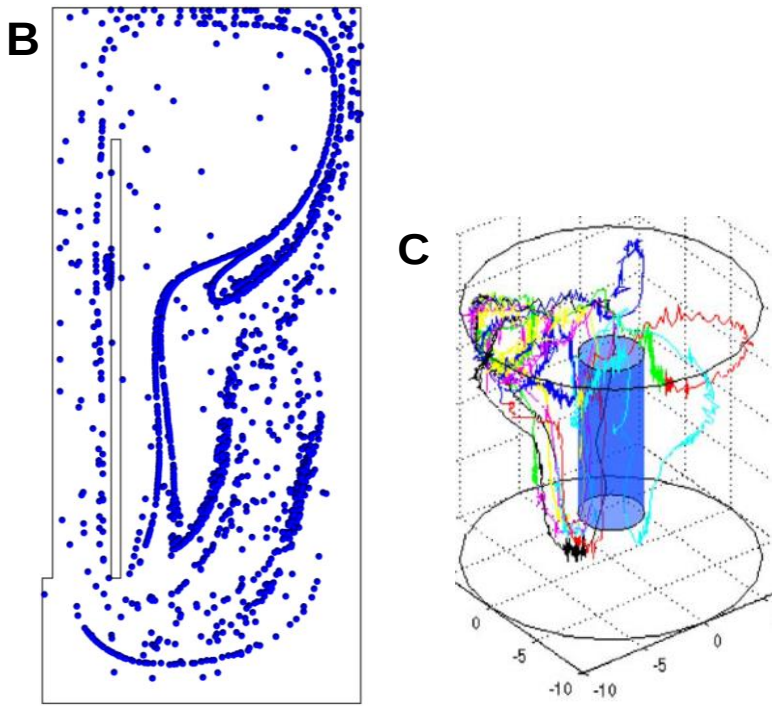

Fig. 4-8 (A) Predicted particle trajectories, (B) typical instantaneous distribution of 2000 particles, and (C) the relevant experimental data (Karim et al. 2004).

As shown in Fig. 4-9A, the major peaks are almost independent from the gas flow rates. However, one separated smaller peak (over θ =1) was found at 28.32 and 56.64 L/h, while a much smoother trend was found at 84.96 L/h. The results of key indicators for RTD and mixing in Table 4-4 showed similar short-circuiting indexes (θ_{10} and θ_p) smaller than the ideal models (0.5 for LFR and 1.0 for PFR), and a considerable increase in the mixing indexes (θ_{90}, θ_g, Morril index, Thirumurthi index and dispersion index) when the gas flow rate increased. This indicates the occurrence of short-circuiting and dead zones, part of which could be mitigated by increasing the gas flow rate, as can be seen from the decrease in number of small peaks. However, the enhancement of mixing and dispersion was limited, reflected by the limited change of the major particle recirculation time at increased gas flow rates.

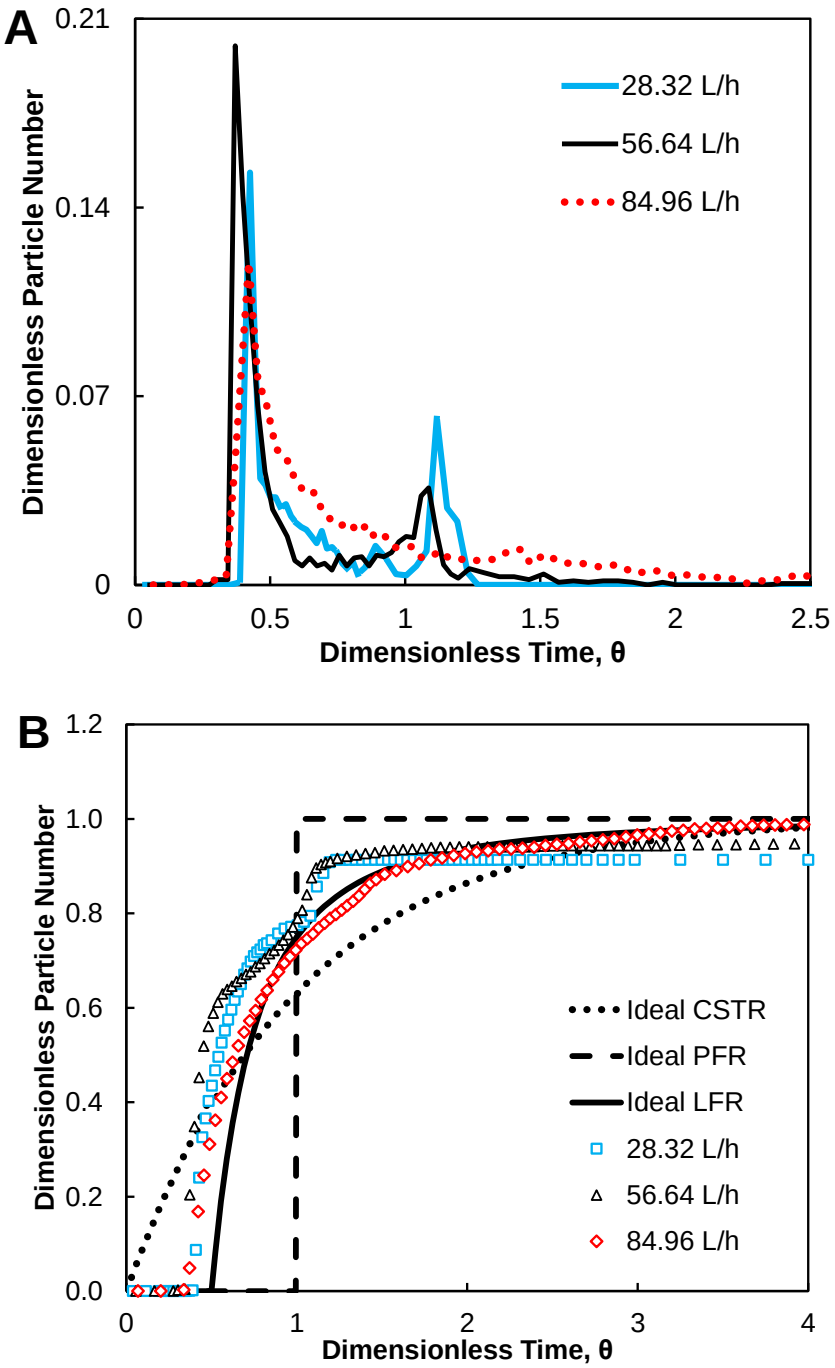

Fig. 4-9 Normalised (A) RTD curve and (B) cumulative distribution curve of the particles in the three gas flow rates.

The mixing behaviour was further characterised using cumulative distribution results, combined with the ideal models. As shown in Fig. 4-9B, besides the steep increase in the beginning, the curves of 28.32 and 56.64 L/h are approaching to the ideal PFR curve after the ideal mean recirculation time (θ =1), due to the considerable number of particles unable

to recirculate (Table 4-4: 8.7% and 5.3%, respectively). However, the trapped particles in 84.96 L/h were much fewer (0.7%) and the curve approached the ideal LFR.

Table 4-4 Indicators of the particles at the three gas flow rates for RTD and mixing evaluation, normalised time applied.

Gas flow rate (L/h)	**28.32**	**56.64**	**84.96**
Time of 10% particles recirculated, θ_{10}	0.41	0.36	0.42
Time to reach peak particle number, θ_p	0.43	0.40	0.42
Time of 50% particles recirculated, θ_{50}	0.54	0.45	0.64
Actual mean recirculation time, θ_g	0.63	0.62	0.91
Time of 90% particles recirculated, θ_{90}	1.19	1.13	1.66
Morril index, θ_{90}/θ_{10}	2.90	3.15	3.98
Thirumurthi index, $1-\theta_p/\theta_g$	0.32	0.36	0.54
Dead zone fraction (%), compared to ideal LFR	15	20	16
Dispersion index, variance	0.004	0.010	0.027
Particles unable to recirculate (%)	8.7	5.3	0.7

Therefore, in the given system, the contribution from the gas-sparging to mixing enhancement was more related to the convection. When the sludge exhibited non-Newtonian and viscous behaviour, the diffusion and dispersion from turbulence became weakened, leading to a more plug-flow pattern with constrained flow regions (short-circuiting), which was demonstrated by the belt-like distributions with condensed particles in Fig. 4-8B. Increasing the gas flow rate could mitigate the problem, but could not change the intrinsic poor mixing regions, and the enhancement was limited to an LFR pattern that is not designed. Hence, to operate the digester in the desired CSTR mode, the limitations of the gas-sparging strategy should be concerned, and improvements for the commonly used gas-lance layout are necessary for scaled-up systems.

4.4 Conclusions

- Bubble size, phase interaction forces, and liquid rheology significantly impacted the two-phase flow hydrodynamics in the studied anaerobic digester. Predictions of the gas phase dispersion and liquid velocity relied on characterisation of the phase interaction forces, which mainly depended on the applied gas-sparging strategy.
- Accurate model development for scaled-up applications requires a critical assessment of experimental data that are used for model validation.

- Evaluation of the mixing showed a performance that was approximated with a laminar-flow reactor (LFR), distinctly deviating from the expected CSTR design. Results indicated that the applied gas-sparging strategy for mixing is not very effective for reaching a CSTR flow regime.
- The results underline the importance of a proper phase-interaction description for achieving a reliable hydrodynamic characterisation and mixing evaluation in gas-mixed digesters.

4.5 References

Achkari-Begdouri, A. and Goodrich, P.R. (1992) Rheological properties of Moroccan dairy cattle manure. Bioresource Technology 40(2), 149-156.

APHA (2012) Standard Methods for the Examination of Water and Wastewater, 22nd Edition, American Public Health Association, American Water Works Association, Water Environment Federation, Washington.

Bello-Mendoza, R. and Sharratt, P.N. (1998) Modelling the effects of imperfect mixing on the performance of anaerobic reactors for sewage sludge treatment. Journal of Chemical Technology and Biotechnology 71(2), 121-130.

Capela, I., Bilé, M.J., Silva, F., Nadais, H., Prates, A. and Arroja, L. (2009) Hydrodynamic behaviour of a full-scale anaerobic contact reactor using residence time distribution technique. Journal of Chemical Technology & Biotechnology 84(5), 716-724.

Celik, I.B., Ghia, U., Roache, P.J. and Freitas, C.J. (2008) Procedure for estimation and reporting of uncertainty due to discretization in CFD applications. Journal of Fluids Engineering-Transactions of the Asme 130(7), 4.

Coughtrie, A.R., Borman, D.J. and Sleigh, P.A. (2013) Effects of turbulence modelling on prediction of flow characteristics in a bench-scale anaerobic gas-lift digester. Bioresource Technology 138, 297-306.

Dapelo, D., Alberini, F. and Bridgeman, J. (2015) Euler-Lagrange CFD modelling of unconfined gas mixing in anaerobic digestion. Water Research 85, 497-511.

Dapelo, D. and Bridgeman, J. (2018) Assessment of mixing quality in full-scale, biogas-mixed anaerobic digestion using CFD. Bioresource Technology 265, 480-489.

de Bertodano, M.L. (1991) Turbulent bubbly flow in a triangular duct. Ph.D. Thesis, Rensselaer Polytechnic Institute, Troy, New York.

Eshtiaghi, N., Markis, F., Yap, S.D., Baudez, J.-C. and Slatter, P. (2013) Rheological characterisation of municipal sludge: A review. Water Research 47(15), 5493-5510.

Karim, K., Thoma, G.J. and Al-Dahhan, M.H. (2007) Gas-lift digester configuration effects on mixing effectiveness. Water Research 41(14), 3051-3060.

Karim, K., Varma, R., Vesvikar, M. and Al-Dahhan, M.H. (2004) Flow pattern visualization of a simulated digester. Water Research 38(17), 3659-3670.

Legendre, D. and Magnaudet, J. (1998) The lift force on a spherical bubble in a viscous linear shear flow. Journal of Fluid Mechanics 368, 81-126.

Lehr, F., Millies, M. and Mewes, D. (2002) Bubble-Size distributions and flow fields in bubble columns. Aiche Journal 48(11), 2426-2443.

Leonard, B.P. and Mokhtari, S. (1990) ULTRA-SHARP nonoscillatory convection schemes for high-speed steady multidimensional flow, NASA Lewis Research Center, United States.

Lindmark, J., Thorin, E., Bel Fdhila, R. and Dahlquist, E. (2014) Effects of mixing on the result of anaerobic digestion: Review. Renewable and Sustainable Energy Reviews 40(0), 1030-1047.

Naumann, Z. and Schiller, L. (1935) A drag coefficient correlation. Z. Ver. Deutsch. Ing. 77, 318-323.

Orszag, S.A., Yakhot, V., Flannery, W.S., Boysan, F., Choudhury, D., Maruzewski, J. and Patel, B. (1993) Renormalization Group Modeling and turbulence simulations, Tempe, Arizona.

Polli, M., Stanislao, M.D., Bagatin, R., Bakr, E.A. and Masi, M. (2002) Bubble size distribution in the sparger region of bubble columns. Chemical Engineering Science 57(1), 197-205.

Roache, P.J. (1994) PERSPECTIVE - A METHOD FOR UNIFORM REPORTING OF GRID REFINEMENT STUDIES. Journal of Fluids Engineering-Transactions of the Asme 116(3), 405-413.

Samstag, R.W., Ducoste, J.J., Griborio, A., Nopens, I., Batstone, D.J., Wicks, J.D., Saunders, S., Wicklein, E.A., Kenny, G. and Laurent, J. (2016) CFD for wastewater treatment: an overview. Water Science and Technology 74(3), 549-563.

Schäfer, R., Merten, C. and Eigenberger, G. (2002) Bubble size distributions in a bubble column reactor under industrial conditions. Experimental Thermal and Fluid Science 26(6), 595-604.

Smith, L.C., Elliot, D.J. and James, A. (1993) Characterisation of mixing patterns in an anaerobic digester by means of tracer curve analysis. Ecological Modelling 69(3–4), 267-285.

Terashima, M., Goel, R., Komatsu, K., Yasui, H., Takahashi, H., Li, Y.Y. and Noike, T. (2009) CFD simulation of mixing in anaerobic digesters. Bioresource Technology 100(7), 2228-2233.

van Leer, B. (1979) Towards the ultimate conservative difference scheme. V. A second-order sequel to Godunov's method. Journal of Computational Physics 32(1), 101-136.

Varma, R. and Al-Dahhan, M. (2007) Effect of sparger design on hydrodynamics of a gas recirculation anaerobic bioreactor. Biotechnology and Bioengineering 98(6), 1146-1160.

Vesvikar, M.S. and Al-Dahhan, M. (2005) Flow pattern visualization in a mimic anaerobic digester using CFD. Biotechnology and Bioengineering 89(6), 719-732.

Wei, P., Tan, Q., Uijttewaal, W., van Lier, J.B. and de Kreuk, M. (2018) Experimental and mathematical characterisation of the rheological instability of concentrated waste activated sludge subject to anaerobic digestion. Chemical Engineering Journal 349, 318-326.

Wicklein, E., Batstone, D.J., Ducoste, J., Laurent, J., Griborio, A., Wicks, J., Saunders, S., Samstag, R., Potier, O. and Nopens, I. (2016) Good modelling practice in applying computational fluid dynamics for WWTP modelling. Water Science and Technology 73(5), 969-982.

Wu, B. (2013) Advances in the use of CFD to characterize, design and optimize bioenergy systems. Computers and Electronics in Agriculture 93(0), 195-208.

Wu, B.X. (2010a) CFD simulation of gas and non-Newtonian fluid two-phase flow in anaerobic digesters. Water Research 44(13), 3861-3874.

Wu, B.X. (2010b) Computational Fluid Dynamics investigation of turbulence models for non-Newtonian fluid flow in anaerobic digesters. Environmental Science & Technology 44(23), 8989-8995.

Chapter 5. Gas-mixing in a full-scale anaerobic digester: assessments of rheological data integration, mixing and recommendations for optimisation using computational fluid dynamics

This chapter is based on a manuscript for a journal submission, with an authorship of Peng Wei, Wim Uijttewaal, Henri Spanjers, Jules B. van Lier and Merle de Kreuk.

Abstract

Gas-mixing is commonly applied in anaerobic digesters, yet the resulting flow and mixing properties are difficult to characterise and evaluate, due to little experimental data obtained from full scale gas-tight digesters, and the uncertainties in integrating sludge rheological data for flow and mixing characterisation. The current study used computational fluid dynamics (CFD) to evaluate the impact of sludge rheological data on flow and mixing predictions in a full-scale biogas-mixed digester. Two rheological models were applied to fit the experimental rheological data, and were integrated into the CFD model. Results showed that the predicted dominant shear rate level in the digester was out of the effective shear rate range of the Ostwald model. This finding limited the model application, since the apparent viscosity underestimation at low shear rates led to flow and mixing overestimation. However, the Herschel-Bulkley model better fitted the low shear rates, and predicted large gradients of apparent viscosity in the poor flow regime. The results revealed distinct flow and mixing compartments based on the gas-sparging height, which included a plug-flow compartment with dominant vertical convection above, and a dead-zone with considerable segregation below. Velocity and time scales of flows and mixing were quantitatively estimated. Although the applied gas-sparging induced insufficient flow and mixing, it may still be useful to mitigate short-circuiting, accumulative sedimentation, and effective volume reduction. Overall, the results clearly indicate that the shear rate level in the digester should be increased, which, however, cannot be reached by simply intensifying the gas-sparging rate. Nonetheless, it is recommended to reduce the distance between the reactor bottom and the outlet of the gas lances, and/or to enlarge the overall bubble size. Moreover, thermophilic operation with lower sludge viscosity could also be an alternative, if the improved operational performance compensates the additional energy requirement.

Keywords: anaerobic digestion, CFD, gas-mixing, sludge rheology, rheological model, optimisation

5.1 Introduction

Effective anaerobic digestion performance relies on good mixing to benefit transfer and interaction between substrates and biomass. In anaerobic digesters that are designed as a continuous stirred tank reactor (CSTR), good mixing needs to be achieved by auxiliary equipment. Commonly, recirculation of produced biogas or gas-mixing is used (Lindmark et al. 2014). However, achieving sufficient mixing is usually challenging in full-scale installations, resulting in relatively low operational performance in practice. In such case, troubleshooting of the operational issue should rely on clear evaluation of the gas-mixing performance. However, despite the fact that the applied gas flow rate is known, evaluating the actual degree of mixing is usually difficult to carry out in an opaque digester. Thus far, only few studies have reported experimental evaluation using a tracer test in full-scale digesters (Capela et al. 2009, Terashima et al. 2009). The studied reactors are mixed by sludge pump recirculation and the obtained flow and mixing characteristics is limited. As a widely-used numerical approach, computational fluid dynamics (CFD) has been applied to gas-mixed digesters, yet most developed models are applied to lab-scale reactors (Coughtrie et al. 2013, Dapelo et al. 2015, Karim et al. 2007, Sajjadi et al. 2016, Vesvikar and Al-Dahhan 2005, Wei et al. 2019). In the few full-scale models, the gas-mixing implemented by bottom-mounted nozzle(s) closely resembles a bubble-column pattern (Dapelo and Bridgeman 2018a, b, Wu 2010b).

Sludge rheology is found to be a significant, influencing factor in design and operation of sludge treatment processes (Eshtiaghi et al. 2013, Kariyama et al. 2018). It has also been considered in some CFD studies, and the integrated rheological data are commonly characterised by the Ostwald or power-law model (Bridgeman 2012, Dapelo et al. 2015, Dapelo and Bridgeman 2018a, Terashima et al. 2009, Wei et al. 2019, Wu 2010d, Wu and Chen 2008), and the Herschel-Bulkley model (Dapelo and Bridgeman 2018a, b). Results of the full-scale models have revealed a considerable rheological impact on sludge flow predictions (Dapelo and Bridgeman 2018a, b, Wu 2010b). However, the referred rheological data are originally from manure slurry (Achkari-Begdouri and Goodrich 1992, Landry et al. 2004). The manure slurry has distinct rheological properties compared to the sewage sludge treated in a municipal wastewater treatment plant (WWTP), which has been characterised in our previous study (Chapter 2 (Wei et al. 2018) and Chapter 3). Hence, for further application in any other full-scale installation, the rheological discrepancy in sludge types or sources should be considered. Moreover, the potential changes in predicted flow and mixing performance are also unclear, which have not been investigated yet. Additionally, the uncertain rheological impact on the gas-mixed flow reported in our lab-scale model (Chapter

4 (Wei et al. 2019)), needs to be further assessed in a full-scale system. From a practical point of view, a better insight into the uncertain correlation between sludge rheology and flow/mixing is also important to propose straightforward and concrete suggestions for troubleshooting and optimisation in full-scale reactors.

This study focused on a full-scale anaerobic digester equipped with a number of vertical lances, through which a recycled biogas flow was injected. Since no experimental approach or data were available, CFD modelling was applied to characterise the resulting flow and mixing in the digester. The study aims to 1) investigate effectiveness and sensitivity of the applied rheological models, including Ostwald and Herschel-Bulkley, on sludge flow and mixing characterisation; 2) assess the flow and mixing performance induced by the applied gas-mixing operation; and 3) propose recommendations or guidelines for optimisation and design in practice.

5.2 Model setup

5.2.1 Geometry, computational domain and mesh

The studied anaerobic digester is located at WWTP De Groote Lucht (The Netherlands). As shown in Fig. 5-1A, the cylindrical digester has a designed effective volume of 4560 m^3, with 19 m diameter and 16 m height. The semi gas-lift pattern is implemented using a gas-sparging system with 21 gas lances. Each gas lance has 5 cm inner-diameter, and is vertically located with a clearance of 1.75 m to the tank bottom. Fig. 5-1B shows a top view of the 21 gas lances: 7 and 14 gas lances are evenly distributed to form an inner circle and an outer circle, respectively. The digester is operated with a solids retention time (SRT) of 27 d. The preliminary simulations showed a negligible effect of the sludge feeding velocity on the overall flow in the digester (data not shown). To focus on the gas-sparging process, a simplified computational domain without the feeding process was developed, based on the regular geometry and layout (the dashed sector in Fig. 5-1B). As shown in Fig. 5-1C, the domain has 1/7 of the whole digester, and contains 3 gas lances in accordance with the segmented layout to the digester centreline. Local mesh refinement was applied in the domain, due to the large dimensional difference between the tank (10^1 m) and the gas lances (10^{-2} m). Regular hexahedron grids were created in the whole domain, with refined grids in regions closely correlated with the gas-sparging (Fig. 5-1D). The optimal mesh containing 4.67 million grid cells was determined for simulations, based on a convergence study with 4 characteristic grid sizes from coarse to fine (data not shown).

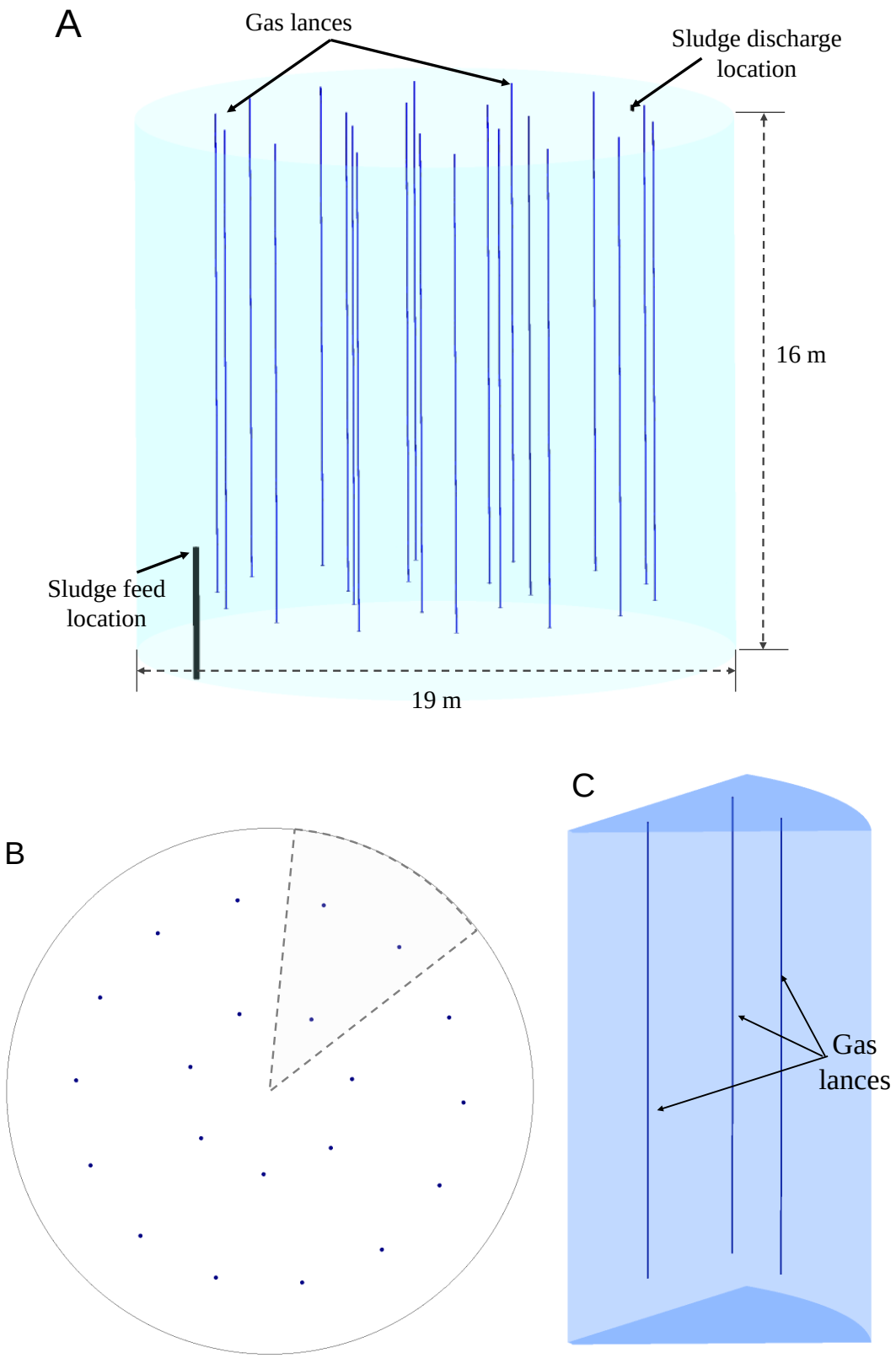
A
Gas lances
Sludge discharge location
16 m
Sludge feed location
19 m
B
C
Gas lances

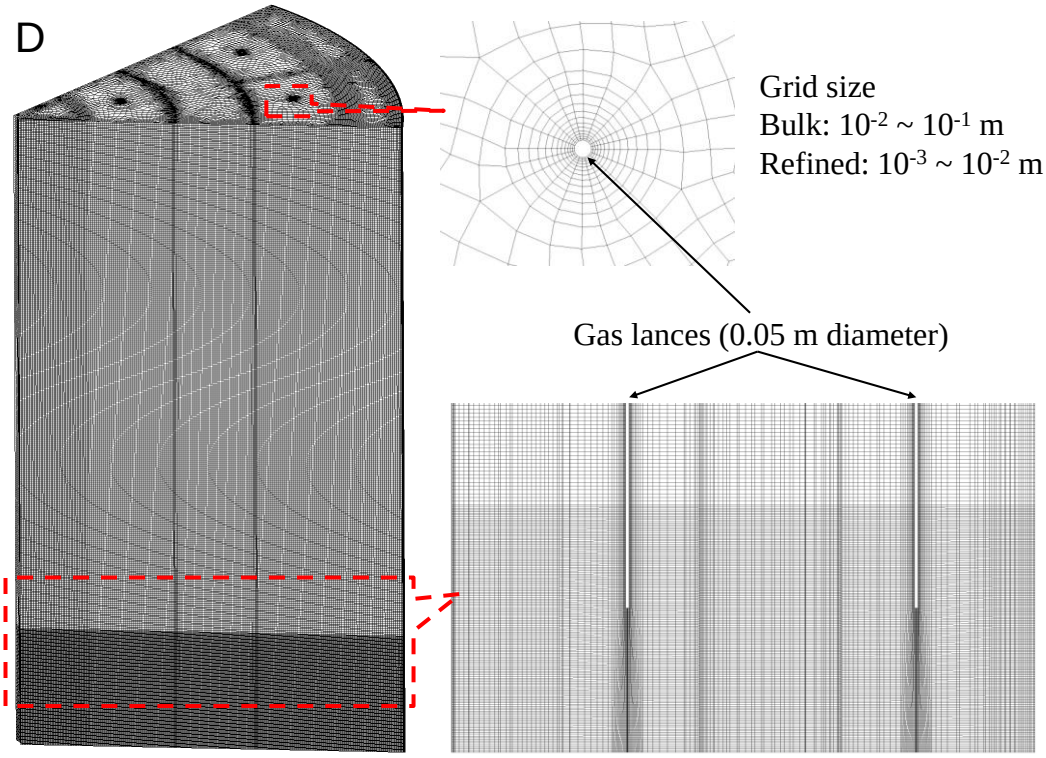

Fig. 5-1 (A), and (B) Geometry of the digester; (C) geometry, and (D) mesh of the computational domain.

5.2.2 Model development

5.2.2.1 Two-phase model

An Eulerian-Eulerian model was applied to simulate the two-phase flow, and both liquid and gas phases were assumed as a continuum. The sludge was set to the liquid phase, and the biogas assumed as a mixture of CH_4 and CO_2 was set to the gas phase. Physical properties of the biogas were proportional to volume fractions of CH_4 (75%) and CO_2 (25%), which slightly differ from commonly observed values in sewage sludge digesters (Andriani et al. 2014). Since proportional changes of the two components had negligible effects on the two-phase flow modelling, any volume fraction discrepancy in biogas between the model setting and reality was not considered. The two-phase model included governing equations for phase volume fraction, mass conservation and momentum conservation. Drag force, lift force and turbulent dispersion force were involved to characterise the gas-liquid interaction. Turbulence was simulated based on the Reynolds-Averaged-Navier-Stokes method, and the RNG k-ε model (Orszag et al. 1993) was applied. Details of all the governing equations and models are described in our lab-scale model setup in Chapter 4 (Wei et al. 2019). Potential bubble shape changes due to enlarged bubble size were considered in this study. Thus

different bubble shapes were involved in the drag force calculation, and the Grace model (Clift et al. 1978) was applied

$$C_D = \alpha_l \cdot max\left(C_{Dsphere}, min\left(C_{Dellipse}, C_{Dcap}\right)\right) \tag{5-1}$$

where C_D denotes the drag coefficient, and α_l the liquid volume fraction. The $C_{Dellipse}$, C_{Dcap} and $C_{Dsphere}$ correlate to specific bubble shapes and are defined as

$$C_{Dsphere} = \begin{cases} \frac{24}{Re_g} & Re_g \leq 0.01 \\ \frac{24 \cdot \left(1+0.15{Re_g}^{0.687}\right)}{Re_g} & Re_g > 0.01 \end{cases} \tag{5-2}$$

$$C_{Dcap} = \frac{8}{3} \tag{5-3}$$

$$\begin{cases} C_{Dellipse} = \frac{4}{3} \cdot \frac{g d_g (\rho_l - \rho_g)}{{U_t}^2 \rho_l} \\ U_t = \frac{\mu_l}{\rho_l d_g} Mo^{-0.149}(J - 0.857) \\ J = \begin{cases} 0.94H^{0.757} & 2 < H \leq 59.3 \\ 3.42H^{0.441} & H > 59.3 \end{cases}, \; H = \frac{4}{3} EoMo^{-0.149} \left(\frac{\mu_l}{0.0009}\right)^{-0.14} \end{cases} \tag{5-4}$$

where Re_g denotes the relative Reynolds number based on the relative velocity between the two phases:

$$Re_g = \frac{\rho_l |\vec{v_g} - \vec{v_l}| d_g}{\mu_l} \tag{5-5}$$

Mo the Morton number

$$Mo = \frac{g(\rho_l - \rho_g){\mu_l}^4}{{\rho_l}^2 \sigma^3} \tag{5-6}$$

and *Eo* the Eötvös number

$$Eo = \frac{g(\rho_l - \rho_g){d_g}^2}{\sigma} \tag{5-7}$$

Where, g denotes the gravitational acceleration, d the diameter, ρ the density, $\vec{v}$ the velocity, and σ the surface tension coefficient. The subscript l and g refer to the primary phase (liquid) and the secondary phase (gas), respectively.

5.2.2.2 Rheological model

Rheological data of the studied sludge were characterised by two widely used rheological models: the Ostwald model (Equation 5-8) and the Herschel-Bulkley model (Equation 5-9).

$$\mu_{sludge} = K\gamma^{n-1} \tag{5-8}$$

$$\mu_{sludge} = \frac{\tau_0}{\gamma} + K\gamma^{n-1} \quad (5\text{-}9)$$

where μ_{sludge} denotes the sludge apparent viscosity, K the flow consistency index, γ the shear rate, n the power index, and τ_0 the yield stress.

5.2.2.3 Tracer simulation and mixing assessment

Tracer simulations were implemented to assess mixing performance. The tracer was set to have the same physical properties as the sludge, with a molecular diffusion coefficient of 1×10^{-9} m^2/s. The turbulent diffusivity was determined by the calculated turbulent viscosity and the turbulent Schmidt number (0.7). To characterise the mixing performance in the entire domain, the tracer was initially concentrated in a small sphere (0.5 m radius) and released from the domain top. The tracer transport equation is

$$\frac{\partial}{\partial t}(\alpha_l \rho_l c_{tc}) + \nabla \cdot (\alpha_l \rho_l c_{tc} \overrightarrow{v_l} - \alpha_l \rho_{tc} D_{tc} \nabla c_{tc}) = 0 \quad (5\text{-}10)$$

where t denotes time, c the tracer concentration, and D the diffusion coefficient including the molecular and turbulent diffusivity. The subscript l and tc refer to the liquid phase and the tracer, respectively. The mixing performance was assessed using coefficient of variance (CoV) of the tracer concentration. All grid cells in the domain were involved, so CoV was calculated as (Etchells and Meyer 2003, Kukuková et al. 2008)

$$CoV = \sqrt{\frac{\sum_{i=1}^{N}\left(\left(\frac{c_i - c_m}{c_m}\right)^2 \cdot V_i\right)}{\sum_{i=1}^{N} V_i}} \quad (5\text{-}11)$$

where c_i denotes the tracer concentration in grid i, c_m the volume-average tracer concentration, V_i the liquid volume in grid i, and N the total grid number. Mixing degrees were specified by CoV values. The 50% mixing degree was determined by CoV of 0.5, and the ideal mixing threshold was set to the 95% mixing degree (CoV of 0.05).

5.2.3 Boundary conditions and main simulation settings

Regarding the simplified domain, a periodic boundary condition was applied for the two rectangular side planes. The domain top was set to a degassing boundary to discharge gas and retain liquid. The end side of the gas lances was set to velocity inlet for gas. All other boundaries were set to a wall condition with no-slip for liquid and free-slip for gas.

Time step sizes were set based on the CFL condition, and the 1st order implicit scheme was applied for transient simulations. The Phase Coupled SIMPLE scheme was used for pressure-velocity coupling. The 3rd order QUICK scheme (Leonard and Mokhtari 1990) was applied

for the momentum equations, and the 1st order upwind scheme for the volume fraction, turbulence, and tracer transport equations. Convergence was determined when all residuals reached an order of 10^{-4}, and the gas phase obtained a well mass balance between the gas inlet and the degassing top (mass imbalance < 5%). The simulations were implemented using the commercial package ANSYS-Fluent 17.0, mainly on a Dell Precision 7910 computer with Intel Xeon E5-2630 and 64 GB RAM.

5.3 Results and Discussion

5.3.1 Rheological data integration: the Ostwald model

5.3.1.1 Plug-flow pattern in flow and mixing

The Ostwald model was applied to characterise the sludge rheological properties and to integrate the best-fit parameters (Table 5-1) in the CFD model. Generally, the Ostwald model is effective in a specified shear rate (γ) range, in which the minimum shear rate (γ_{min}) correlates to the maximum apparent viscosity (μ_{max}), and vice versa. Constant apparent viscosity μ is assumed out of the effective range. Fig. 5-2 (Ostwald, 35°C) shows a good model fitting performance to the experimental data. It should be noticed that within the effective range, the μ change becomes quite sensitive at low shear rates in a shear-thinning scenario (n<1). Hence, a sensitivity study on the effective range determination was carried out, which was described in Supplementary D. The results showed considerable changes in flow and mixing predictions when the effective range only had small differences in γ_{min}. To minimise the γ_{min} effect on the flow and mixing predictions, the smallest γ_{min} value obtained in a good model fitting was applied, and thus the largest effective γ range was set from 1 to 300 s^{-1}.

Table 5-1 Sludge rheological data obtained from model fitting using Ostwald and Herschel-Bulkley.

Sludge	**Rheological properties**		
	K, Pa·s^n	**n**	**τ_0, Pa**
Ostwald, 35°C	1.4	0.292	-
Herschel-Bulkley, 35°C	0.49	0.526	1.45
Herschel-Bulkley, 55°C	0.39	0.525	1.15

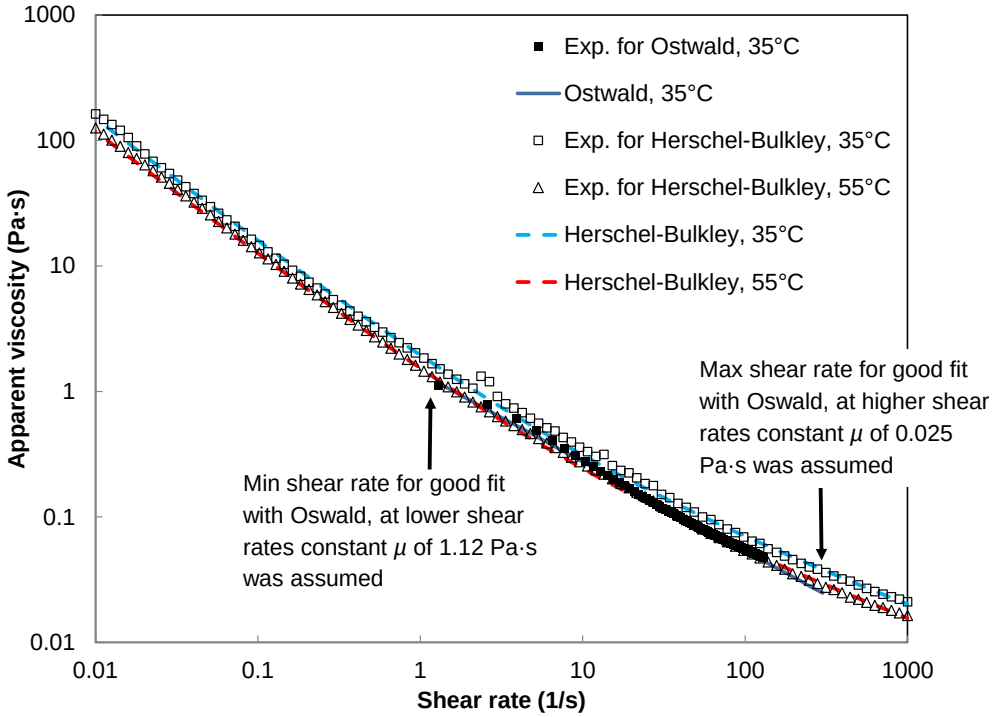

Fig. 5-2 Sludge rheological data, experimental and model fitting by Ostwald and Herschel-Bulkley.

Fig. 5-3 (A, B and C) demonstrates the simulation results using a cross section containing two gas lances. Generally, the gas phase was mainly constrained in regions close to the gas lances, and dispersed slightly from the gas inlet to the tank top (Fig. 5-3A). Induced sludge flows correlated to the gas phase distribution, with high velocities close to the gas lances (Fig. 5-3B). Vertical-dominant flows were obtained, due to the major velocity component in vertical direction and small components in horizontal directions. This flow behaviour was also demonstrated in streamline distributions (Fig. 5-3C): most streamlines (or flow loops) had a size comparable to the length scale of the gas lance; some large vortices with small velocity magnitude were formed and sparse streamlines were found near the tank bottom, indicating poor-flow regions.

The flow results revealed a plug-flow pattern between the lances, induced by the gas-sparging, which was also reflected in the tracer simulation results. As shown in Fig. 5-3D, after released from the top (0 s), the tracer had limited dispersion first (1000 s) in accordance with the dominant vertical flows. The radial dispersion was still weak even after 2000 s, and became more apparent over 3000 s. Regarding tracer mass transfer, convection by the vertical flows was dominant, while dispersion by the horizontal flows and turbulence was weak. Compared to our lab-scale results (Wei et al. 2019), the full-scale flow and mixing results indicated

similar localised plug-flow behaviour. Thus, similar mixing problems were expected in a scaled-up process of the gas-mixed digesters.

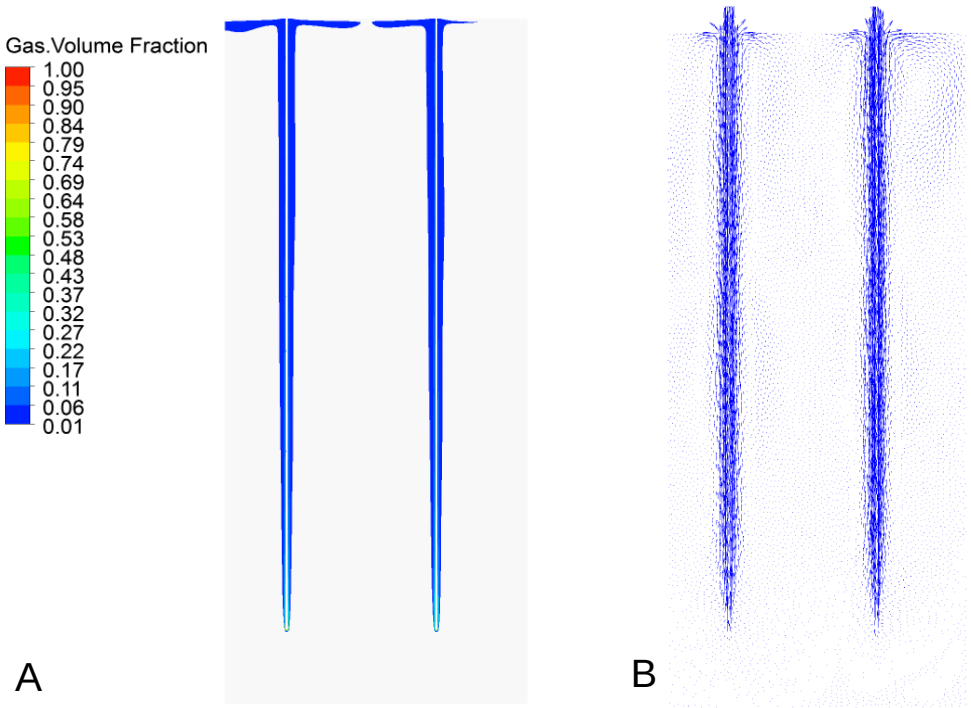

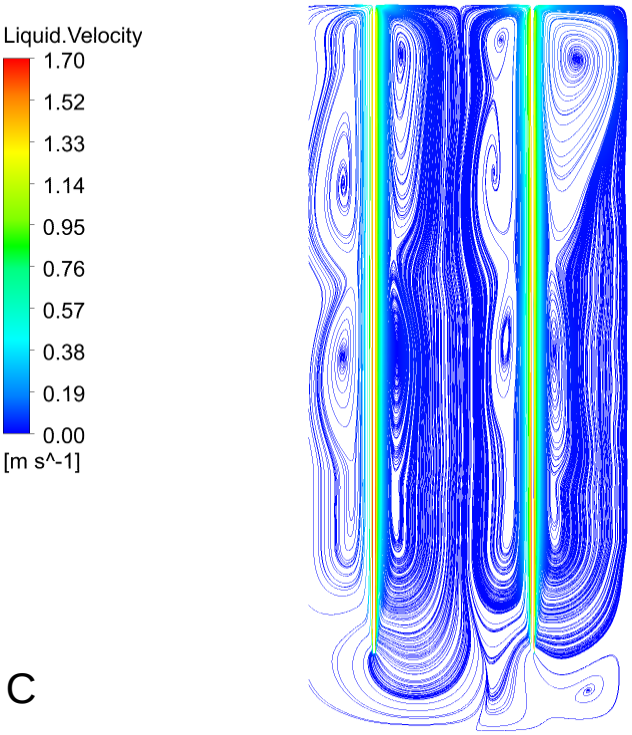

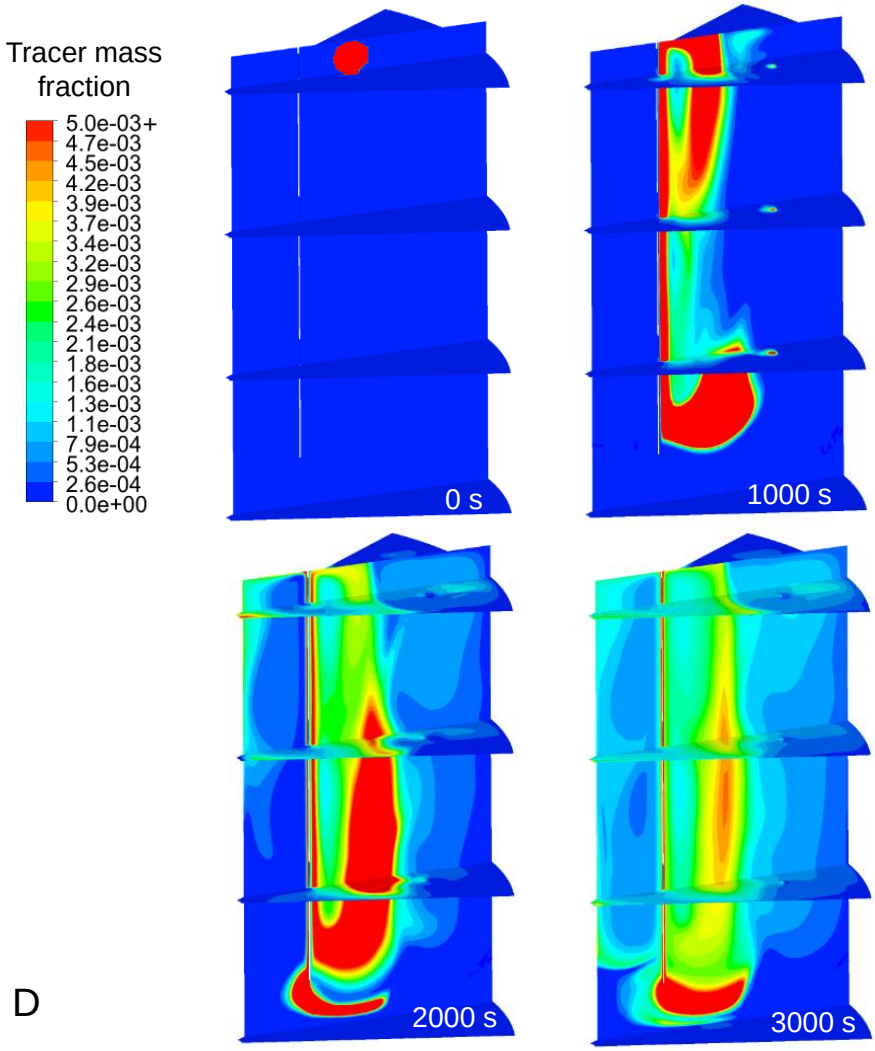

Fig. 5-3 Simulation results of Ostwald, 35°C: (A) gas phase distribution; (B) liquid velocity vector distribution; (C) liquid streamlines; and (D) tracer dispersion.

5.3.1.2 Model effective range: effectiveness and limitation on flow and mixing characterisation

The sludge velocity data (Fig. 5-4A) showed that the major part of the domain was covered by velocities in a range <0.1 m/s, and the low velocity level (<0.01 m/s) was mainly distributed near the bottom of the digester. The considerable velocity heterogeneity also correlated to the mixing performance which was assessed using the tracer's CoV data. As shown in Fig. 5-4B, the CoV curve had a varying deceasing tendency, with an exponential decay when approaching to the ideal (or 95%) mixing degree (Fig. 5-4B). As discussed in Supplementary D, the CoV results indicated that the medium and high velocity levels above the gas inlet mainly accounted for reaching a medium mixing degree of 75%. However, for

reaching a higher degree of mixing or even ideal mixing, the relatively small volume fraction characterised by a low velocity level (<0.01 m/s) became more important. This volume fraction is directly correlated to the apparent dead zone in the digester.

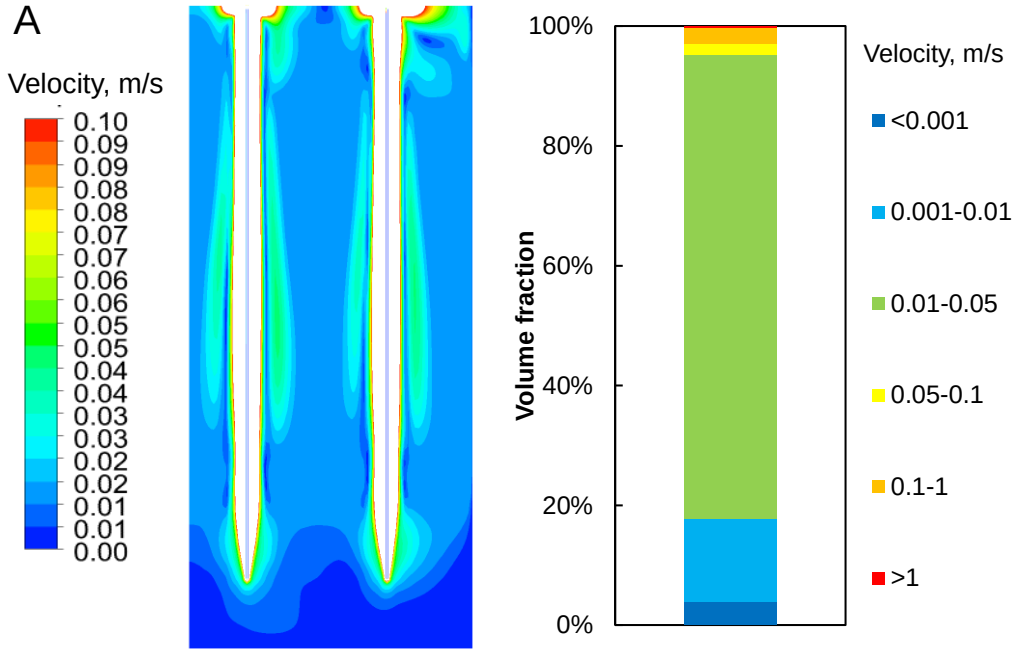

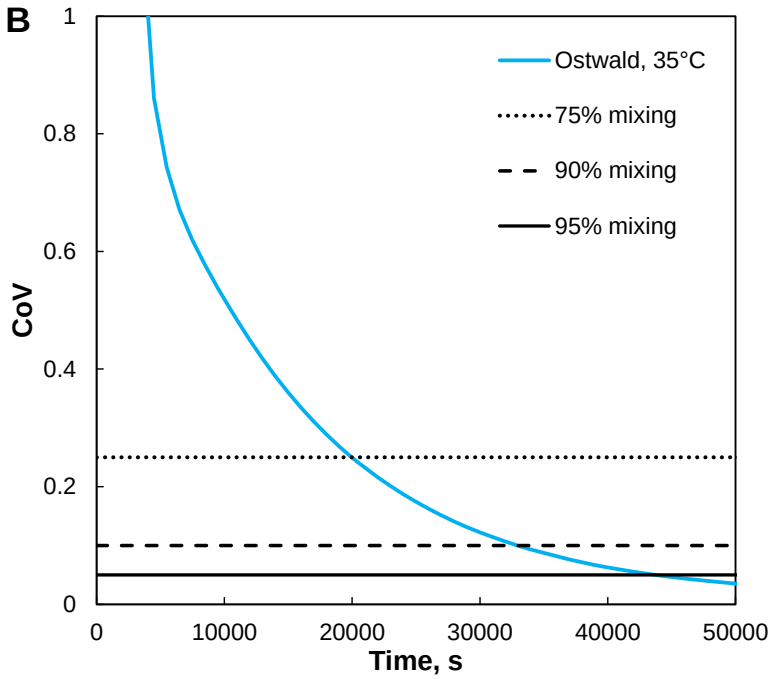

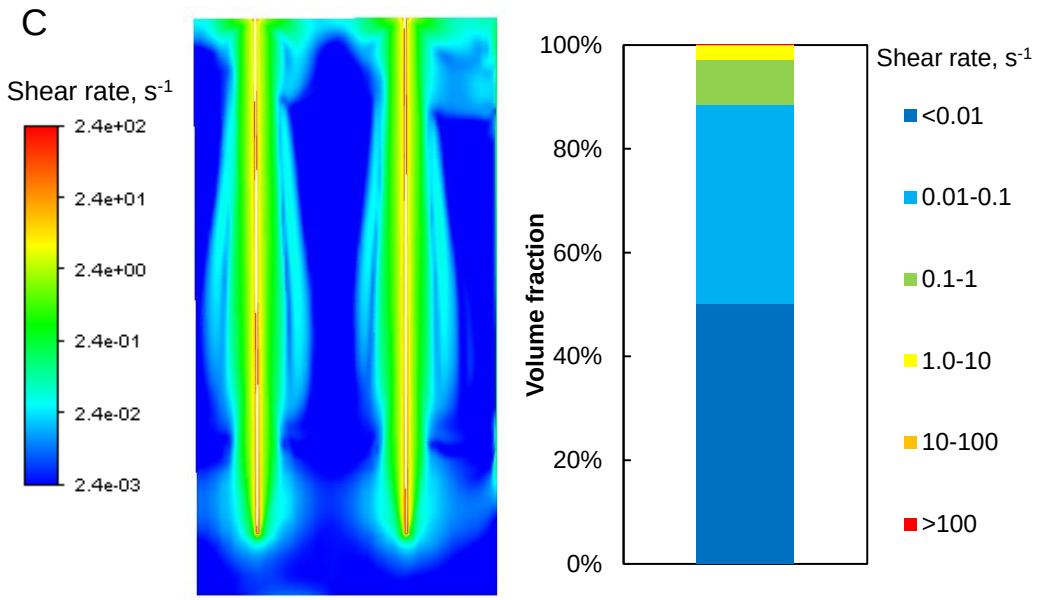

Fig. 5-4 Flow and mixing data of Ostwald, 35°C: (A) sludge velocity contour (left) and volume fraction (right) distributions; (B) CoV curve; and (C) shear rate contour (left) and volume fraction (right) distributions.

It should be noticed that different dead zone definitions have been employed in previous studies (Bridgeman 2012, Karim et al. 2004, Mendoza et al. 2011, Vesvikar and Al-Dahhan 2005, Vesvikar et al. 2005). In some studies, the dead zone is defined by velocities below 5% of the maximum velocity (v_{max}) (Bridgeman 2012, Vesvikar and Al-Dahhan 2005, Vesvikar et al. 2005). However, this definition relies on flow field stability, and seems not be very useful due to strong v_{max} fluctuations in the digester (Dapelo and Bridgeman 2018a). Although our results obtained small v_{max} fluctuations, the highest velocity level (>1 m/s) was mainly located in the constrained regions near the gas lances; the volume fraction was too small (<0.2%) to represent or affect the dominant velocity level. Hence, the definition was not appropriate to apply in this study. Besides, the dead zone determination can correlate to Stokes' settling velocity ($v_{settling}$), which is calculated by (Lamb 1994)

$$v_{settling} = \frac{\rho_p - \rho_l}{18\mu_l} g {d_p}^2 \quad (5\text{-}12)$$

where d_p denotes the particle diameter. This dead zone definition has also been applied in some studies, and the $v_{settling}$ specific to the referred biomass (diameter 250 µm and density 1050 kg/m^3) is in the order of 10^{-3} m/s (Karim et al. 2004, Mendoza et al. 2011). However, the estimation is based on a μ_l level comparable to water viscosity, and thus needs to be adapted for our sludge scenario. Referring to biomass with similar characteristics, the highest

$v_{settling}$ determined by μ_{min} (0.025 Pa·s) in this study was in a much lower order of 10^{-5} m/s, resulting in almost no dead zone predictions. In addition, it has been reported that the characteristic sludge-particle sizes in digesters are usually smaller than 250 μm (Kim et al. 2003, Zhang et al. 2018), and the sludge density does not change much to the solids content level (Wu and Chen 2008). So any further changes in the biomass density and particle size would not result in much higher $v_{settling}$, indicating inappropriate dead zone determination for the studied sludge. However, this definition could still be useful for interpreting the considerable sand/gravel sedimentation observed in the studied digester. Regarding fine gravel (density 1600 kg/m^3) with 5 mm diameter, the dead zone determined by $v_{settling}$ obtained a large volume fraction of 31%. Hence, the applied gas-sparging strategy could moderately maintain the sludge matrix in suspension, but seems not enough to prevent accumulative sedimentation of other contained denser materials (such as fine gravel), which could lead to a considerable reduction of the effective volume in long-term operation.

Moreover, the Ostwald model results revealed an important role of the effective range in flow and mixing predictions, which could limit applications of the Ostwald model. The Ostwald model generally fits well at medium and high shear rates, so the determined γ_{min} is usually not low. As shown in Table 5-2, γ_{min} of 11 s^{-1} has been determined for fitting the experimental rheological data (Achkari-Begdouri and Goodrich 1992, Landry et al. 2004), and thus referred in many CFD modelling studies (Bridgeman 2012, Dapelo et al. 2015, Dapelo and Bridgeman 2018b, Terashima et al. 2009, Wu 2010d, Wu and Chen 2008). However, the γ levels in predicted flows are only reported in one full-scale model, with average γ values around 0.2 s^{-1} (Dapelo and Bridgeman 2018b). This magnitude is smaller than the referred γ_{min}, but the difference has not been further discussed. In this study, a comparable volume-average γ value of 0.14 s^{-1} was obtained. Similarly, it was still smaller than the applied γ_{min} of 1 s^{-1} that was much smaller than the γ_{min} of 11 s^{-1} in literature. In addition, Fig. 5-4C also shows considerable γ gradients in the whole domain. As discussed in Supplementary D, the obtained dominant γ level was out of the effective range, leading to an almost 'Newtonian fluid' prediction with constant μ_{max} in most regions.

According to the authors' knowledge, the effect of the effective range determination on flow and mixing characterisation has not been investigated thus far. But its importance, especially for γ_{min}/μ_{max} determination, was clearly revealed in our results. The Ostwald model can perform well to describe sludge rheological properties, but should be carefully integrated to assess flow and mixing. Due to less model complexity, the Ostwald model can be a better option than the other rheological models, when the dominant γ level in an installation is in the effective range. However, regarding the good agreement in the γ predictions between this

study and the reference (Dapelo and Bridgeman 2018b), the dominant γ level in realistic full-scale gas-mixed digesters could be expected in the same order of 0.1 s^{-1}. Hence, underestimation of the overall μ level due to the limited effective model range, may result in overestimation of the flow and mixing performance. Solution of the uncoupled shear rate challenge requires better rheological model fittings, and also more accurate rheological measurements at low shear rates.

Table 5-2 Shear rate and apparent viscosity ranges in different datasets.

	Ostwald		**Herschel-Bulkley**	
	γ, s^{-1}	**μ, Pa·s**	**γ, s^{-1}**	**μ, Pa·s**
Determined in the rheological model	1-300	0.025-1.12	0.01-1000	0.02-162
Predicted in the CFD model	-236*	0.029-1.12	-1007*	0.02-297
Rheological model applied in reference (Bridgeman 2012, Dapelo et al. 2015, Dapelo and Bridgeman 2018b, Terashima et al. 2009, Wu 2010d, Wu and Chen 2008)	11-702	0.006-0.17	0.01-30	0.02-13.3

* with very small γ_{min} (<10^{-4} s^{-1})

5.3.2 Rheological data integration: the Herschel-Buckley model

5.3.2.1 Flow and mixing performance (mesophilic)

The Herschel-Bulkley model was applied to improve the model fitting quality at low shear rates, and to further assess the effectiveness of the rheological data integration. As shown in Fig. 5-2, a good model fitting was also obtained, with a larger effective range from 0.01 to 1000 s^{-1} (Table 5-2). The apparent viscosity μ out of the effective range (<γ_{min}) was calculated by (Fluent 2017)

$$\mu = \frac{\tau_0}{\gamma_{min}} \cdot \left(2 - \frac{\gamma}{\gamma_{min}}\right) + K \cdot {\gamma_{min}}^{n-1} \cdot \left(2 - n + \frac{(n-1)\gamma}{\gamma_{min}}\right) \quad (5\text{-}13)$$

Compared to Ostwald, much larger μ magnitude was obtained by Herschel-Bulkley at low shear rates (γ <1 s^{-1}). As shown in Fig. 5-5A and 5B, the data of Herschel-Bulkley, 35°C obtained large volume fractions with velocities <0.5 m/s and γ <0.1 s^{-1} (57% and 68%, respectively).

Fig. 5-5C shows viscosity distribution results of the Ostwald and Herschel-Bulkley models. Effective viscosity (μ_{eff}) was applied to involve a turbulence impact, which is a sum of apparent viscosity (μ_{sludge}) and turbulent viscosity (μ_{turb})

$$\mu_{eff} = \mu_{sludge} + \mu_{turb} \quad (5\text{-}14)$$

The two models showed distinct μ_{eff} distributions in the domain. For the Ostwald model, the volume-average μ_{sludge} was close to μ_{max} (1.12 Pa·s), so μ_{turb} (volume-average 26.6 Pa·s) was the dominant component in μ_{eff}. As shown in Fig. 5-5C (Ostwald, 35°C), high μ_{eff} levels (μ_{turb} dominant) were found above the gas inlet, especially in regions between the gas lances. However, the Herschel-Bulkley model (35°C) obtained opposite results: the volume-average μ_{sludge} of 69.5 Pa·s was much higher than μ_{turb} (volume-average 3.9 Pa·s), and became dominant in μ_{eff}. Much larger μ_{eff} gradients were obtained and the high μ_{eff} levels were mainly distributed below the gas inlet (Fig. 5-5C, Herschel-Bulkley, 35°C), consistent with the low velocity and shear rate regions.

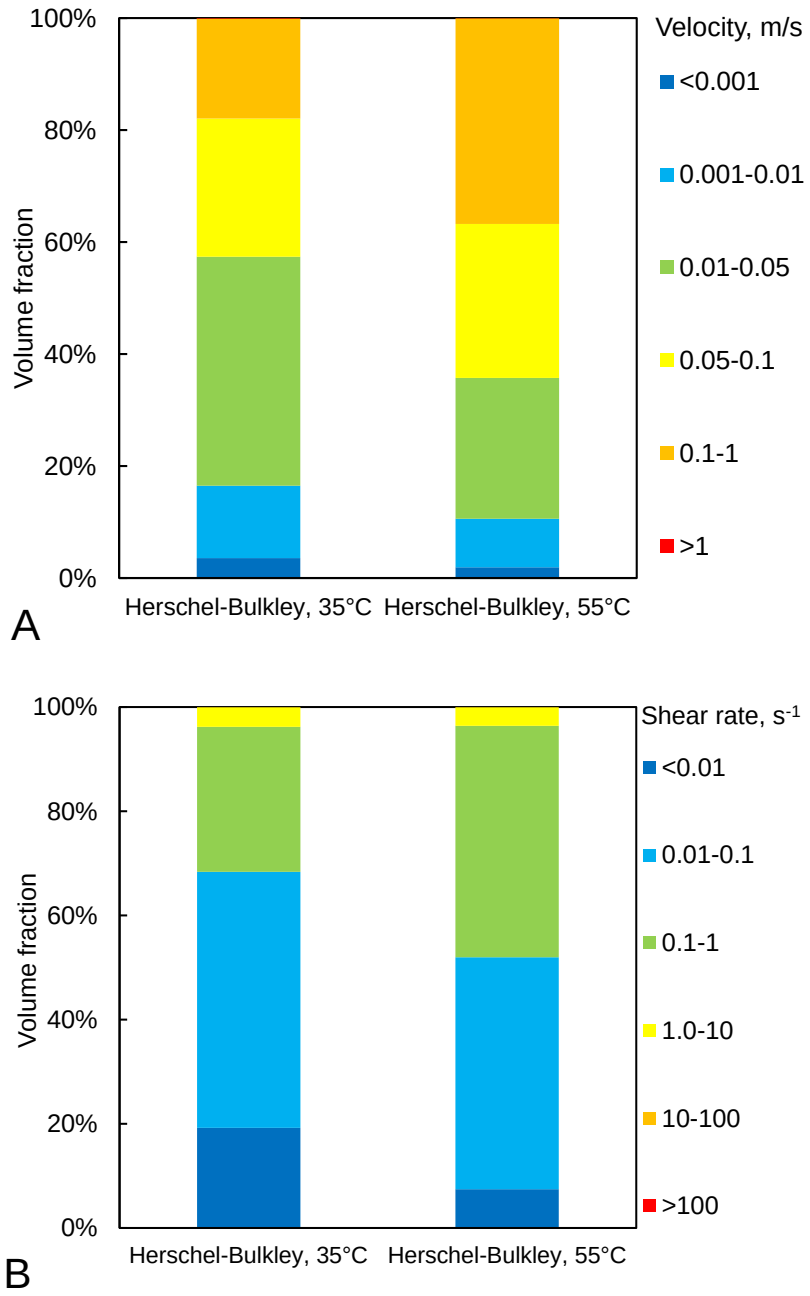

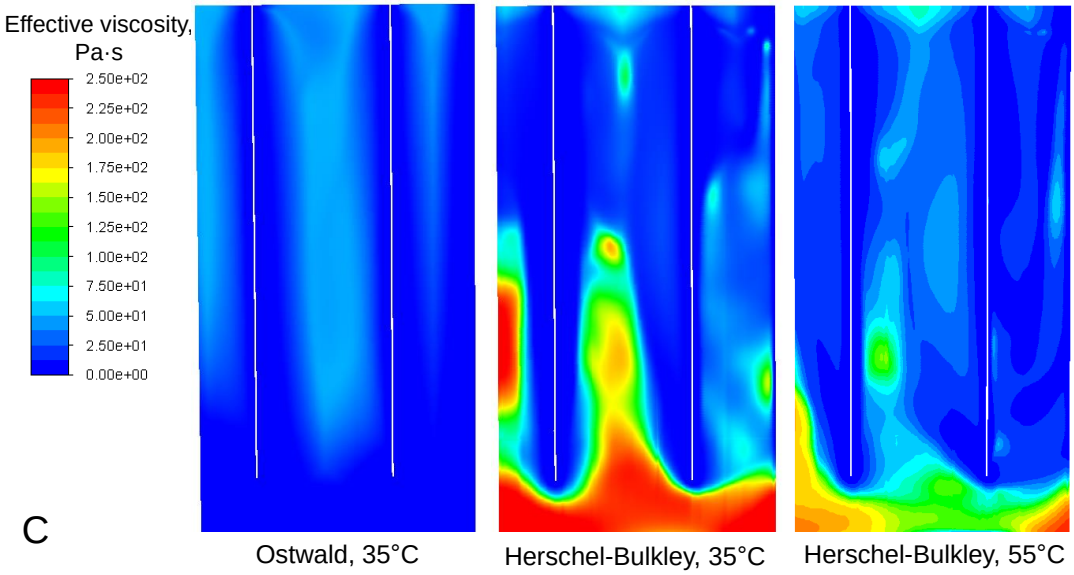

Fig. 5-5 Flow behaviour of the Ostwald and Herschel-Bulkley models: (A) velocity; (B) shear rate; and (C) effective viscosity.

The distinct μ_{eff} distributions correlated to the corresponding mixing behaviour between Ostwald and Herschel-Bulkley. Fig. 5-6A shows variation of the area-average tracer concentration at two heights: 1.5 m (just below the gas inlet), and 0.1 m (near the bottom). Here dimensionless mixing time θ was used, normalised by the ideal mixing time:

$$\theta = \frac{t}{t_{95\%\ mixing}} \tag{5-15}$$

The two Ostwald 35°C curves (1.5 m and bottom) showed a similar tendency: the lag of the tracer dispersion from 1.5 m to the bottom was not much, and the concentration difference became negligible when $\theta > 0.5$. However, the two Herschel-Bulkley 35°C curves showed distinct tendencies. The 1.5 m curve obtained shorter θ for the first appearance of the tracer, and then had a steep and monotonic increase to a plateau. The bottom curve obtained the lag θ similar to the Ostwald model, but then had a much slower increase. When reaching the ideal mixing (θ=1), the concentration difference between the two curves was still not negligible. Hence, the Herschel-Bulkley model revealed a different tracer dispersion pattern, and considerable segregation occurred. The highly heterogeneous μ_{eff} distribution accounted for the segregation: the tracer transfer from top to the gas inlet height was easy; but further penetration to the bottom became much difficult. These localised differences were further reflected in the overall mixing performance. As illustrated in Fig. 5-6B, considerable differences were observed after reaching the 75% mixing degree between Ostwald and Herschel-Bulkley (35°C). Similar to Fig. 5-4B, the Ostwald curve also had an exponential

decay. But the Herschel-Bulkley curve had a power-law decay, and took much more time to reach the ideal mixing degree. Accordingly, $t_{95\%\ mixing}$ values of Ostwald and Herschel-Bulkley had an order of magnitude difference, which were 3.1×10^{3} s and 7.0×10^{4} s, respectively.

The dramatic discrepancy in flow and mixing predictions further revealed the intrinsic limitation of the Ostwald model. The simplified μ assumption at low shear rates led to the absence of the segregation prediction, and thus the considerable flow and mixing overestimation. This limitation was negated using the Herschel-Bulkley model, due to more accurate descriptions of the highly sensitive μ changes at low shear rates. Besides, the predicted segregation pattern directly correlated to poor mixing performance, and thus was more meaningful to determine the dead zone than the several definitions discussed in Section 5.3.1.2.

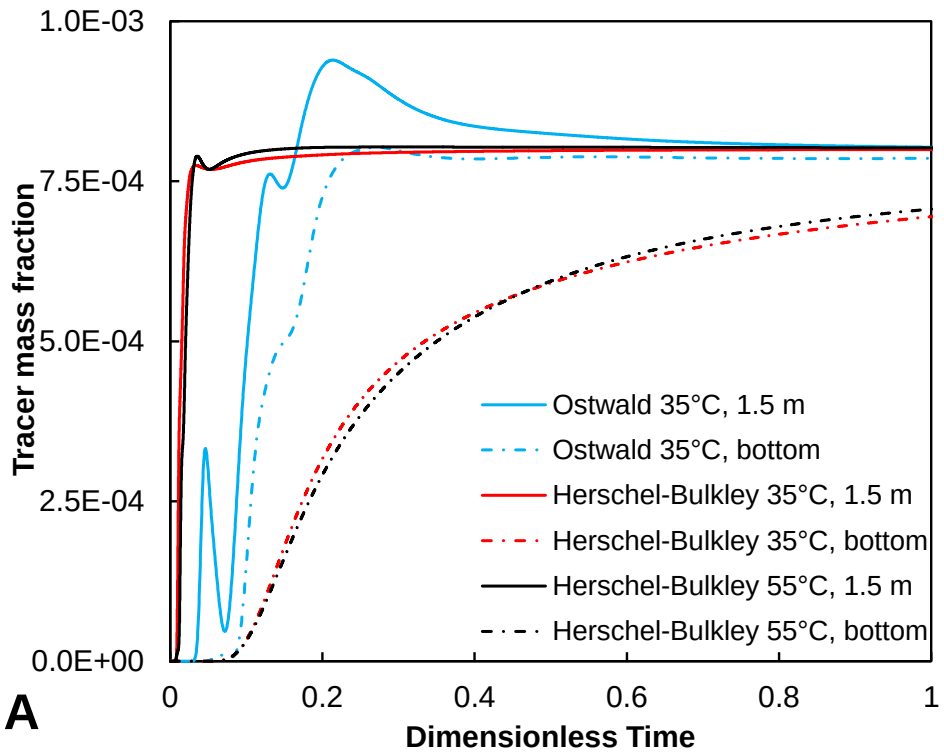

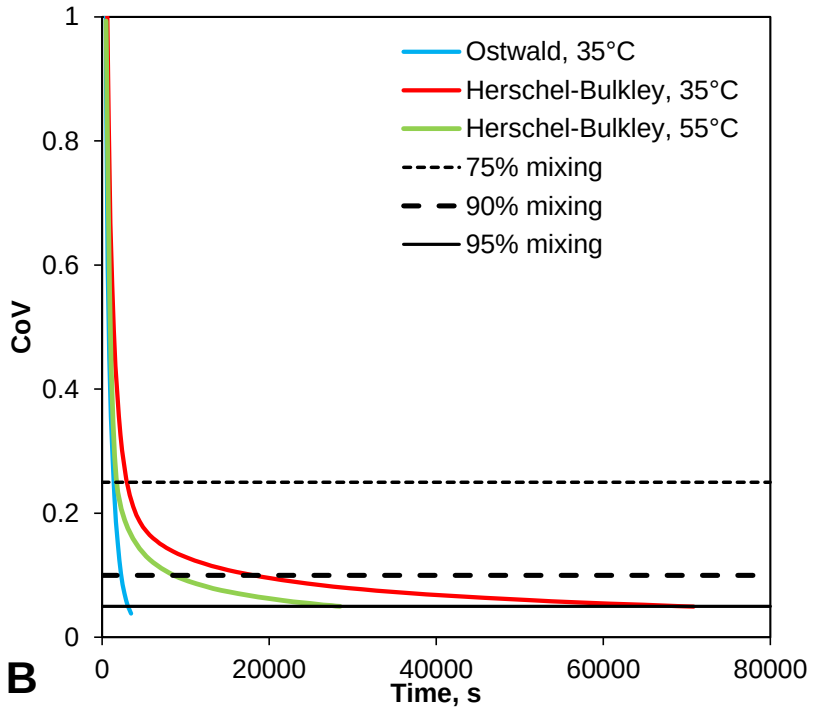

Fig. 5-6 Mixing behaviour of the Ostwald and Herschel-Bulkley models, (A) area-average tracer concentration at local heights; and (B) CoV in the whole domain.

5.3.2.2 Mesophilic vs. thermophilic, the rheological impact on flow and mixing

The aforementioned simulations were based on the mesophilic digestion mode operated at 35°C. Anaerobic digestion is also commonly implemented in the thermophilic mode, which is operated at 55°C (Buhr and Andrews 1977). As reported in Chapter 3, the studied sludge had a systematic 20% decrease in μ from 35°C to 55°C (also shown in Fig. 5-2). Hence, potential changes in resulting flow and mixing were assessed by simulations of the thermophilic temperature. As shown in Fig. 5-5 and 5-6, the Herschel-Bulkley 55°C scenario had a volume fraction decrease of 22% in velocity <0.5 m/s, and 16% in γ <0.1 s^{-1}, compared to Herschel-Bulkley 35°C. Besides, the volume-average μ_{eff} in the domain had a dramatic decrease of 49% to 37.2 Pa·s. However, the changes were not qualitative: μ_{sludge} (volume-average 30 Pa·s) was still dominant, and the μ_{eff} gradients were still considerable. This similarity to Herschel-Bulkley 35°C indicated that the segregation still occurred, which was clearly reflected in the similar mixing performance at local heights (Fig. 5-6A) and the whole domain (Fig. 5-6B). The 55°C CoV curve also had a power-law decay after reaching the 75% mixing degree. But the time scale was much smaller, and the ideal mixing time reduced 59% to 2.8×10^4 s.

Compared to mesophilic, the thermophilic mode has been reported to take some advantages,

including higher destruction rate of organic solids, improved dewatering characteristics and lower production of pathogenic organisms (Buhr and Andrews 1977). Our results revealed more advantages: better flow and mixing performance resulting from lower μ of the sludge matrix, and thus a better use of the whole effective volume. If the benefit from the improved operational performance compensates the extra energy required by the higher working temperature, thermophilic digestion could be an alternative for optimisation in the studied digester.

5.3.3 Role of gas-sparging in mixing: assessment and guidelines for optimisation

5.3.3.1 Flow and mixing enhancement by the gas-sparging

More tracer data at local heights were also analysed to assess the flow and mixing performance. Besides the aforementioned two heights (1.5 m and bottom), three heights above the gas inlet were included, which are nearly 1/3 (5 m), 2/3 (10 m), and the whole height (15 m) of the digester, respectively. As shown in Fig. 5-7 (Herschel-Bulkley 35°C), the curves at the three additional heights had more fluctuations before being stabilised, which was different from the plateau tendency in the 1.5 m curve. The different curve tendencies indicated distinct tracer dispersion patterns referring to the gas inlet height (1.75 m). Above the gas inlet, the tracer dispersion had a plug-flow pattern. Motion of the concentrated tracer bulk was mainly affected by the vertical-dominant flows, and tracked by the peaks in the three curves. A characteristic dispersion rate of 0.06 m/s was estimated, based on the peak time differences among the three heights. Below the gas inlet, the tracer dispersion to the bottom had a monotonic penetration pattern due to the considerable segregation, and had a much slow rate around 0.2 mm/s. Therefore, two compartments with distinct flow and mixing behaviour were obtained based on the gas inlet location: a plug-flow compartment above, and a dead-zone compartment below.

Furthermore, several representative flow and mixing time scales were estimated. An effective vertical dispersion through the major part of the domain (above 1.5 m) had a time scale up to 600 s. An effective horizontal dispersion had a time scale around 2000 s, when obtaining negligible differences in the tracer concentration among all heights above 1.5 m. Therefore, the applied gas-sparging operation was supposed to enhance flow and mixing with: 1) a fast vertical dispersion in an order of 10^2 s (<10 min); 2) a slower centre-side dispersion in an order of 10^3 s (> 20 min); and 3) a much larger time scale of ideal mixing in an order of 10^4 s (> 3 h).

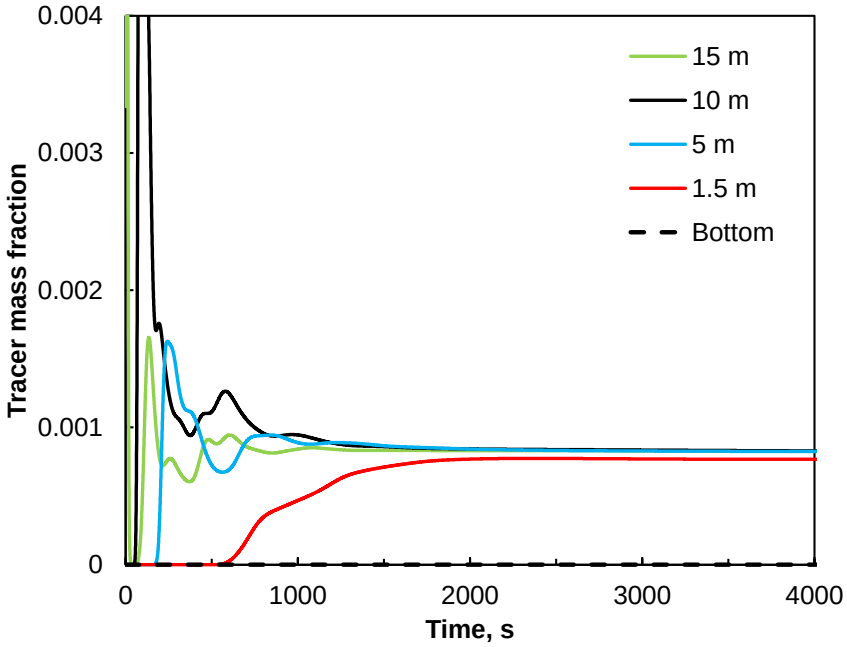

Fig. 5-7 Variation of area-average tracer concentration at different heights, Herschel-Bulkley 35°C.

Although the insufficient mixing and resulting flow created a considerable gap with the ideal CSTR expectation, the applied gas-sparging operation could still be of importance for the operation of the studied digester. Regarding the layout (Fig. 5-1A), the location difference between the sludge feed point (4.25 m height) and the discharge point (16 m height, opposite side to the feed point) could easily result in short-circuiting, if no gas-sparging would be applied. As shown in Fig. 5-8A, the gas-sparging by the 21 gas lances created considerable vertical-dominant convection through the digester. Thus, it could moderately maintain the effective volume and mitigate the short-circuiting, which is of high importance to attain the long-term digestion performance. However, the considerable segregation in the dead-zone compartment was a critical shortcoming, and should be solved to improve the gas-sparging performance. In addition, Fig. 5-8 also demonstrates different flow patterns between the two sludge sources, and a much better flow performance (Fig. 5-8B) was obtained using the referred sludge (Achkari-Begdouri and Goodrich 1992, Landry et al. 2004). Results show another limitation that was not further explored in the previous studies (Bridgeman 2012, Dapelo et al. 2015, Dapelo and Bridgeman 2018b, Terashima et al. 2009, Wu 2010d, Wu and Chen 2008): if the rheological data integration does not match with the sludge source treated in the installation, there is a risk of incorrect assessment on flow and mixing performance.

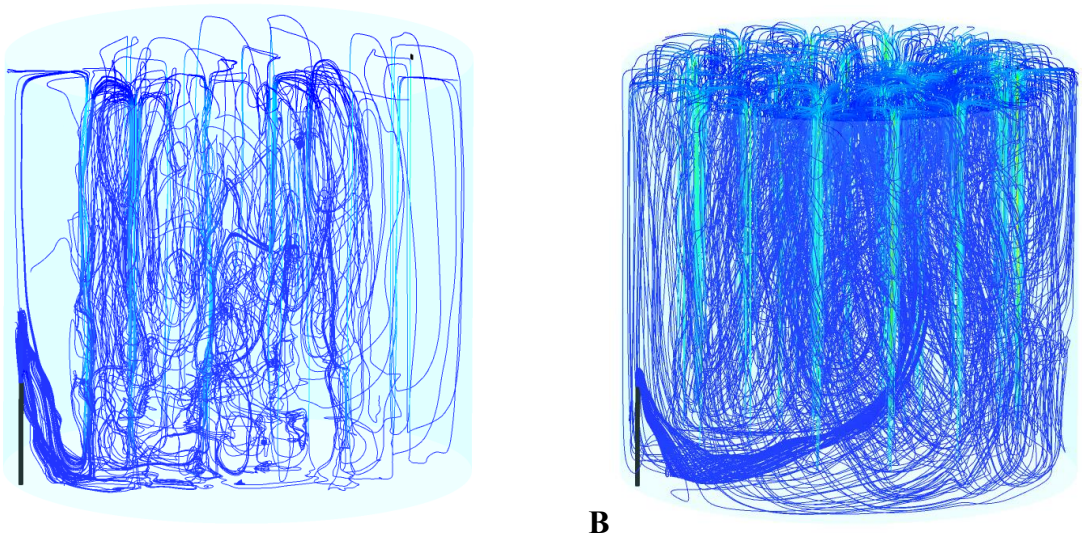

A B

Fig. 5-8 Schematic streamlines in the whole digester filled with different sludge sources, (A) the locally treated sewage sludge; and (B) referred manure slurry (Achkari-Begdouri and Goodrich 1992, Landry et al. 2004).

It should be notified that our present work does not include the randomly produced biogas bubbles in the digestion process itself. In the studied digester, an average biogas production of 2450 m^3/day is obtained (full scale data, not shown), which is randomly released, resulting in biogas bubbles of different sizes. Very likely, also the laminar and turbulent flows brought about by these biogas bubbles contribute to the mixing and prevention of short circuiting between inlet and outlet of the digester.

5.3.3.2 Guidelines for optimisation and design in practice

(1) Gas-sparging intensity

Based on all aforementioned results, guidelines were proposed for process optimisation at full scale. The gas-sparging intensity was firstly assessed, which was quantified by calculating the injected biogas flow rate that was controlled by the capacity of the applied compressor. The injected biogas flow rate was calculated to be 300 m^3/h in the studied digester. Two more biogas flow rates were considered to investigate the gas-sparging intensity effect on flow and mixing predictions, including 150 and 450 m^3/h, which agree with a 50% decrease and 50% increase of 300 m^3/h, respectively. As shown in Fig. 5-9, an increased biogas flow rate resulted in a decreased volume fraction of the low velocity level (<0.01 m/s), but the decrease was not considerable. In addition, similar volume fractions of the high velocity level (>0.1 m/s) were obtained. Table 5-3 demonstrates the mixing results, using dimensionless mixing time normalised by the ideal mixing time of the 300 m^3/h

scenario. Similarly, the mixing performance did not differ much with the biogas flow rate, and almost the same ideal mixing time was obtained for 300 and 450 m^3/h.

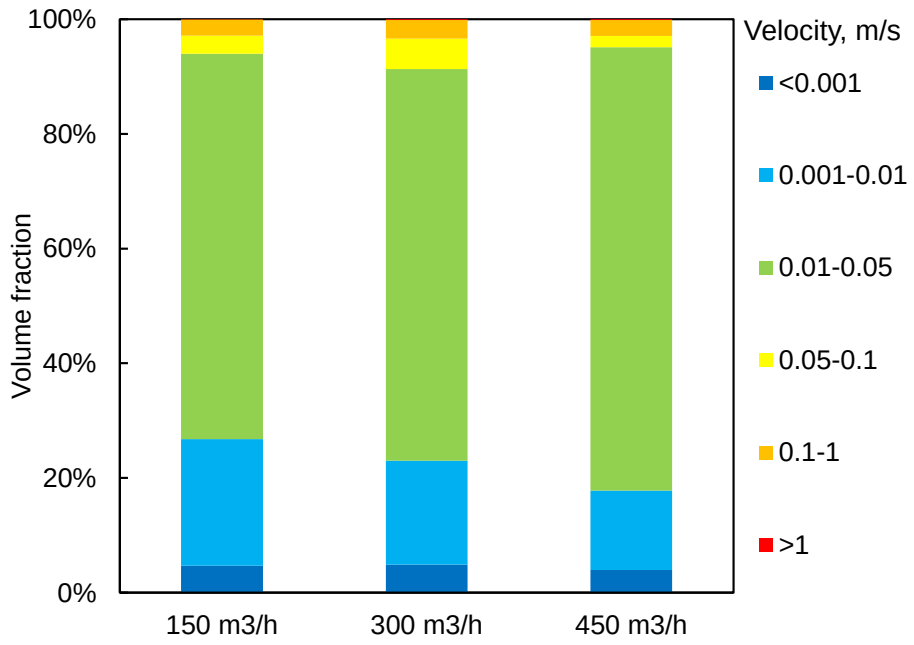

Fig. 5-9 Volume fraction data of sludge velocity, with different gas-sparging rates.

The small changes in flow and mixing to the biogas flow rate had a qualitative agreement with our lab-scale model results (Wei et al. 2019) and the lab-scale experimental results in a previous study (Karim et al. 2004). From a practical point of view, the flow and mixing enhancement was insufficient regarding the applied large increase of biogas flow rate (a factor 3, from 150 to 450 m^3/h). Energy consumption was also evaluated based on the power input calculation (McFarland 2001)

$$E = P_1 \cdot Q \cdot ln\left(\frac{P_2}{P_1}\right) \tag{5-16}$$

where Q denotes the gas flow rate; and P_1 and P_2 the absolute pressure in the tank headspace (1 atm) and at the gas-sparging inlet (3 atm), respectively. The mixing energy level (*MEL*) can be estimated by (Stukenberg et al. 1992)

$$MEL = \frac{E}{V} \tag{5-17}$$

where V denotes the effective volume of the digester. The 300 m^3/h scenario obtained a *MEL* value of 2.1 W/m^3, which was close to 2.2 W/m^3 reported in another full-scale gas-mixed digester (Dapelo and Bridgeman 2018b), while it was much smaller than the recommended range of 5-8 W/m^3 for proper mixing (EPA 1979). To match the recommended range, the

current compressor capacity should at least increase 240% to 740 m^3/h. This change requires more investment, more technical adjustment and much larger energy consumption, which may not be applicable to the studied digester. Therefore, the results did not reveal efficient enhancement of flow and mixing by simply intensifying the gas-sparging rate, and the recommended *MEL* criterion appears unsuitable for the studied digester.

(2) Bubble size

The bubble size impact on flow and mixing in the full-scale model was further assessed, as a further step to our lab-scale study (Wei et al. 2019). Compared to the lab-scale scenario, bubble size distribution is expected to be distinct and complicated in the full-scale scenario due to the large dimension (16 m height), the different gas-sparging equipment and potential size changes from bubble coalescence or break-up. However, no experimental data on bubble size have been obtained in the studied digester. Thus necessary simplifications were made, and an identical bubble size was still assumed. A size of 5 mm was set first based on our lab-scale model (Wei et al. 2019), but larger sizes up to 30 mm were considered due to the quite large hydrostatic pressure change (over 1.5 atm) and large diameter of the gas lances. As shown in Fig. 5-10, the bubble size had a considerable effect on the velocity volumetric distributions. In particular, the volume fraction of velocity > 0.05 m/s obtained a large increase when the size increased to over 10 mm. The dramatic changes were also reflected in the mixing performance shown in Table 5-3, and the scenarios with the size over 10 mm had a much smaller time scale to reach each mixing degree.

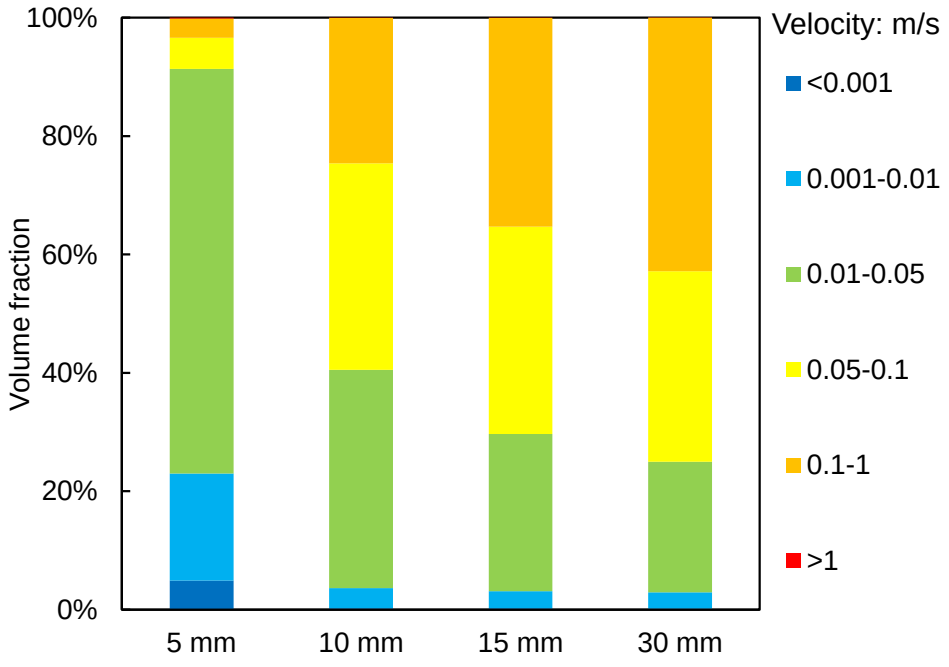

Fig. 5-10 Volume fraction data of sludge velocity, with different bubble sizes.

Moreover, the flow and mixing differences became much less when the bubble size setting was over 15 mm. Apparently, the 15 mm scenario had both a moderate bubble size, and moderate flow and mixing performance and was thus applied in most simulations shown in this study. It should be noticed that the simplifications in the bubble size setup were a necessary trade-off between simulation accuracy and feasibility. So it is difficult and inappropriate to expect that the realistic flow and mixing performance has a good quantitative agreement with one specific bubble size scenario. However, the predicted qualitative tendencies of flow and mixing were more important, since larger bubbles accounted for stronger phase interactions and thus stronger disturbance in sludge flows. Hence, increase in overall bubble size could be proposed to improve flow and mixing performance in the studied digester. The applied gas lances are basically long open tubes with little size control of released bubbles. Thus, a layout modification, or a new design of the gas lances could be an option for generating larger bubbles. In addition, biogas production from sludge digestion creates bubbles of different diameters in the digester. Owing to sludge rheology (yield stress) these bubbles may reach very large dimensions, causing biogas eruptions from the sludge, particularly when the sludge is not well mixed. While escaping from the liquid stagnant zone, these bubbles likely cause regions of turbulence, which are not considered in our current work. Future work should combine the impact of the generated biogas bubbles on the flow and mixing patterns of digesters.

Table 5-3 Mixing time data of different scenarios, normalised by the ideal mixing time of the 300 m^3/h scenario (5 mm bubble size). The specified mixing degree in % was determined by the CoV data, as described in Section 5.2.2.3.

Variable		**Dimensionless mixing time**			
		50%	**75%**	**90%**	**95% (ideal)**
Gas-sparging rate	**150 m^3/h**	0.19	0.37	0.65	1.2
	300 m^3/h	0.20	0.40	0.69	1.0
	450 m^3/h	0.25	0.48	0.79	1.0
Bubble size	**5 mm**	0.20	0.40	0.69	1.0
	10 mm	0.05	0.08	0.13	0.2
	15 mm	0.02	0.03	0.06±0.01	0.08±0.01
	30 mm	0.02	0.03	0.04±0.01	0.06±0.02
Gas inlet height	**1.75 m**	0.03	0.07	0.43	1.68
	0.5 m	0.02	0.03	0.09	0.33

(3) Height of the gas inlet

As discussed in Section 5.3.3.1, the gas inlet location determined the two-compartment pattern. To mitigate the segregation in the dead-zone compartment, more simulations were implemented using a lower gas inlet height of 0.5 m. Fig. 5-11 shows the γ distribution data (mesophilic). Compared to 1.75 m, the 0.5 m scenario obtained a considerable decrease in volume fraction (from 19.2% to 6.4%) in $\gamma < 0.01$ s^{-1}, and the volume-average μ_{eff} reduced 41% to 43.4 Pa·s. As shown in Table 5-3, also the time to reach a specific mixing degree distinctly decreased. Moreover, similar flow and mixing changes were obtained between the two height scenarios in the thermophilic mode (data not shown).

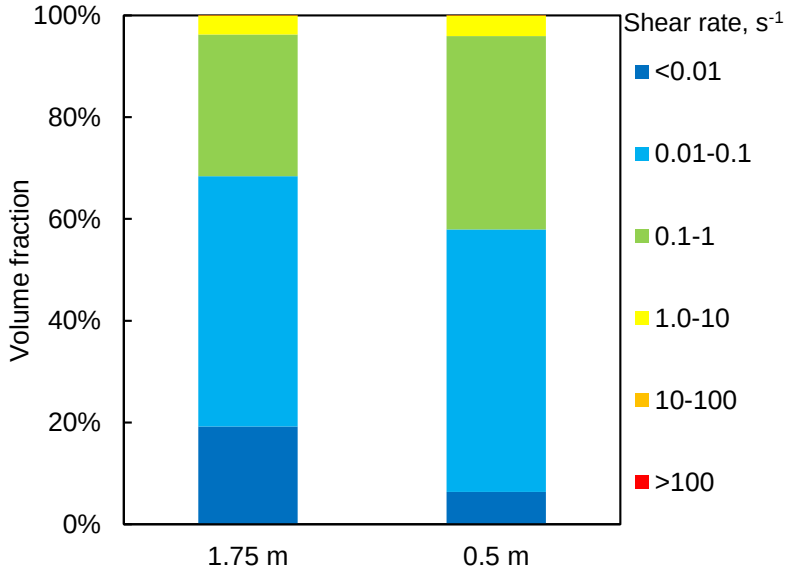

Fig. 5-11 Volume fraction data of shear rate, with different settings of gas inlet height, mesophilic mode.

With the low gas inlet height, the gas-sparging operation activated more sludge motion close to the bottom. The overall velocity and shear rate levels had a considerable increase (14.8% and 16.8%, respectively), resulting in reduced space of the dead-zone compartment. Besides, the low gas inlet height helps to further mitigate short-circuiting, sedimentation and to maintain the effective volume in long-term operation. Unlike the thermophilic mode change, the gas inlet height adjustment did not reduce the μ_{sludge} level, but still considerably enhanced the flow and mixing performance. From a practical aspect, it is more feasible to implement this in an existing system for operational optimisation, yet more attention should be paid on any potential blockage issues, e.g., with accumulating sand/gravel.

5.4 Conclusions

This study revealed considerable dependency of the flow and mixing characterisation in a full-scale digester, with the treated sludge rheological data input. The predicted dominant shear rate level in the digester was out of the effective shear rate range of the Ostwald model. This finding limited the model application, since the apparent viscosity overestimation at low shear rates led to flow and mixing overestimation.

However, the Herschel-Bulkley model better fitted the low shear rates, and predicted large gradients of apparent viscosity in the poor flow regime. The results revealed distinct flow and mixing compartments, based on the gas-sparging height, which included a plug-flow compartment with dominant vertical convection above, and a dead-zone with considerable segregation below. Velocity and time scales of flows and mixing were quantitatively estimated. Although the applied gas-sparging induced insufficient flow and mixing, it may still be useful to mitigate short-circuiting, accumulative sedimentation and effective volume reduction.

Overall, the results clearly indicate that the shear rate level in the digester should be increased, which, however, cannot be reached by simply intensifying the gas-sparging rate. Nonetheless, it is recommended to reduce the distance between the reactor bottom and the outlet of the gas lances, and/or to enlarge the overall bubble size. Moreover, thermophilic operation with lower sludge viscosity could also be an alternative, if the improved operational performance compensates the additional energy requirement.

5.5 References

Achkari-Begdouri, A. and Goodrich, P.R. (1992) Rheological properties of Moroccan dairy cattle manure. Bioresource Technology 40(2), 149-156.

Andriani, D., Wresta, A., Atmaja, T.D. and Saepudin, A. (2014) A Review on optimization production and upgrading biogas through CO2 removal using various techniques. Applied Biochemistry and Biotechnology 172(4), 1909-1928.

Bridgeman, J. (2012) Computational fluid dynamics modelling of sewage sludge mixing in an anaerobic digester. Advances in Engineering Software 44(1), 54-62.

Buhr, H.O. and Andrews, J.F. (1977) The thermophilic anaerobic digestion process. Water Research 11(2), 129-143.

Capela, I., Bilé, M.J., Silva, F., Nadais, H., Prates, A. and Arroja, L. (2009) Hydrodynamic behaviour of a full-scale anaerobic contact reactor using residence time distribution technique. Journal of

Chemical Technology & Biotechnology 84(5), 716-724.

Clift, R., Grace, J.R. and Weber, M.E. (1978) Bubbles, drops, and particles, Academic Press, New York.

Coughtrie, A.R., Borman, D.J. and Sleigh, P.A. (2013) Effects of turbulence modelling on prediction of flow characteristics in a bench-scale anaerobic gas-lift digester. Bioresource Technology 138, 297-306.

Dapelo, D., Alberini, F. and Bridgeman, J. (2015) Euler-Lagrange CFD modelling of unconfined gas mixing in anaerobic digestion. Water Research 85, 497-511.

Dapelo, D. and Bridgeman, J. (2018a) Assessment of mixing quality in full-scale, biogas-mixed anaerobic digestion using CFD. Bioresource Technology 265, 480-489.

Dapelo, D. and Bridgeman, J. (2018b) Euler-Lagrange Computational Fluid Dynamics simulation of a full-scale unconfined anaerobic digester for wastewater sludge treatment. Advances in Engineering Software 117, 153-169.

EPA, U. (1979) Process design manual for sludge treatment and disposal. Center for environmental research in formation technology transfer.

Eshtiaghi, N., Markis, F., Yap, S.D., Baudez, J.-C. and Slatter, P. (2013) Rheological characterisation of municipal sludge: A review. Water Research 47(15), 5493-5510.

Etchells, A.W. and Meyer, C.F. (2003) Mixing in Pipelines. Handbook of industrial mixing, 391-477.

Fluent, A. (2017) ANSYS Fluent Theory Guide, Release 18.0. Ansys, Inc.

Karim, K., Thoma, G.J. and Al-Dahhan, M.H. (2007) Gas-lift digester configuration effects on mixing effectiveness. Water Research 41(14), 3051-3060.

Karim, K., Varma, R., Vesvikar, M. and Al-Dahhan, M.H. (2004) Flow pattern visualization of a simulated digester. Water Research 38(17), 3659-3670.

Kariyama, I.D., Zhai, X. and Wu, B. (2018) Influence of mixing on anaerobic digestion efficiency in stirred tank digesters: A review. Water Research 143, 503-517.

Kim, J., Park, C., Kim, T.-H., Lee, M., Kim, S., Kim, S.-W. and Lee, J. (2003) Effects of various pretreatments for enhanced anaerobic digestion with waste activated sludge. Journal of Bioscience and Bioengineering 95(3), 271-275.

Kukuková, A., Noël, B., Kresta, S.M. and Aubin, J. (2008) Impact of sampling method and scale on the measurement of mixing and the coefficient of variance. Aiche Journal 54(12), 3068-3083.

Lamb, H. (1994) Hydrodynamics, 6th Edition, Cambridge university press.

Landry, H., Laguë, C. and Roberge, M. (2004) Physical and rheological properties of manure products. Applied Engineering in Agriculture 20(3), 277-288.

Leonard, B.P. and Mokhtari, S. (1990) ULTRA-SHARP nonoscillatory convection schemes for high-speed steady multidimensional flow, NASA Lewis Research Center, United States.

Lindmark, J., Thorin, E., Bel Fdhila, R. and Dahlquist, E. (2014) Effects of mixing on the result of anaerobic digestion: Review. Renewable and Sustainable Energy Reviews 40(0), 1030-1047.

McFarland, M.J. (2001) Biosolids engineering, McGraw-Hill Education.

Mendoza, A.M., Martínez, T.M. and Fajardo, V. (2011) Modeling flow inside an anaerobic digester by CFD techniques. International Journal of Energy and Environment 2(6), 963-974.

Orszag, S.A., Yakhot, V., Flannery, W.S., Boysan, F., Choudhury, D., Maruzewski, J. and Patel, B. (1993) Renormalization Group Modeling and turbulence simulations, Tempe, Arizona.

Sajjadi, B., Raman, A.A.A. and Parthasarathy, R. (2016) Fluid dynamic analysis of non-Newtonian flow behavior of municipal sludge simulant in anaerobic digesters using submerged, recirculating jets. Chemical Engineering Journal 298, 259-270.

Stukenberg, J.R., Clark, J.H., Sandino, J. and Naydo, W.R. (1992) Egg-Shaped Digesters: From Germany to the U.S. Water Environment & Technology 4(4), 42-51.

Terashima, M., Goel, R., Komatsu, K., Yasui, H., Takahashi, H., Li, Y.Y. and Noike, T. (2009) CFD simulation of mixing in anaerobic digesters. Bioresource Technology 100(7), 2228-2233.

Vesvikar, M.S. and Al-Dahhan, M. (2005) Flow pattern visualization in a mimic anaerobic digester using CFD. Biotechnology and Bioengineering 89(6), 719-732.

Vesvikar, M.S., Varma, R., Karim, K. and Al-Dahhan, M. (2005) Flow pattern visualization in a mimic anaerobic digester: experimental and computational studies. Water Science and Technology 52(1-2), 537-543.

Wei, P., Mudde, R.F., Uijttewaal, W., Spanjers, H., van Lier, J.B. and de Kreuk, M. (2019) Characterising the two-phase flow and mixing performance in a gas-mixed anaerobic digester: Importance for scaled-up applications. Water Research 149, 86-97.

Wei, P., Tan, Q., Uijttewaal, W., van Lier, J.B. and de Kreuk, M. (2018) Experimental and mathematical characterisation of the rheological instability of concentrated waste activated sludge subject to anaerobic digestion. Chemical Engineering Journal 349, 318-326.

Wu, B.X. (2010a) CFD simulation of gas and non-Newtonian fluid two-phase flow in anaerobic digesters. Water Research 44(13), 3861-3874.

Wu, B.X. (2010b) Computational Fluid Dynamics investigation of turbulence models for non-Newtonian fluid flow in anaerobic digesters. Environmental Science & Technology 44(23), 8989-8995.

Wu, B.X. and Chen, S.L. (2008) CFD simulation of non-Newtonian fluid flow in anaerobic digesters. Biotechnology and Bioengineering 99(3), 700-711.

Zhang, J., Li, N., Dai, X., Tao, W., Jenkinson, I.R. and Li, Z. (2018) Enhanced dewaterability of sludge during anaerobic digestion with thermal hydrolysis pretreatment: New insights through structure evolution. Water Research 131, 177-185.

Chapter 6. Summary, further discussion and outlook

In this chapter the research findings are summarised and placed in the actual context of the Water Authorities in The Netherlands and municipal wastewater treatment in general.

6.1 Summary

This summary is based on all the conclusions in the previous chapters, and reorganised into four sub-topics in line with the thesis outline setup in Chapter 1.

6.1.1 Rheological characterisation of sewage sludge

(1) Complex rheological properties of waste activated sludge (WAS): Chapter 2

The studied sewage sludge demonstrated complex rheological properties, especially the concentrated WAS samples. The obtained yield-pseudoplastic behaviour showed varying flow curve patterns in a wide shear rate range, and was better characterised by hybrid model fitting of defined shear rate segments. A new mathematical expression was developed to improve the fitting quality. However, the limited applicability of the empiric models reflected the samples' transient rheological behaviour rather than intrinsic properties, challenging the included parameters definition. The rheological instability was characterised by the distinct flow status and transitions, and became more pronounced at increased TS concentrations. The determined rheological instability could give more insight in viscoelasticity and thixotropy of the concentrated WAS, which complicate its flow and mixing characterisation in full-scale WAS treatment systems. Moreover, recommendations for developing a proper rheological measurement protocol were also formulated.

(2) Digestate (DGT) rheology, and further investigation on thixotropy and the temperature impact: Chapter 3

Regarding the DGT samples from the same WWTP, the yield-pseudoplastic behaviour was well characterised by the Herschel-Bulkley model.

Under the long-term shearing conditions, the complex thixotropic behaviour was well characterised by two quantified limitation states: Initial and Stable. For the concentrated WAS samples, the two states showed distinct rheological properties; while this rheological difference was small for the DGT samples.

Temperature had a striking impact on the sludge rheological properties, which was strongly

correlated with the solids content. The AD or aging process also had a considerable effect on the sludge rheology. Besides the observed distinct difference in thixotropic behaviour between WAS and DGT, the results showed a large decrease in yield stress and apparent viscosity to temperature for WAS, whereas this was not observed for DGT. The discrepancy in impact between long-term shearing and temperature implied the existence of different mechanisms, which are responsible for shifting the force equilibrium of hydrodynamic and non-hydrodynamic interactions that are responsible for the structural deformation and subsequent recovery of the sludge matrix.

6.1.2 Flow behaviour of sewage sludge

(1) Single-phase sludge pipe flow: Chapter 3

The distinct rheological properties between Initial and Stable states were clearly reflected in the pipe flow behaviour of the concentrated WAS, revealing a concrete link between lab-measured sludge rheology and its practical flow performance. Our results also showed that the complex rheological properties of WAS in pipe flows and the associated pressure drop were well assessed using the developed CFD model with effective rheological data integration, which is promising for practical purposes and optimisation of energy consumption in sewage sludge handling.

(2) Two-phase flow in digesters: Chapter 4 and 5

Detailed characterisation of the gas-sludge flow was implemented in a refined lab-scale CFD model with experimental validation (Chapter 4). Bubble size, phase interaction forces, and liquid rheology significantly impacted the two-phase flow hydrodynamics in the studied anaerobic digester. Predictions of the gas phase dispersion and liquid velocity relied on the characterisation of the phase interaction forces. A more reliable and complete model validation was obtained by performing a critical comparison, using the referred experimental data and the CFD models reported in other studies. Additionally, justifiable corrections and predictions of the sludge flow behaviour in detail were obtained.

Results of the full-scale model (Chapter 5) revealed considerable dependency of the flow characterisation, with the treated sludge rheological input data. The predicted dominant shear rate level in the digester was out of the effective shear rate range of the Ostwald model. This finding limited the model application, since the apparent viscosity overestimation at low shear rates led to flow overestimation. However, the Herschel-Bulkley model better fitted the low shear rates, and predicted large gradients of apparent viscosity in the poor flow regime.

A plug-flow pattern with dominant vertical convection was predicted above the gas-sparging nozzle that was situated at a height of 1.75 m from the bottom. However, below the gas-sparging nozzle a large dead zone was predicted.

6.1.3 Mixing performance in digesters

Mixing in the lab-scale digester was evaluated using an Euler-Lagrange method (Chapter 4). The mixing performance approximated a LFR that distinctly deviated from the expected CSTR design. Results indicated that the applied gas-sparging strategy for mixing is not very effective for reaching a CSTR flow regime. The results underline the importance of a proper phase-interaction description for achieving a reliable hydrodynamic characterisation and mixing evaluation in gas-mixed digesters.

In the full-scale model (Chapter 5), the considerable dependency on the rheological input data was also revealed in the mixing performance. Mixing overestimation was found in the Ostwald model, which was also attributed to the inability of the Ostwald model to properly describe the low shear rate regime. Similarly, distinct mixing compartments were predicted by the Herschel-Bulkley model, with considerable segregation below the gas-sparging nozzle height at 1.75 m from the bottom. Besides, velocity and time scales of flows and mixing were quantitatively estimated. Although the applied gas-sparging induced insufficient flow and mixing, it may still be useful to mitigate short-circuiting, accumulative sedimentation and effective volume reduction.

6.1.4 Practical aspects: recommendations/guidelines for design and operation

Validations, bend to experimental data without a critical assessment, may lead to an inaccurate model for further scaled-up applications (Chapter 4). From lab-scale to full-scale (Chapter 5), the considerable dimensional differences aggravated the insufficient degree of the induced mixing and the gap to the ideal CSTR expectation. Overall, the results clearly indicate that the shear rate level in the full-scale digester should be increased, which, however, cannot be reached by simply intensifying the gas-sparging rate. Nonetheless, it is recommended to reduce the distance between the reactor bottom and the outlet of the gas lances, and/or to enlarge the overall bubble size. Moreover, thermophilic operation with lower sludge viscosity could also be an alternative, if the improved operational performance compensates the additional energy requirement.

Regarding the full-scale modelling, model reliability or effectiveness should be scrutinized

using any available experimental data, but should not merely rely on experimental validation. Generally, discrepancies in operations and conditions between design and reality are difficult to be thoroughly identified and foreseen, and thus necessary simplifications have to be employed in the model. With this aspect, sensitivity analysis and assessment, as well as tendency predictions are more important than an agreement with experimental data.

6.2. Further discussion and outlook

Based on the obtained conclusions, the research objectives are discussed in a broader context, and recommendations for future research are proposed. The sub-chapter is also organised into four sub-topics.

6.2.1 Rheological characterisation: method, data accuracy and mechanism

As discussed in Chapter 2, it is necessary to develop a proper protocol for sludge rheological measurements. The method of hysteresis loop creation has been widely used to determine thixotropy, which was also applied in Chapter 2 but not in Chapter 3. The Initial state can be determined in the first half procedure of the hysteresis method with increased shear rates. However, the second half procedure may just obtain an intermediate state due to the short time or history of shearing. It means that thixotropy is just qualitatively determined, while the Stable state cannot be clearly characterised. In addition, the measurement settings such as the shear rate range in a hysteresis loop are usually artificial, which limit the method standardisation and applications of the quantitative data or correlations in practice. Hence, the hysteresis method was not appropriate to use in Chapter 3, and the complex thixotropic behaviour was determined by the proposed measuring method, which has not been reported in literature. The initial purpose was not to develop a new method, but the proposed method could be promising to determine the potential limiting states of the thixotropic behaviour, and to assess the corresponding limiting flow and mixing behaviour. Regarding the current methodology for measuring complicated sludge rheology and linking the results to practical applications, further developments are needed in the future.

The wall effect has been reported to be an error source in rheological measurements (Eshtiaghi et al. 2013). Particular attention has been addressed to minimise the effect in capillary rheometers, requiring the proper length to diameter ratio of the capillary tube (Eshtiaghi et al. 2013, Seyssiecq et al. 2003). Similarly, the potential wall effect should also be considered in rotational rheometers, and use of the device with rough surface is

recommended (Seyssiecq et al. 2003). In our study, only a measuring bob with smooth surface was available for the measurements, so the wall effect on data accuracy was not considered. This effect was identified when a new measuring bob with rough surface could be used only recently. Sewage sludge samples from Kralingseveer WWTP, Rotterdam (kindly provided by Ir. A. Gonzalez Ortega, TU Delft), including WAS (TS 7.9%) and DGT (TS 3.3%), were measured using the two measuring bobs. Results are shown in Fig. 6-1 (non-published results). The WAS flow curves (Fig. 6-1A) were found to be almost the same when shear rates > 20 s^{-1} were applied. But considerable differences were found at shear rates < 20 s^{-1}, in which the smooth bob obtained lower values of shear stress and apparent viscosity (20±8%) than in the case of using the rough bob. Fig. 6-1B shows the data of the DGT samples, for which only very small differences were found at very low shear rates (< 1 s^{-1}). Results shown in Fig. 6-1A indicate that the wall effect at low shear rates in the concentrated WAS needs to be considered; and the use of the smooth bob could lead to an underestimation of apparent viscosity. Besides, important qualitative differences were not observed between the used sludges, implying that the similarities in the rheological complexity as shown in Chapter 2, will still be obtained using the rough bob. Hence, regarding minimising the wall effect, the rough bob is recommended for further rheological measurements.

Moreover, the complex rheological properties were found to strongly correlate to solids content and temperature. These results indicate that the impact of the solids content, and especially the effects related to the key components and interactions in the sludge matrix, is very important in the rheological complexity. However, these effects are still unclear and out of the thesis scope. Thus, the rheological consequences related to sludge matrix structure, components, physical/chemical interactions, and relevant changes to temperature, needs to be further explored.

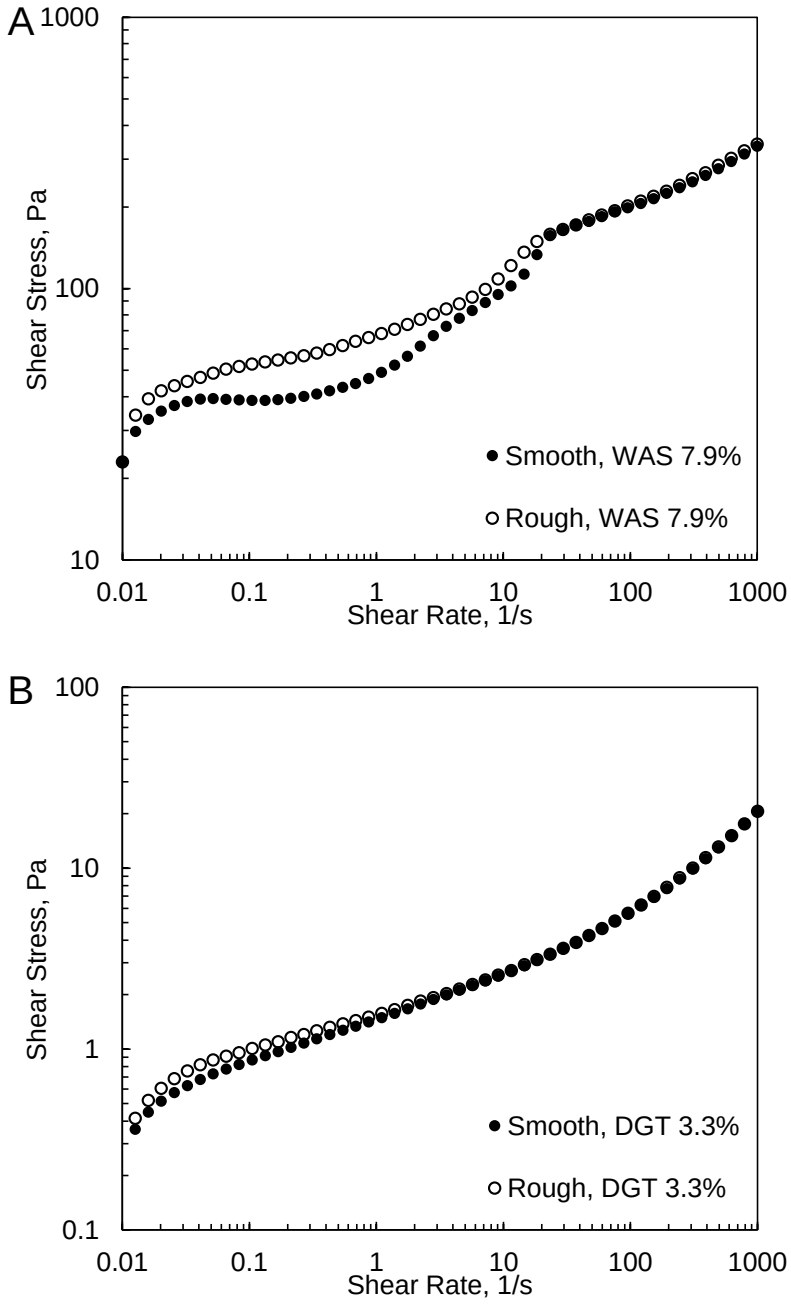

Fig. 6-1 Rheograms of (A): WAS with TS 7.9%, and (B): DGT with TS 3.3%, by measuring bobs with smooth surface and rough surface. The samples were provided by Ir. A. Gonzalez Ortega, TU Delft, non-published results.

6.2.2 Rheological characterisation: effectiveness to practical applications

On the one hand, the aforementioned wall effect should be minimised to obtain more accurate data in rheological measurements in laboratory. On the other hand, effectiveness of the rheological data to assess sludge flow and mixing in practice should be considered. If the studied sludge is pumped in a smooth pipeline or mixed by an impeller with smooth blades

in reality, a slip layer adjacent to the smooth surface can be formed due to the wall effect (Baudez et al. 2007). Thus, the considerable differences in the predicted apparent viscosity (~ 20%) need to be considered for pumping- or mixing-related energy assessment. In this case, the wall effect may not be recognised as an error source, but is attributed to the sludge intrinsic property. The smooth bob's data reflect 'effective' rheological properties in conditions of contacting smooth surfaces, which may be more meaningful to refer in practice. Similar discussion could also be held on other sludge types, i.e. primary sludge. Its components are usually more diverse and complex, and specific pre-treatment (like filtration or sieving) is necessary for a qualified rheological measurement. However, whether the rheological data of the refined sample can be representative to assess flow and mixing of the original sample in reality, needs to be determined. Therefore, similar to the data accuracy, the effectiveness of sludge rheological characterisation needs to be better evaluated in future research.

Furthermore, as discussed in Chapter 2 and 3, the regressed model parameters were more meaningful for a good data fitting performance rather than a clear representation of specific physical properties of the sludge matrix. Hence, definitions of the model parameters and correlations to sludge intrinsic physical properties need to be further determined.

6.2.3 Limitations in modelling of non-Newtonian flows

The limitation in turbulence modelling should be noticed in simulating non-Newtonian flows. Applications of more RANS models, and even Large Eddy Simulation in digesters have been reported (Bridgeman 2012, Coughtrie et al. 2013, Wu 2010b, d, 2011, 2012c), but the intrinsic challenge in turbulence modelling has not been discussed yet. As described in Chapter 1, the diffusion term in the momentum conservation equation is determined based on Reynolds decomposition in a RANS model (i.e. *k*-*ε*)

$$\frac{\partial}{\partial x_j}\left(\nu_{mol}\left(\frac{\partial \overline{u_i}}{\partial x_j}+\frac{\partial \overline{u_j}}{\partial x_i}-\frac{2}{3}\delta_{ij}\frac{\partial \overline{u_j}}{\partial x_j}\right)-\overline{u_i'u_j'}\right) \tag{6-1}$$

where δ_{ij} denotes the Kronecker delta (0 if $i \neq j$; 1 if $i=j$). The term $\overline{u_i'u_j'}$ is solved by this RANS model. When sludge rheology is involved, the kinematic viscosity ν_{mol} is determined by a specific rheological model, and thus is no longer constant but a function of shear rate γ

$$\nu_{mol} = f(\gamma) \tag{6-2}$$

Since γ is determined by mean-flow shear strain $\left(\frac{\partial \overline{u_i}}{\partial x_j}+\frac{\partial \overline{u_j}}{\partial x_i}\right)$, the data accuracy relies on

resolution of predicted Reynolds-averaged flow field. In a turbulence-dominant flow, γ can also be determined by Kolmogorov-scale shear strain:

$$\gamma_{Kolmo} = \sqrt{\varepsilon / \nu_{mol}} \tag{6-3}$$

where ε is the energy dissipation rate. It should be noticed that γ_{Kolmo} is also dependent on the ν_{mol} change when involving rheology, leading to more complicated predictions of the smallest scale in turbulent flow, compared to a Newtonian fluid. Hence, the rheological data integration increases model complexity and uncertainty, especially when local ν_{mol} is sensitive to γ and turbulence is dominant. In our full-scale model, considerable differences were found between the predicted mean-flow γ and γ_{Kolmo}. These differences did not play an important role, since the turbulence-dominant regions were only localised and constrained. Solutions for the limitations in the non-Newtonian turbulence modelling is still a fundamental challenge thus far, and is also out of the thesis scope. However, it should be further explored in the future, especially in digesters with more intense turbulent flows (i.e. the mechanical stirring mode).

The gas phase was set as bubbles with an identical size in this study. The assumption was appropriate in the lab-scale model (Chapter 4), but essentially not enough in the full-scale model with an effective height over 16 m (Chapter 5). In this case, an effect of the hydrostatic pressure difference (> 1.5 atm) on bubble size should be considered, when bubbles rise from bottom to top. This effect was considered by an ideal gas assumption in the model, but the modelling required more computational consumption and confronted more non-stabilised and divergent problems. Hence, the current identical bubble size setup was a trade-off with respect to modelling feasibility. However, this simplification needs to be improved to better characterise the bubble-induced flow and mixing in a system with a large hydrostatic pressure difference. Besides, potential dynamic size changes due to bubble coalescence and break-up should also be considered in the future.

Although some simplifications were applied, the full-scale simulations still had large computational consumption. The time step size was required to be set in the order of 10^{-4}~10^{-2} s to achieve good convergence. The simulations usually took over one month to reach a fully-developed flow state, even using the maximum 16 cores in ANSYS-Fluent. Hence, the huge computational consumption was also a critical limitation in this study, which needs to be optimised in the future.

Furthermore, our full-scale model still lacks available experimental data to validate. Although experimental data collection in full-scale digesters is usually challenging, a concrete correlation between CFD modelling and experiments is still necessary for optimisation of

operation and design in practice.

6.2.4 Mixing in anaerobic digesters

As discussed in Chapter 5, it is not appropriate to simply determine the dead zone in the digester by a specified velocity (maximum or settling) as proposed in previous studies. The large variability in materials that are contained in the sludge matrix should be considered, such as sand and gravel, Thus, the dead zone assessment by instantaneous flow or mixing behaviour (up to 10^1 h) with a short-term aspect may not be enough. Regarding the long SRT (10^1 d) in AD, an accumulative effect of poor flow and mixing on the long-term operation seems more meaningful in practice, which still lacks concrete methodology to characterise and should be in focus in the future.

The mixing enhanced by the recirculated biogas was assessed in Chapter 5. However, flow and mixing induced by the produced biogas was not considered in this thesis, which has not been in focus yet according to the author's knowledge. Only limited clues can be found in literature. Fig. 6-2 shows both experimental and simulated tracer data in a full-scale digester using a pump recirculation mode (Terashima et al. 2009). A good agreement has been found between the experimental and simulation data, but the biogas production process was not considered in the CFD modelling. The paper does not explicitly describe whether the tracer experiment was implemented under normal operational conditions with biogas production. But if yes, the good agreement implies a negligible effect from the produced biogas on flow and mixing. However, this is not a straightforward evidence, and as addressed in paragraph 6.1.4, the effect was possibly to be weakened by some unknown influencing factor(s), prevailing in reality but not involved in the model. As mentioned in Chapter 5, the biogas production performance is also dependent on the mixing performance. Thus, the flow and mixing induced by produced biogas are expected to be uncertain and complicated, but necessary to assess in the future research work.

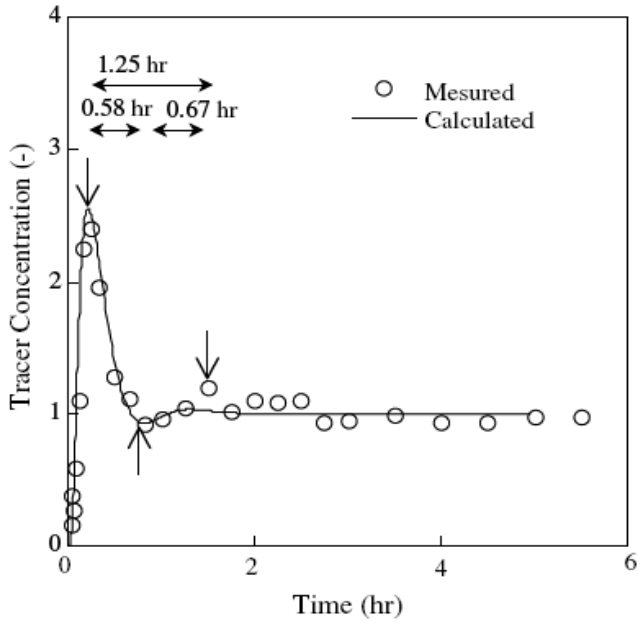

Fig. 6-2 Tracer response of experimental and simulation data (Terashima et al. 2009).

To develop concrete recommendations or guidelines for full-scale digesters in practice, the mixing assessment needs to be linked to operational parameters, such as biogas production rate and temperature gradients. Research on correlations between flow/mixing, and the AD biokinetic process or heat transfer is still limited (Bello-Mendoza and Sharratt 1998, Keshtkar et al. 2003, Wu 2012b, Yu et al. 2013). So, a model of integrating hydrodynamics, heat transfer and AD biokinetics, such as the Anaerobic Digestion Model No. 1, needs to be explored in the future.

6.3 References

Baudez, J.C., Ginisty, P., Peuchot, C. and Spinosa, L. (2007) The preparation of synthetic sludge for lab testing. Water Science and Technology 56(9), 67-74.

Bello-Mendoza, R. and Sharratt, P.N. (1998) Modelling the effects of imperfect mixing on the performance of anaerobic reactors for sewage sludge treatment. Journal of Chemical Technology and Biotechnology 71(2), 121-130.

Bridgeman, J. (2012) Computational fluid dynamics modelling of sewage sludge mixing in an anaerobic digester. Advances in Engineering Software 44(1), 54-62.

Coughtrie, A.R., Borman, D.J. and Sleigh, P.A. (2013) Effects of turbulence modelling on prediction of flow characteristics in a bench-scale anaerobic gas-lift digester. Bioresource Technology 138, 297-306.

Eshtiaghi, N., Markis, F., Yap, S.D., Baudez, J.-C. and Slatter, P. (2013) Rheological characterisation of municipal sludge: A review. Water Research 47(15), 5493-5510.

Keshtkar, A., Meyssami, B., Abolhamd, G., Ghaforian, H. and Khalagi Asadi, M. (2003) Mathematical modeling of non-ideal mixing continuous flow reactors for anaerobic digestion of cattle manure. Bioresource Technology 87(1), 113-124.

Seyssiecq, I., Ferrasse, J.-H. and Roche, N. (2003) State-of-the-art: rheological characterisation of wastewater treatment sludge. Biochemical Engineering Journal 16(1), 41-56.

Terashima, M., Goel, R., Komatsu, K., Yasui, H., Takahashi, H., Li, Y.Y. and Noike, T. (2009) CFD simulation of mixing in anaerobic digesters. Bioresource Technology 100(7), 2228-2233.

Wu, B.X. (2010a) CFD simulation of gas and non-Newtonian fluid two-phase flow in anaerobic digesters. Water Research 44(13), 3861-3874.

Wu, B.X. (2010b) Computational Fluid Dynamics investigation of turbulence models for non-Newtonian fluid flow in anaerobic digesters. Environmental Science & Technology 44(23), 8989-8995.

Wu, B.X. (2011) CFD investigation of turbulence models for mechanical agitation of non-Newtonian fluids in anaerobic digesters. Water Research 45(5), 2082-2094.

Wu, B.X. (2012a) Integration of mixing, heat transfer, and biochemical reaction kinetics in anaerobic methane fermentation. Biotechnology and Bioengineering 109(11), 2864-2874.

Wu, B.X. (2012b) Large eddy simulation of mechanical mixing in anaerobic digesters. Biotechnology and Bioengineering 109(3), 804-812.

Yu, L., Ma, J.W., Frear, C., Zhao, Q.B., Dillon, R., Li, X.J. and Chen, S.L. (2013) Multiphase modeling of settling and suspension in anaerobic digester. Applied Energy 111, 28-39.

Nomenclature

Roman

A	Coefficient in the Vogel-Tammann-Fulcher model, specified unit
A_{in}	Interfacial area per unit volume, m^{-1}
c	Tracer dimensionless concentration, -
$C_{1\varepsilon}$, $C_{2\varepsilon}$, C_{μ}	Constants in the RNG k-ε model, = 1.42, 1.68, 0.0845, respectively, -
$C_{2\varepsilon}^{*}$	Parameter in the RNG k-ε model, -
C_D	Drag coefficient, -
C_L	Lift coefficient, -
$C_{L,\ lowRe}$, $C_{L,\ highRe}$	Parameters in the Legendre-Magnaudet model, -
C_T	Model constant in the Lopez de Bertodana Model, =1
C_{VM}	Virtual mass coefficient, = 0.5, -
C_v	Parameter in the Differential Viscosity Model, ≈ 100, -
d	Gap width between rheometer measuring bob and cup, m
d_{eff}	Width of localised shear layer, m
d_g , d_{pt}	Diameter of the secondary phase, m
D	Pipe diameter, m
D_{tc}	Diffussion coefficient of the tracer, m^2/s
E	Power input for mixing, W
E_a	Activation energy, $J \cdot mol^{-1}$
Eo	Eötvös number, -
f	Fanning friction factor, -
F, $\vec{F}$	External body force, or additional force on a particle, N
$\vec{F}_D$	Drag force, N
$\vec{F}_L$	Lift force, N
$\vec{F}_{PI}$	Phase interaction forces (gas-liquid), N
$\vec{F}_{PG}$	Pressure gradient force, N
$\vec{F}_{SL}$	Saffman lift force, N
$\vec{F}_T$	Turbulent dispersion force, N
$\vec{F}_{VM}$	Virtual mass force, N
g, $\vec{g}$	Gravitational acceleration, 9.8 $m \cdot s^{-2}$
G	Production of turbulent kinetic energy, $J \cdot s^{-1}$
i, j	Number index as subscript in equations, -
k	Turbulent kinetic energy, $m^2 \cdot s^{-2}$
K	Flow consistency index, $Pa \cdot s^n$

K_n	Adjusted K, $Pa^{1/2}\cdot s^{n/2}$
L	Pipe length, m
m	Rate constant in Cross model, -
m_{pt}	Particle mass, kg
Mo	Morton number, -
MEL	Mixing energy level, W/m^3
n, n'	Flow behaviour index, -
N	Total number of phases, -
p, P	Pressure, Pa
Q	Flow rate, kg/s
R	Gas constant, $J\cdot K^{-1}\cdot mol^{-1}$
$R1$	Electrical resistance, Ohm
R_i	Radius of measuring bob, m
R_o	Radius of measuring cup, m
Re	Reynolds number, -
Re_g, Re_{pt}	Relative Reynolds number, -
Re_ω	Vorticity Reynolds number, -
Sr	Parameter in the Legendre-Magnaudet model, -
t	Time, s
T	Temperature, °C or K
Ta	Taylor number, -
$v, \vec{v}$	Velocity, $m\cdot s^{-1}$
$\overline{v_l}, \overline{v_l}$	Mean liquid velocity, $m\cdot s^{-1}$
v_i', v_l'	Velocity fluctuation, $m\cdot s^{-1}$
V	Volume, m^3
V_p	Mean pipe-flow velocity, m/s
x_i, x_j	Spatial coordinates, -
X	Parameter in the Herschel-Bulkley-based Re expression, -

Greek

α	Volume fraction, -
α_0	Bingham infinite apparent viscosity, Pa·s
$\alpha_k, \alpha_\varepsilon$	Inverse effective Prandtl numbers for k and ε, both ≈1.393, -
β	Constant in the RNG k-ε model, =0.012, -
β_{mc}	Parameter in the master curve equation, -
$\gamma, \dot{\gamma}$	Shear rate, s^{-1}
$\dot{\gamma}_{eff}$	Effective shear rate of localised shear layer, s^{-1}

Γ	Normalised shear rate, -
δ_{ij}	Kronecker delta, -
ΔP	Pressure difference, Pa
ε	Rate of dissipation of turbulent energy, $m^2 \cdot s^{-3}$
ζ	Normally distributed random number, -
η_0	Constant in the RNG k-ε model, =4.38, -
θ	Normalised time referred to theoretical mean recirculation time, -
λ_{Ca}	Time coefficient in Carreau model, s
λ_{Cr}	Time coefficient in Cross model, s^m
μ	Dynamic viscosity or apparent viscosity, Pa·s
$\hat{\mu}$	Parameter in the Differential Viscosity Model, -
μ_0	Zero-shear viscosity, Pa·s
μ_∞	Infinite rate apparent viscosity, Pa·s
μ_B	Bingham viscosity, Pa·s
μ_{eff}, μ_{eff_MR}	Effective dynamic viscosity, Pa·s
μ_T	Reference viscosity of the interstitial fluid, Pa·s
υ	Kinematic viscosity, m^2/s
ρ	Density, kg/m^3
σ	Surface tension coefficient, kg/s^2
τ	Shear stress, Pa
$\boldsymbol{\tau}$	Stress-strain tensor, $N \cdot m^{-2}$
τ_0	Yield stress, Pa
$\tau_{1/2}$	Critical shear stress in Ellis model, Pa
τ_C	The critical shear stress in the new expression, Pa
τ_{pt}	Particle relaxation time, s
τ_W	Wall shear stress, Pa
T	Normalised shear stress, -
φ	Rheological parameter correlated by the VTF model, specified unit
ω	Angular velocity, rad/s

Abbreviations

AD	Anaerobic digestion
CARPT	Computer automated radioactive particle tracking
CFD	Computational fluid dynamics
CFL	Courant-Friedrichs-Lewy
CoV	Coefficient of variance
CSTR	Completely stirred tank reactor

CT	Computed tomography
DGT	Digestate
GCI	Grid convergence index
GT	Gravitational thickened
HRT	Hydraulic retention time
LFR	Laminar-flow reactor
MUSCL	Monotonic upstream-centered scheme for conservation laws
PFR	Plug-flow reactor
QUICK	Quadratic interpolation for convective kinetics
RANS	Reynolds-averaged Navier-Stokes
RMSE	Root mean squared error
RNG	Re-normalisation group
RP	Redox potential
RTD	Residence time distribution
SIMPLE	Semi-implicit method for pressure linked equations
SRT	Solids retention time
SSE	Sum of squared errors
THP	Thermal-hydrolysis process
TS	Total solids
VFC	Vacuum-filtration-concentrated
VS	Volatile solids
VTF	Vogel-Tammann-Fulcher
WAS	Waste activated sludge
WWTP	Wastewater treatment plant

Supplementary

A. Fitting results of more rheological models (Chapter 2)

Besides Fig. 2-2 in Chapter 2, fitting data of the models with a higher degree of complexity are shown in Table S-1. For the GT sludge, the Casson model performed very well, with regressed a yield stress value (0.44 Pa) quite close to the measurement (0.43 Pa), and reasonable asymptotic μ_∞ (4.1 mPa·s) compared to the minimum apparent viscosity (7.7 mPa·s). Contrarily, the Sisko model deviated at high shear rates (>100 s^{-1}) and predicted an unreasonable μ_∞. Although returning acceptable fitting below 2 s^{-1}, the most complicated Cross model and Carreau model deviated at high shear rates too and largely overestimated μ_∞. The Ellis model did not result in a fit at all so was not discussed more.

Fitting quality improvement by adjustments was limited. Only Sisko returned a quite good fit when discarding the data of segment 1. Assuming a reasonable value for μ_∞ (4.1 mPa·s) in Cross and Carreau, a better trend (Fig. 2-2B) was obtained, but the overall quality (SSE and RMSE values) was not improved.

Similar but lower performance was obtained for the VFC sludge curves without segment 1. Casson still predicted acceptable τ_0 and μ_∞, but SSE and RMSE values were no longer low. Cross and Carreau did not produce a satisfactory fit either, even though μ_∞ was removed since no relevant trend was observed in the curves. Hence, the general fitting advantage in a wide shear rate range when using the models with higher complexity, was not demonstrated for the VFC sludge curves revealing no asymptotic trend. Moreover, although having distinct expressions, Sisko, Cross and Carreau usually returned similar μ_∞, SSE and RMSE.

Table S-1 Fitting results of the models with limiting parameters, the data of the adjusted model fitting are in parentheses.

Sludge TS	Model	Parameters						SSE	RMSE
		K	n	τ_0	μ_0	μ_∞	Other		
1.2%	Casson			0.45		$4.1\cdot10^{-3}$		0.03	0.02
	Sisko	0.79 (0.31)	0.15 (0.31)			~0 ($4.4\cdot10^{-3}$)		63.3 (~0)	0.81 (~0)
	Cross				63.37 (66.45)	0.16 ($4.1\cdot10^{-3}$)	m = 1.30 (1.26) λ_{Cr} = 272 (245)	21.1 (22.6)	0.47 (0.48)
	Carreau		-0.16 (-0.13)		50.07 (50.54)	0.12 ($4.1\cdot10^{-3}$)	λ_{Ca} = 80 (83)	15.0 (15.8)	0.40 (0.41)
	This paper	K_n= 0.06	1.00				τ_C = 0.45	0.03	0.02
3.6%	Casson			8.52		0.04		17.3	0.50
	Sisko	6.68	0.18			0.20		1.3	0.14
	Cross				$1.6\cdot10^5$ ($1.8\cdot10^5$)	0.20 (-)	m = 0.82 (0.79) λ_{Cr} = $2.5\cdot10^4$ ($2.6\cdot10^4$)	1.3 (2.5)	0.14 (0.19)
	Carreau		0.18 (0.21)		$1.4\cdot10^3$ ($1.3\cdot10^3$)	0.20 (-)	λ_{Ca} = 669 (729)	1.3 (2.5)	0.14 (0.19)
	This paper	K_n= 2.27	0.35				τ_C = 0.12	0.6	0.09
6.0%	Casson			71.5		0.22		245.3	1.8
	Sisko	51.67	0.08			3.11		407.3	2.3
	Cross				$1.7\cdot10^6$ ($1.1\cdot10^7$)	3.11 (-)	m = 0.93 (0.90) λ_{Cr} = $3.3\cdot10^4$ ($2.0\cdot10^5$)	407.8 (799.7)	2.3 (3.2)
	Carreau		0.08 0.11		$7.0\cdot10^4$ $5.3\cdot10^4$	3.11 -	λ_{Ca} = $2.4\cdot10^3$ ($2.2\cdot10^3$)	407.3 (799.6)	2.3 (3.2)
	This paper	K_n= 8.02	0.27				τ_C ~ 0	23.0	0.5

B. Supplementary rheological and pipe-flow data (Chapter 3)

Table S-2 Rheological properties of WAS and DGT in the Initial and Stable states.

State, WAS 6.7%	Yield stress τ_0 (Pa)	Segment 1 K1 (Pa·s^n)	n1	τ_1 (Pa)	Transition γ (1/s)	Segment 2 K2 (Pa·s^n)	n2
Initial	108	32	0.626	47	25.8	156	0.181
Stable	55	25	0.743	22	9.6	104	0.149
1h rest	109	29	0.647	52	25.8	150	0.185

State, DGT 2.6%	Parameters K (Pa·s^n)	n	τ_0 (Pa)
Initial	0.42	0.549	0.74
Stable	0.33	0.571	0.63

Table S-3 Model parameters for WAS 7.0% at the 5 temperatures.

Temperature (°C)	Yield stress τ_0 (Pa)	Segment 1 K1 (Pa·s^n)	n1	τ_1 (Pa)	Transition γ (1/s)	Segment 2 K2 (Pa·s^n)	n2
10	131	39	0.66	67	15.2	171	0.19
20	126	32	0.63	54	30.5	163	0.18
35	83	22	0.64	38	34.3	126	0.18
45	63	16	0.70	33	38.5	118	0.17
55	46	11	0.69	20	34.3	68	0.21

Table S-4 Mass flow rates of Initial and Stable sludge under different pressure-driven conditions.

Sludge	Pressure-driven condition (Pa/m)	Flow rate, Initial, kg/s	Flow rate, Stable, kg/s	Difference, %
WAS 6.7%	**2500**	2.3	4.4	96.6
	5000	11.8	68.8	482.5
	10000	96.1	172.4	79.5
	25000	294.5	324.7	10.27
DGT 2.6%	**100**	17.7	19.6	10.7
	150	25.9	26.9	4.1
	250	37.5	38.7	3.0
	500	58.0	58.3	0.5
	1000	85.3	85.5	0.2
	2500	140.1	141.1	0.7

As shown in Fig. S-1, a good agreement is achieved between theoretical and simulated velocity profiles of the water. Predictions of non-Newtonian flows in more Re cases are also

acceptable, especially in the turbulent regime. However, an agreement in laminar regime was difficult. The materials in this study and the referred experiments (Ostwald, (Pinho and Whitelaw, 1990)) had distinct rheological properties. At low shear rates, τ_0 became important and could result in different laminar curves with a smooth or plateau region ('plug flow' pattern) towards the pipe centre and high velocity gradient near the wall. Hence, the non-Newtonian velocity profiles showed a higher rheological dependency, increasing the complicity to determine the laminar/turbulent regime.

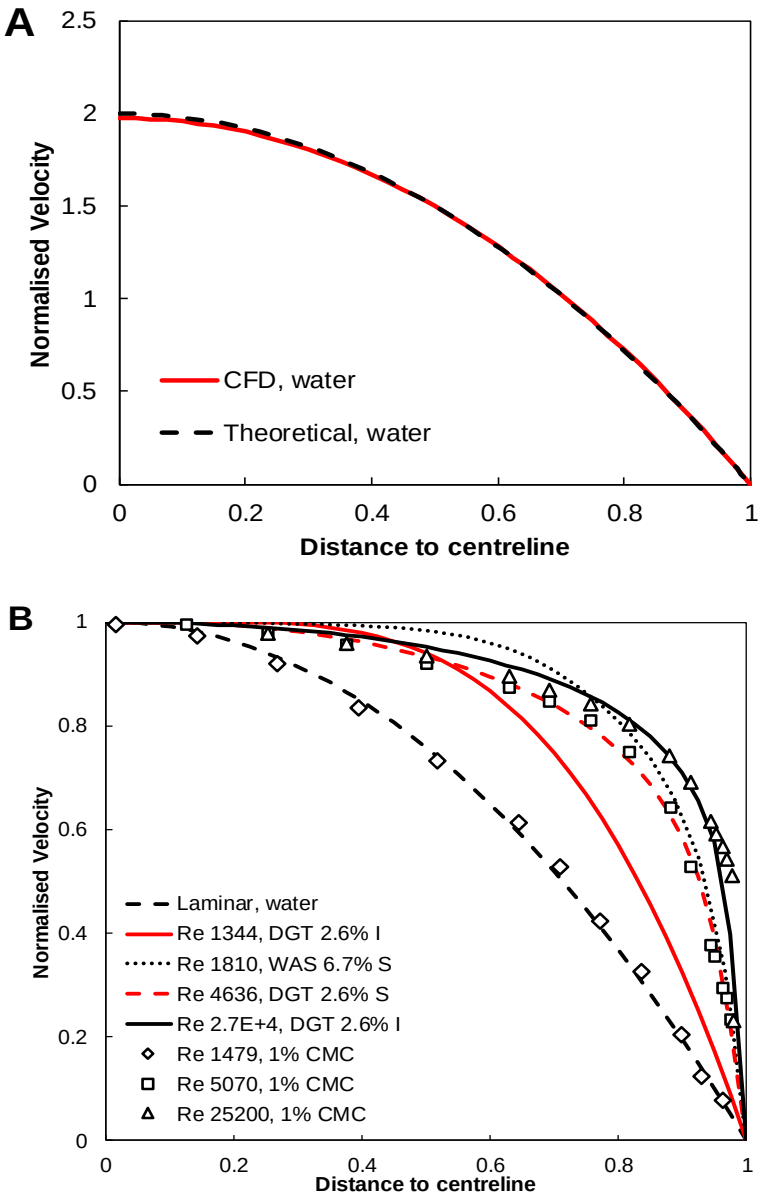

Fig. S-1 Comparisons of simulated and reference data of the normalised axial velocity from A: Newtonian (water), and B: non-Newtonian (carboxy methyl cellulose (Pinho and Whitelaw, 1990)) Flows.

As shown in Fig. S-2, in each WAS group of the same pressure-driven condition, a large flow-rate increase and a weakened 'plug flow' pattern are found in Stable. Similar tendency is also found in DGT data with much smaller differences between Initial and Stable. However, the 150 Pa/m case is an exception (red curves in Fig. S-2B), because compared to the laminar Initial, the Stable flow was in transition to turbulence.

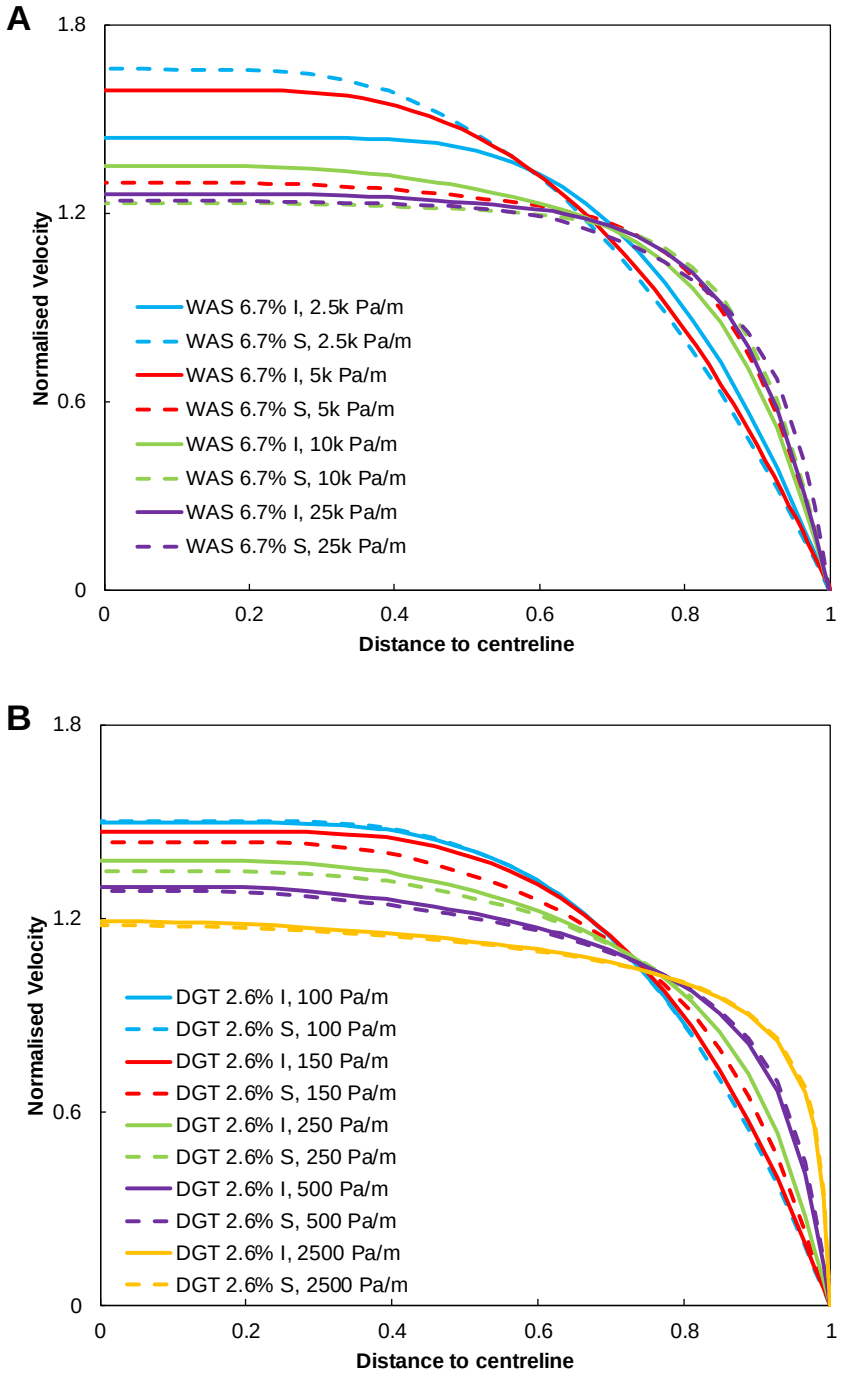

Fig. S-2 Normalised axial velocity (to mean velocity) of Initial (I) and Stable (S) under different pressure-driven conditions, A: WAS 7.6%, and B: DGT 2.6%.

Reference

Pinho FT, Whitelaw JH. Flow of non-newtonian fluids in a pipe. Journal of Non-Newtonian Fluid Mechanics 1990; 34: 129-144.

C. Grid independence test (Chapter 4)

Fig. S-3 shows liquid axial velocity data of the 5 grid sizes (Mesh A-E) at heights of 11.25 cm (1/2 depth) and 18.25 cm (1/5 depth) and Table S-5 shows relevant GCI assessment results. As shown in Table S-5, each GCI assessment group contains three adjacent characteristic grid sizes from Mesh A to E. To better assess the phase interaction region, the mean velocity inside the draft tube was also analysed separately. According to the GCI method (Roache 1994, Celik et al. 2008), mesh independence can be indicated by reaching an asymptotic range (Asymptotic value ~ 1). However, this is not the only criterion. Although a good asymptotic range was obtained for both Group 1 and 3 (values of Asymptotic_{ABC} and Asymptotic_{CDE} in Table S-5), the velocity profile of Mesh B/C still got considerable difference (with high GCI values) when compared to Mesh D and E (Fig. S-3). So based on the GCI results, in combination with qualitatively assessing the overlapping degree of the velocity profiles, Mesh D and E were reaching mesh independence. Since having smaller number of grid cells and thus less computational consumption than Mesh E, Mesh D was selected as optimal for the following simulations.

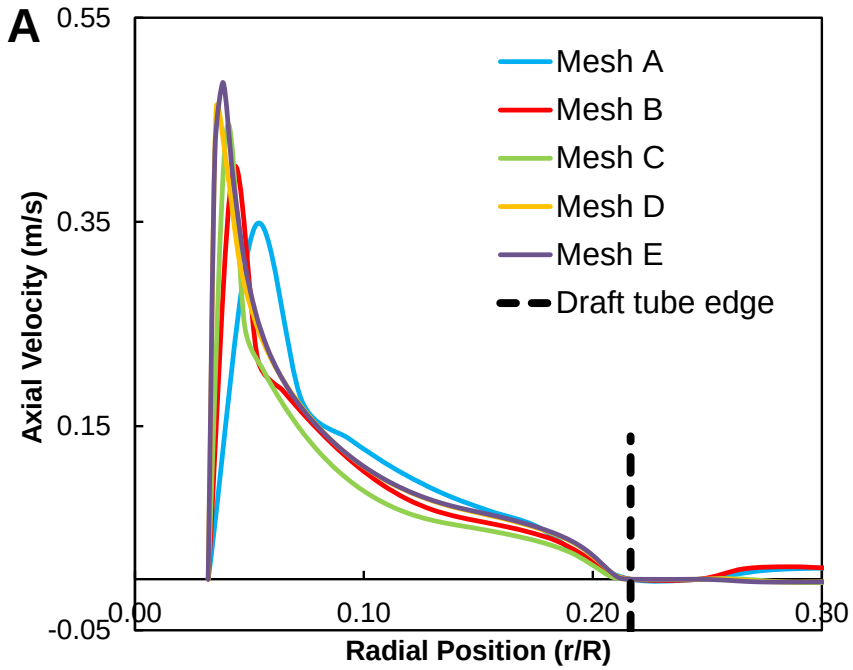

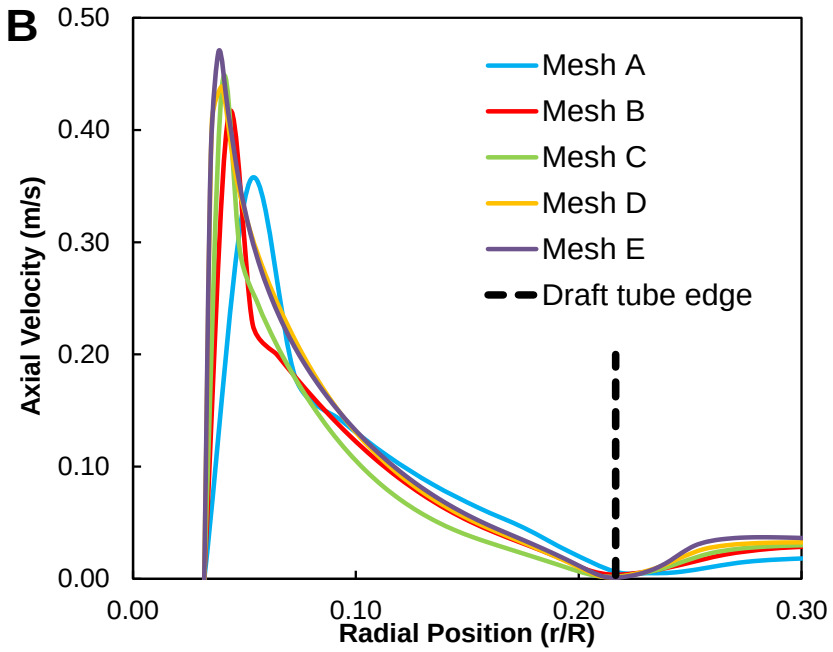

Fig. S-3. Liquid axial velocity profiles of the 5 grid sizes at heights of (A) 11.25 cm and (B) 18.25 cm; gas flow rate 28.32 L/h.

Table S-5 GCI assessment results of the mean axial velocity of the draft tube and the whole region, heights of 11.25 cm and 18.25 cm.

		Height 11.25 cm		Height 18.25 cm	
		Draft tube	**Whole region**	**Draft tube**	**Whole region**
Mean axial velocity (m/s)	**Mesh A**	0.124	0.029	0.125	0.029
	Mesh B	0.094	0.022	0.098	0.027
	Mesh C	0.087	0.019	0.095	0.025
	Mesh D	0.106	0.023	0.116	0.030
	Mesh E	0.107	0.023	0.119	0.032
Group 1, Mesh A, B & C	**GCI_{AB}, %**	13.5	45.1	4.7	26.5
	GCI_{BC}, %	3.8	29.6	0.6	20.0
	$Asymptotic_{ABC}$	0.92	0.84	0.97	0.94
Group 2, Mesh B, C & D	**GCI_{BC}, %**	6.9	119	0.7	4.1
	GCI_{CD}, %	14.6	116	4.1	10.3
	$Asymptotic_{BCD}$	0.19	0.85	0.03	0.13
Group 3, Mesh C, D & E	**GCI_{CD}, %**	1.4	0.9	2.5	8.5
	GCI_{DE}, %	0.08	0.03	0.2	2.3
	$Asymptotic_{CDE}$	1.01	1.01	1.02	1.05

D. Sensitivity study on the effective range of the Ostwald model (Chapter 5)

Here we investigated an impact of the effective range of the Ostwald model, especially the γ_{min}/μ_{max} setup, on flow and mixing predictions. As shown in Fig. S-4 (curves of Ostwald 1, 2 and 3), three γ_{min}/μ_{max} values were determined based on the same data fitting quality. The γ_{min} change was small (from 1 to 9 s^{-1}, 2.7% of the whole effective range), yet the corresponding μ_{max} change was considerable (from 1.12 to 0.3 Pa·s, 73% reduction).

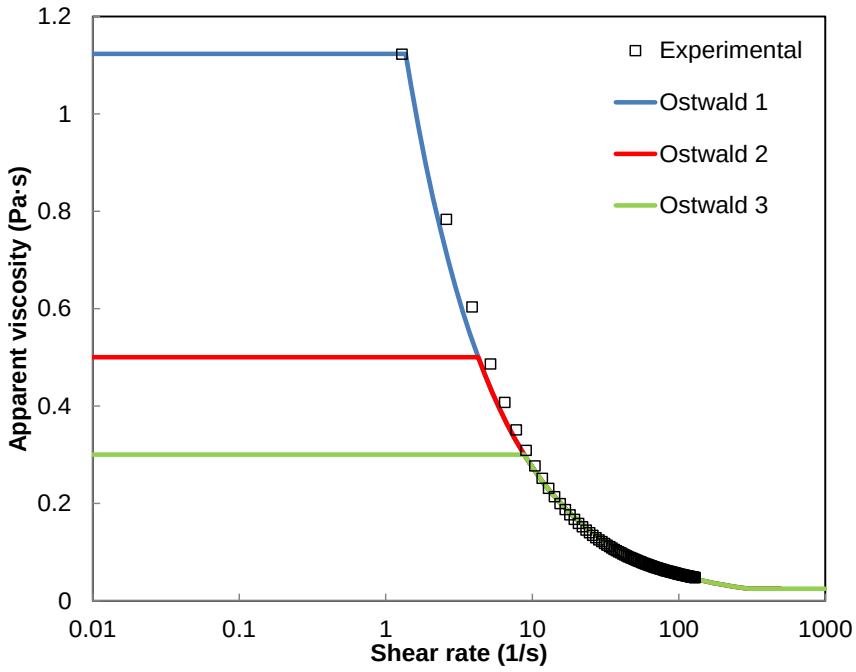

Fig. S-4 Sludge rheological data, experimental and the Ostwald model fitting (with 3 μ_{max} settings).

Sludge velocity data of the three Ostwald cases are shown in Fig. S-5A, zooming in to velocities <0.1 m/s. The zoomed velocity range was found to cover the major part of the domain, and the overall velocity magnitude increased considerably from Ostwald 1 to 3, especially in regions above the gas inlet. Fig. S-5B demonstrates considerable heterogeneity of the velocity distributions in the whole domain, and more differences in volume fraction among the three cases. As μ_{max} decreased from Ostwald 1 to 3, the volume fraction of the low velocity level (< 0.01 m/s) also decreased, correlating to the increased medium and high velocity levels. Especially for velocity > 0.05 m/s, the volume fraction considerably increased from 2.9% to 13.4%.

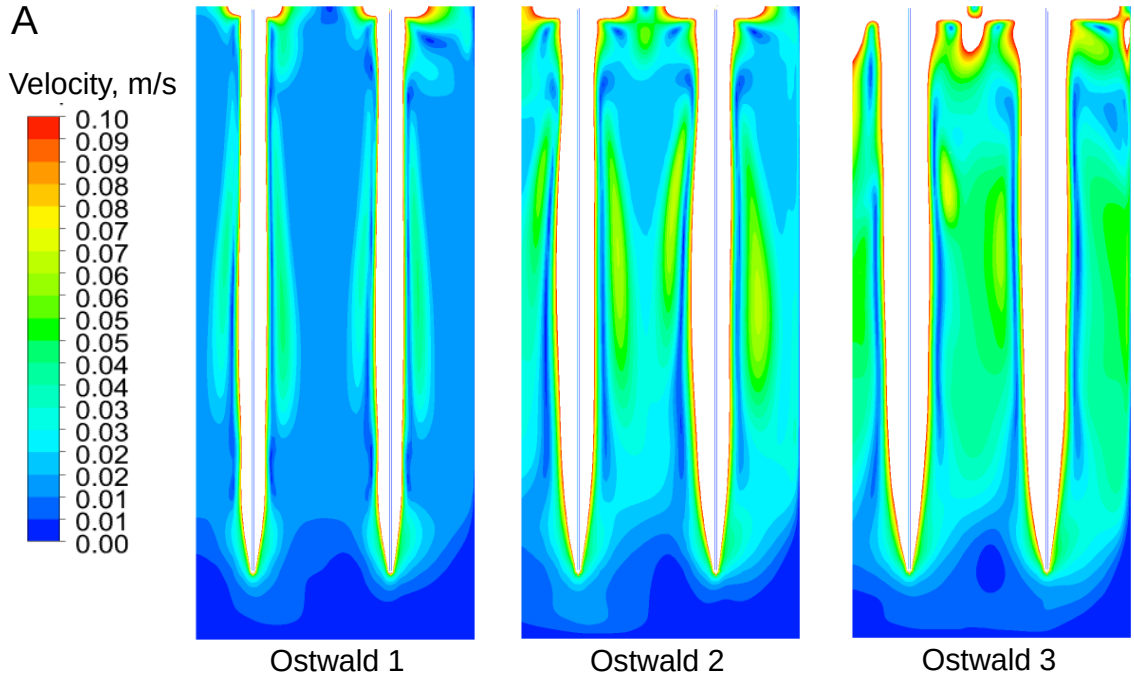
A
Velocity, m/s
0.10
0.09
0.09
0.08
0.08
0.07
0.07
0.06
0.06
0.05
0.05
0.04
0.04
0.03
0.03
0.02
0.02
0.01
0.01
0.00
Ostwald 1
Ostwald 2
Ostwald 3

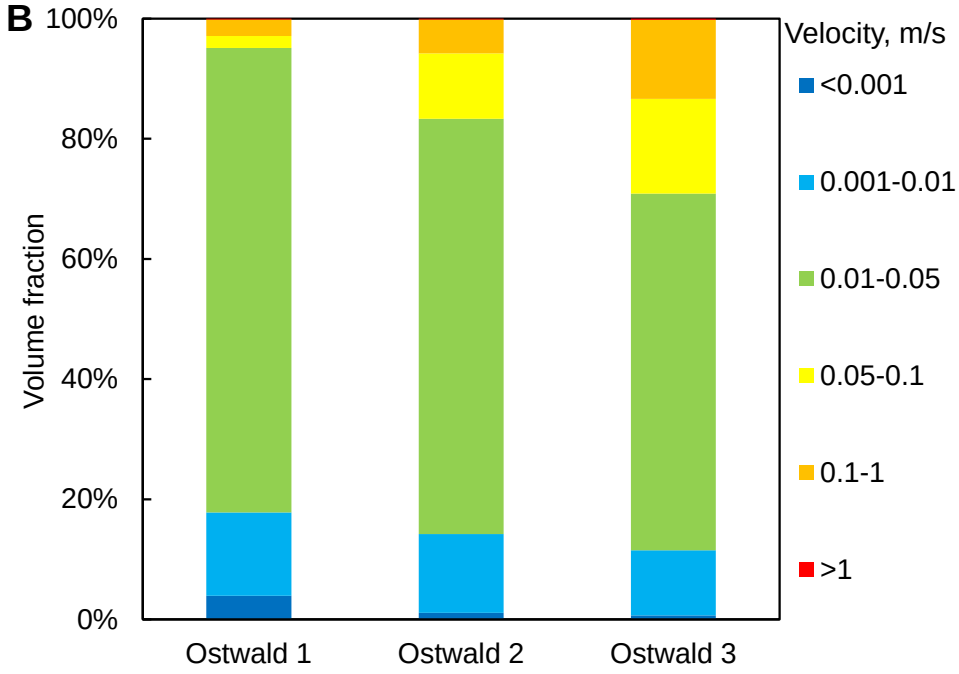
B
100%
80%
60%
40%
20%
0%
Volume fraction
Ostwald 1
Ostwald 2
Ostwald 3
Velocity, m/s
<0.001
0.001-0.01
0.01-0.05
0.05-0.1
0.1-1
>1

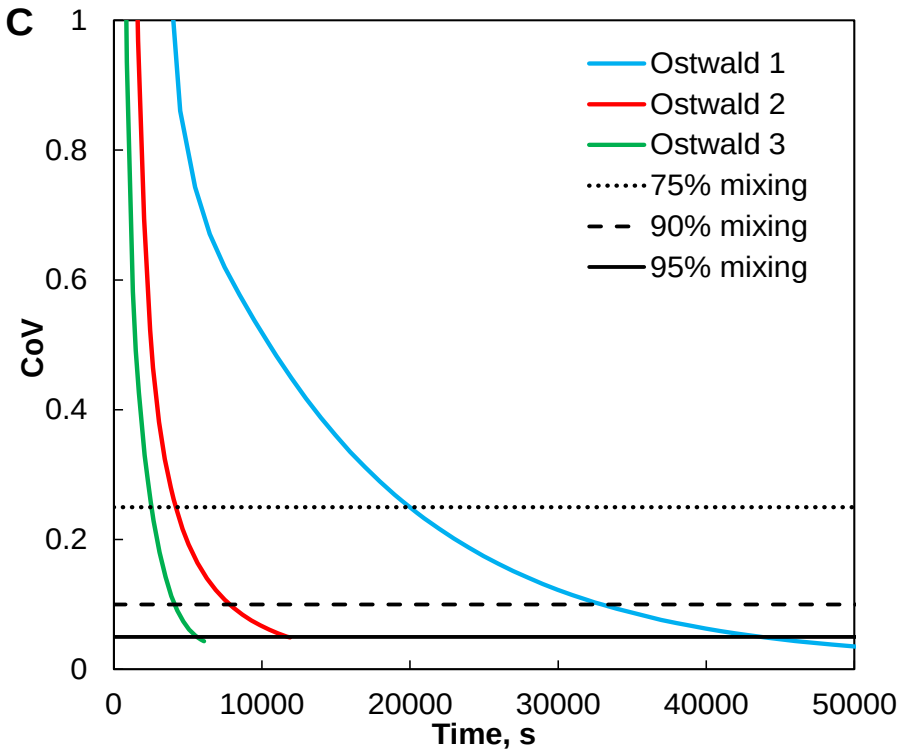

Fig. S-5 Flow (A and B) and mixing (C) results of the three Ostwald cases.

The mixing performance was assessed using the tracer's CoV data. As shown in Fig. S-5C, the three cases had even larger differences in time to reach specific mixing degrees. The high velocity level (>0.05 m/s) mainly accounted for reaching a medium mixing degree, such as 75%. Regarding the corresponding volume fraction, Ostwald 2 and 3 had relatively small differences, and the CoV curves mainly had a quantitative difference but a similar tendency to reach the 75% mixing degree. The medium and low velocity levels (<0.05 m/s) became more important when reaching further mixing degrees, so the CoV curve tendency also became different between Ostwald 2 and 3. Ostwald 1 had the smallest volume fraction in the high velocity level, and the largest in the low velocity level (<0.01 m/s), especially in the range < 0.001 m/s. Thus the CoV curve had a different tendency from an early stage. The predicted ideal (or 95%) mixing time of 4.4×10^4 s, was much larger than the time of Ostwald 2 and 3, which was 1.2×10^4 s and 5.6×10^3 s, respectively. Hence, although with small differences in volume fraction, the low velocity level (<0.01 m/s) was still crucial for reaching the ideal mixing degree.

Moreover, the γ distribution data (Fig. S-6A) demonstrated that over 97% total volume obtained γ <1 s^{-1}, which was out of the applied effective range. In line with the high velocity locations, the γ levels within the effective range were only constrained in the regions

surrounding the gas lances (orange and red in Fig. S-6B). The apparent viscosity distribution data (Fig. S-6C) showed the same pattern: in most regions the sludge did not behave shear-thinning, but 'Newtonian' with constant μ_{max}. These large differences in the overall apparent viscosity level among the three cases accounted for the distinct flow and mixing performance described in Fig. S-5. Hence, these results indicated an important role of the effective range determination in flow and mixing predictions, which could limit applications of the Ostwald model.

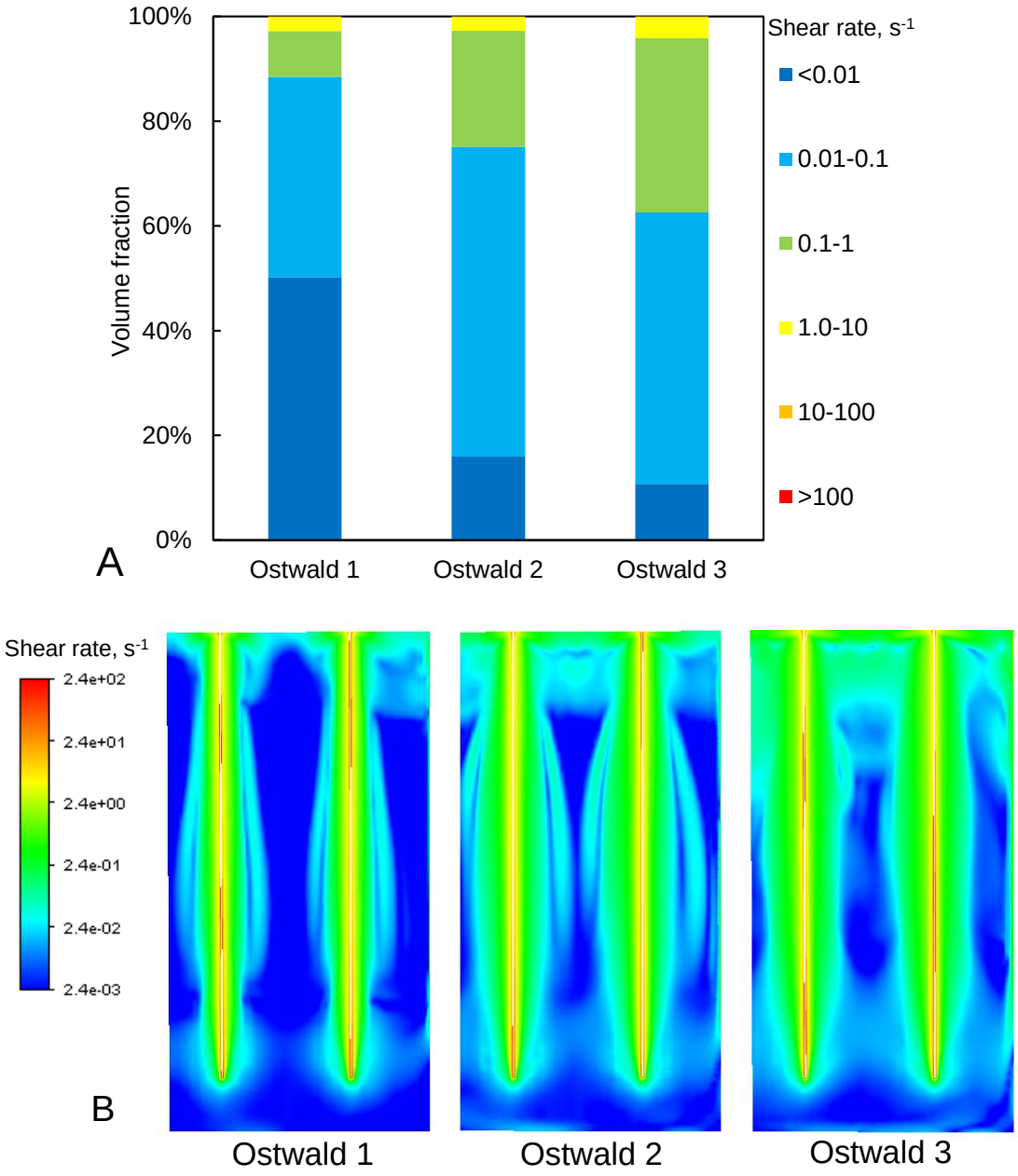

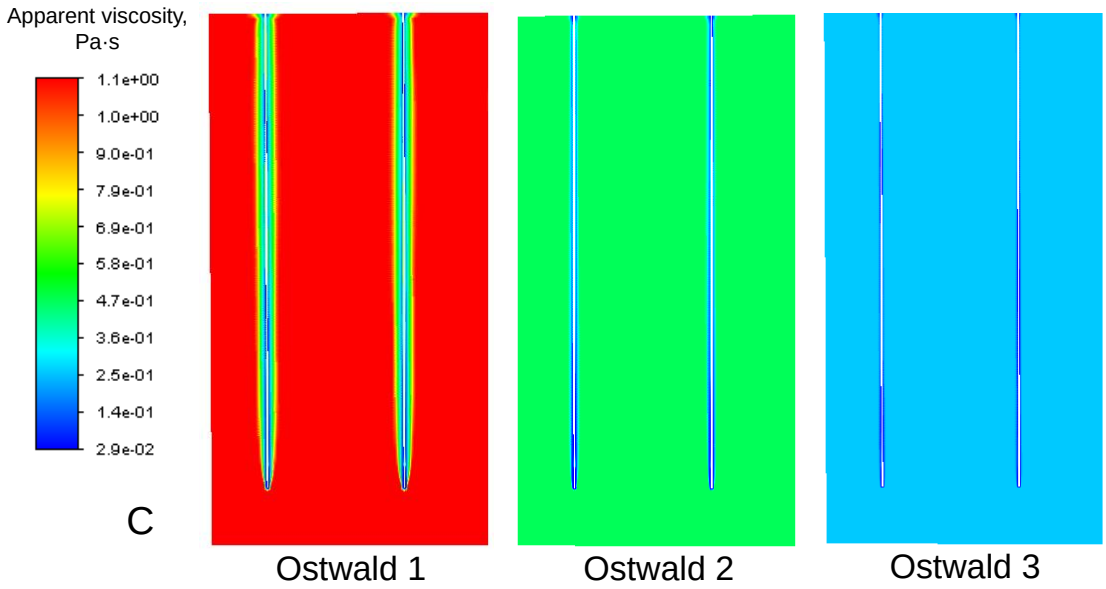

Fig. S-6 Shear rate (A and B) and apparent viscosity (C) distributions predicted in the three Ostwald cases.

Acknowledgements/致谢

The long journey is eventually going to an end, and there are so many people I really would like to appreciate. First gratitude to my promotors: Jules, Merle, and Wim, for supervising my PhD study. Many thanks to Jules for leading me to the world of anaerobic digestion. You taught and inspired me a lot about what an academic researcher should be and how to do scientific research. Your views and remarks were crucial to orient and shape this thesis. Many thanks to Merle for guiding me on the PhD track in detail. All concrete elements in the thesis were constructed based on the discussion at our regular meetings. Your supports were both technical, like useful guidelines and corrections to my scientific writing and presentation; and mental, like the way to overcome frustrations. Many thanks to Wim as well. Your critical and conducive comments were crucial for my work on fluid dynamics and modelling, which was a basic pillar of the thesis. Although sometimes really challenging, your remarks were indeed to the point to improve my research and develop my expertise. What I have learned from you all not only served for the current thesis, but will also benefit my future academic career. Particularly, I acknowledge China Scholarship Council and Lamminga Fonds for the financial supports on my living and research in The Netherlands.

I do appreciate Henri for all kinds of supports in the first few years. Your personality and expertise helped me a lot adapt to the new circumstance, and to shape the thesis objectives. Each meeting or talk with you encouraged and inspired me a lot, regardless of topics. My particular appreciation to Luuk, for your offer to pursue my PhD here after our meeting in Xiamen, and your open mind to the supervision transfer.

I would like to express my sincere gratitude to Rob. The communications with you were not early, but quite efficient to proceed with my modelling work. Also thank you so much for the opportunity to join the postdoc project I have been working on. Many thanks to Cees for useful help and suggestions on Fluent usage. Great appreciation is also to Mark for providing the sludge samples and the nice collaborations with De Groote Lucht wastewater treatment plant. Many thanks to Qiuman for the collaborated work on the sludge rheological measurements. Many thanks to Rosario for our collaborations on the multiphase flow modelling.

Great gratitude is to Armand, Tonny, and Mohammed for all the assistance to implement my experimental work in Water Lab. I do appreciate Mariska, Jennifer, Anouk, Tamara, and Riëlle a lot, for all kinds of administrative supports and help.

Besides, I am grateful to my officemates and friends in Room 4.59: Xuedong, Annelies,

Guido, Hongxiao, Adrian, Ka Leung, Juan, Alex, Thabo, Deva, Rokhsareh, Dhruve, Marij, Sara, and Lenno, for the enjoyable time to stay in this 'warm' office. Also, would like to thank the other colleagues and friends in Water Lab and our section, especially Zhongbo, Hale, Evren, Maarten, Marjolein, Julian, Mostafa, Dara, Niels, Ljiljana, Andre, Adithya, and Irene, for the nice time we had been communicating or collaborating with.

Special thanks to the other Chinese colleagues and friends for sharing the colourful time and all kinds of help in and out of the campus: Gang, Ran, Jingyi, Feifei, Xiaochen, Haoyu, Yu, Nan, Zheyi, Weigang, Wei Wang, Liangfu, Xuefeng, Bensheng, Ying, Xinyue, Shunwen, Wei Fang, Hongbo, Lihua, Mingliang, Max, Zhe, Bin, Qi, Guoshuai, Shuo, Xinyu, and Yuke; Yujia, Mingsheng, Lingshan, Jinlong, Tian, Liwei, Shilong, Bowei, Xu Huang, Hong Li, Ruxin, Jiafang, Tao, Die, Liangyuan, Zhongbing, Zejian, Jun, Xueqing, Peijuan, Xinlei, Ru, and Yaya. Maybe I still missed some names, but I really cherish the time we were together abroad.

Finally, deepest gratitude and love to my family, which cannot be simply expressed in words. Thank my cousin Xiaojie for the thesis cover design. Thank my parents for everything devoted to me, which never changed to time or distance. Thank my parents-in-law for all your supports and love in these years. 感谢表妹晓捷的论文封面设计。感谢父母养育之恩及无条件的付出和关爱，大爱无言，铭记在心。感谢岳父岳母多年来给予的全方面支持、包容和关爱。感谢儿子与妻子的爱和陪伴。Thank my little boy Mario, and my wife Cuijie. Mario, you are the most important gift I have ever had, filling so much meaningfulness in my life. The current world became unusual, hope everything will go back normal when you grow up. My deepest thanks and love to Cuijie, for everything we experienced together so far. This journey was filled with all kinds of tastes, including a lot of tough moments, and I could not complete it without your accompany.

Peng Wei 魏鹏

Delft

16 June, 2021

List of publications

Peer reviewed journal papers

- **P. Wei***, W. Uijttewaal, J. van Lier, M. de Kreuk. Impacts of shearing and temperature on sewage sludge: rheological characterisation and integration to flow assessment. *Science of the Total Environment*, 2021, (774) 145005. (Chapter 3)
- **P. Wei***, R. Mudde, W. Uijttewaal, H. Spanjers, J. van Lier, M. de Kreuk. Characterising the two-phase flow and mixing performance in a gas-mixed anaerobic digester: Importance for scaled-up applications. *Water Research*. 2019, (149) 86-97. (Chapter 4)
- **P. Wei***, Q. Tan, W. Uijttewaal, J. van Lier, M. de Kreuk. Experimental and mathematical characterisation of the rheological instability in concentrated waste activated sludge subject to anaerobic digestion. *Chemical Engineering Journal*. 2018 (349) 318-326. (Chapter 2)
- **P. Wei**, K. Zhang*, W. Gao, L. Kong, R. Field. CFD modeling of hydrodynamic characteristics of slug bubble flow in a flat sheet membrane bioreactor. *Journal of Membrane Science*. 2013 (445): 15-24.
- K. Zhang, **P. Wei**, M. Yao, R. Field, Z. Cui*. Effect of the bubbling regimes on the performance and energy cost of flat sheet MBRs. *Desalination*. 2011 (283): 211-216.

Peer reviewed journal papers in preparation

- **P. Wei***, W. Uijttewaal, J. van Lier, M. de Kreuk. Gas-mixing in a full-scale anaerobic digester: assessments of rheological data integration, mixing and recommendations for optimisation using computational fluid dynamics. *To be decided*, in preparation. (Chapter 5)

Conference proceedings and oral presentations

- **P. Wei***, R. Mudde, W. Uijttewaal, H. Spanjers, J. van Lier, M. de Kreuk. Mixing characterisation in gas-mixed anaerobic digesters: scaled-down evaluation and scaled-up implication. *The 16th IWA World Conference on Anaerobic Digestion,* 2019, The Netherlands.
- **P. Wei***, H. Spanjers, W. Uijttewaal, J. van Lier, M. de Kreuk. Improved hydrodynamic characterisation of two-phase flow in gas-mixed anaerobic digester by CFD modelling. *The 15th IWA World Conference on Anaerobic Digestion,* 2017, China.
- **P. Wei***, H. Spanjers, W. Uijttewaal, J. van Lier, M. de Kreuk. CFD modelling of

hydrodynamic characteristics in gas-mixed anaerobic digester. *Frontiers International Conference on Wastewater TreatMent,* 2017, Italy.

- **P. Wei***, H. Spanjers, W. Uijttewaal, J. van Lier, M. de Kreuk. Hydrodynamics characterisation of gas mixing in anaerobic digesters. *IX International Conference on Computational Heat and Mass Transfer*, 2016, Poland.
- **P. Wei***, H. Spanjers, W. Uijttewaal J. van Lier, M. de Kreuk. Hydrodynamic characterization of gas mixing in a full-scale anaerobic digester. *The 4th Young Water Professional BeNeLux Regional Conference*, 2015, The Netherlands.
- G. Zhang, **P. Wei**, H. Liu, K. Zhang*. Antifouling performance of membrane bioreactors with slug bubbling for municipal wastewater reuse. *The 8th International Conference on Sustainable Water Environment*, 2012, China.

Biography

Peng Wei (魏鹏) was born in Jiangxi, China, on June 8, 1984. He obtained his BSc. degree (cum laude) in Environmental Engineering at Beijing Normal University in 2007. He obtained his MSc. degree in Environmental Engineering at Graduate University of Chinese Academy of Sciences in 2010. His master thesis was entitled "*Investigation on hydrodynamic characteristics of flat sheet MBR module with slug bubbling*". Since July 2010, he had been working as a research assistant at Institute of Urban Environment, Chinese Academy of Sciences for over three years. He had been in Institute for Frontier Materials, Deakin University, as a visiting academic from March to June in 2012. In April 2014, he started his PhD research on the current topic on sewage sludge rheology and mixing in gas-mixed anaerobic digesters. Since July 2018, he has been working as a postdoctoral researcher on an ERA CoBioTech project entitled "*Computation for rational design: from lab to production with success*".

His research interests mainly include computational fluid dynamics (CFD) on multiphase flows, viscous/non-Newtonian fluids, CFD-biokinetics coupling, cost-effective technologies and resource recovery applications in (waste)water treatment, and scale-up/-down process optimisation.